THUNDERSTORM ELECTRIFICATION:

PRECIPITATION VERSUS CONVECTION

by

Earle Rolfe Williams

B.A., Swarthmore College
(1974)

SUBMITTED IN PARTIAL FULFILLMENT
OF THE REQUIREMENTS OF THE
DEGREE OF

DOCTOR OF PHILOSOPHY

at the

MASSACHUSETTS INSTITUTE OF TECHNOLOGY

June 1981

Signature of Author_____
Department of Earth and Planetary Sciences
June 17, 1981

Certified by_____
Theodore R. Madden
Thesis Advisor

Accepted by_____
Theodore R. Madden
Chairman, Department Committee

THUNDERSTORM ELECTRIFICATION:

PRECIPITATION VERSUS CONVECTION

by

EARLE R. WILLIAMS

Submitted to the Department of Earth and Planetary Sciences
on June 17, 1981 in partial fulfillment of the
requirements for the Degree of Doctor of Philosophy in
Geophysics

ABSTRACT

The processes of precipitation and convection have been
examined to evaluate their relative contributions to
thunderstorm electrification. These studies demonstrate that
convection is essential to the energetics of
electrification, but that convection alone cannot account for
the generation of lightning.

An energy analysis has shown that the gravitational
potential energy of precipitation is of the order of 5-10% of
the available convective energy, and that this gravitational
energy must be efficiently converted to electrical energy if
classical gravitational separation is to account for the
electrification of active thunderstorms. Efficient energy
conversion requires electric force modifications in the fall
speeds of the precipitation particles of several meters per
second with respect to still air.

The results of a search for abrupt velocity changes with
a vertically pointing Doppler radar at the time of nearby
lightning discharges do not support the view that the
precipitation particle motions are contributing to the
pre-discharge accumulation of electrostatic energy. They do,
however, provide strong evidence that precipitation particles
may be highly charged.

The existence of precipitation at mid-levels (6-8 km) of
the cloud during initial electrification when convective
initiation is questionable, and the strong correlation between
vigorous electrical activity and precipitation at upper levels
in mature stages of the electrical development, both indicate
that precipitation is playing a fundamental role in the
electrification process.

The precipitation and convective motions which are potential contributors to electrification may be distinguished on the basis of velocity. Scaling law tests which incorporate this distinction unanimously support charge transport by convection. Highly correlated records of pressure and electric field beneath thunderstorms substantiate the view that electric charge is transported by air motions. The association of low radar reflectivity and large vertical air velocity with inferred breakdown regions is additional evidence for generative charge transport by convection in the upper part of the cloud.

A simple kinematic model for convective transport of screening layer charge supports the original assertion of Grenet (1947) and Vonnegut (1953) that externally derived electric charge may make a substantial contribution to electrification. This analysis results in optimal electric Reynolds numbers, which may be achieved by terrestrial thunderstorms. Because the decrease in dielectric strength with altitude is less rapid than the increase of electrical conductivity with altitude, the current flow to large clouds may be far greater than to small ones. Estimates of conductivity and dielectric strength in other planetary atmospheres suggest that this feedback mechanism may be a common feature of planetary electrification.

A comparison of continental and oceanic thunderstorm lightning rates has shown that continental storms are 2-4 times more electrically active. This difference may be attributed to the paucity of corona space charge available for convective transport in oceanic storms, or to a systematic difference in the size of continental and oceanic thunderclouds.

Thesis Advisor: Theodore R. Madden

Title: Professor of Geophysics

ACKNOWLEDGMENTS

I am very grateful for the diversity in my fellow graduate students (and their spouses), who became an important part of day to day life and learning at MIT. They are (in order of

We may not be able to formulate an exact law
between one large event and another, between a
thundercloud and where the lightning strikes... But
we are to believe that we suffer these uncertainties
only because we lack the detail. To grow more
assured, we need only (we are assured) divide the
phenomenon more finely: to map every electric
charge... On this view nature is continuous, and
her parts and processes can be divided indefinitely.
We shall find her mechanism if we go on looking for
smaller and smaller hairsprings.

From an essay entitled
"The Logic of Nature"
by Jacob Bronowski (1955)

Table of Contents

xiv

xvi

Chapter I

Introduction

I-1 The Problem Addressed

This study is concerned with the electrification of
thunderstorms, with special emphasis on the mechanism of
electric charge transport in the hope of distinguishing between
convection and precipitation theories for electrification.
These studies show that convection is necessary for the energy
of electrification, and many correlative phenomena demonstrate
an intimate connection between convection and electrification.
Other comparisons indicate the importance of precipitation, and
suggest that it may be necessary in initiating the
electrification process.

Electrical energy in thunderstorms results from the
mechanically forced motions of charged particles against the
local electric fields. Two general classes of particles are
available for charge transport: the cloud particles and the
precipitation particles. In the cloud particle class are
cloud droplets, ice crystals, and atmospheric ions whose sizes
range from a few tens of microns downward, and whose terminal
velocities under gravity are negligible when compared with
typical air velocities ($\sim$10 m/sec). In the precipitation
particle class are the raindrops, graupel, and hailstones
whose linear dimensions range from a hundred microns to
several centimeters and whose terminal velocities are appre-
ciable when compared with the air velocities of the cloud. As

1

a result of these particle velocity characteristics, charged
cloud particles will faithfully follow the motions of the air
(except in the presence of strong electric fields), whereas the
precipitation particles will move relative to the air around
them.

The principal question addressed in this thesis is: which
charged particle motion makes the larger contribution to
thunderstorm electrification? Or symbolically, which particle
type is the larger contributor to $\int -\overline{J} \cdot \overline{E} dV$?, where $\overline{J}$ is
the local current density associated with the charged
particle motion, $\overline{E}$ is the local electric field, and the
integration is performed over the volume of the thundercloud.

In a broader context, the problem addressed is one of
determining the relative importance of thermal (cloud
particles) versus nonthermal (precipitation particles)
convection.* This controversy has arisen in other geophysical
problems including the origin of the geomagnetic field (Busse,
1979) and the driving mechanism for plate tectonics (McKenzie,
1969).

I-2   The Precipitation Hypothesis

The preferential acquisition of charge by precipitation
particles through contact with cloud particles, and their
subsequent gravity-driven descent with respect to the

---

* We will not, however, refer to precipitation motion
  as convection in this thesis.

2

oppositely charged cloud particles left behind forms the basis for the classical hypothesis for thunderstorm electrification (Chalmers, 1967). As far as charge segregation and electrical energy generation are concerned the convective air motions play no role whatever in precipitation-powered electrification. According to this hypothesis, the formation of the characteristic positive thunderstorm electric dipole results from the preferential acquisition of negative charge by the falling precipitation particles. Although many mechanisms for this charge acquisition have been proposed in the past century, only two are now seriously considered (Latham, 1981).

The older of these two ideas is the induction charging process in which surface charge induced by the ambient field is selectively transferred during particle collisions. Originally formulated for liquid particle interactions by Elster and Geitel (1885), this mechanism was later extended to liquid-solid and solid-solid interactions (Muller-Hillebrand (1954), Sartor, (1967); and Mason (1972).

The second (and at this writing the more popular) mechanism involves the interaction between ice crystals and graupel and in the original laboratory study (Reynolds et al., 1957) was interpreted as a thermoelectric effect. More recently, an electronic surface states interpretation is in vogue (Caranti and Illingworth, 1980).

3

I-3 The Convection Hypothesis

The convection hypothesis asserts that the motion of charged cloudy air, driven in turn by the convective overturn of the cloud, is responsible for the generation of thunderstorm electrical energy. Such a process, unlike gravitational separation by precipitation, requires the existence of a volume space charge density in regions of electrical power generation. Such space charge accumulations may develop as a result of the segregation effects of a precipitation process, the redistribution of fair weather space charge, the deposition of charge by lightning, the unipolar corona currents from the Earth's surface, or the selective ion capture from the relatively conductive clear air at the cloud boundary. The latter two processes are fundamental to the convective theory proposed by Vonnegut (1953), which has been closely identified with the convective hypothesis.

I-4 Organization of Thesis

The problem addressed in this thesis is by no means new, and has been the subject of investigations far too numerous to adequately review here. In spite of these efforts, the question of the origin of thunderstorm electrification remains controversial, the purpose here has been to seek out new approaches to this problem. These approaches are the subjects of chapters which we now summarize.

Chapter II is concerned with a critical examination of the energetics of the precipitation hypothesis. The

4

conditions on precipitation particle charge and size necessary
for maximum conversion of gravitational potential energy to
electrical energy are derived and compared with the
predictions of the popular precipitation mechanisms and with
in situ thundercloud data. Incoherent radar estimates of the
total gravitational power associated with falling
precipitation in thunderstorms are compared with their
simultaneous electrical outputs to place constraints on the
energy contribution of falling precipitation.

The results of Chapter II show that if falling
precipitation is chiefly responsible for thunderstorm
electrical energy, then the fallspeeds of the precipitation
particles will be modified. Chapter III is largely concerned
with a search for charged precipitation particle velocity
variations associated with lightning discharges with a
zenith-pointing Doppler radar. In addition, these data have
been analyzed to investigate the vertical velocity and
reflectivity structures during a period of initial
electrification and during a period of vigorous convection to
examine the relative importance of precipitation and convection
at these times.

If the particle motion in breakdown regions of the cloud
is responsible for that breakdown, then a knowledge of the
nature of the particles and their motions is essential in
distinguishing the contributions of convection and
precipitation. Comparisons between radar reflectivity and the
location of sources of VHF emission which are likely
indicative of breakdown regions are treated in Chapter IV.

Chapter V is primarily concerned with scaling law predictions which distinguish the contributions of precipitation and convection on the basis of the velocity by which electric charge is transported. These predictions are tested with cloud height and lightning flash rate data. The variation of lightning flash energy with cloud size, which is important to this argument as well as to the discussion of energetics in Chapter II, is given particular attention.

More speculative scaling relationships concern the subcloud corona current (which is fundamental to the convective theory (Vonnegut, 1953)), the gravitational power associated with falling precipitation, and the existence of lightning in warm clouds. These relationships are treated in the final section of Chapter V.

Chapter VI considers pressure measurements beneath thunderstorms with microbarographs responsive to periods typical of cumulus convection. Specific causes for pressure fluctuations are discussed and many examples of correlated pressure and electric field behavior at the earth's surface are presented. Vertically-pointing Doppler observations are integrated with these other data to examine the hypothesis of large scale convective charge transport in the end of storm oscillation (EOSO) (Moore and Vonnegut, 1977).

The final three chapters (VII, VIII and IX) deal with very different subjects, but all share a common original purpose: to evaluate the convective mechanism for electrification proposed by Vonnegut (1953).

Chapter VII extends the treatment of screening layer charge transport beyond the "back of the envelope" stage to quantify the importance of a conductive atmosphere at the cloud top and to determine the electrical power this mechanism might provide under optimal conditions.

The other feedback feature of the convective theory is the positive space charge produced by point discharge at the earth's surface. In Chapter VIII existing global lightning data is used to compare the electrical outputs of continental storms (where positive corona space charge is plentiful) with oceanic storms (where this space charge contribution may be scarce).

The final Chapter X was originally concerned with an evaluation of the electrical conductivity structure in other planetary atmospheres in which lightning is now known to occur in a search for similarities in non dimensional parameters. This Chapter was later extended to consider other parameters relevant to the question of precipitation versus convection.

Chapter II

Thunderstorm Energetics and the Gravitational Power Associated with Falling Precipitation

II-1 Introduction

This Chapter is concerned with an examination of the energy available for thunderstorm electrification, with particular attention devoted to the energy available to precipitation charging mechanisms.

In Section II-1, the flow of energy in thunderstorms is considered and some limits on energy conversion are derived so that the energy available for precipitation-and convection-driven electrification may be compared.

A parameter critical to the analysis in this Chapter is the lightning flash energy. Section II-2 is concerned with estimates of this quantity in light of recently available electric field soundings in thounderclouds (Winn et al., 1980).

The remainder of the Chapter concerns the energy contribution of falling precipitation to electrification, and is adequately introduced in Section II-4.

II-2 Thunderstorm Energy Flows and Efficiences

The two general classes of theories for thunderstorm electrification may be distinguished on the basis of how a fraction of the latent heat (chemical) energy is ultimately transformed to electrical energy. The energy cascade for the

precipitation and convection classes is represented in Figures
II-1 and II-2, respectively. This section is concerned with
the maximum efficiencies which can be achieved in each step of
the energy transformation.

Common to both classes is the conversion of latent heat
energy (E) to kinetic energy. Twenty five hundred joules is
released when 1 gram of water vapor condenses, a substantial
quantity of energy for a molecular reaction. An additional 300
joules is released when 1 gram of liquid water freezes. Some of
this energy heats the air and thereby contributes to the
internal energy (I) of the atmosphere, and the remainder is
used to increase the atmospheric potential energy (PE) through
buoyant expansion. The relative amounts are determined
according to the First Law of thermodynamics:

$$\Delta E = \Delta I + p\Delta V$$

$$= C_V \Delta T + p\Delta V = C_p \Delta T$$

where all energy changes are on a per mole basis. C_p and C_V
are the heat capacities of atmospheric air at constant pressure
(1000 joule/kg/°K) and constant volume (720 joule/kg/°C),
respectively. Since the change in potential energy is simply
the pressure expansion work done, we have

$$\Delta(PE) = p\Delta V = (C_p - C_V)\Delta T$$

Only the potential energy can be ultimately used to create
electrical energy, and so the efficiency of
chemical-to-potential energy conversion is of interest:

$$Eff = \frac{\Delta(PE)}{\Delta E} \frac{C_p - C_V}{C_p} = 29\%$$

9
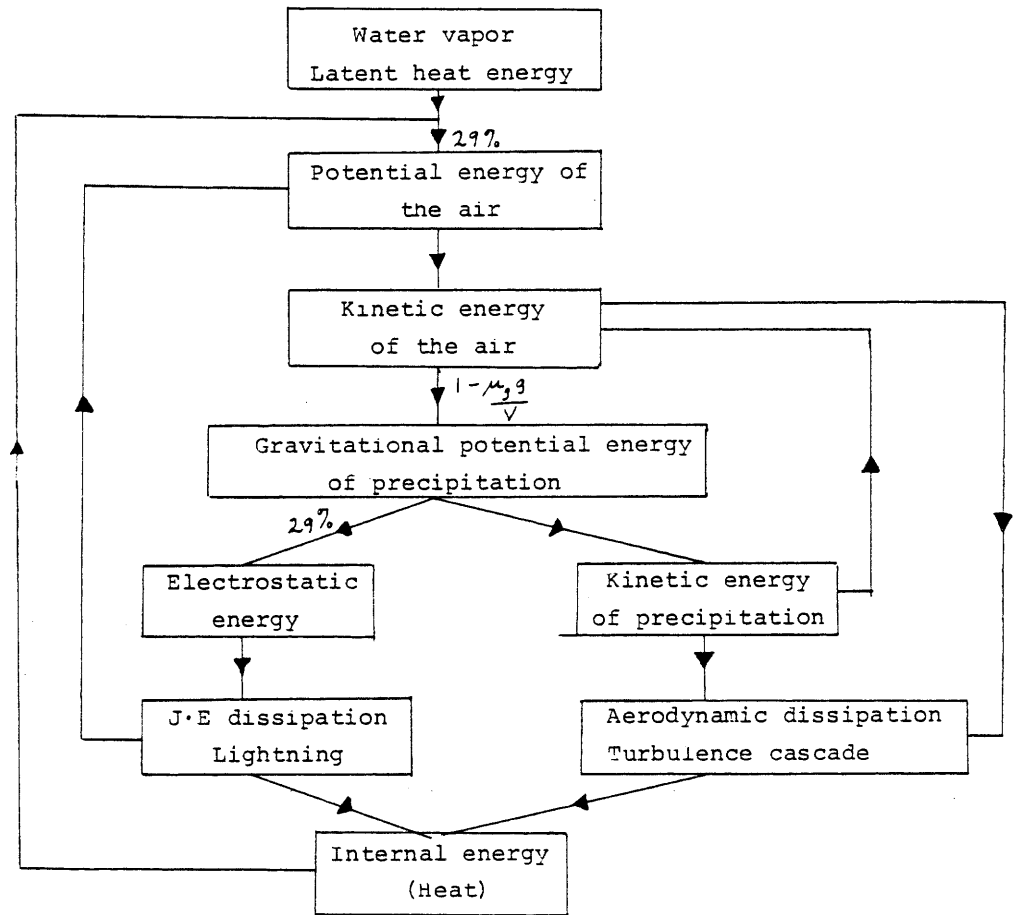
Figure II-1

Energy cascade for precipitation driven electrification
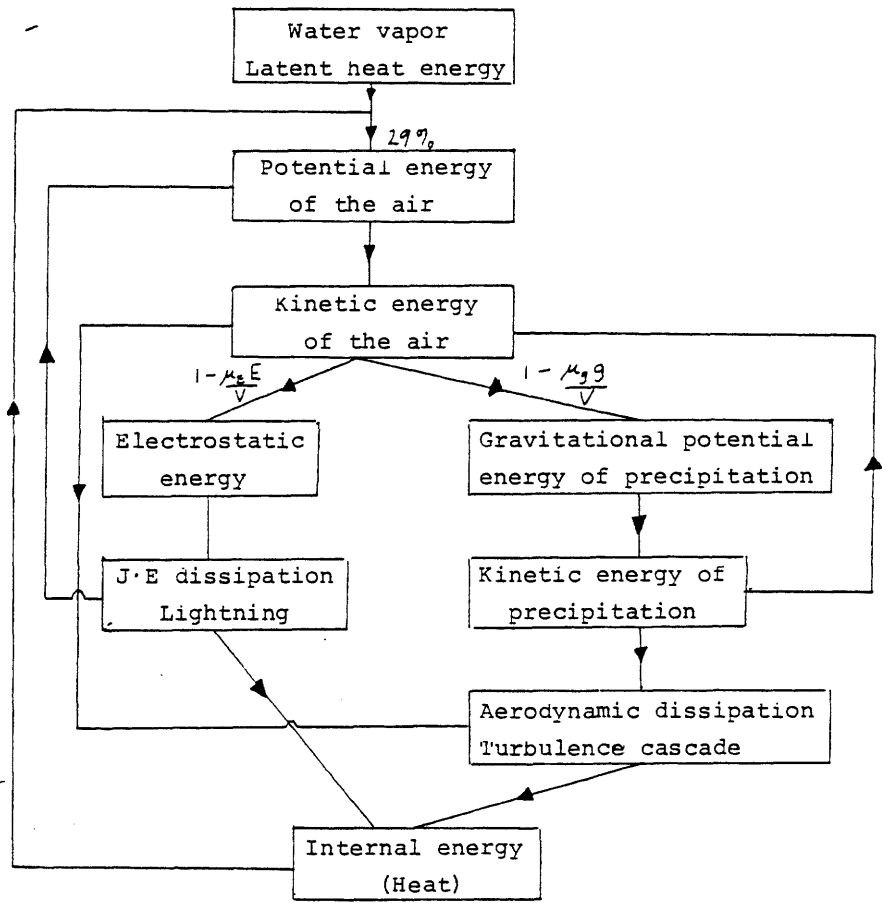
Figure II-2

Energy cascade for convective electrification

This ratio will be only weakly dependent on height in the atmosphere.

Condensation and freezing and the subsequent creation of potential energy takes place on scales of hundreds of meters to kilometers, scales much larger than the scales at which kinetic energy is viscously dissipated, and so virtually all 29% of the latent heat energy may be transformed to kinetic energy (locally). What fraction of this kinetic energy may be subsequently transformed to electrical energy?

Consider an element of kinetic energy, a small parcel of air moving upward at velocity V. If electrical energy is to be created, the parcel must contain space charge which is transported against a local electric field. In this case, assume a single positively charged particle (ion or cloud droplet) and a downward directed electric field E. In a reference frame fixed with respect to the Earth, the particle's motion is retarded by the electric field and its velocity in this frame is V-v. For cloud particles, the gravity force is neglected for reasons mentioned in Chapter I. The velocity v is determined by Stokes' Law in the moving frame

$$qE = 6\pi\eta av$$

where q is the particle's electric charge. Energetics in the fixed frame (for instance) are

Electrical power generated = F_e · velocity = $qE(V-v)$

Dissipated power = F_{drag} · velocity

$$= 6\pi\eta av \cdot v$$

The local overall efficiency of conversion of kinetic to electrical energy is

$$\text{Eff} = \frac{\text{Generated power}}{\text{Total power}} = \frac{qE(V-v)}{qE(V-v) + 6\pi\eta av^2} = \frac{V-v}{V} = 1 - \frac{\mu_e E}{V} \quad (1)$$

where $\mu_e = v/E$ is the particle's electric mobility.

Since the drift velocities of ions and charged cloud particles are often less than a few meters per second in fields of thunderstorm magnitude, and since the upward velocity in a vigorous thunderstorm updraft may exceed 20 meters/sec, the efficiency calculated according to (1) may be well over 90%, and in certain cases, virtually 100%. By combining this result with our earlier thermodynamic result in which we ignored turbulent dissipation processes in the medium, we obtain an upper bound on the efficiency with which chemical (latent heat) energy may be converted to electrical energy (29%).

By shear coincidence, this efficiency is numerically equal to the fraction of gravitational potential energy of precipitation which is available for electrification, a result derived in Section II-4. Since the total gravitational potential energy of a thunderstorm is roughly 5% of the latent heat energy (Braham, 1952), the original assertion is still upheld: convectively driven electrification has 10-20 times as much energy as that available for precipitation driven electrification.

II-3 The Energy Associated with Lightning

The electrostatic energy transformed in a lightning flash
will take on an important role in constraining the contribution
of falling precipitation to cloud electrification (to be
discussed in II-3), and therefore deserves discussion.
Estimates of this quantity, derived from electrostatic (Wilson,
1920; Bohannon, 1980), acoustic (Dawson et al., 1968; Few et
al., 1970), and laboratory spark optical (Krider et al., 1968;
Uman et al., 1968) approaches, vary by 2-3 orders of magnitude.
Hill (1977, 1979) thoroughly reviews past work, but
unfortunately confines his attention to the energy dissipated
per unit length in the return stroke channel; we are interested
in representative values for the total energy given up in an
entire flash. We therefore present our own estimates based on
recently available data from New Mexico thunderclouds.

Figure II-3 from Winn et al. (1980) shows vector electric
field profiles extending from the ground (3.2 km MSL) to levels
above the negative charge region within active thunderclouds.
By integrating these profiles from the ground to the electric
field zero crossing, we have estimated cloud-to-ground
potential differences of $1-2 \times 10^8$ volts for each of these
cases. Representative values for total negative charge brought
to ground in New Mexico cloud-to-ground lightning range from
10C (Brook et al., 1962) to 70 C (Krehbiel et al., 1979).
Recalling the result of Winn and Byerley (1975) that the
fractional decrease in electric field is usually less than 50%
and often much less (see Section V-6), we may conclude that the
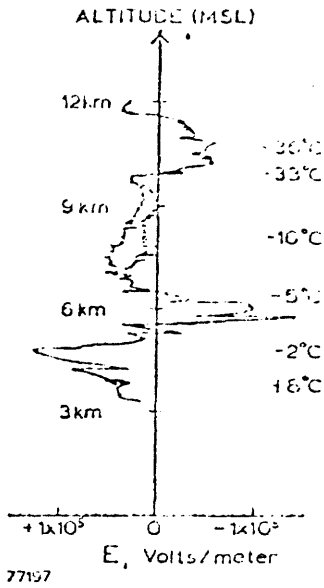
ELECTRIC FIELD VS. ALTITUDE,
JULY 16, 1977, NEW MEXICO.
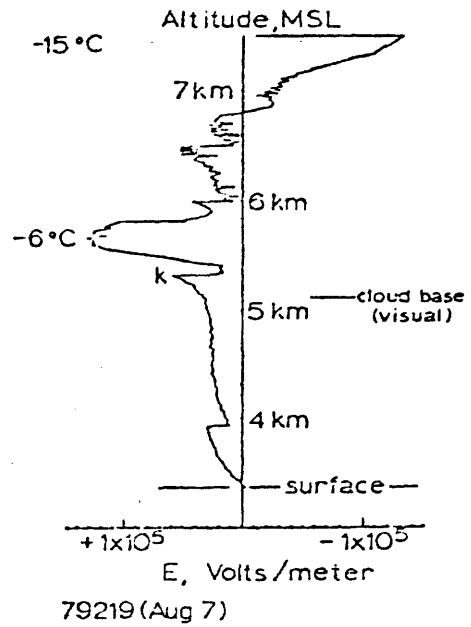
ELECTRIC FIELD VS. ALTITUDE,
AUC. 7, 1979, NEW MEXICO.

from: Winn et al. (1980)

Figure II-3
Electric Field Soundings
in Thunderclouds

15

predischarge cloud-to-ground potential difference ΔV is not annihilated by the discharge, but only reduced. The electrostatic energy dissipated by these discharges will therefore be approximately $\Delta Q \cdot \Delta V$. The resulting range in energy is 10^9 to 10^{10} joules.

No good data are currently available which map the electric field between negative and upper positive charge centers in thunderclouds, and so we have no direct way to estimate the energies involved in intra-cloud discharges. Since the field changes at the ground are of comparable magnitude with those of cloud-to-ground discharges, we have reason to believe that the net electric charge changes are also of comparable magnitude. One study (Nakano, 1979) suggests that intra-cloud charge magnitudes may be even larger (see also Figure V-8 in Chapter V).

Our best guess is that the energies involved in intra-cloud discharges will be comparable with the values determined above.

In Chapter V on thunderstorm scaling laws we present evidence that the energy involved in a lightning flash is roughly independent of the size of the cloud which produces it.

II-4 Gravitational Power, Optimal Charging, and Maximum Power Conversion for Falling Precipitation

This section is concerned with the gravitational potential energy available to precipitation mechanisms for thunderstorm electrification. As we discussed in the first section of this

chapter, the gravitational potential energy of thunderstorm precipitation is only a few per cent of the latent heat energy (Braham, 1952), and so from the standpoint of energetics alone, one would conclude that convectively-driven electrification is favored over a precipitation powered mechanism. In order to investigate what constraints energy conservation places on the classical precipitation hypothesis, we derive the required microphysical conditions necessary to maximize the conversion of gravitational to electrical power for falling precipitation. We compare these results with the predictions of the popular precipitation mechanisms (Section II-6), with the available in situ observations (local comparisons) in Section II-7, and finally compare incoherent radar estimates of thunderstorm gravitational power with simultaneously observed electrical outputs (global comparisons) in Section II-8.

An upper limit to the steady state electrical power available from any precipitation mechanism is MgV, where M is the total precipitation mass, g is the acceleration due to gravity, and V is the effective terminal fall velocity; this quantity is simply the rate at which the gravitational potential energy of precipitation is given up. Not all the available gravitational power may be converted to electrical power, but a realizable bound for electrical power may be determined by maximizing the current contributions of charged particles falling in local vertical electric fields.

The terminal velocity of precipitation particles as a function of their mass (m), charge (q) and the local vertical

17

electric field (E) is given by Gay et al. (1974):

$$V = \frac{\nu}{2r}(0.08) \times \left[\frac{8(mg-qE)}{\pi \rho_a \nu^2}\right]^{0.8} \tag{1}$$

where r is the particle radius, ρ_a is the air density, ν is the kinematic viscosity of air, and x is an empirical parameter dependent on the Q number (the quantity in brackets on the right hand side of equation (1)).

If electric charge is nondimensionalized so that q^* is the fraction of the charge necessary to balance the particle against gravity

$$q^* = \frac{qE}{(4/3)\pi r^3 \rho g} \tag{2}$$

We obtain a simplified expression for velocity

$$V = V_0 (1-q^*)^{0.8} \tag{3}$$

where V_0 is the charge free terminal velocity.

The current contribution of this falling particle is the product of charge and velocity

$$I = q^* V = V_0 q^*(1-q^*)^{0.8} \tag{4}$$

The electrical power will be greatest[**] for any vertical electric field when this current is maximized with respect to the nondimensional charge q^*.

$$\frac{dI}{dq^*} = 0 \rightarrow q^* = 0.555 \tag{5}$$

[**]The equivalent calculation in the Stoke's regime is analytic and is included in Appendix A.

Solving for the optimal charge yields a value which is 56% of the balance charge and substitution in the velocity equation (1) shows that optimally charged particles will fall at about 52% of their charge-free terminal velocities.

The maximum fraction of gravitational potential energy which may be delivered as electrical power may now be calculated. This fraction F is the difference between the gravitational power given up, MgV, and the aerodynamic dissipation rate, normalized to available power, MgV_O.

$$F = \frac{MgV - (1/2)\rho_a V^2 C_D \pi r^2 V}{MgV_O} \qquad (6)$$

In the charge-free case, all gravitational power is dissipated aerodynamically:

$$MgV_O = 1/2 \rho_a V_O{}^2 C_{DO} \pi r^2 V_O \qquad (7)$$

Substituting equation (7) into equation (6) simplifies the expression for F

$$F = \frac{V}{V_O} \frac{C_{DO}}{C_D} \left(\frac{V}{V_O}\right)^3 \qquad (8)$$

$$= q^* \left(\frac{V}{V_O}\right)$$

Substituting the optimal values for q^* and V/V_O into (8) yields the maximum achievable fraction of 0.29. This result is in effect the inefficiency imposed on all precipitation mechanisms by the Second Law of thermodynamics.

A maximum 29% of the gravitational potential energy of precipitation may be converted to electrical energy. A precipitation rate of 1 mm/hr corresponds to a gravitational power density of 2.7×10^{-3} watt/m^3. At a 29% conversion rate, we have a realizable limit on electrical power output of 8.2×10^{-4} watt/m^3 per mm/hr of precipitation rate. This result is a more severe constraint by a factor of three than the original estimate by Latham (1971) in his assessment of precipitation mechanisms.

II-5 Precipitation Particles in Horizontal Electric Fields

In deriving the preceding results, it has been assumed that a component of electric field is aligned with gravity. Only in this case can gravitational energy be converted to electrical energy. Horizontal field components will always drive charged precipitation dissipatively, as Vonnegut has noted before (private communication, 1975). Since horizontal field components of large magnitude are present in thunderclouds (Rust and Moore, 1974; Winn et al., 1974), we wish to examine their impact on precipitation mechanisms of electrification.

Since gravity is unimportant when considering horizontal particle motions, the result of Gay et al (1974) for terminal velocity will be applicable when the mg term is eliminated from the Q number in brackets in equation (1). The precipitation particle horizontal velocity V_H is then simply

$$V_H = K(qE_H)^{0.8} \tag{9}$$

where K is similar to the constant defined previously (equation (4)).

If we let the precipitation particle take on a charge which is some fraction f of the charge necessary to balance the particle in the local <u>vertical</u> field E_V, we have

$$V_H = K \left(\frac{f \; 4/3 \pi r^3 \rho g}{E_V} E_H \right)^{0.8} \tag{10}$$

The Gay <u>et al.</u> result for the vertical velocity is (as shown before)

$$V_V = K(mg - qE_V)^{0.8}$$

$$= K \left(\frac{4}{3} \pi r^3 \rho g \right)^{0.8} (1 - f)^{0.8} \tag{11}$$

The horizontal and vertical velocities will be equal when

$$\frac{V_H}{V_V} = \left(\frac{f}{1-f} \cdot \frac{E_H}{E_V} \right)^{0.8} = 1 \tag{12}$$

or when the ratio of horizontal to vertical electric field is

$$\frac{E_H}{E_V} = \frac{1-f}{f} \tag{13}$$

For ideally charged precipitation particles (f = 0.555), this ratio is 0.80, and in a field inclined at

$$\Theta_{crit} = \arctan (E_H/E_V) = 39° \tag{14}$$

with respect to the vertical, the terminal velocities will be equal.

A similar analysis comparing the vertical (ideal) generation of electrical power with the horizontal dissipation of energy

21

leads to the result that dissipation balances generation when

$$\frac{E_H}{E_V} = \frac{1-f}{f} = 0.91 \text{ for } f = 0.555 \tag{15}$$

and $\Theta_{crit} = \arctan(E_H/E_V) = 42°$.

In summary, no net electrical energy is generated by ideally charged precipitation particle motion in electric fields inclined at angles greater than 42° with respect to the vertical.

Although the gross electrical structure of a thunderstorm is of the form of a vertical electric dipole, at least one study has shown the dipole to be inclined at 50° with respect to the vertical (Reynolds and Neill, 1955) on occasion. A later study (Ogawa and Brook, 1969) suggested that wind shear was responsible for inclined electrical structures. Since the most severe electrical storms probably are associated with the strongest shear, it would appear that thunderstorms are able to generate electrical energy in spite of large horizontal fields, but that precipitation mechanisms are not likely candidates.

It should be noted that the critical condition (15) is strongly dependent on f, the fraction of the balance charge which the particle contains. If f is much less than its ideal value, then horizontal dissipation competes with vertical only when the ratio of vertical to horizontal field components is small. Of course, departures of f from ideality require a sacrifice in gravitational power. Again, the overall efficiency of the gravitational separation mechanism depends both on

particle charge distributions and on the three dimensional

electric field configuration in the cloud.

II-6 Gravitational Power for Specific Precipitation Charging Mechanisms

The general results derived in Section II-4 are applicable

to any precipitation mechanism. The charging predictions of the

popular precipitation mechanisms are now tested in light of

these general results.

II-6.1 Field Dependent Charging Mechanisms

For idealized spherical precipitation particles, the maximum

charge attainable in either the Wilson ion capture or the

induction mechanism, is the equilibrium charge (or Wilson

charge), $Q_{Wilson} = 3\pi\epsilon D^2 E$, where D is the particle diameter and

E the local vertical field. Consistent with the previous

formalism (equation (2)) the charge is nondimensionalized

$$q^* = \frac{Q_{Wilson}}{Q_{Balance}} = \frac{18\epsilon E^2}{\rho g D} \qquad (17)$$

Substituting (17) into equation (3) and then into (8) yields

the gravitational-to-electrical efficiency:

$$q^* \left(\frac{V}{V_o}\right) = \left(\frac{18\epsilon E^2}{\rho g D}\right)\left(1 - \frac{18\epsilon E^2}{\rho g D}\right)^{0.8} \qquad (18)$$

for inductively charge-saturated particles of diameter D and ρ

density falling in a vertical field E.

For a spectrum of particle sizes, the overall efficiency may

be determined by weighting the individual particle efficiencies

according to their respective gravitational power contributions.

23

Assuming an exponential distribution of particle sizes and a terminal velocity relation $V_O \sim D^{0.5}$, which is sufficiently accurate for particle sizes which contribute significantly to gravitational power, we have:

$$\text{overall efficiency} = \frac{\int_O^{D_{max}} \text{Eff}(D)^{7/2} \exp(-\Lambda D) dD}{\int_O^{D_{max}} D^{7/2} \exp(-\Lambda D) dD} \qquad (19)$$

In the limit $q^* \ll 1$, the electrical force effects on terminal velocity may be ignored, and the efficiency simplifies to

$$\text{Eff} = \text{Eff}(D) = \frac{18 \epsilon E^2}{\rho g D} \qquad (20)$$

In this case, equation (18) may be solved analytically to get:

$$\text{overall efficiency} = \frac{36 \Lambda \epsilon E^2}{7 \rho g} \qquad (21)$$

For the case $Q_{Wilson} \sim Q_{balance}$, the electrical and gravitational forces are comparable, and the integral in (19) was solved numerically. The overall efficiency over three decades of vertical electric field strength and for particle densities of 0.5 and 1.0 gm/cm^3 is shown in Figure II-4. The efficiencies begin to bend over and approach the optimal value (29%) when the electric forces exert an appreciable influence on the particle motions. However, the optimal efficiency can be achieved only when the vertical electric field strength approaches values of breakdown magnitude. Since regions of intense electric field occupy only a small fraction of a
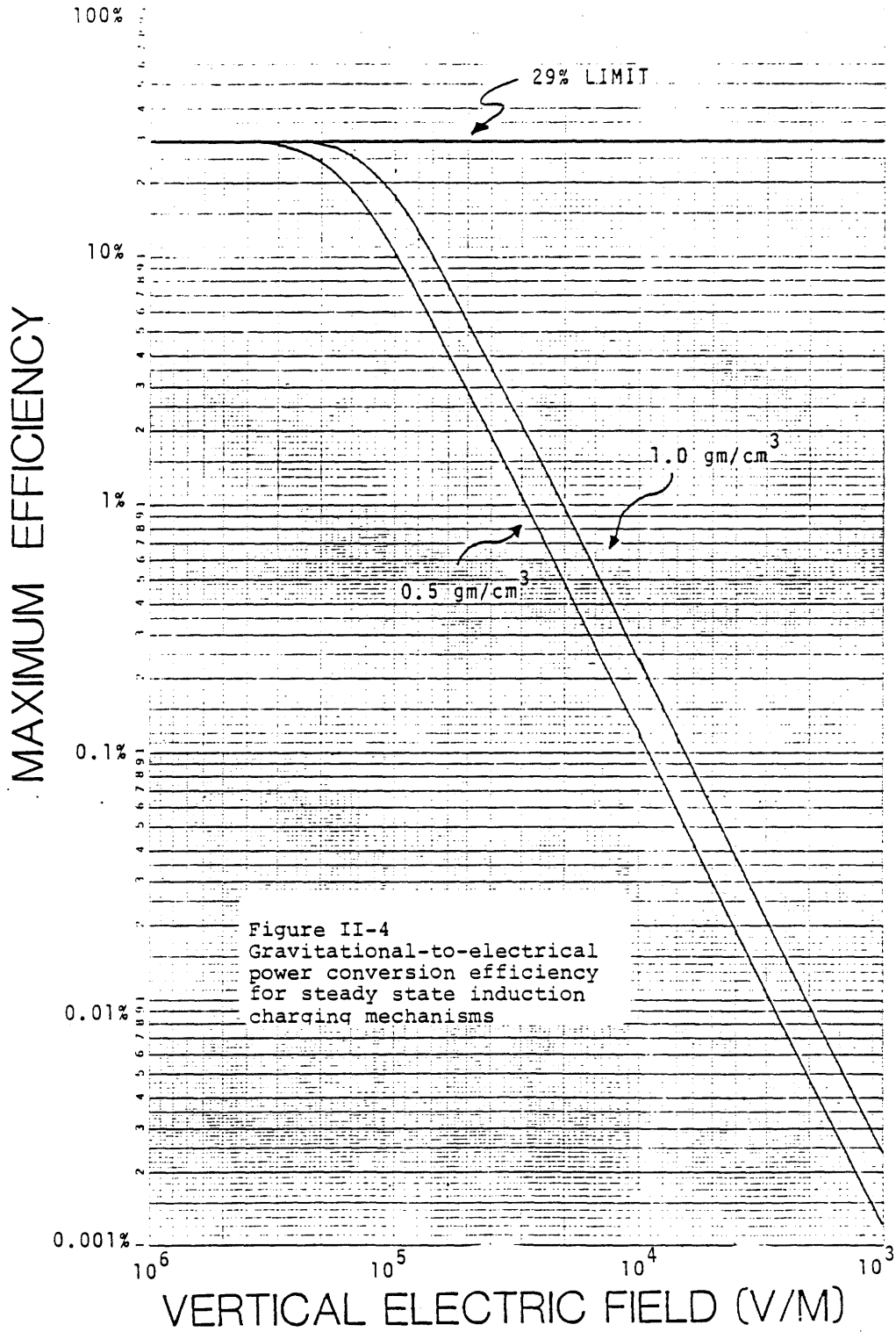
Figure II-4
Gravitational-to-electrical
power conversion efficiency
for steady state induction
charging mechanisms

thunderstorm volume (Winn et al., 1974), the overall efficiency

of field dependent mechanisms will be far less than 29%.

II-6.2 Field Independent Charging Mechanisms

Although many precipitation charging mechanisms which are

independent of the electric field have been proposed, the most

popular in recent years has been the ice crystal-graupel

interaction. This mechanism was first studied by Reynolds et

al. (1957) and has received additional attention from Takahashi

(1978), Marshall et al. (1978), Hallett and Saunders (1979),

and Gaskell and Illingworth (1980). In this section we apply

the results of Section II-4 to this charging mechanism to see

how efficiently it can operate under ideal conditions.

We therefore seek the electric charge Q of a falling graupel

pellet as a function of its radius R. A fixed charge q is

transferred to the pellet with each ice crystal collision; the

ice crystals have a uniform volume concentration n. The pellet

is assumed to grow by efficient accretion of supercooled water

droplets; the cloud liquid water content is M, and is also

uniform.

With these assumptions, it is easy to show that the pellet

radius will increase linearly with its distance of fall

$$\frac{dR}{dz} = \frac{M}{\rho_L} \qquad\qquad (22)$$

where ρ_L is the density of the supercooled water. The pellet's

geometric (πR^2) collision cross section for ice crystals, of

concentration n, leads to a prediction for the rate of pellet charging

$$\frac{dQ}{dz} \mp \pi R^2 nq \qquad (23)$$

Equations (21) and (22) may be integrated and combined to yield the pellet charge as a function of its radius:

$$Q(R) = [(\frac{\pi}{3}) (\frac{4\rho_L}{M}) nq] R^3$$

The charge Q is (not surprisingly) proportional to the pellet volume, since the accumulated charge is proportional to the volume of accreted material.

Recalling the result from Section II-4 that the optimal charge for gravitationally sedimenting precipitation particles is proportional to R^3, we may immediately conclude that the gravitational-to-electrical conversion efficiency for the graupel-ice crystal charging mechanism will be independent of particle size. In fact,

$$\text{Efficiency} = (\frac{Q}{Q_{BAL}}) (\frac{V}{V_0}) \cong \frac{Q}{Q_{BAL}} \qquad \text{for E} \ll \text{E breakdown}$$

$$= (\frac{\rho_L}{M}) (\frac{nq}{\rho_p g}) E$$

Taking values for the parameters consistent with other evaluations of this charging mechanism, (Illingworth and Latham, 1977) we have

$n = 10^5 \ m^{-3}$ $\qquad$ $q = 10^{-14} \ C$ $\qquad$ $\rho_L = 10^3 \ kg/m^3$

$M = 10^{-3} \ kg/m^3$ $\qquad$ $q = 9.8 \ m/sec^2$ $\qquad$ $\rho_p = 5 \times 10^2 \ kg/m^3$

27

which result in an efficiency:

$$\text{Efficiency} = (2 \times 10^{-7}) E$$

where the vertical electric field E is expressed in
volt/meter.

Unlike the efficiency for field dependent charging
mechanisms which varies as E, the efficiency for this mechanism
is only linearly dependent on the vertical electric field. For
vertical field strengths of a few tens of kilovolts per meter,
which are typical within thunderclouds (Winn et al., 1978), the
estimated efficiencies are only a fraction of one percent.
However, for field strengths approaching breakdown values
(4×10^5 volt/meter), the electrical and gravitational forces
acting on the graupel particles will be comparable and the
efficiency is substantial. We would therefore predict a
modification in the fall speeds of graupel particles which
should be detectable with a zenith pointing Doppler radar, an
experiment described in Chapter III.

II-7 Local Measurements and Comparisons with Theory

To evaluate how efficiently precipitation charge transport
is operating in real thunderclouds, we may compare the optimal
charge prediction with in situ measurements of electric charge.
Since the optimal charge is a function of the local electric
field (see equations (2) and (5)), the field information is
also required, but several investigators (Gaskell et al., 1978;
Christian et al., 1980; Marshall and Winn, 1980) have succeeded
in measuring these quantities. Results for maximum values of

28

charge and particle size from these studies (at times when the particle motion was enhancing the local vertical field), are shown in Figure II-5.

Included for comparsons in Figure II-5 are loci of optimal charge (proportional to R^3) for various vertical electric fields, loci of field dependent Wilson charge (proportional to R^2) for various fields, and the Rayleigh bursting limit (proportional to $R^{3/2}$). The two stippled vertical lines bracket the range of particle sizes which contribute most to a thunderstorm's gravitational power.

These results show that although the measured charge values often exceed the Wilson charge (Gaskell et al., 1978), they are at least an order of magnitude less than optimal values.

The implications of this result are more clearly seen when local power generation values, $-J \cdot E$, are compared with the theoretical limit. Early measurements in the vicinity of cloud base (Rust and Moore, 1974; Gaskell et al., 1978) showed dissipative motion of falling precipitation, but more recent probing at high levels in the cloud has shown evidence for generative motion (Christian et al., 1980). A compilation of the generations results to date, including maximum $-J \cdot E$ values, local precipitation rates, and a calculation of the local conversion efficiency of gravitational to electrical power is shown in Table II-1. Consistent with the particle charge comparisons, the peak local efficiencies are at least an order of magnitude less than the theoretical limit of 29%.

Figure II-5
Precipitation Particle
Electric Charge
vs. Size
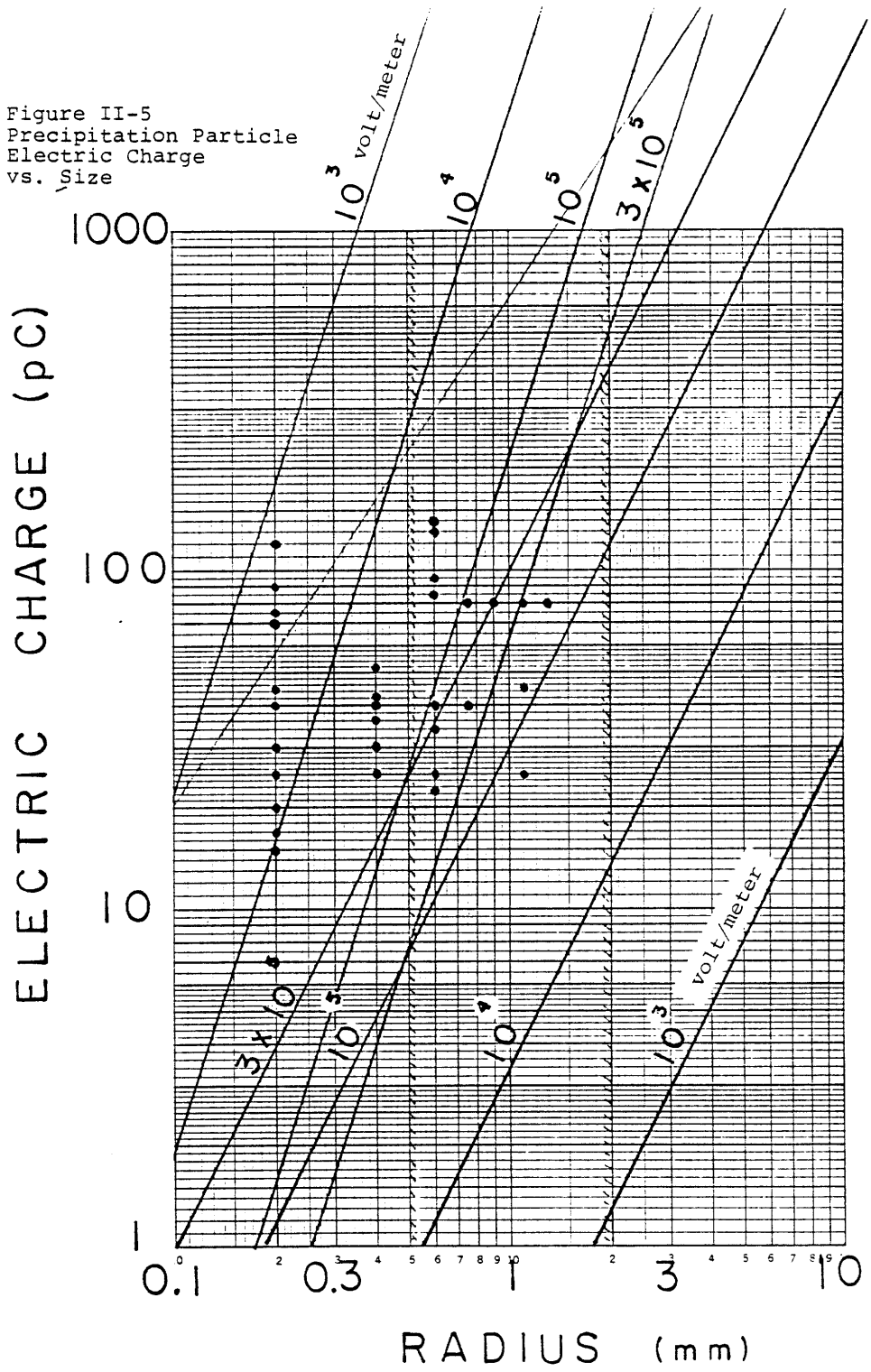
Table II-1

Compilation of In Situ Measurements of the Energy Contribution of Precipitation

igators	$J(nA/m^2)$	$E(kV/m)$	$-J \cdot E(watt/m^3)$	$p(mm/hr)$	I
nd Moore (1974)	−	−	3×10^{-7}	10	
1 et al. (1978)		(dissipative motion)			
ian et al. (1980)	2	5	1.2×10^{-4}	22 ± 11	
	2.5	75	1.3×10^{-5}	15 ± 7	
	12	30	9×10^{-4}	34	
11 and Winn (1980)	40	30	1.2×10^{-3}	27	

The single exception is the 5% value of Marshall and Winn (1980), who attribute their large current density (40 nA/m^2) to lightning-deposited charge on precipitation, rather than to a pre-discharge charging mechanism.

A careful examination of the available in situ data indicates that the calculated efficiences in Table II-1 may all be over-estimated. At the root of this problem is the limited dynamic range of the particle charge measuring devices. The trends in the number-charge distributions from both Gaskell et al. (1978) and Marshall and Winn (1980) indicate that there are significant numbers of particles whose charges are less than the lower limit for detection. The large particle charges contribute most to the current density estimate, and this quantity may not be badly underestimated. However, the weakly charged particles which contribute to precipitation rate will not be counted, and this quantity may be grossly underestimated. The efficiency estimates (the ratio of $-J \cdot E$ to precipitation rate converted to gravitational power density) are therefore probably exaggerated.

Regardless of these possible errors, the few available results suggest that falling precipitation does not generate electrical energy efficiently. Though this result conflicts with the exigencies of global gravitational power estimates in the next section, it is at least consistent with two other local measurements. The low gravitational-to-electrical efficiency implies that the electrical forces acting on precipitation elements will not appreciably influence their

32

motions. Balloon measurements by Winn and Byerley (1975)
showed a linear growth of electric field between lightning
discharges, suggesting that the charge transport mechanism was
field independent. Such behavior is not expected in a
thundercloud whose precipitation particles are near-optimally
charged. Also, our measurements of precipitation particle
motion during lightning discharges with Doppler radar (Chapter
III) indicate that only in rare cases are the particle
velocities disturbed (at the one meter per second level) by
abrupt changes in electric field. Again the indication is that
the electrical forces acting on precipitation particles are
small compared to gravitational forces.

II-8 Global Measurements and Comparisons with Theory

The classical precipitation hypothesis for thunderstorm
electrification relies on the gravitational potential energy of
precipitation particles. To determine how efficiently falling
precipitation need be in generating electrical energy if this
hypothesis is correct, we have measured the available
gravitational power of precipitation for several thunderstorms
and compared these values with estimates of the simultaneous
electrical outputs.

The gravitational power estimates were derived from three
dimensional radar reflectivity data. Empirical relationships
were used (Geotis, 1971) to convert reflectivity values to
local precipitation rates and are discussed in Appendix B. The
precipitation rate is a mass flux, which when multiplied by g,

33

the acceleration due to gravity, is a gravitational power density. These latter values were then integrated over the scanned storm volume to arrive at a total gravitational power.

The electrical outputs of the storms studied were estimated by counting lightning flashes, for lack of a more sophisticated procedure. A justification for this procedure is presented in Chapter V in which we examine the scaling behavior of flash energy with storm size. We have neglected the ohmic contribution to dissipation within the cloud because it is probably small (Griffiths and Myers, 1974), and the dissipation contribution from external currents and field-driven cloud and precipitation particle motions because we do not know them.

The resulting flash rates and corresponding gravitational power estimates are plotted in Figure II-6. Two points are plotted for each storm: the righthand point designates the available gravitational power and the lefthand point the maximum possible electrical power if precipitation is driving the electrification. The lines in the upper left relate electrical power to flash rate, for a fixed energy per flash as indicated.

The low flash rate storms tend to be widespread, low-level rainshower systems which produced occasional lightning. The high flash rate storms were of two types: frontal and air mass thunderstorms. For the low flash rate storms it is immediately apparent that the available gravitational power is more than adequate to account for their electrification. For increasingly active storms, the margin between electrical and

34

Figure II-6
Lightning Flash Rate
vs. Gravitational Power

● Thunderstorms

✛ Widespread Rainshower
  Systems

35
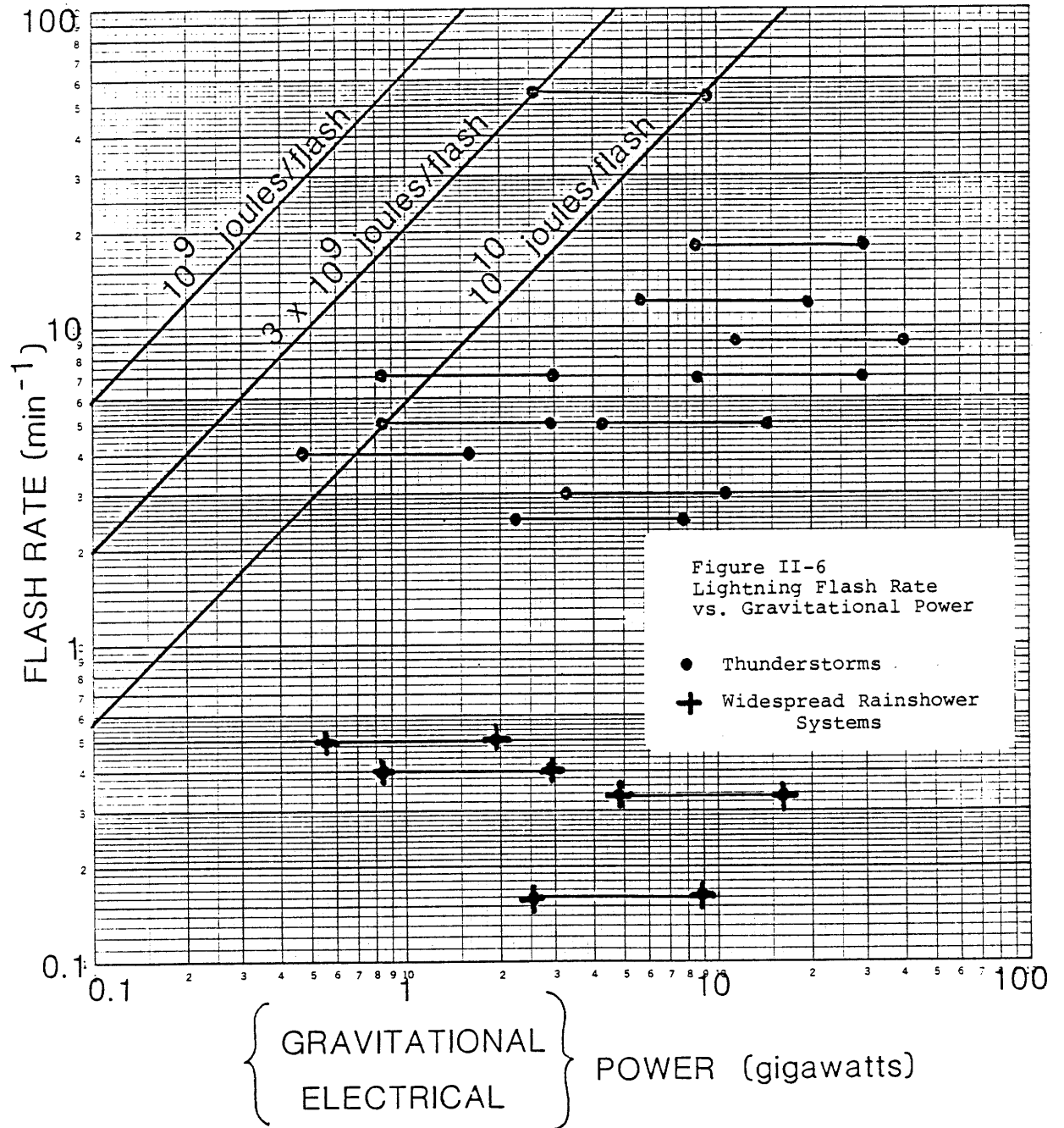
gravitational power shrinks considerably. Noteworthy is the fact that a factor of two or three increase in available gravitational power can result in an order of magnitude or more increase in electrical output.

The <u>apparent</u> global gravitational-to-electrical power efficiencies for three New England storms and one Florida storm[*] are all a few per cent or larger if a flash energy of 10^9 joules is assumed (see Section II-3), and are therefore greater than all but one of the <u>in situ</u> local efficiency estimates (Table II-1).

The gravitational power calculations were most reliably performed on the Florida storm data, in which specific electrical power-producing storm cells could be identified and evaluated. The calculations for New England squall lines were performed (see Appendix B) over a 10 km radius cylindrical volume in which lighning flash rates were estimated from single station electric field data. Orville and Spencer (1979), on the basis of satellite lightning observations, conclude that 1 flash/sec in a 10 km x 10 km area is a reasonable value for an active squall line. Since the storm area over which we evaluated gravitational power (314 km^2) is more than three times this latter area, and because the reported flash rate of

---

[*] P.R. Krehbiel has recently informed the author that the field changes associated with the high flash rate (50-60 min^{-1}) period of the Florida thunderstorm analyzed in detail by Lhermitte and Krehbiel (1979) are small and has suggested that the flash energies are anomalously low. The tendency for field change magnitudes to decrease with increasing flash rate is however a feature consistent with scale independent flash energy, as discussed in Section V-6.

1 sec^{-1} is three times larger than our largest estimates for New England (see Figure II-6), it appears likely that apparent gravitational-to-electrical efficiencies are significantly larger than those reported in this thesis.

Gravitational power values at times of maximum flash rate are plotted in Figure II-6. Seldom do the times of peak flash rate and peak gravitational power coincide, and the temporal evolutions of these quantities are poorly correlated. This assertion is illustrated in Figure II-7, where the evolution of these parameters is plotted for the August 13, 1978 Florida thunderstorm.

To test the idea that the ice crystal-graupel charging mechanism (Reynolds et al., 1957) is responsible for the electrification, we have plotted the gravitational power above the altitude of 6 km, as well as the total gravitational power associated with precipitation. The total gravitational power in Figure II-7 is poorly correlated with the discharge rate at 1907 GMT, and the peak discharge rate at 1908 GMT is associated with a slight decrease in total gravitational power.

A far better correlation with discharge rate is the vertical air velocity data at upper levels of the cloud. Maximum vertical velocities are plotted as far as they are available.

Also well correlated with the electrical output is the gravitational power above 6 km, particularly at the time of the dramatic onset in discharge rate when both quantities increase by large factors. It is possible that the ice is playing a

Figure II-7
Discharge Rate, Precipitation
Gravitational Power, and
Vertical Air Motion for the
August 13, 1978 Thunderstorm
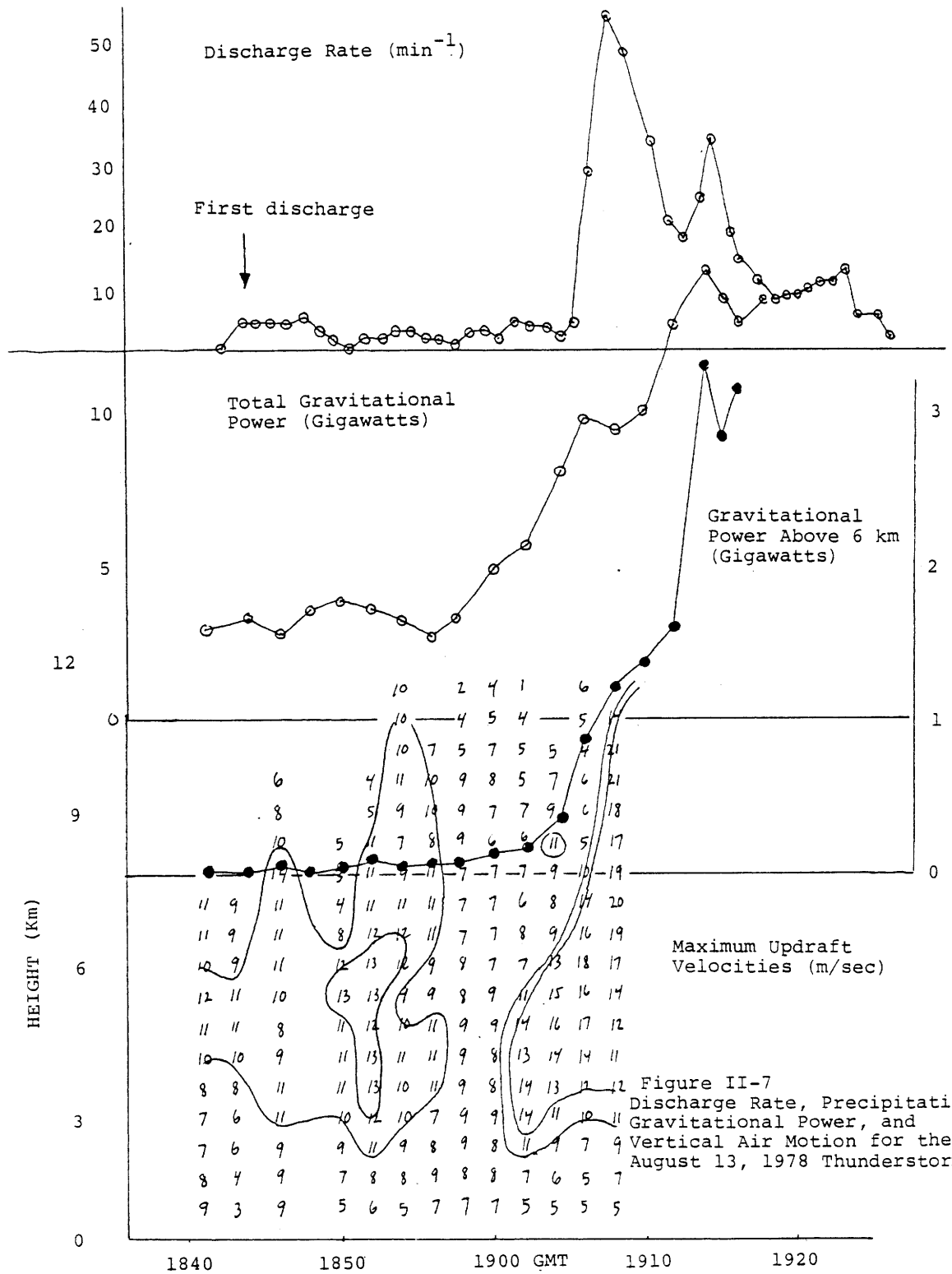
major role in the electrification, or alternatively, that the vigorous vertical air motion observed simultaneously is responsible for both the electrification, and the rapid growth of precipitation particles at higher levels through accretion of supercooled water. Since the gravitational power available for electrification at high levels continues to increase <u>after</u> the peak discharge rate, and doubles in value as the discharge rate declines to less than half its peak value, we favor the latter interpretation.

II-9 <u>The</u> <u>Spatial</u> <u>Distribution</u> <u>of</u> <u>the</u> <u>Precipitation</u> <u>Gravitational</u> <u>Power</u>

An additional constraint may be placed on the role of falling precipitation by examining the distribution of gravitational power with height in the storm. Figure II-8 shows this distribution for the active storm just discussed. Superimposed on this profile is the distribution of negative charge neutralizations found in similar Florida storms (Jacobson and Krider, 1976).

The precipitation hypothesis holds that the positive dipole structure of a thunderstorm is maintained by the descent of negatively charged precipitation particles in the central dipole region. If the negative charge neutralizations shown in Figure II-8 are indicative of the lower (negative) end of the classical dipole, it is immediately obvious that only a small fraction (less than 10% in this case) of the available gravitational power of precipitation lies in the supposed generation region.

39

NEGATIVE CHARGE LOCATIONS

Negative charge location
data from Jacobson and
Krider (1976)

Figure II-8
The Distribution of
Precipitation Gravitational
Power and Negative Charge
Locations with Height

HEIGHT (KM m.s.l.)

GRAVITATIONAL POWER (GIGAWATTS/KM)
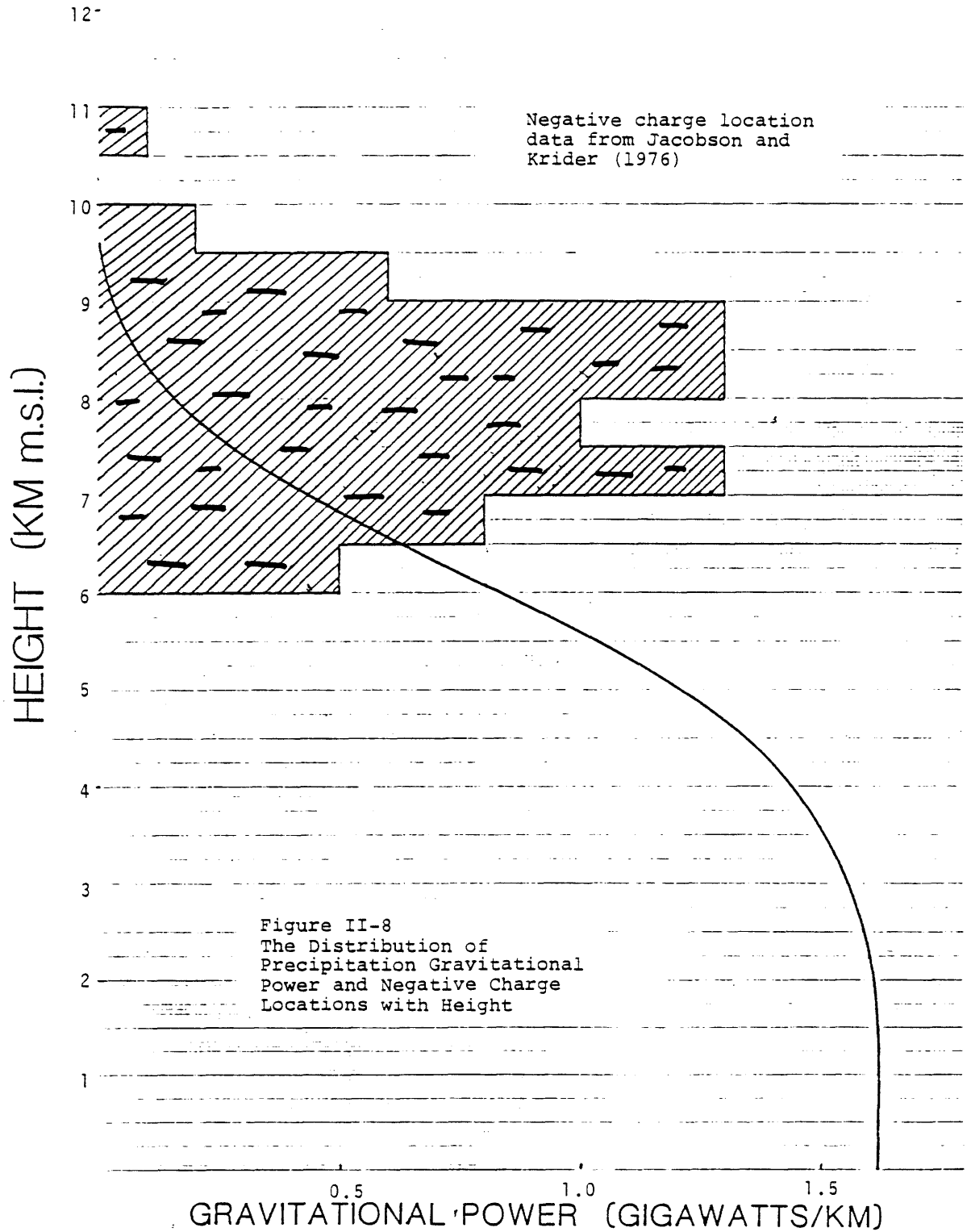
The bulk of the available gravitational power within the cloud lies below the region of negative charge. Observations in this region to date (see Christian et al., 1980) show a tendency for negatively charged precipitation falling in upward directed electric fields, a dissipative configuration. If this preliminary result has general validity in electrically active clouds, the calculations presented in this chapter indicate that precipitation must be falling with high efficiency higher in the cloud if it is the major contributor to cloud electrification.

The largest fraction of available gravitational power lies in the subcloud region. At levels near the ground in which the so-called mirror-image relation between precipitation current and electric field is upheld, the falling precipitation will be generating electrical energy. However, if Wilson ion capture of point discharge ions is responsible for this phenomenon, as Rust and Moore (1974) have argued, we can conclude that the associated gravitational-to-electrical conversion efficiency cannot be very large.

II-10 Conclusions

A consideration of the energetics of falling precipitation and its contribution to the electrification of thunderstorms has led to the following conclusions:

(1) A maximum of 29% of the gravitational potential energy of precipitation may be converted to electrical energy. This

41

result places a realizable limit on electrical power density of 8.2×10^{-4} watt/m^3 per mm/hr of precipitation rate.

(2) Efficient conversion of gravitational to electrical energy requires the modification of precipitation particle fall velocities.

(3) The existence of horizontal components of electric field will result in dissipative precipitation particle motion.

(4) Specific hypothesized precipitation charging mechanisms are predicted to operate most efficiently in regions of intense vertical field.

(5) Modest flash rate storms contain sufficient gravitational power associated with precipitation to account for their electrification as Braham's (1952) estimates had shown. The totalitarian principle in physics (that which is not prohibited, is compulsory) would lead one to conclude that falling precipitation makes a significant contribution to the electrification of such storms. Although most of the _in situ_ measurements to date by other investigators show dissipative precipitation motion, the presently available generation evidence (Table II-1) is consistent with the low apparent global efficiences for electrically inactive storms (Figure II-6).

(6) Storms which are electrically active (several flashes per minute) may be producing electrical power which is of the same magnitude as the available gravitational power of falling precipitation. The analysis presented in this Chapter (Section II-4),taken together with the available data (Sections II-7 and II-8),suggests that if precipitation is the major contributor to

electrification, then the particles must be falling with high efficiency. This last conclusion is however not consistent with our zenith-pointing Doppler radar results (Chapter III).

(7) The gravitational power structure of a thunderstorm is not entirely consistent with the classical, positive dipole-embodying, precipitation hypothesis. The bulk of the gravitational power is not available for electrical power generation in the central dipole region, but instead lies in a region in which falling precipitation may make a negative contribution to the electrification of the cloud. The gravitational power at upper levels (above 6 km) is well correlated with the electrical output, but appears inadequate to account for the energy of electrification.

Chapter III

Vertically Pointing Doppler Radar Measurements

III-1 Introduction

An understanding of the motion fields within thunderclouds is essential to a quantification of the relative importance of precipitation and convection to electrification. This chapter is concerned with thundercloud observations with Doppler radar, which is currently the most valuable technique for getting at this information.

Both precipitation particle motions and vertical air motions are examined in this chapter. Section III-2 is specifically concerned with a search for changes in the velocities of precipitation particles during lightning discharges, and Section III-3 is concerned with vertical velocity profiles and their relationship with the simultaneously observed electrification.

III-2 A Search for Precipitation Particle Velocity Changes Associated with Lightning Discharges

III-2.1 Motivations for the Experiment

The principal motivation for the vertically pointing Doppler experiment is the result in Chapter II that the electrical power generated by active thunderstorms is comparable with the gravitational power associated with falling precipitation. If charged precipitation is chiefly responsible for this electrical output, it follows that the

44

electrical and gravitational forces acting on these particles will be of comparable magnitude in certain regions of the cloud. We have demonstrated in Chapter II that efficient conversion of precipitation gravitational power to electrical power requires an approximate halving of the zero field precipitation particle fall speeds with respect to still air.

Additional motivations for the Doppler experiment are the following:

(1) In a numerical study of cloud electrification Chiu (1978) concludes that rain particle terminal velocities can "...decrease by a few meters per second in a region where the electric field strength grows beyond 2×10^5 or 3×10^5 v/m".

(2) The existing data on the electric charge carried by individual precipitation particles within thunderclouds (Christian et al., 1980; Marshall and Winn, 1980) show values of many tens of picocoulombs. Twenty picocoulombs on a 1 mm diameter raindrop is sufficient to levitate such a particle in a field of breakdown magnitude (4×10^5 v/m).

(3) Schonland's (1950) hypothesis for the raingush phenomenon is based on the sudden release of precipitation at the time of the lightning discharge: "With the passage of the flash within the cloud the electric charges momentarily disappear... and the rain... is free to fall."

The basis for all predicted velocity changes lies in the necessary re-equilibration of forces when the electric force is abruptly modified as a result of a lightning discharge.

45

The response of precipitation particles to step function forcing has been studied by Hilst (1949), Wilson (1970), and Wang and Pruppacher (1977). The predicted rapid response of these particles make such velocity transitions distinguishable from the buoyant and advective velocity fluctuations which are common features in zenith-pointing Doppler radar data (Battan, 1980).

III-2.2 Methodology

Searches for velocity changes associated with the occurrence of nearby lightning were carried out as part of the TRIP (Thunderstorm Research International Program) experiments. A vertically pointing Doppler radar was operated on the mountain ridge near Langmuir Laboratory (3.2 km MSL) near Socorro, New Mexico during the months of July and August in 1979 and 1980. The operating characteristics of these radars, a block diagram of the Doppler equipment, and a more detailed discussion of instrumentation are included in Appendix C.

During 1979, only a single radar range gate was available, situated at 6.8 km MSL in a region thought to be of importance in the production of charged precipitation (Krehbiel et al., 1979). In addition to recording the Doppler signals on analog tape, we listened to one Doppler channel with an audio amplifier to check for lighting associated Doppler frequency changes in real time.

46

Substantial improvements in the 1980 experimental setup included multiple radar range gates spaced by 255 meters, real time digital processing of the mean of the Doppler velocity spectrum at 150 msec intervals, and the real time color CRT display of mean velocity and electric field. This latter feature permitted the instant recognition of substantial velocity changes.

A field mill located within 100 meters of the radar was used to monitor the electric field during overhead thunderstorms. This information on lightning occurrence was occasionally supplemented with the output of a HF radio receiver.

III-2.3 1979 Observations

Figure III-1 (a,b) shows a rapid decrease of 1 m/sec in particle mean downward velocity coincident with the occurrence of a lightning discharge indicated by the burst of HF radiation shown on the same time scale. Figure III-1(b) shows a time expanded display of the velocity change which allows an accurate determination of the response time of approximately 1.5 seconds, consistent with the inertial effects of millimeter size particles. If we assume that the electric field was diminished by the discharge, this abrupt velocity change is indicative of predischarge dissipation.

The upward velocity shown in Figure III-2 suggests a case of particle levitation in a strong predischarge electric field which ends abruptly at the time of the discharge (see Figure II-2(c)), thereby allowing the particles to move

47
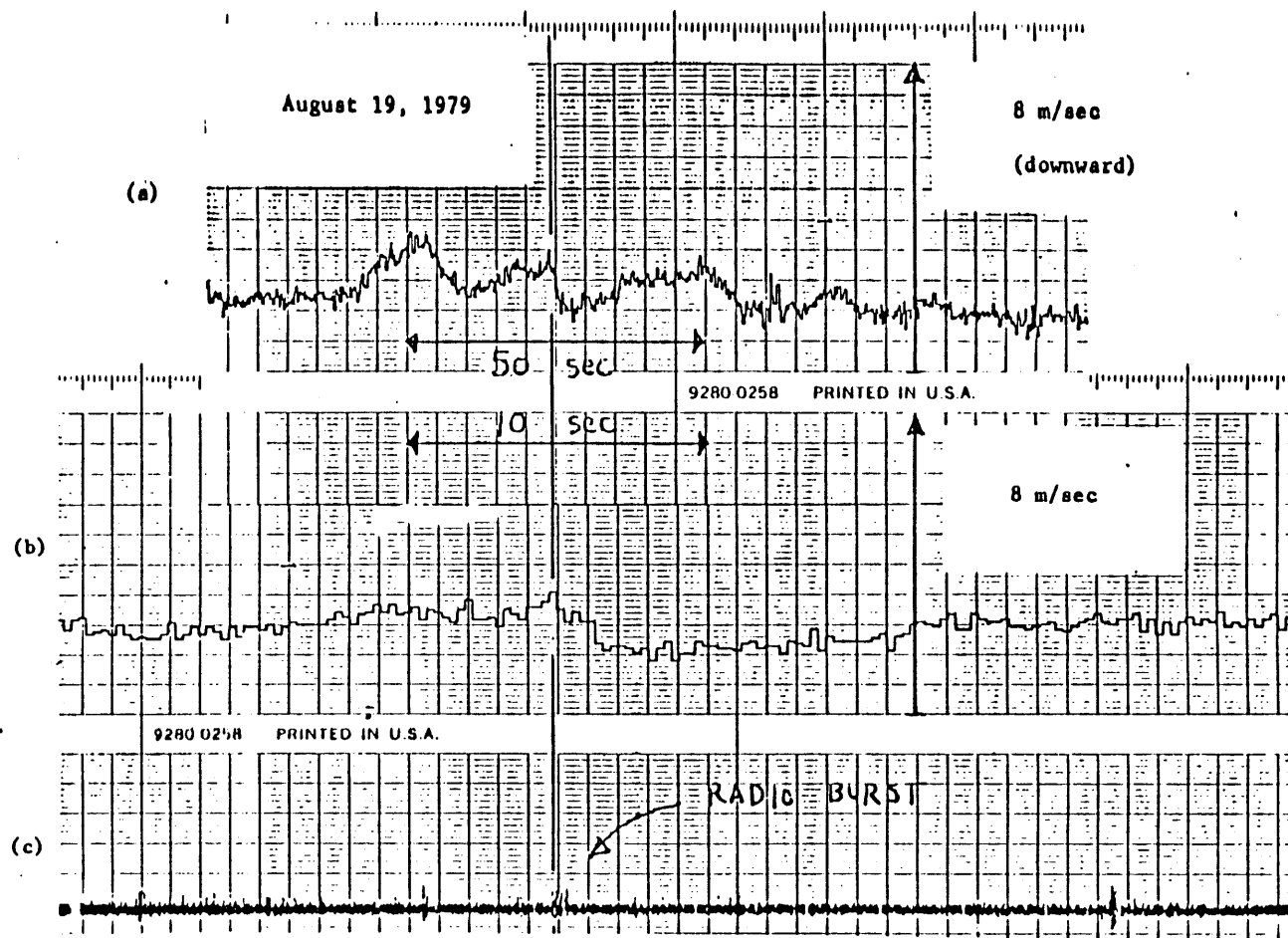
Figure III-1

a) Sudden decrease in downward particle motion associated with a lightning
   discharge and observed at an altitude of 3.2 km above the radar.
b) Expanded time scale of the event showing that the transition lasts
   slightly more than 1 sec.
c) HF radiation burst associated with the discharge, observed simultaneously
   and presented on the same time scale as a).
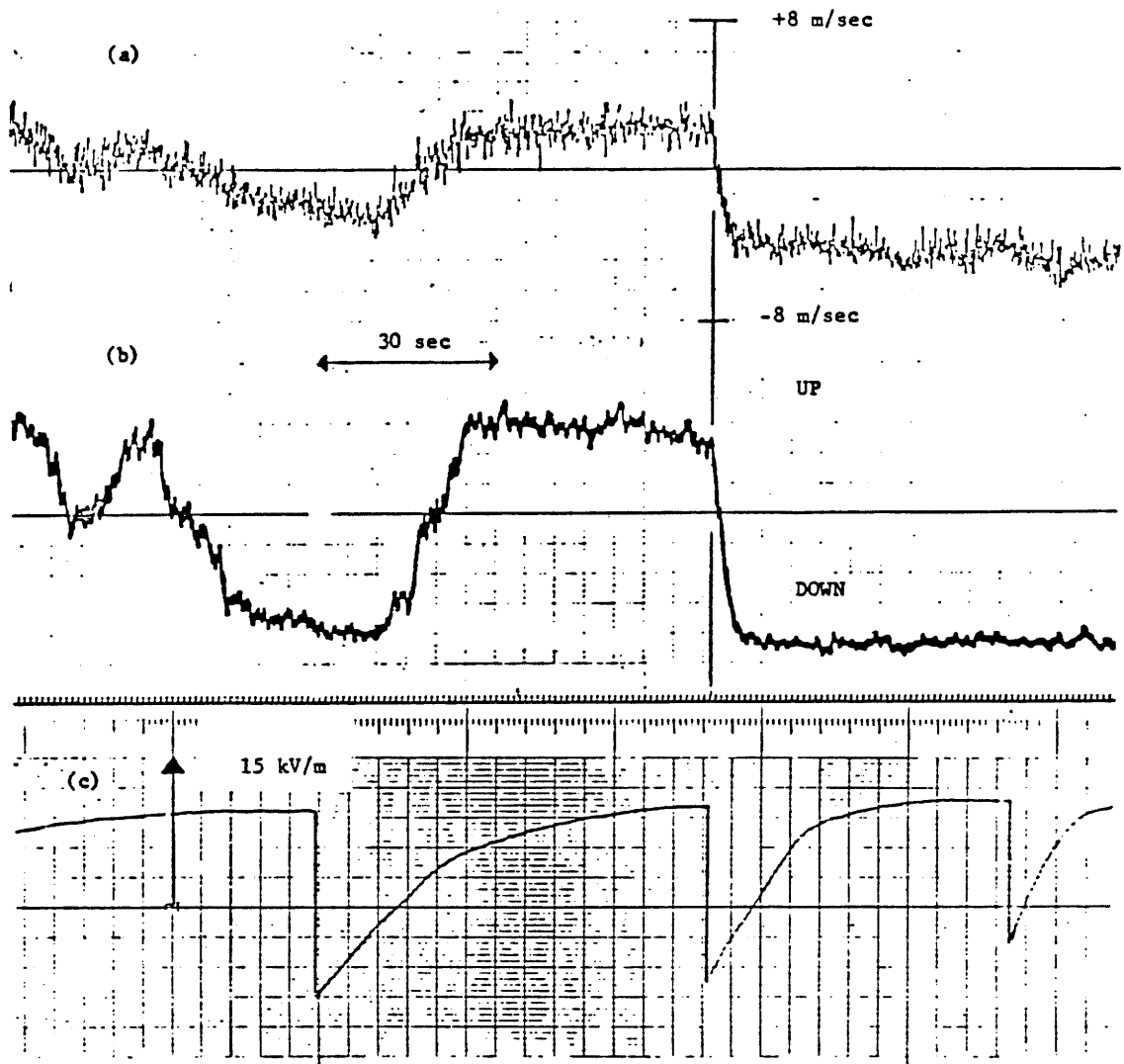
Figure III-2
a) Doppler vertical velocity versus time indicates possible levitation of particle by the electric field which ends abruptly at the time of the discharge.
b) Lead-Lag behavior of the Doppler signal indicating the probability of sign in Doppler spectrum obtained from the zero crossing method.
c) Electric field at the ground near the radar.

downward. The post discharge (downward) vertical velocity is consistent with the terminal velocity of precipitation particles in the form of graupel or small size hail, which suggests that vertical air velocity is not significant in the storm at this time. The fact that upward velocity is observed prior to the discharge suggests that the electrical forces exceed the gravitational forces acting on the particles. The information in Figure II-5 and reasonable assumptions about the magnitude of the field in the cloud lead to the conclusion that the precipitation particle charges at the time of the discharge were several hundred picocoulombs. The net particle motion appears to be electric field-driven just prior to the discharge and therefore cannot be contributing to the accumulation of electrostatic energy. It is however quite possible that gravity driven generative motion was occurring prior to the onset of levitation, as well as following the discharge.

A rather large field change (~17 kV/m) was recorded at the Solar Tower site for this discharge. To further confirm the proximity of the discharge to the radar range gate overhead, we have examined acoustic reconstructions of the thunder sources for this event, which were kindly provided by the New Mexico Institute of Mining and Technology. Figures III-3 and III-4 show projections of these sources on the vertical and horizontal planes, respectively. The acoustic source heights cluster around the altitude of the range gate, and the nearest identifiable source was displaced horizontally only 1500 meters from the range gate.

Figure III-3
Thunder sources for the
Lightning Discharge of
Figure 2: Vertical Plane

Figure III-4
Thunder Sources for the
Lightning Discharge of
Figure 2: Horizontal
Plane
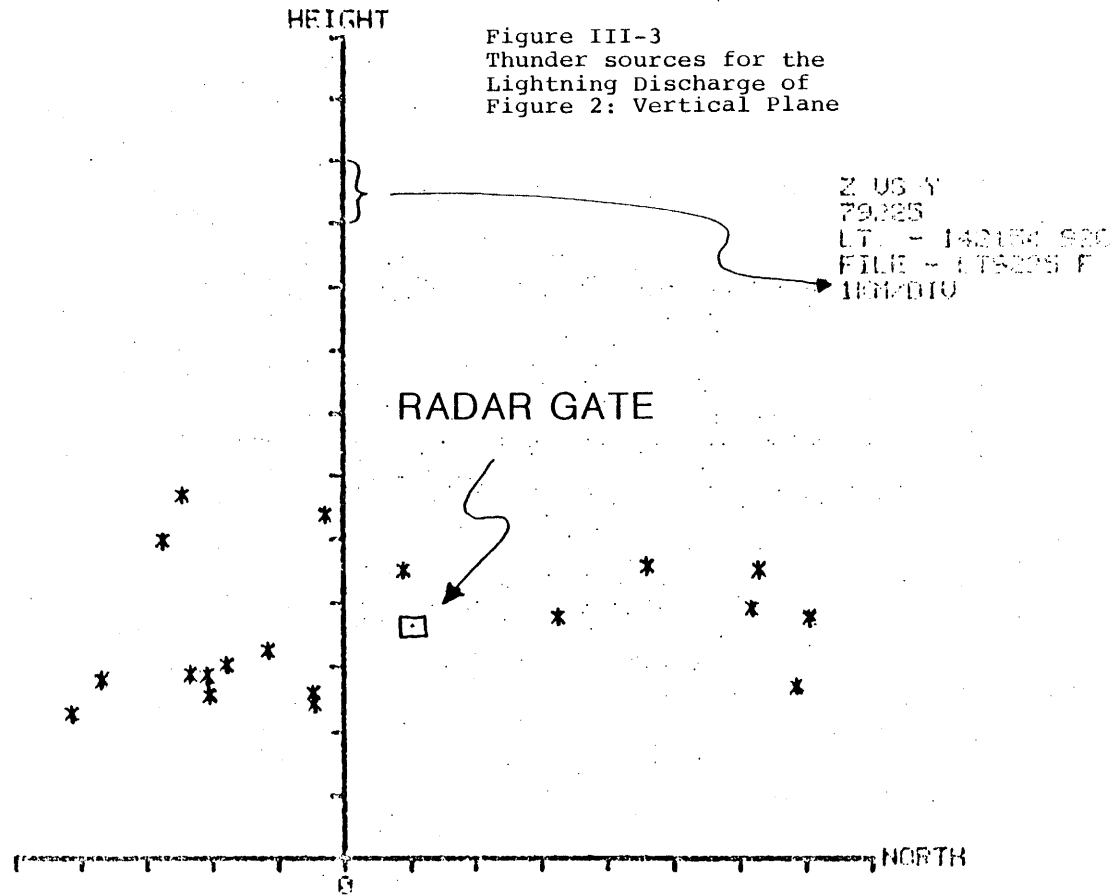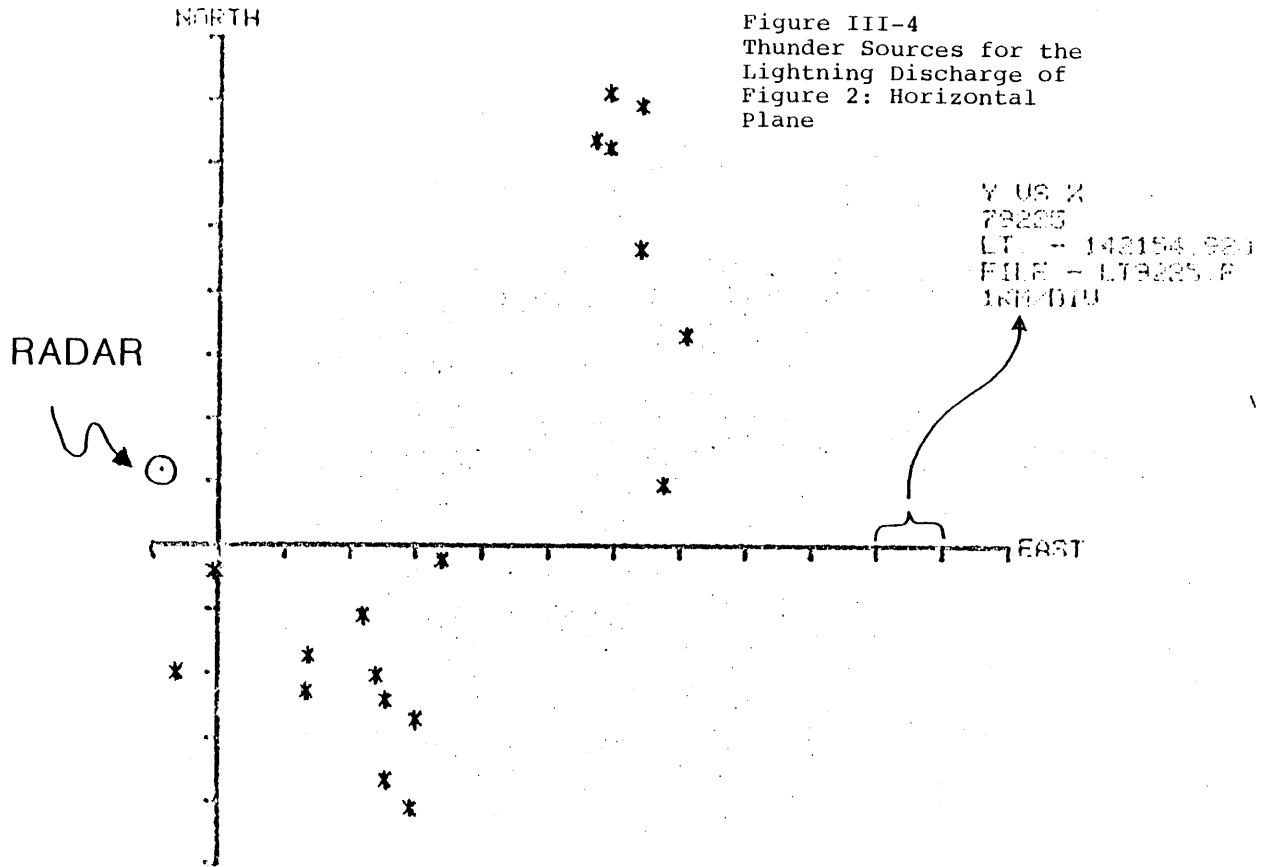
Figure III-5 shows evidence for more gradual variations of the downward vertical velocity which exhibit a high correlation with electric field changes. Such behavior still suggests a close coupling between the electric field and the motion field, but is less easily interpreted. These variations were observed within one kilometer of the radar cloud top during a brief flurry of discharges when the cloud top and pressure signals were highly coherent (see Figure VI-6; August 13, 1979, 1326-1331 MST). The pre-and post-discharge velocity behaviors to not show the systematic asymmetry which characterizes the other velocity perturbations, and the discharge times are not always centered on discharge maxima. Colgate (1967) has suggested that turbulent eddies of characteristic size 100 meters and characteristic velocity 5 m/sec are responsible for the initiation of lightning discharges. This prediction is not inconsistent with the observations in Figure III-5.

During approximately eleven hours of thunderstorm Doppler observations in 1979, only four clear cut discharge-coincident velocity changes were observed. In three of these cases, the downward velocity increased at the time of the lightning (as in Figure III-1), and in the fourth case apparent electric field levitation of the particles was taking place (as in Figure III-2). If we assume that the magnitude of the electric field is reduced by the discharge (in agreement with the in situ balloon observations of Winn and Byerley (1975)), then we conclude that the pre-discharge precipitation particle motion was dissipating electrical energy in all cases.

53
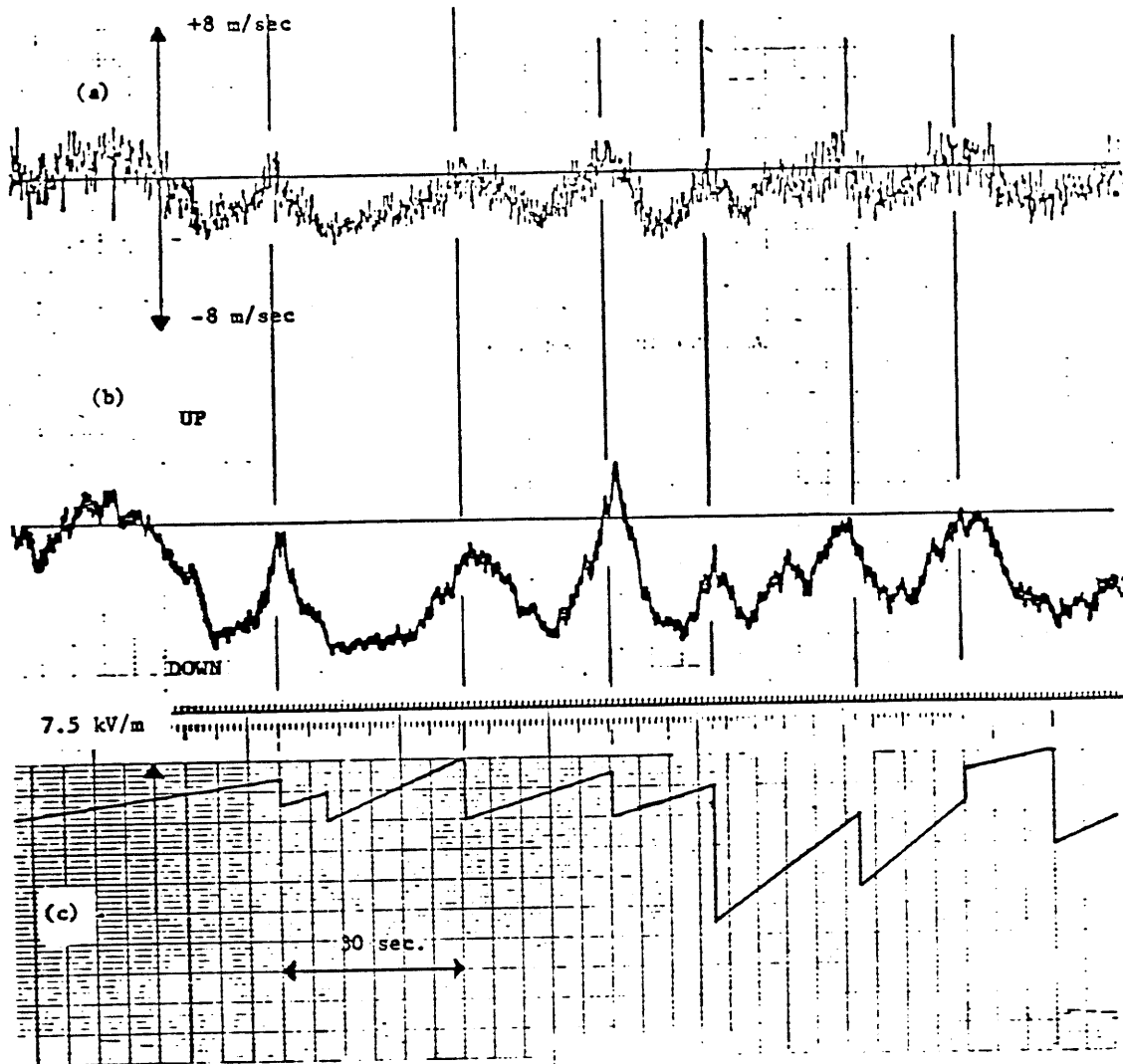
Figure III-5

a) Fluctuating Doppler velocity versus time at the same altitude as Fig. 1 and Fig. 2.

b) Sign of Doppler velocity (same as 2b).

c) Electric field at the ground near the radar.

III-2.4 1980 Observations

A few additional velocity changes during nearby lightning discharges were observed during Summer 1980, and the multiple radar range gate capability contributed a great deal to defining the structural context of these events.

Time-height profiles of radar reflectivity and mean Doppler velocity for the July 6, 1980 thunderstorm are shown in Figure III-6. Also included is the simultaneous electric field as measured at the ground approximately 50 meters from the radar, which clearly shows the discontinuities associated with lightning discharges. No abrupt velocity changes are discernible in these data until the seventh discharge at 151330 MST, at which time pronounced downward motion appears at an altitude of 8-8.5 km MSL. The variation of mean Doppler velocity in Gate 19 (8.0 km MSL) is depicted in Figure III-7 on an expanded time scale. Though the apparent vertical acceleration of these targets is 2-3 meter/sec^2, this velocity transition is not sufficiently abrupt to be attributed to a sudden change in electric force, but instead is probably associated with the advection of a rainshaft into the radar beam. An alternative possibility is the existence of a discharge stimulated raingush (Vonnegut and Moore, 1960), which is suggested by the substantial reflectivity increase (at a rate of 80 dB per minute) coincident with both the lightning discharge and velocity increase. Because only fixed beam radar data is available at this time, we are unable to distinguish advecting features from true time variations.

55

Figure III-6
Time-Height Profiles of
Radar Reflectivity and
Mean Doppler Velocity:
July 6, 1980, New Mexico

Figure III-7
Pronounced Downward Motion
Subsequent to a Lightning
Discharge

GATE 19
8.0 KM MSL
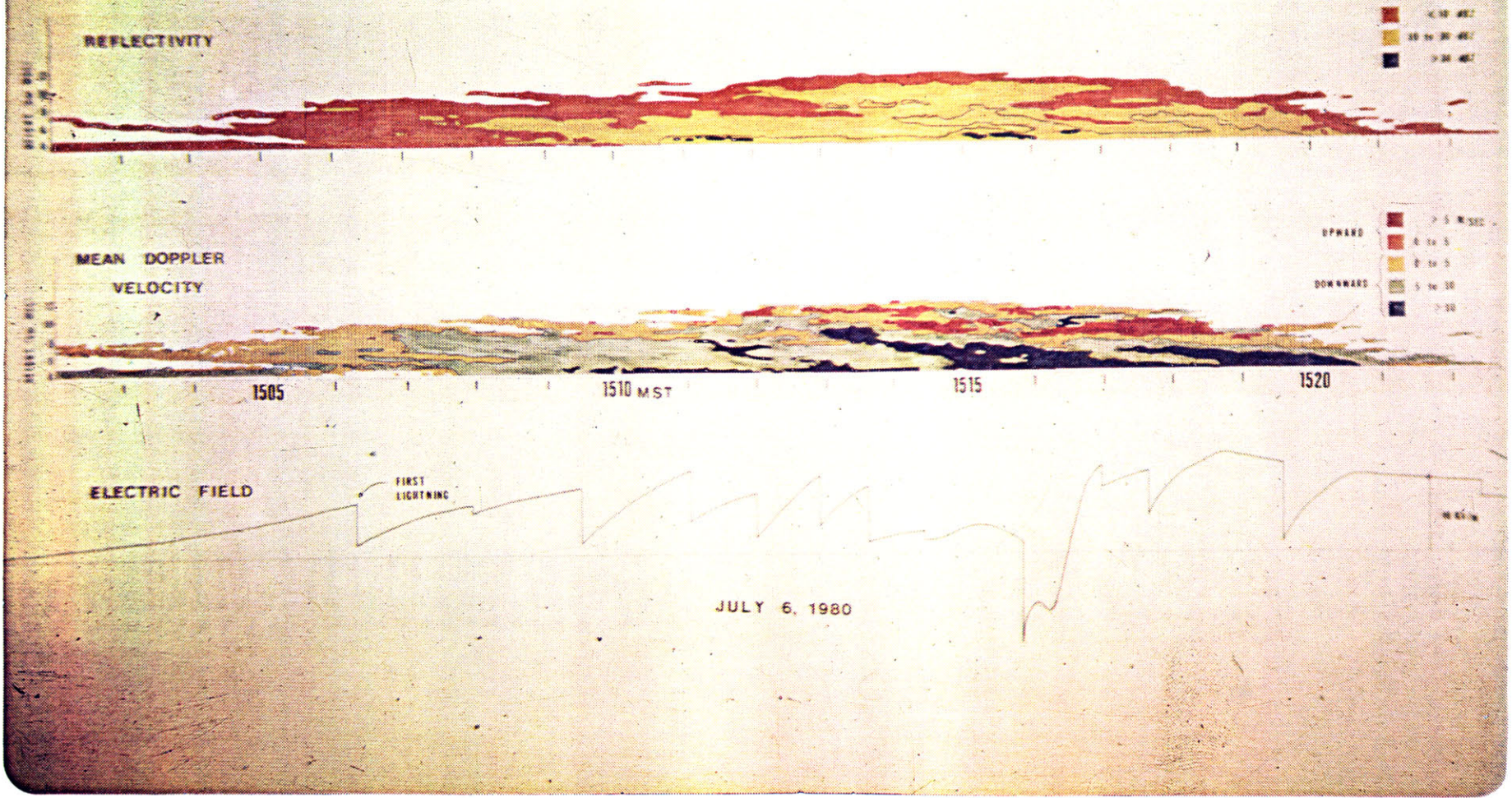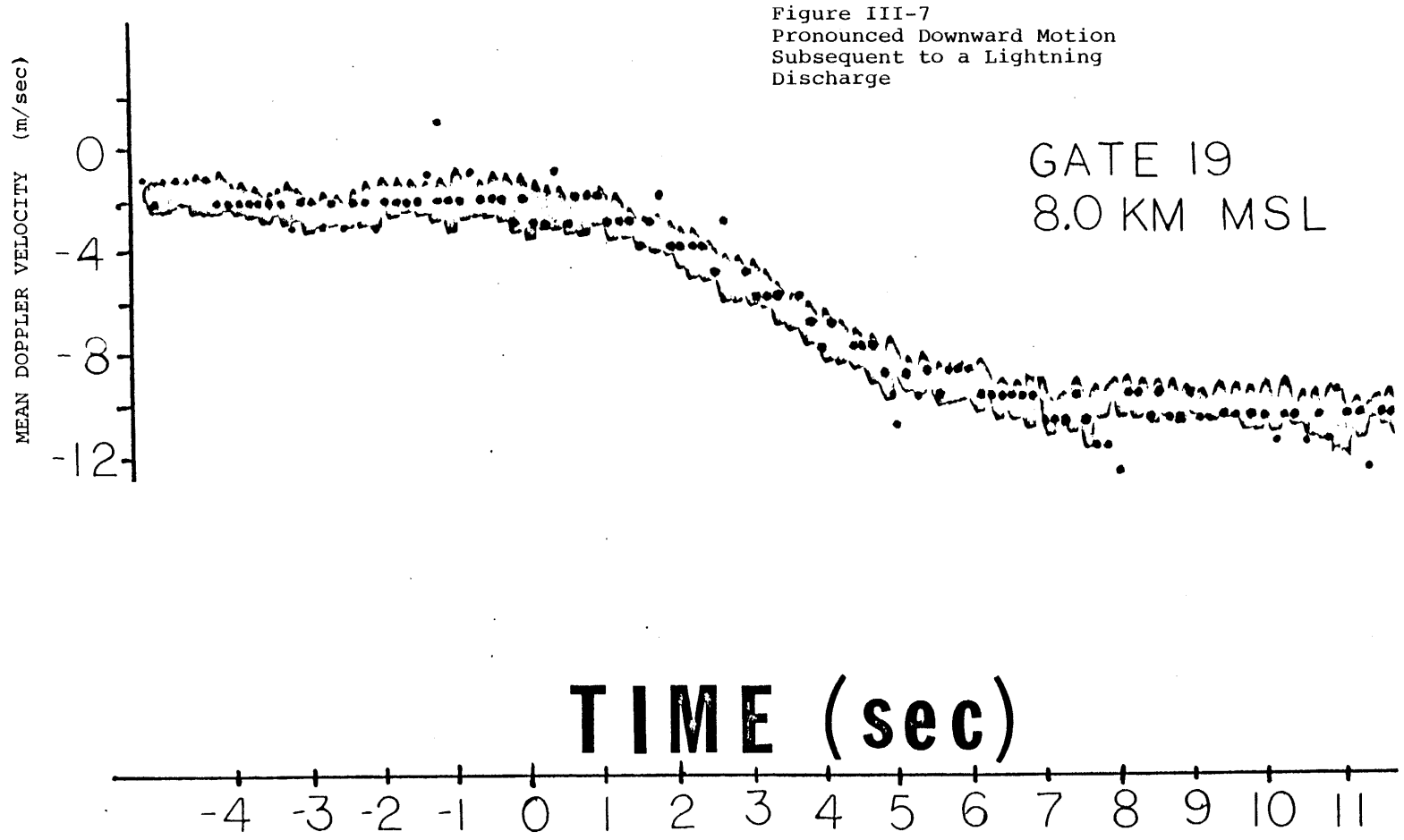
Of particular interest is the fact that this downward motion persists (see Fig. III-6) through a period of diminished discharge rate and depressed foul weather field and reaches the ground (3.2 km MSL) at the termination of this period (151540 MST), which is marked by a discharge and large field change which reverses the polarity of the electric field. Velocity changes were observed in several range gates at this time.

Figure III-8 illustrates the velocity behavior in those radar gates of interest at the time of this latter lightning discharge. The most pronounced changes occurred in adjacent gates within 1500 meters of the top of the radar cloud. A cursory look at the increases in downward motion at this time suggests that the particles were suddenly released when the electric field collapsed. However, the large 8 meter/sec change at Gate 25 (9.6 km MSL) would require the existence of large particles (D > 3mm) to be consistent with this interpretation. The low radar reflectivity (13 dBZ) at this time, the rapid (<1 sec) response time of the particles, and the fact that this gate is located near the top of the cloud all indicate that these targets are quite small (D<1 mm) and therefore will have zero-field terminal velocities of at most 4 m/sec. We prefer the interpretation that these particles are field-driven upward at ~4 m/sec against a ~5 m/sec downdraft prior to the discharge and then approach the ground at the combined downdraft-terminal velocity of 9 m/sec when the field collapses.

Figure III-8(a)
Multiple Range Gate
Velocity Changes Attributed
to a Lightning Discharge

GATE 26
9.8 KM MSL

13 DBZ

MEAN DOPPLER VELOCITY (m/sec).

TIME (sec)

59

Figure III-8(b)

GATE 25
9.6 KM MSL

13 DBZ

MEAN DOPPLER VELOCITY (m/sec)

+4

0

-4

-8

-12

TIME (sec)

-4 -3 -2 -1 0 1 2 3 4 5 6 7 8 9 10 11

09

Figure III-8(c)

GATE 24
9.3 KM MSL

12 DBZ

GATE 19
8.0 KM MSL

16 DBZ

TIME (sec)
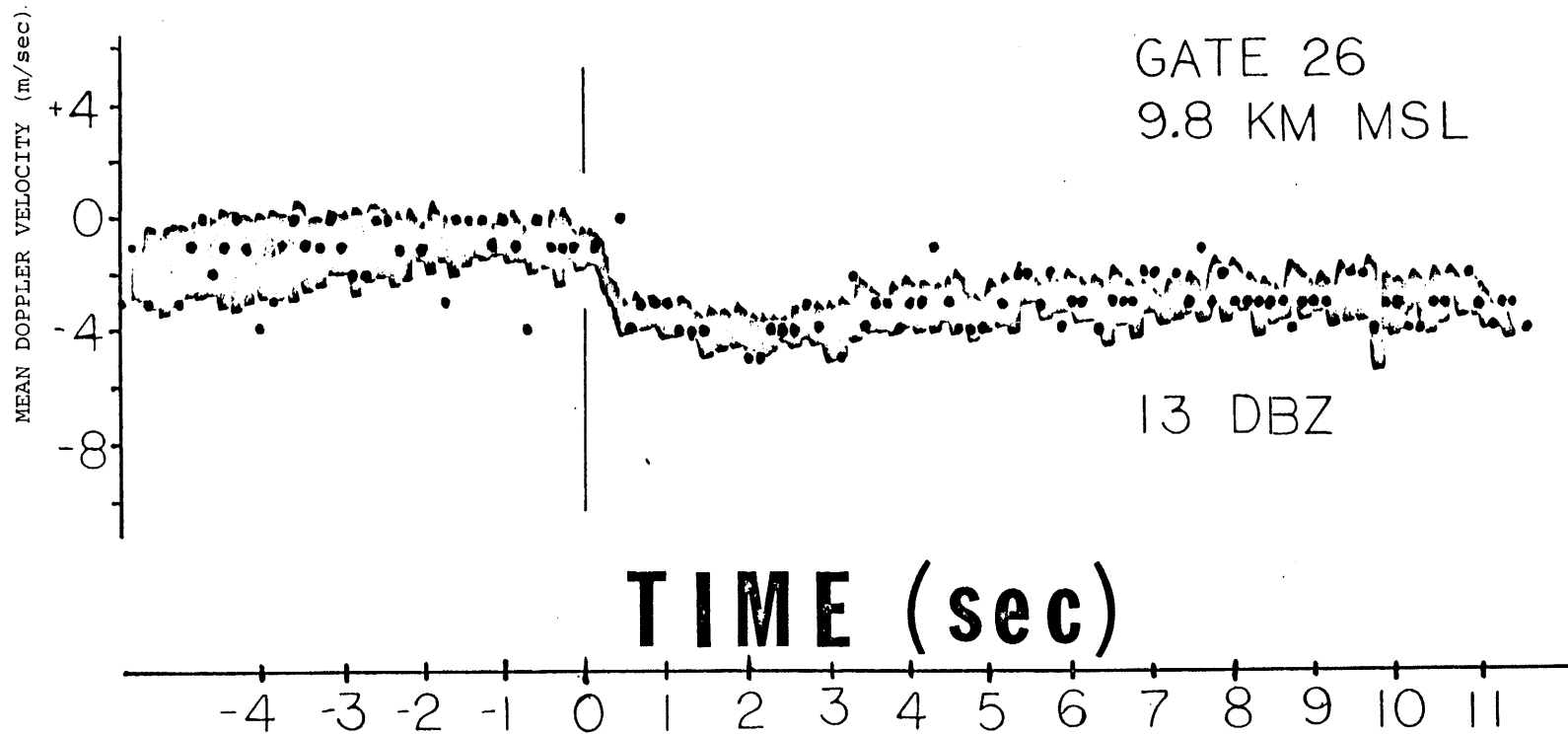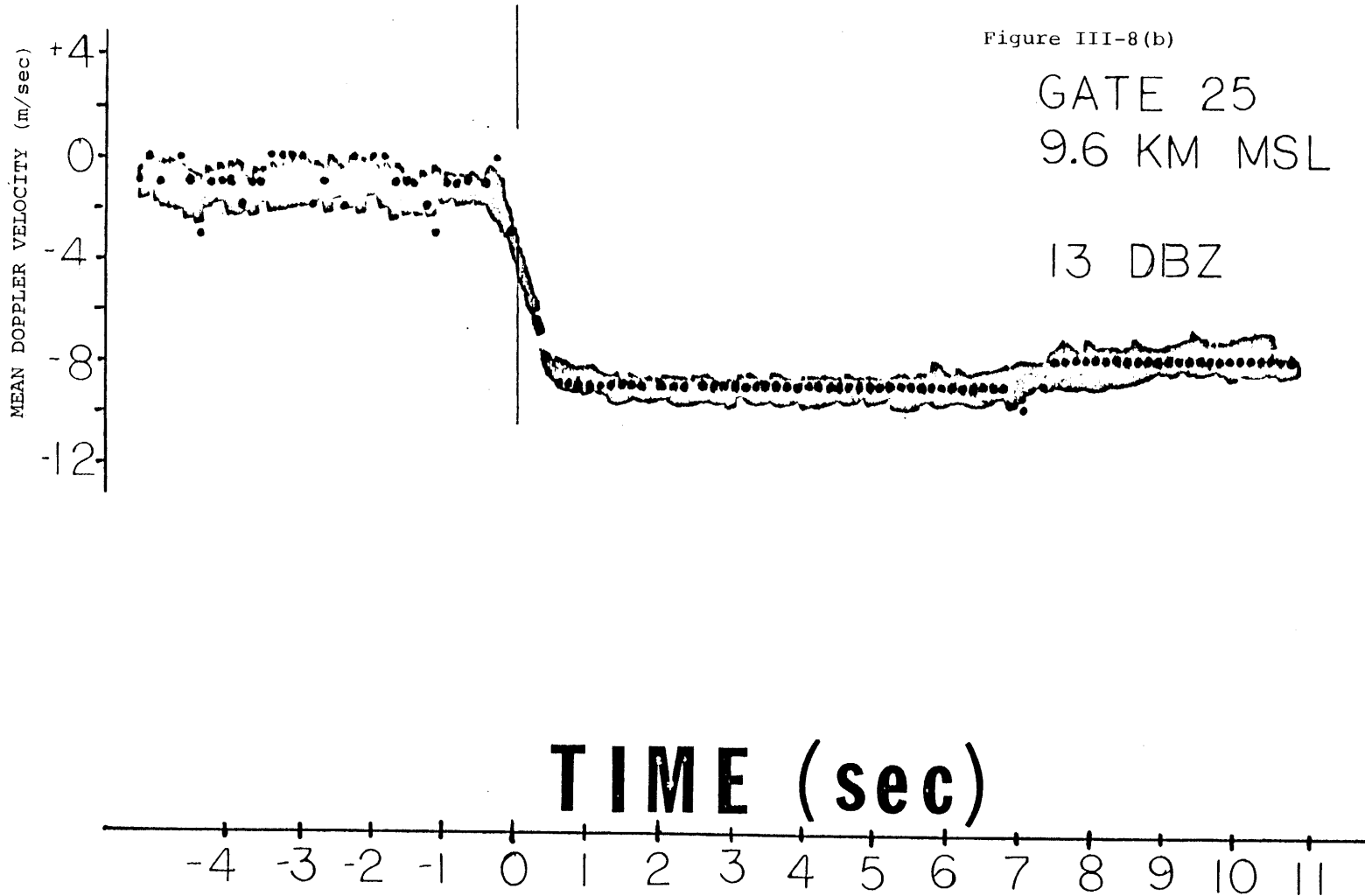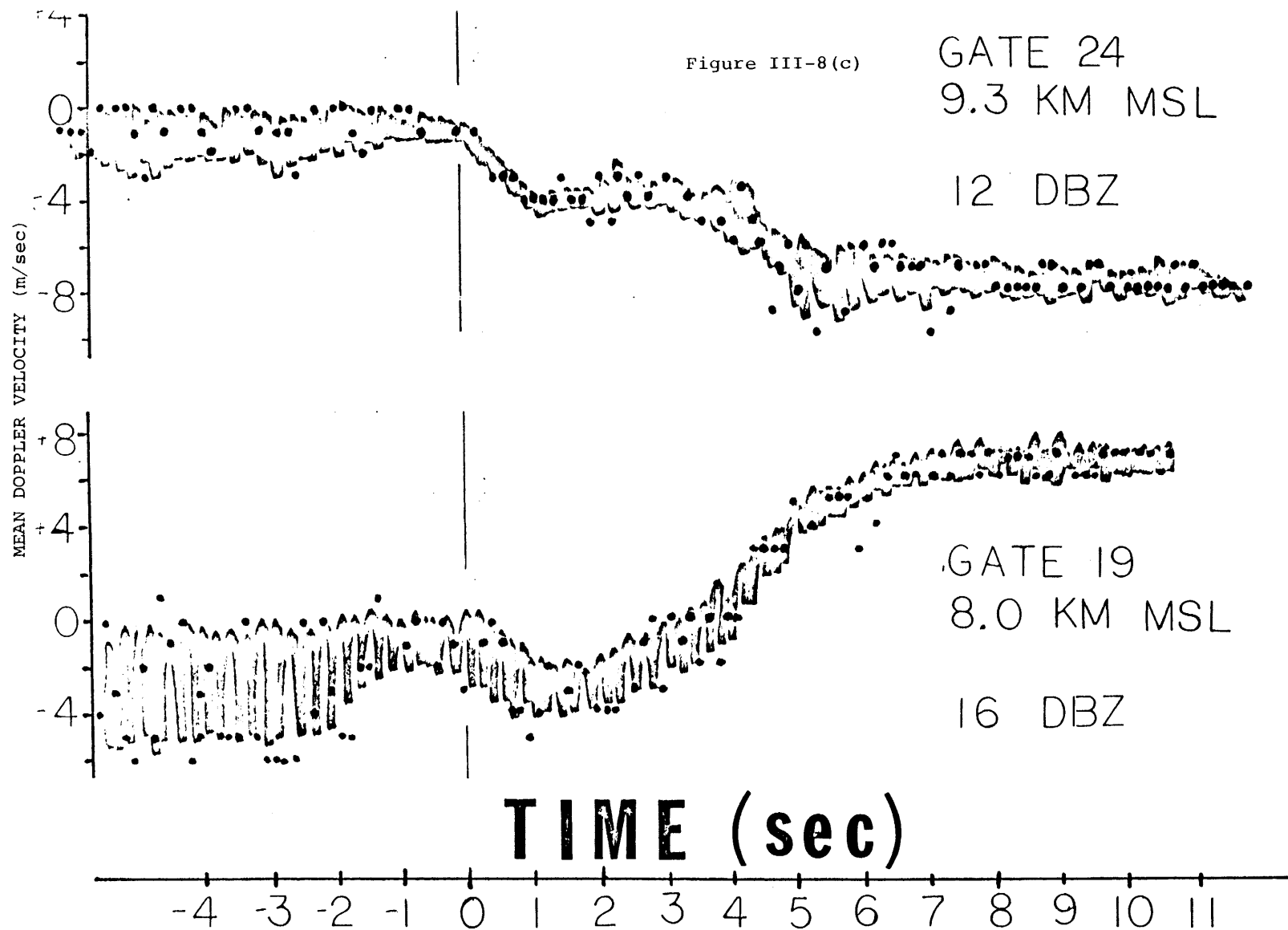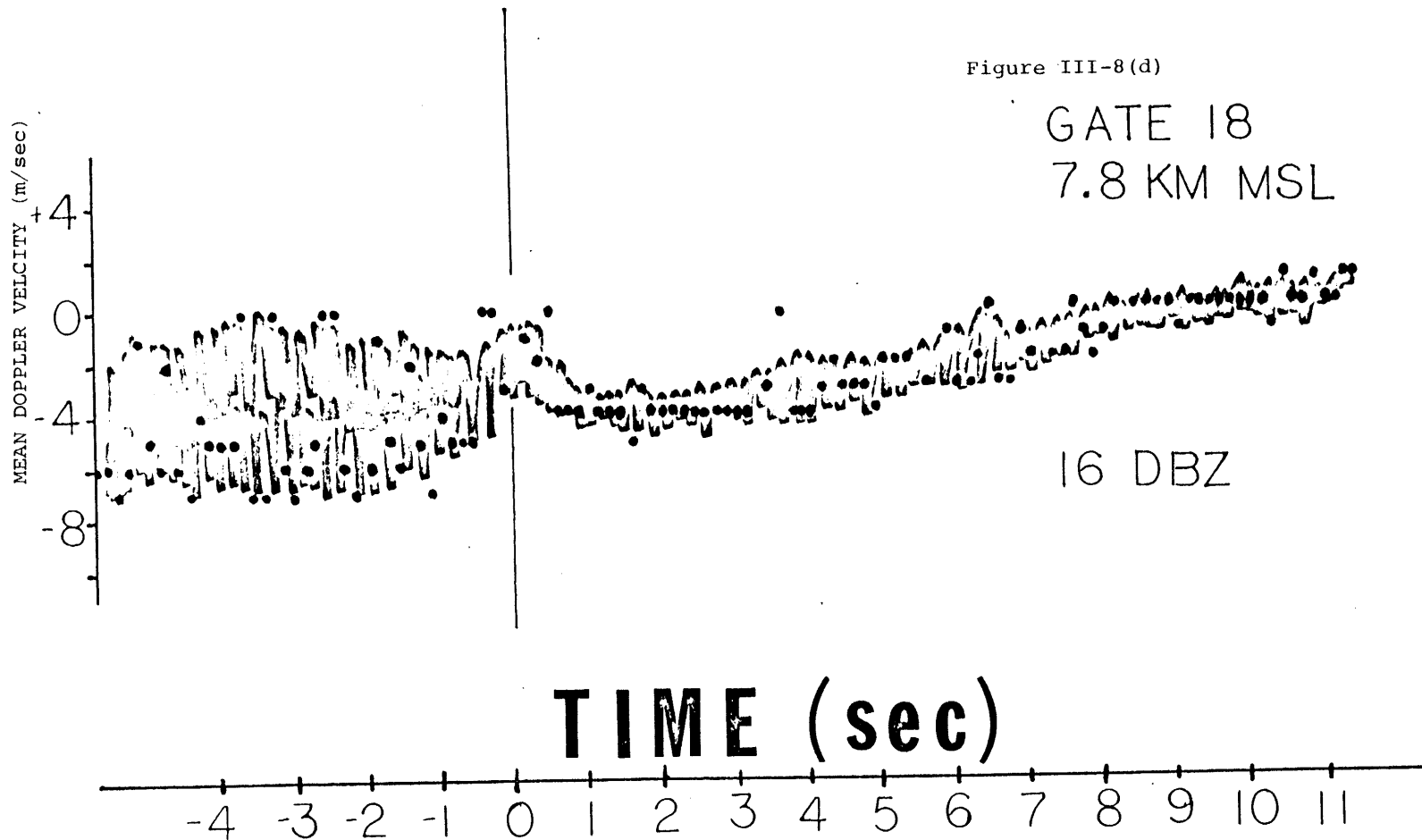
Figure III-8(d)

GATE 18
7.8 KM MSL

16 DBZ

MEAN DOPPLER VELCITY (m/sec)

+4

0

-4

-8

TIME (sec)

-4 -3 -2 -1 0 1 2 3 4 5 6 7 8 9 10 11

Figure III-8(e)

GATE 12
6.3 KM MSL

30 DBZ

GATE 4
4.2 KM MSL

MEAN DOPPLER VELOCITY (m/sec)

TIME (sec)
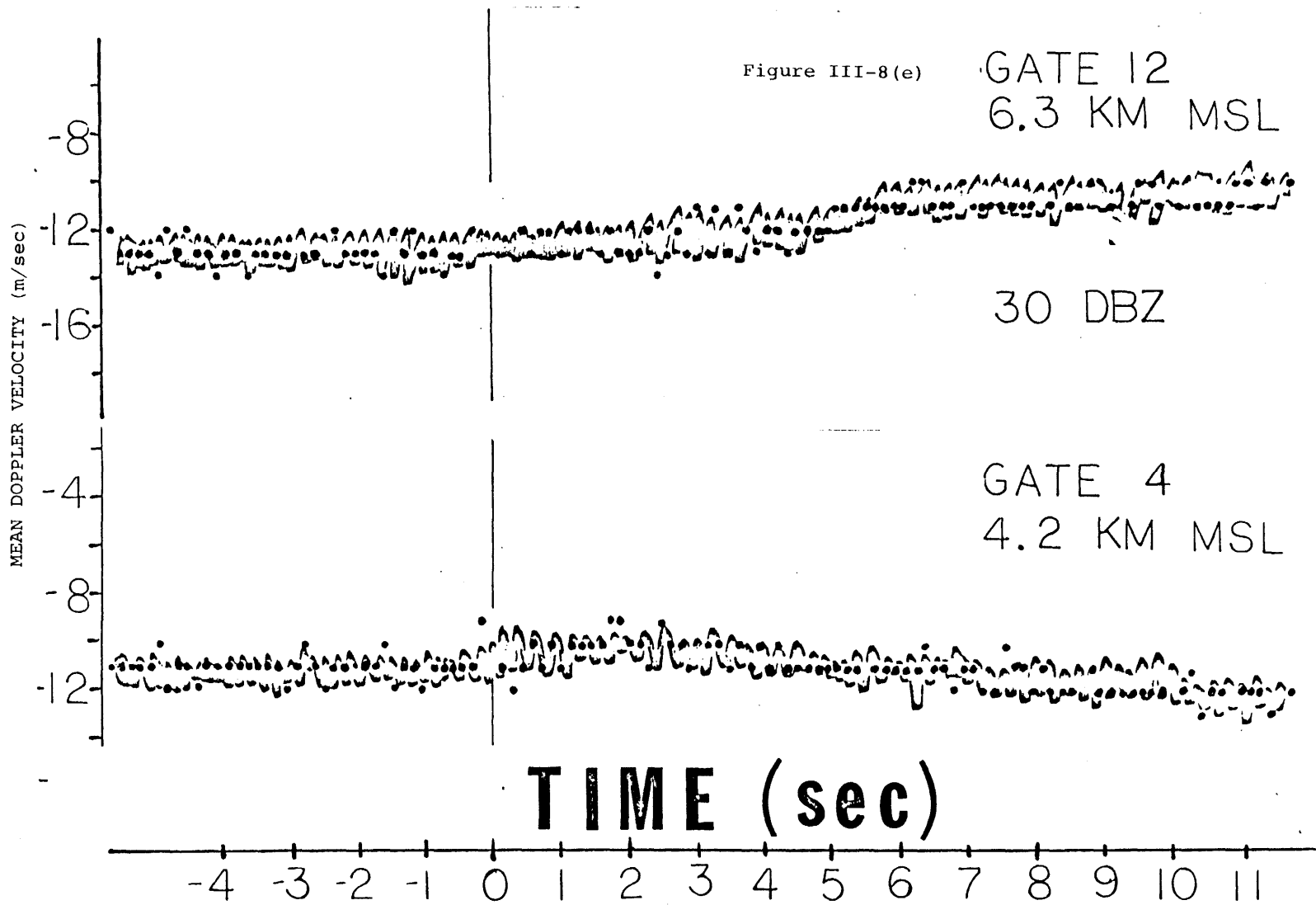
We need not invoke a downdraft to explain the smaller

velocity increases in the adjacent gates 24 and 26 and in such

a case it is possible that these targets are falling against

the predischarge electric field. An _upper_ bound on the rate of

generation of electrical energy in each of these gates is

(0.29)MgV where M is the precipitation mass per unit volume,

g is the acceleration due to gravity, and V is the zero-field

terminal velocity of the particles.

In Gate 25 the particles were constrained to be

field-driven against gravity, and thus the predischarge

electric force exceeds the gravitational force acting on these

particles. A _lower_ bound on the rate of dissipation of

electrical energy (ρEV) is therefore MgV, where V is the

field-driven velocity with respect to still air.

Since the radar reflectivities in these three adjacent

gates are comparable, the mass densities M associated with the

precipitation targets are closely matched. Summing the

contributions of Gates 24, 25 and 26 to electrical power, we

have a _lower_ limit on net dissipation of $2(0.29)$MgV $-$MgV $=$

-0.42 MgV. If the mass density corresponding to the radar

reflectivity of 12-13 dBZ is 10^{-2} g/m^3 (Battan, 1973), we have

a lower limit on net dissipation due to precipitation particle

motion of 1.6×10^{-4} watt/m^3 within a substantial volume of the

cloud.

Velocity excursions at lower levels of the cloud (Gates 18

and 19)) are insufficiently rapid to be attributed to an

electric field discontinuity. These changes may be associated with the advection of inhomogeneities into the radar beam, but the coincidence with the time of the lightning remains a puzzle.

We have also looked for velocity changes at levels in the cloud where negative charge inferred to have been neutralized by lightning has been located (Krehbiel et al., 1979). No discernible velocity adjustments exist in Gate 12 at a height of 6.3 km MSL. Nor are there apparent velocity changes in the heavier precipitation in the lower part of the cloud at Gate 4 (4.2 km MSL).

A noticeable general feature of Figure III-8 is the tendency for the standard deviation of the mean Doppler velocity estimate to be larger prior to the discharge than following it. This behavior may be attributed to either rapid fluctuations in the electric field prior to the discharge, or to an electric field broadening of the Doppler spectrum. If electric forces contribute significantly to the individual particle velocities, it may be shown that in certain circumstances an increase in velocity spectral width will result when the electric field increases prior to the discharge. Specific cases in which this may occur are examined in Appendix D.

III-2.5 Fixed Horizontal Beam Observations

To investigate the possible dissipative motions of charged precipitation particles (see section II-5) in the

65

horizontal electric fields which are known to exist in
thunderclouds (Rust and Moore, 1974; Winn et al., 1974) we
conducted a few Doppler experiments with a fixed beam at low
antenna elevation angles (a few degrees above the horizon).
Such an opportunity was afforded by the New Mexico
thunderstorms which developed away from the mountaintop but
were sufficiently close to allow the recording of
lightning-associated electric field changes.

One advantage of horizontal Doppler probing is the reduced
spectral width and smaller standard deviation in the mean
Doppler velocity estimates. In spite of this improvement in
sensitivity to velocity changes, we observed no dramatic
perturbations in horizontal velocity during 20-30 discharges in
the clouds under surveillance.

III-2.6   Conclusions

Precipitation particle velocity changes of several meters
per second have been observed at the time of nearby lightning
discharges, and are attributed to abrupt changes in electric
force acting on these charged particles. Most, if not all, of
these velocity changes occurred in the upper half of the cloud
in regions of weak reflectivity, a result consistent with the
conclusions drawn in Chapter IV concerning the location of
breakdown regions in the cloud. Since the volume of the cloud
under Doppler surveillance may be several hundred cubic meters,
we may infer that, at least on occasion, a substantial
population of precipitation particles is predominantly charged

66

with a single polarity. Though the observations presently available do not support the view that precipitation motion is contributing to predischarge electrification, the question of generation versus dissipation cannot be fully assessed with this Doppler technique. Velocity changes of a meter per second or less may often be smaller than the standard deviation in the mean velocity estimate and may escape detection, but may be associated with significant amounts of energy. Also, it is possible that particles are highly charged but suffer only small velocity changes because the lightning-associated field change in the cloud is small (see Section V-6 for a discussion of this evidence). The observation of Doppler spectral evolution during lightning discharges should provide additional sensitivity to velocity change detection.

Although this experiment has provided an exciting new opportunity for investigating the contribution of precipitation to cloud electrification, we emphasize the result that precipitation velocity changes associated with lightning discharges are rare events. Two storm seasons, 30-40 hours of observations, and many hundreds of discharges within a few kilometers of the radar produced only a dozen velocity changes with clear-cut associations with lightning discharges. This absence of results places a constraint on the energy contribution of precipitation which is difficult to quantify for reasons we have already mentioned.

III-3 Vertical Profiles of Mean Doppler Velocity and Radar Reflectivity

III-3.1 Vertical Profiles Prior to the Initial Lightning Discharge

Previous attempts to distinguish the roles of precipitation and convection in electrification have concentrated on cloud development prior to the occurrence of the first lightning discharge (Reynolds and Neill, 1955; Moore et al., 1958; Lhermitte and Krehbiel, 1979). Unfortunately, we were able to obtain Doppler data on a storm in this stage on only one occasion: an isolated thundercloud which formed over the radar on July 6, 1980. Vertical profiles of radar reflectivity and mean Doppler velocity, together with the electric field signal at the ground near the radar, are shown in Figure III-6.

Consistent with earlier results in New Mexico (Reynolds and Neill, 1955) is the appearance of a weak radar echo associated with precipitation and an electric field reversal at the ground from fair to foul weather polarity about 8 minutes prior to the time of the initial lightning discharge.

Local charge conservation forbids the simultaneous appearance of positive and negative charges at different locations, and therefore the accumulation of space charge responsible for this growth of foul weather field must be initiated either by preferentially charged precipitation particles or by an organized motion of pre-existing space charge.

68

If the pre-existing fair weather space charge is to make an initiating contribution, as Vonnegut (1953) has suggested, it must be swept into the cloud by updrafts. Doppler indications of the vertical air motions in the lower cloud which are uniformly downward, do not support this hypothesis. Since the time interval between the onset of corona and the first discharge is only 3 minutes, the positive corona space charge is also not likely to make a significant contribution to the first lightning, in agreement with the conclusions drawn from a cloud model by Winn et al. (1980).

The largest vertical motions observed overhead prior to the first lightning are not air motions but precipitation particle motions (4-5 m/sec), which are available for segregating electric charge. The proximity of the initially developing precipitation echo to the negative charge region observed in other studies (Winn et al., 1981; Krehbiel et al., 1979) further suggests this region as the origin of the initial charge generation.

Although we believe that precipitation is playing a role in initiating the electrification process, its energy contribution remains a problem. The maximum reflectivity overhead at the time of the first discharge is only 5 dBZ, and corresponds with an equivalent precipitation rate of less than 0.01 mm/hr (Battan, 1973) and a gravitational power density of 2.5×10^4 watts/km^3. Although larger reflectivities may be present in regions displaced from the vertical beam, we can make the generous assumption that the maximum radar observed

precipitation rate was present everywhere within a volume of 100 km^3 during the entire 8 minute period of field growth. In such a case, the gravitational potential energy given up by the time of the first lightning is 10^{10} joules. In view of the anticipated inefficient conversion of gravitational to electrical energy in these early stages (see Chapter II), there is some doubt as to whether adequate energy will have been made available for a discharge requiring 10^9 joules (see Section II-3). We note further that no increases in downward particle velocity were noted in any of the 22 range gates under Doppler surveillance at the time of the first lightning.

This difficulty with explaining the first lightning with existing precipitation mechanisms is reflected in theoretical modelling studies (Illingworth and Latham, 1977), which require 20 minutes of sustained precipitation rate of 4 mm/hr to achieve dielectric breakdown in a wide cloud (6.4 km).

We are of the opinion that the air motions occupying a cloud volume far larger than the radar-observed volume contribute to the energy necessary for electrification once it has been initiated. Doppler observations during convectively vigorous and electrically active clouds in the next section provide insight into how this might occur.

III-3.2 Vertical Profiles in a Convectively Vigorous Storm

Figure III-9 shows time-height profiles of radar reflectivity, mean Doppler velocity and the electric field near

Figure III-9
Time-Height Profiles of
Radar Reflectivity and
Mean Doppler Velocity:
August 4, 1980
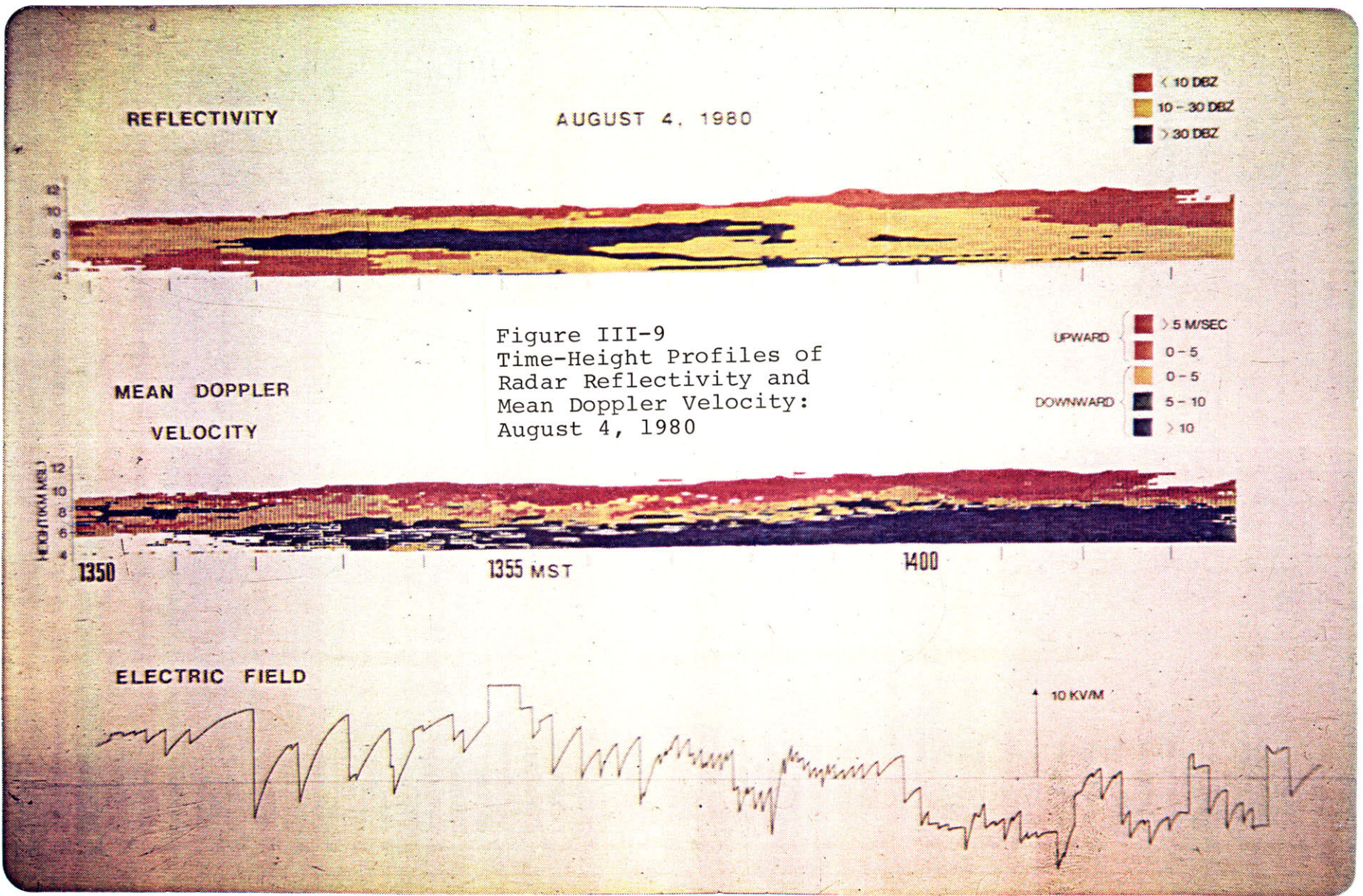
the radar during an unusually electrically active New Mexico thunderstorm. The vertical air velocity reached 22 m/sec and the flash rate exceeded 10 min^{-1} during the 14-minute period shown. Noteworthy is the consistent nature of the draft structure, and its continued intensification which parallels the increase in flash rate and decrease in field change magnitude (recall Section V-6). Also well developed is the reflectivity at mid-levels (35-40 dBZ) which indicates the presence of ice phase precipitation. We note however that the high flash rate is sustained following the decline in reflectivity around 1358 MST, whereas the vertical velocity continues to intensify.

The vertical velocity structure is most intense at 1401 MST and Figure III-10 shows profiles of mean Doppler velocity, calculated vertical air velocity, and radar reflectivity at this time. Note here that the difference between the two velocity profiles represents the terminal velocity of the precipitation particles at the respective levels in the cloud. It is immediately obvious that the precipitation particle terminal velocities are everywhere small compared to the air motions.

We interpret the vertical profiles in Figure III-10 as evidence for a tilted updraft-downdraft structure, with the updraft overlying the downdraft. Such structures probably develop to accomodate the opposing tendencies of latent heat induced positive buoyancy and the negative buoyancy effects of growing precipitation particles. Note that the maximum

72

Figure III-10
Vertical Profiles of
Velocity and Reflectivity
August 4, 1980 New Mexico

RADAR REFLECTIVITY (dBZ)

Mean Doppler Velocity

Radar Reflectivity

Inferred Air Velocity

HEIGHT (km MSL)

DOWNWARD MOTION (m/sec)

UPWARD MOTION (m/sec)

73
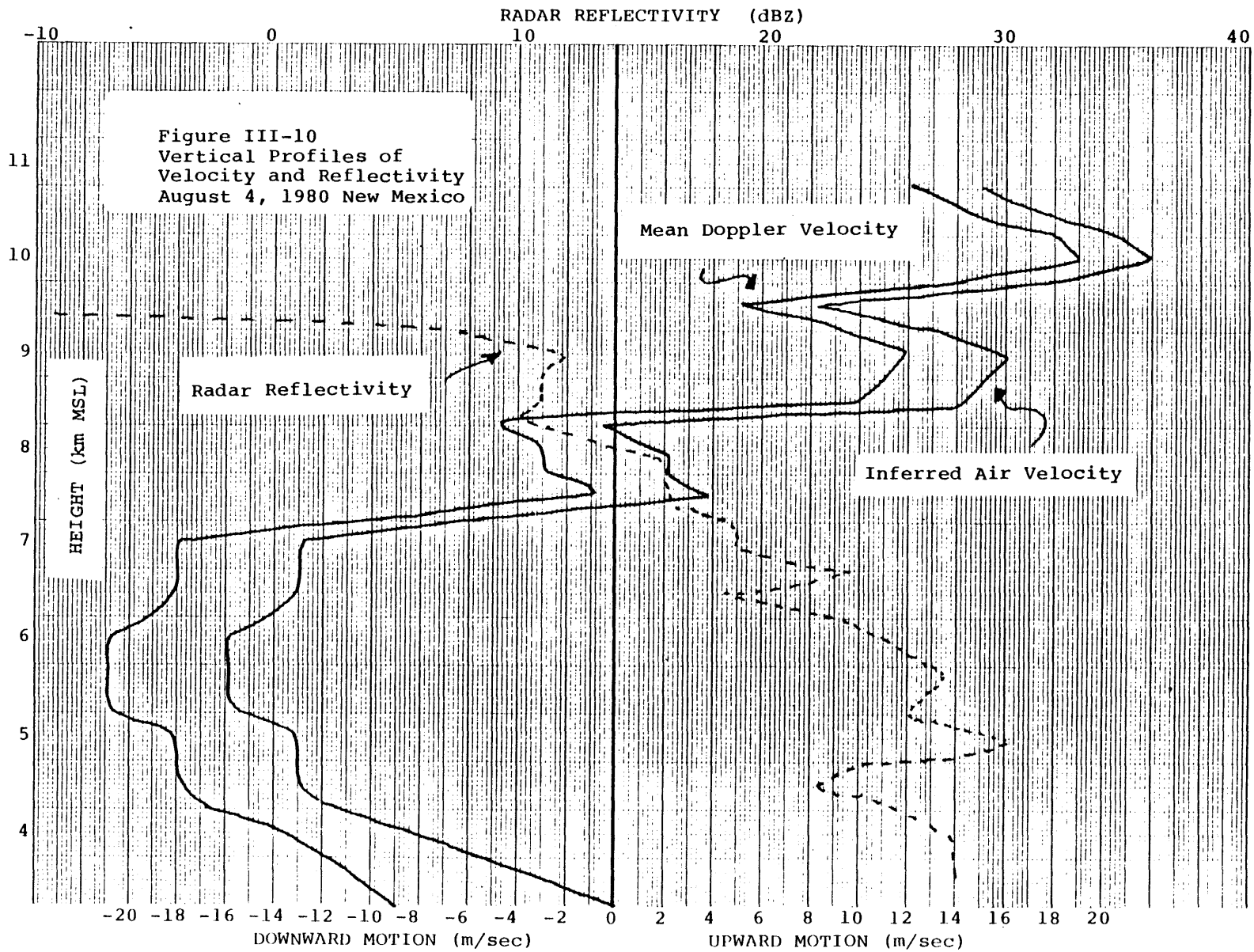
vertical gradient in reflectivity coincides with the transition from downward to upward air motion.

Such tilted draft structures are apparently characteristic of many thunderstorms. Figure III-11 shows two-dimensional Doppler data for a Colorado thunderstorm (Kropfli and Miller, 1976). A zenith pointing Doppler radar positioned as shown would record a vertical profile similar to the one in Figure III-10.

The gross electrical structure of the thunderstorm is that of a positive dipole with negative charge at 5-7 km in New Mexico (Winn et al., 1981; Krehbiel et al., 1979) and positive charge at higher, but less well specified levels. If these respective positive and negative space charge regions coincide with the updraft and downdraft, respectively, then a dipole "stretching" may occur at a rate which in this case may be as large as 38 meters per second, the relative velocity between maximum updraft and downdraft. This velocity is at least 5 times greater than the differential motion resulting from sedimenting precipitation.

Two means are imagined by which electrical energy could be derived from the kinetic energy of air motion in such a flow configuration. A cooperative structure might be established by a precipitation mechanism operating in the transition zone between the updraft and downdraft structures, or by a feedback mechanism like the one proposed by Vonnegut (1953) in which volumes of high density space charge are induced by pre-existing fields. Either mechanism is capable of
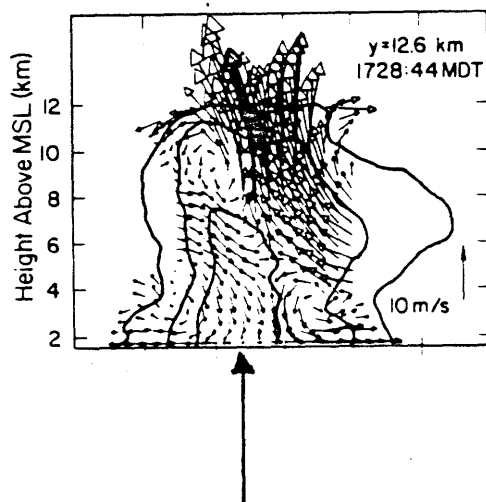
Zenith-pointing Doppler
Radar located here would
record profile shown in
Figure III-10

Figure III-11
Example of Tilted Updraft-
Downdraft Structure from
Kropfli & Miller (1976)

segregating electric charges of opposite sign and making it available for convective transport against the local fields.

A precipitation charging mechanism operating in the updraft (where precipitation growth is likely to occur) and selectively transferring charged precipitation to the downdraft beneath would enable the storm to utilize kinetic energy of air motion for the generation of electrical power.

Alternatively, the asymmetrical flow structure which Figure III-10 implies and which Figure III-11 clearly shows may facilitate the feedback mechanism proposed by Vonnegut (1953). This asymmetry allows a spatial decoupling between updraft and downdraft. The tilted updraft, seen at upper levels in the cloud overhead, may originate at low levels and carry positive space charge to higher levels. For storms whose precipitation cores were displaced from the vertical radar beam, we observed a greater frequency of upward air motion at low levels and a persistence of large amplitude foul weather fields, both of which will facilitate the vertical transport of positive corona space charge to higher levels in the cloud. The downdraft which is often observed at the periphery of the cloud in Doppler radar data, where the radar echo is often very weak (see Figure III-11), may successfully transport negative charge downward if a screening layer has formed there. A model for this process is treated in Chapter VII.

Unfortunately, the energetics of this storm are not well constrained and one can not distinguish definitively the roles of precipitation and convection on this basis. With only

vertical beam data for this storm, the total gravitational

power has not been determined, but no precipitation particle

velocity changes were observed during the period shown in

Figure III-9.

Chapter IV

Thunderstorm VHF Radiation
and Local Radar Reflectivity

IV-1 Introduction

The charged particle motion against the electric field which
is responsible for cloud electrification is expected to operate
effectively in breakdown fields. It is in fact this expectation
that led us to look for (but not find) decreased downward motion
of precipitation particles prior to lightning discharges
(Chapter III). This chapter is concerned with the nature of the
particles in the regions of an active thunderstorm from which
VHF radiation is emitted, very likely regions in which
dielectric breakdown is occurring. We may distinguish
precipitation particles from cloud particles on the basis of
radar reflectivity (since the reflectivity is proportional to
the sixth power of the particle diameter), and inferred
breakdown regions may be accurately located by inverting
multiple VHF receiver data.

IV-2 The Available Data

Radar reflectivity data were obtained with the
sector-scanning C-band Doppler radar which was operated at the
Kennedy Space Center during the August 13, 1978 storm. The
radar beam swept out twelve 60 degree sectors from low to high
elevation angles. This procedure was then reversed, requiring a
total volume scan time of about two minutes. The times at which

particular sectors were scanned was known to within a few seconds. Radar reflectivity estimates were quantized in 5 dB increments, and were available with 600 meter spatial resolution.

VHF source locations were provided by the LDAR (Lightning Detection and Ranging) network of receivers operating in the 30-50 MHz band (Poehler, 1978). This system consists of two independent, four-station time of arrival networks of the 120°-Y configuration. The time arrival data is inverted by computer to locate sources in space with an accuracy often superior to the resolution of the radar data.

IV-3 VHF Source Location Errors

To ensure that the errors in VHF source location were less than the radar resolution of 600 meters, we compared VHF locations evaluated independently from the two separate 4-station arrays. The results of this comparison for over one hundred locations are shown in Figure IV-1. Except for the 15-20% of the locations which had quite large errors (and which were discarded from our comparisons), the discrepancies in location for the two arrays were well within the 600 meter resolution of radar reflectivity (imposed by the finite beam width at the distance of this storm (~ 20 km)).

IV-4 Radar Reflectivity Coincident with VHF Source Locations

Figure IV-2 shows the results of the radar-VHF comparisons. To ensure excellent temporal as well as spatial resolution,

79

Figure IV-1
VHF Source Location Errors

Figure IV-2
Distribution of Radar
Reflectivity at VHF Source
Locations

81
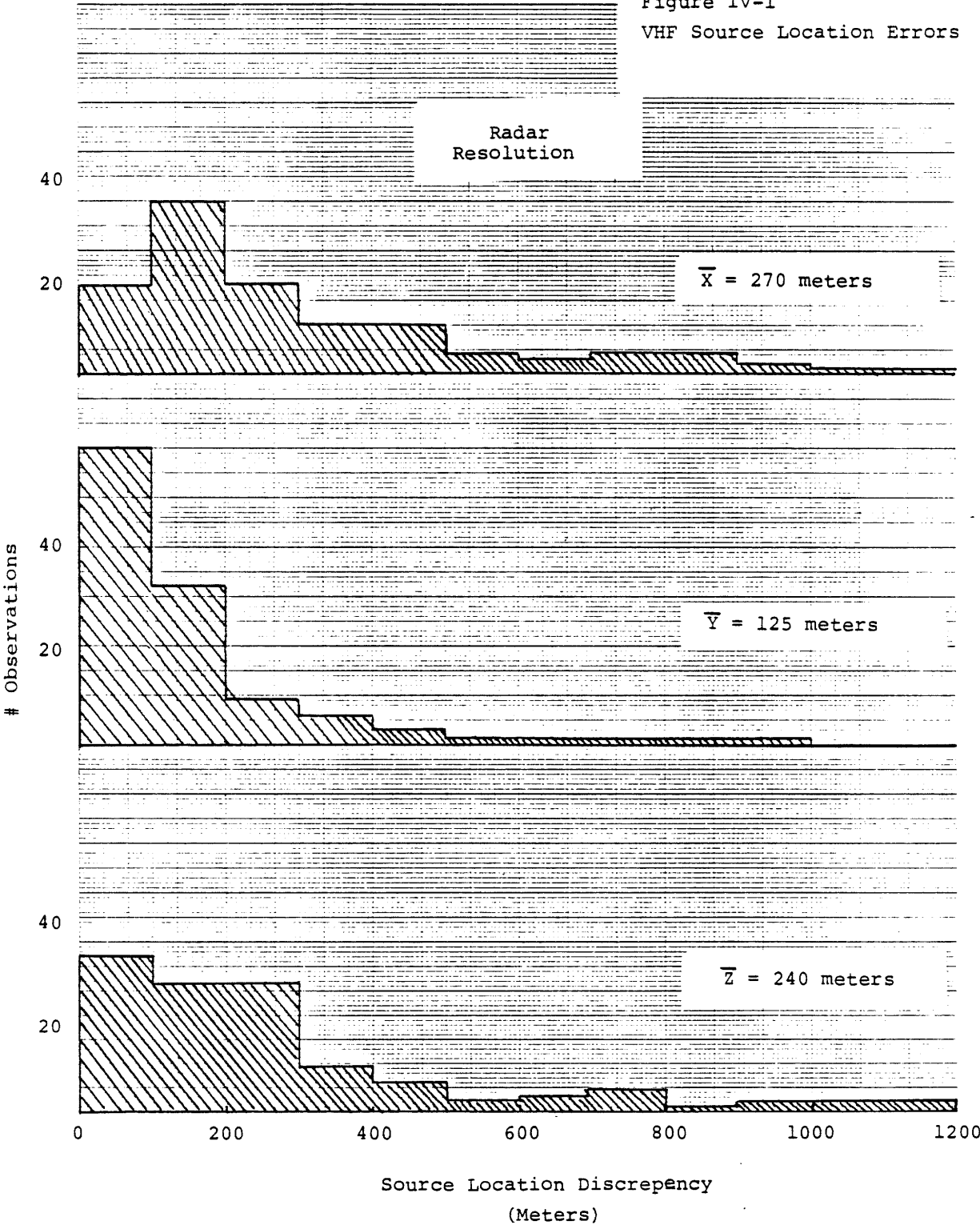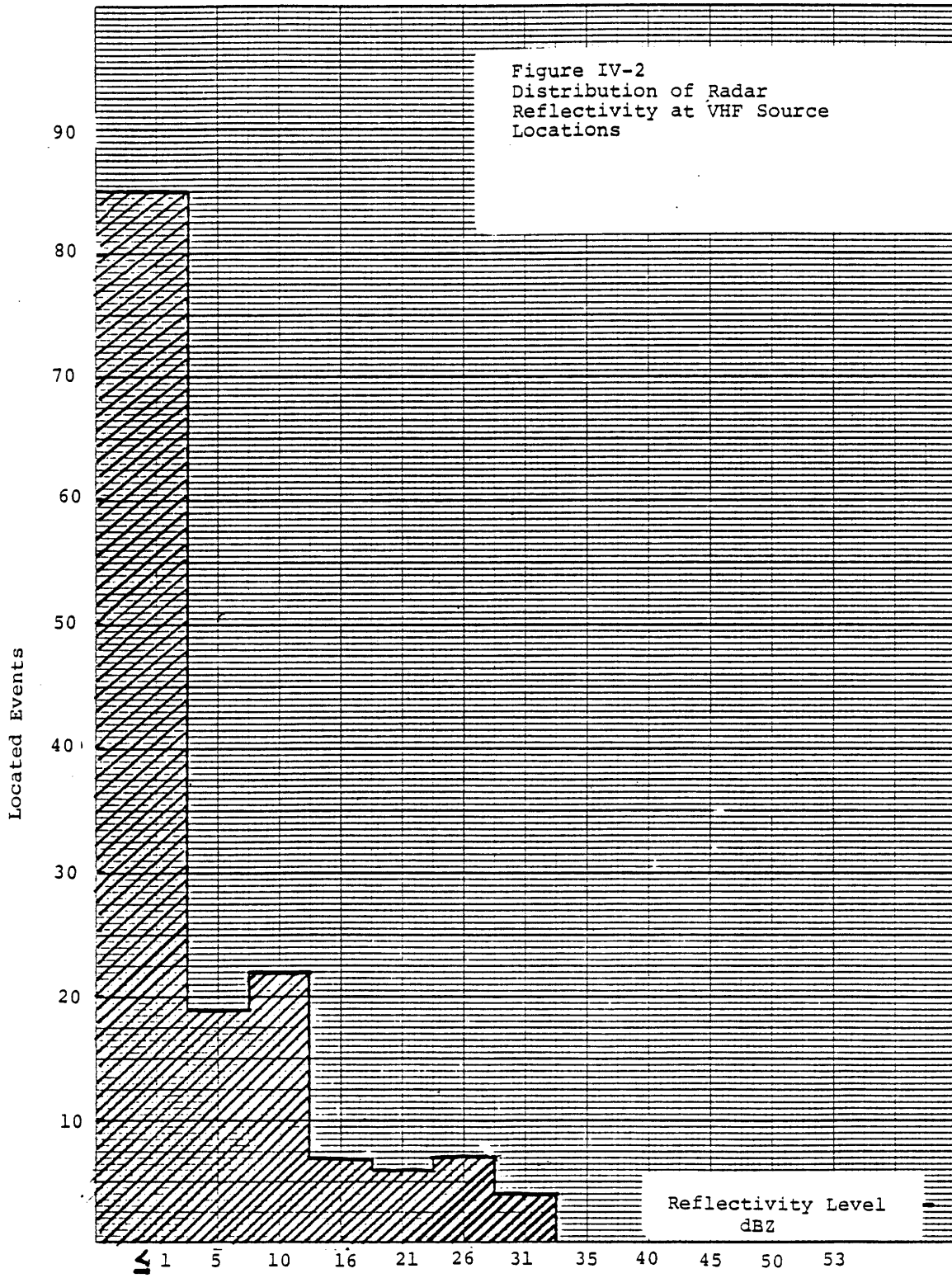
only VHF origins which occurred within 30 seconds and 600
meters of a particular sector scan were selected for
comparison. In keeping with our intent to determine the origin
of dielectric breakdown in the cloud, only the first pulse of a
discharge event was located for comparison.

In spite of these restrictions, approximately 120
comparisons were possible within an active 25 minute storm
period. Well over half of the VHF origins occurred where the
radar reflectivity was below the recording threshold (about 0
dBZ). Only about 10% of the VHF origins coincide with
reflectivities in excess of 20 dBZ. The maximum reflectivity
which coincides with a VHF origin is 30 dBZ, whereas the core
of this storm exhibited reflectivities in excess of 50 dBZ.

These results indicate that regions of VHF emission are <u>not</u>
regions of intense precipitation.

IV-5 <u>VHF</u> <u>Emission</u> <u>and</u> <u>Reflectivity</u> <u>Intensification</u>:
      <u>Determination</u> <u>of</u> <u>Precedence</u>

In order to further constrain the interpretation of these
data, we have also looked at the evolution of the VHF radiation
and reflectivity structures. Figure IV-3 is the first of three
figures which will show radar sector scans at a common
elevation angle but separated in time by the interval required
to complete a set of sector scans at several elevation angles
(in this case about 3-4 minutes). Radar reflectivity values
are coded as shown, with 600 meter grid spacing.
Reflectivities greater than 25 dBZ are contoured with a black

82

North

Storm
Motion

Radar
Location

0 = 5 dBZ
1 = 10
2 = 16
3 = 21
4 = 26
5 = 31
6 = 35

Figure IV-3
Radar Scan at 190624 GMT;
Reflectivity and VHF
Source Locations ●

83
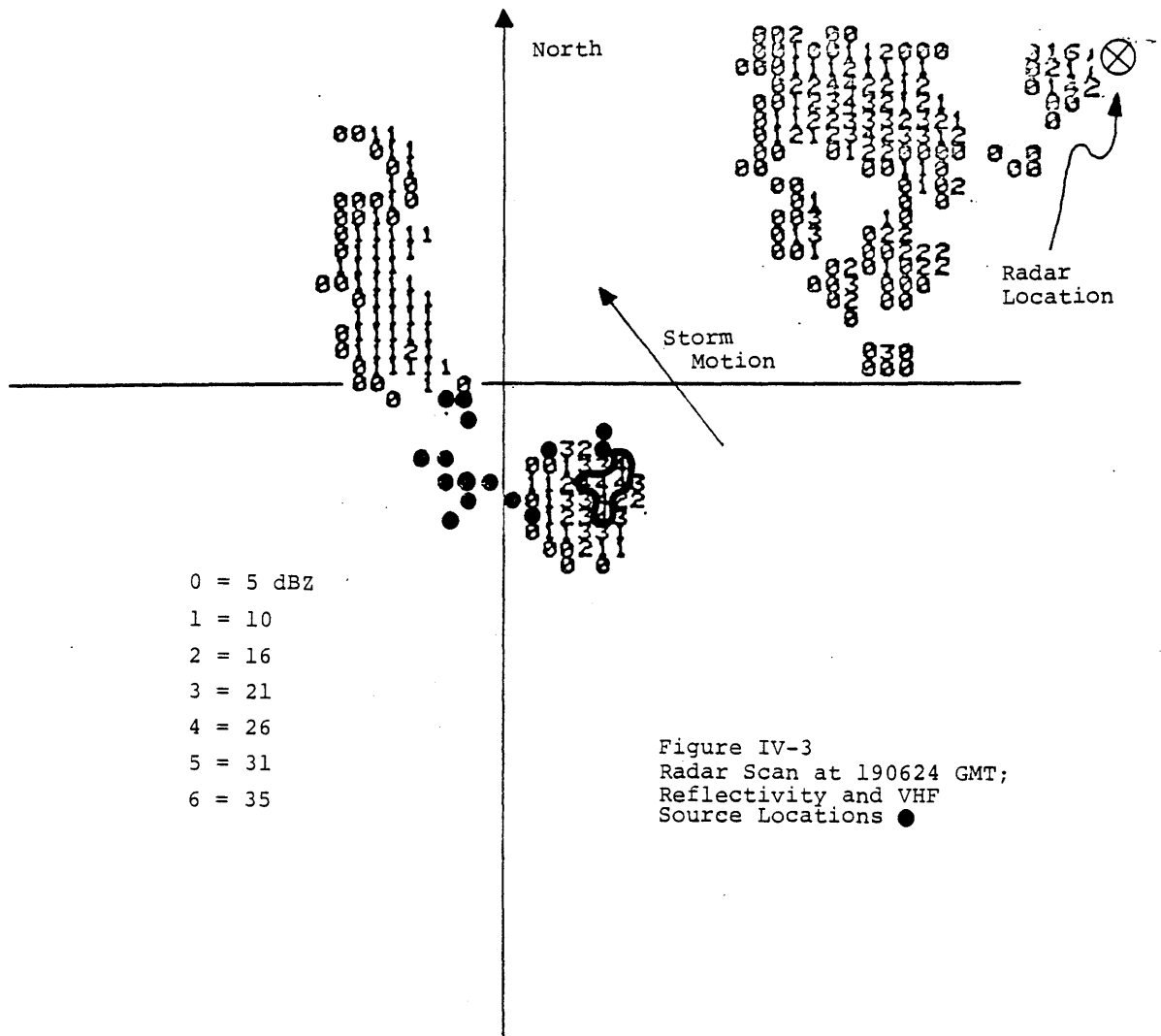
line. These particular sector scans intersect the storm at a

height of 8.7 km which is near the center of the maximum VHF

activity. Superimposed as dots on the reflectivity data are

the VHF source locations. Note that in this scan the VHF

sources are located in weak reflectivity and are displaced from

the radar echo maxima, in this case 1-3 km to the northwest

which is the direction of storm motion. In Figure IV-4

(3 minutes later) the VHF sources are again displaced to the

northwest, but now the reflectivity maximum is located where

the VHF sources occurred in the last scan. In Figure IV-5, the

third scan, the reflectivity maximum again coincides with the

VHF source locations 3-4 minutes earlier. VHF locations for

this scan were not available.

These data show a clear tendency for VHF emission to

precede the development of substantial radar reflectivity.

IV-6 Comparisons with the Dual-Doppler Derived Wind Field

Lhermitte and Krehbiel (1979) have presented Doppler data

for the August 13, 1978 storm. Figure IV-6 shows a storm

cross-section approximately aligned with the storm's direction

of translation (at the time of our VHF comparisons), which

displays both the dual-Doppler derived wind field and the

reflectivity structure. Though the velocity data lack the

temporal resolution available with the sector-scanned

reflectivity, it can be seen that the maximum updraft

velocities are, like the VHF origins, displaced 1-2 kilometers

North

Storm
Motion

Radar
Location

0 = 5 dBZ
1 = 10
2 = 16
3 = 21
4 = 26
5 = 31
6 = 35

Figure IV-4
Radar Scan at 191005 GMT;
Reflectivity and VHF
Source Locations ●

North

Storm
Motion

Radar
Location

0 = 5 dBZ
1 = 10
2 = 16
3 = 21
4 = 26
5 = 31
6 = 35

Figure IV-5
Radar Scan at 191427 GMT;
Reflectivity Data Only

Updraft Core

Reflectivity Core

Direction of Storm Motion

10 m/sec

$19^h 07^m$ TO $19^h 09^m$ GMT

Figure IV-6
Velocity and
Reflectivity Structure
August 13, 1978

Lhermitte and Krehbiel
(1979)

9

6

3

HEIGHT (km)

50

45

40
35

45

10 km

87 .

downstream from the region of maximum reflectivity. It is
therefore quite likely that an updraft with weak reflectivity
and the VHF source region closely coincide.

IV-7 Vertical Distributions of VHF Source Locations, Air Velocity, and Gravitational Power

In Figure IV-7 are shown the vertical distribution of VHF
source locations, the vertical profile of maximum vertical air
velocity, and the gravitational power profile associated with
the radar-observed precipitation during the most active storm
period. The updraft maximum coincides closely with the VHF
source locations, whereas the bulk of the available
gravitational power lies several kilometers lower in the storm.

IV-8 Discussion of Results

The interpretation of the results presented in this Chapter
is by no means unique. Several possibilities exist and will be
discussed in turn.

(1) The possibility exists that the initial VHF source
locations are not reliable indicators of breakdown regions. It
is possible that the radiation at VHF is weak during the
initial breakdown phase and that a sufficiently high LDAR
threshold would prevent its detection. This situation is
unlikely, however, since other studies of the preliminary
breakdown period prior to the stepped leader have demonstrated
the existence of VHF pulses prior to or simultaneous with the
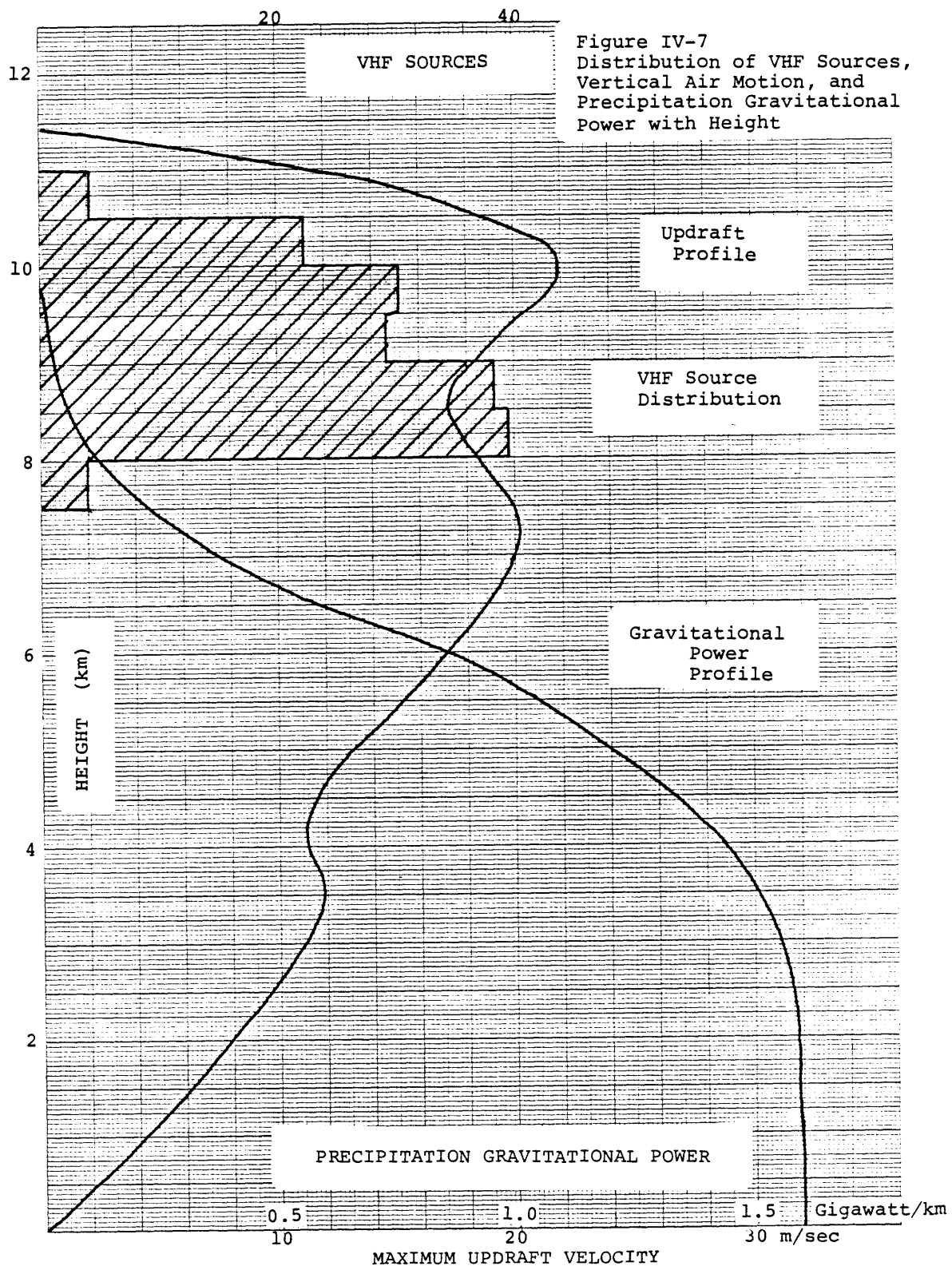
Figure IV-7
Distribution of VHF Sources,
Vertical Air Motion, and
Precipitation Gravitational
Power with Height

89

earliest signatures in other detectors (Rustan et al., 1980;

M. Brook, private communication). The systematic evolution of

the VHF sources relative to the reflectivity development

(Section IV-5) supports the view that these source locations

are meaningful in the sense suggested in the Introduction.

(2) Perhaps the generation of electrical energy due to

falling precipitation is taking place in weak field regions

where breakdown is unlikely to occur. One could probably

fabricate a thunderstorm model in which the bulk of the

charging current was located in weak field regions, and in

which the maximum field region contained very little charging

current, yet was responsible for breakdwon initiation. Though

this scenario may be marginal from an energy standpoint (see

Chapter II), it cannot be ruled it out. However, the

necessarily large gravitational-to-electrical efficiency in

weak field regions will require the existence of large charges

on precipitation particles (thousands of picocoulombs; see

Figure II-5). Such charge magnitudes are larger by an order of

magnitude than any which have been measured (Gaskell et al.,

1978; Marshall and Winn, 1980). At least one precipitation

mechanism, induction charging, requires the co-existence of

intense precipitation and large vertical field for efficient

operation.

(3) Regions of intense precipitation may somehow dissipate

the local field and prevent the occurrence of breakdown. A

justification of this assertion for regions of liquid

precipitation has been put forward by Vonnegut (1968). Such a

scenario could explain the absence of VHF emission in regions

of large reflectivity, but argues strongly against

precipitation as the major contributor to cloud

electrification.

(4) Lhermitte and Krehbiel (1979) have suggested that

breakdown may occur at the edge of a highly charged

precipitation region, where the electric field is expected to

be greatest. If we make the simplest assumption that the

charge on the precipitation is proportional to its reflectivity

signature, then the "edge" of the inferred precipitation charge

region (and the resultant breakdown location) should correspond

with maximum values of $Z \nabla(dBZ)$ where Z is the local

reflectivity and $\nabla(dBZ)$ is the gradient in logarithmic

reflectivity. Our comparisons indicate that not only do the

VHF sources lie in regions of low reflectivity, but they also

lie well outside the reflectivity "edge" as specified by this

latter criterion (see Figure IV-6).

(5) A final possible interpretation, and the one favored

here is that the progression to breakdown takes place as the

result of the motion of cloud particles (of low radar

reflectivity). The existence of intense vertical air motion in

the region in question (Figure IV-6) supports this view.

The intensification of reflectivity subsequent to the time

of VHF emission and inferred breakdown may be explicable in

terms of the raingush mechanism described by Vonnegut and Moore

(1960) in which electrical forces hasten the coalescence of

oppositely charged cloud particles.

IV-9   Conclusion

Sources of VHF emission in an active thunderstorm are
conspicuously absent in regions of large radar reflectivity and
predominate in weak reflectivity regions high in the cloud.
These sources also coincide with a region of substantial
vertical motion and precede the growth of radar reflectivity.
The interpretation of these results is that the motion of
charged cloudy air is responsible for dielectric breakdown (and
consequent VHF emission), a process which in turn may promote
the coalescence of cloud particles and intensify the local
reflectivity.

Chapter V

Scaling Law Tests For Thunderstorm Electrification

V-1   Introduction

This chapter is concerned with scaling relationships for parameters relevant to electrification. One relationship of particular interest is how the electrical output of a thunderstorm depends on its size and how this dependence may distinguish between precipitation- and convection-driven electrification.

Section V-2 through V-4 are concerned with the dependence of cloud potential, charge transport velocity, charging current, and steady state electrical power, respectively, on cloud size. Flash rate and cloud height data from several different sources are used to check these predictions in Section V-5. These arguments lead naturally to an examination of the scaling behavior of lightning flash energy in Section V-6.

Scaling relationships for which we lack adequate data to test concern the subcloud corona current (Section V-7), the precipitation gravitational power (Section V-8), and the existence of lightning in warm clouds (Section V-9).

The electric Reynolds number, a scaling parameter common to electrohydrodynamics and which surfaces in the treatment of screening layer convective charge transport in Chapter VII, is discussed in the final section (V-10).

V-2   Scaling Behavior of Cloud Charging Current and Potential Difference

Thunderstorms tend to be equidimensional, with the exception of squall line systems, and so can be characterized by a single length parameter L.   Simple scaling relationships for a thunderstorm with gross positive dipole structure are shown in Figure V-1.

Gauss' Law relates a spatial first derivative of electric field to the space charge density, and therefore the electric field will scale as L, assuming the space charge density is a local property and hence scale independent.   The potential difference across the thunderstorm dipole is the spatially integrated electric field and therefore scales as L^2.   The charging current I is the current density integrated over the storm cross-sectional area and scales as the product of the charge transport velocity and L^2.   Such relationships were first discussed by Vonnegut (1963).

V-3   Charge Transport Velocity

A distinction between charge transport by precipitation and charge transport by convection may be drawn on the basis of how the velocity V depends on storm size.   Precipitation terminal velocities are not strongly dependent on storm size and to first order are scale independent.   Convective air velocities, on the other hand, increase with the size of the cloud.   The velocity of buoyant bubble-like convection scales as $L^{1/2}$ (Scorer, 1958).   The velocity dependence in real clouds appears to be more strongly dependent on size.
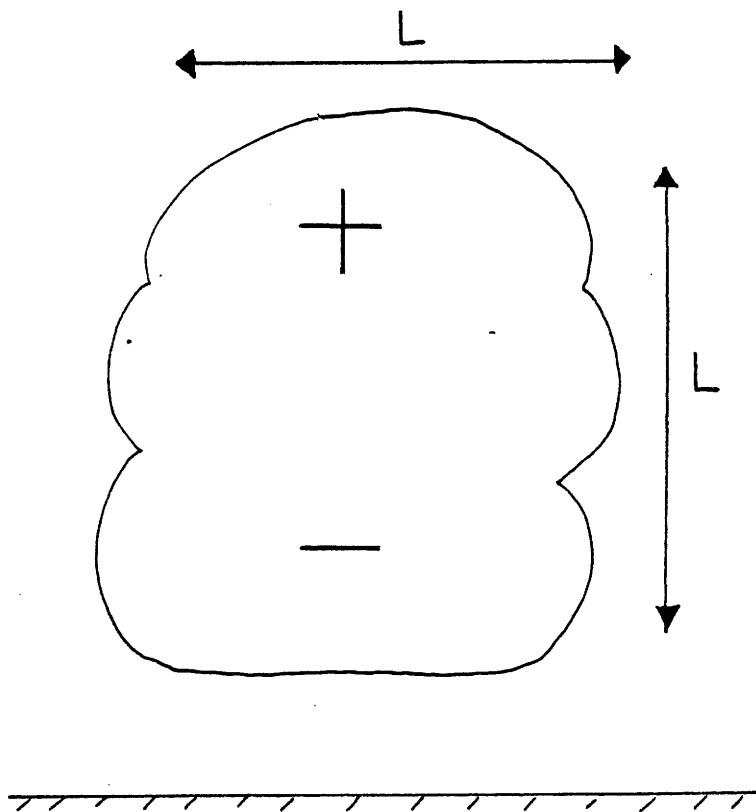
Electric Field (E)

Gauss' Law $\nabla \cdot E = \rho / \varepsilon$

$\rightarrow E \sim \rho L \sim L$

Potential Difference (P.D.)

$P.D. = \int E \cdot dl \sim \rho L^2 \sim L^2$

Charging Current (I)

$I \sim J \cdot (area) \sim \rho V L^2 \sim V L^2$

Electrical Power (P)

$P = I \cdot (P.D.) \sim V L^2 \cdot L^2 \sim V L^4$

Figure V-1
Scaling Relationships

Figure V-2 presents a partial compilation from the literature of cloud heights and their associated maximum air velocities. Data were obtained from both aircraft measurements and vertical Doppler radar estimates. Although data from large storms are scarce, estimates based on the observed stratospheric penetrations result in updraft velocities in excess of 100 m/sec (Vonnegut and Moore, 1958).

Also shown in Figure V-2 are the theoretical $L^{1/2}$ prediction and a linear scaling law, which is a better fit to the data.

V-4   Electrical Power Scaling

The electrical power generated is the product of charging current and potential difference and scales as the product of charge transport velocity and the fourth power of cloud size. With the results from Sections V-2 and V-3, we now have predictions for the electrical power scaling behaviors for precipitation- and convection-driven electrification. For precipitation, electrical power varies as the fourth power of the cloud size and for convection should vary in the range $L^{9/2}$ to L^5.

V-5   Scaling Law Tests: Flash Rate and Cloud Height Data

In testing these predictions, we use the mean sea level height of a thunderstorm as a measure of its size L, and assume for the moment that the lightning flash rate is a reliable measure of the electrical power produced by the storm (a thorough discussion of flash energy scaling is found in

Figure V-2
Convective Velocity vs.
Cloud Size

Maximum Velocity (m/sec)

CLOUD HEIGHT (km)

Data from: Adler & Penn (1979)
Battan (1975)
Battan & Theiss (1965, 1970)
Donaldson (1967)
Kelly et al, (1978)
Kropfli & Miller (1976)
Lawson (1979)
Malkus (1954)
Shenk (1974)
Shmeter & Silaeva (1966)
Steiner & Rhyne (1964)
Telford & Warner (1962)
Warner (1969)
Wilson & Fujita (1979)
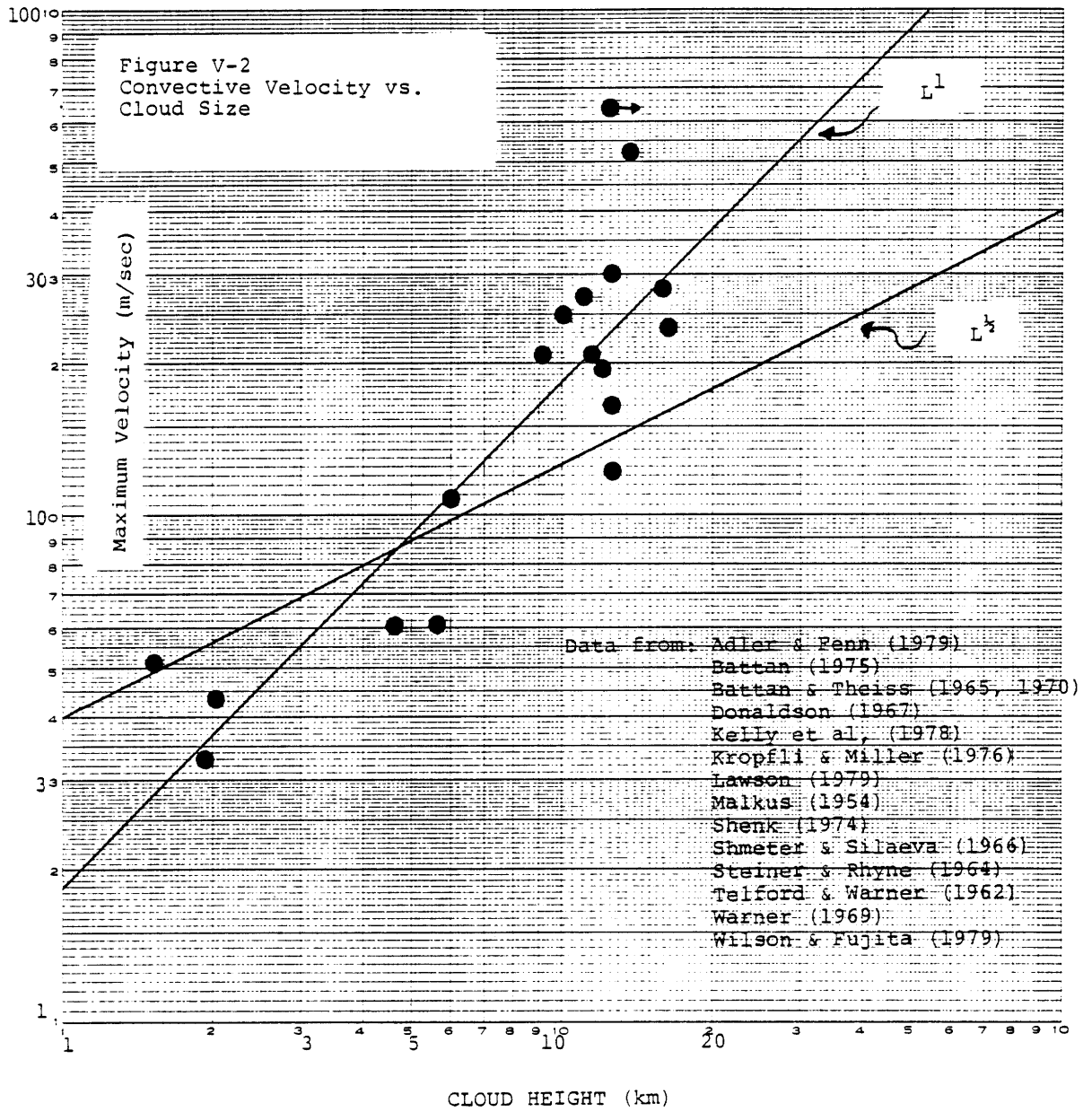
Section V-6). Two sets of data from the literature

(Shackford, 1960 and Jacobson and Krider, 1976; Livingston and

Krider, 1978), as well as data collected at Langmuir

Laboratory, were used to test the scaling law predictions.

The literature data, one set from Florida and one set

from New England, are shown in Figure V-3. Flash rates were

averaged for storms over 1 km height intervals, and the

standard deviations resulting from this procedure are shown.

The Florida data showed a slope of 4.6 and the New England

data a slope of 5.0.

More reliable data on thunderstorm heights were obtained

in New Mexico. Again the flash rate-storm height data showed

considerable variability, but the data from the most active

storms in each height interval, which would most likely

follow the predictions of a steady state model, did show more

consistent behavior. Figure V-4 shows the results for the

most electrically active storms. The least squares fit to the

data has a slope of 4.4 with a standard deviation of 0.5.

Data for the top two flashing rates in each height interval

(not plotted in Figure V-4) showed a steeper slope of 4.9 with

a standard deviation of 0.4.

In summary, all the data presently available are in closer

agreement with the convective charge transport prediction than

with the precipitation prediction. We note, however, that the

two predictions are not sufficiently different to allow a

definitive distinction between precipitation and convection.

98
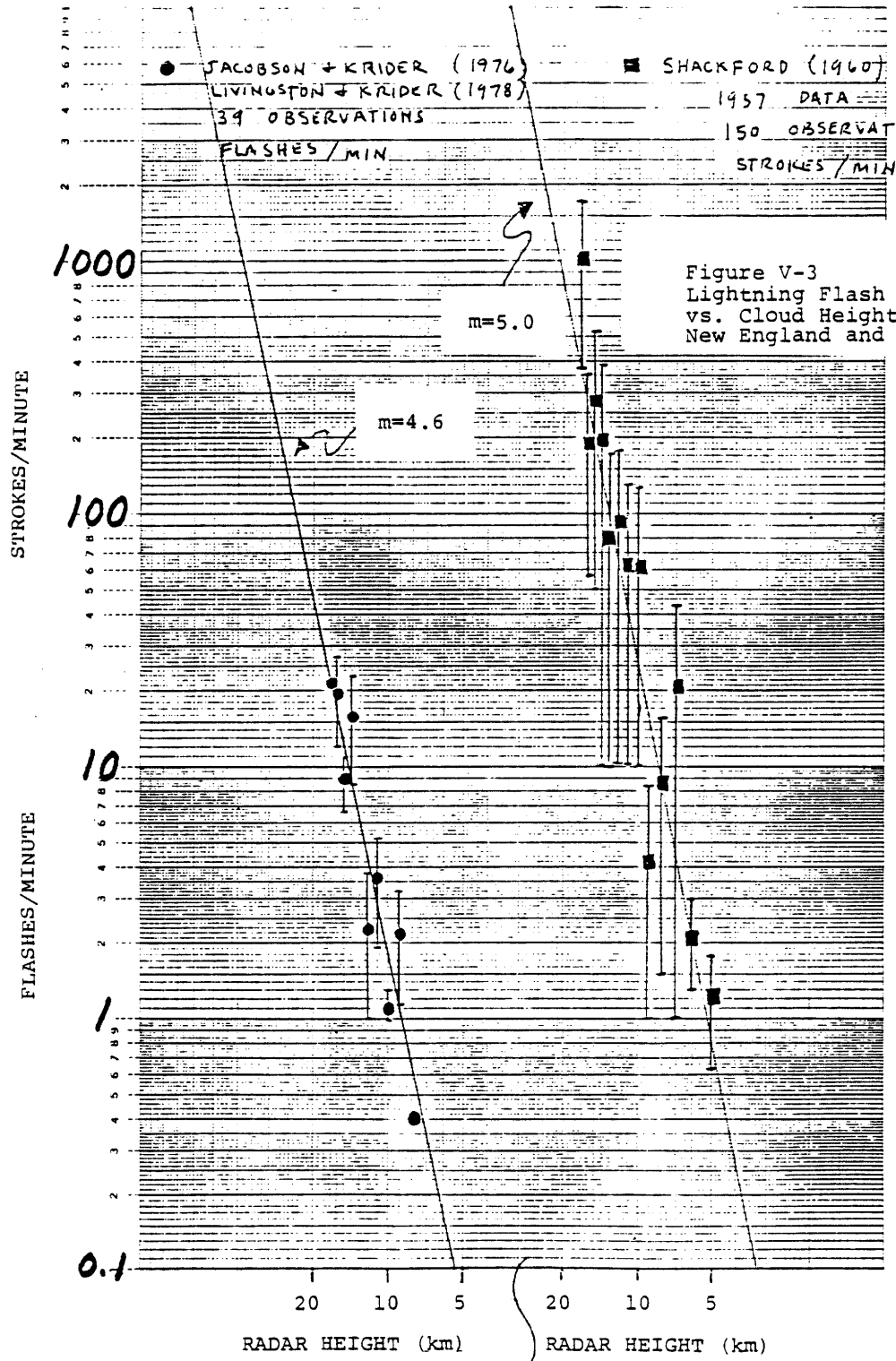
Figure V-3
Lightning Flash Rate
vs. Cloud Height:
New England and Florida

Figure V-4
Lightning Flash Rate
vs. Cloud Height:
New Mexico

(Most active storms)

RADAR HEIGHT   (Km MSL)
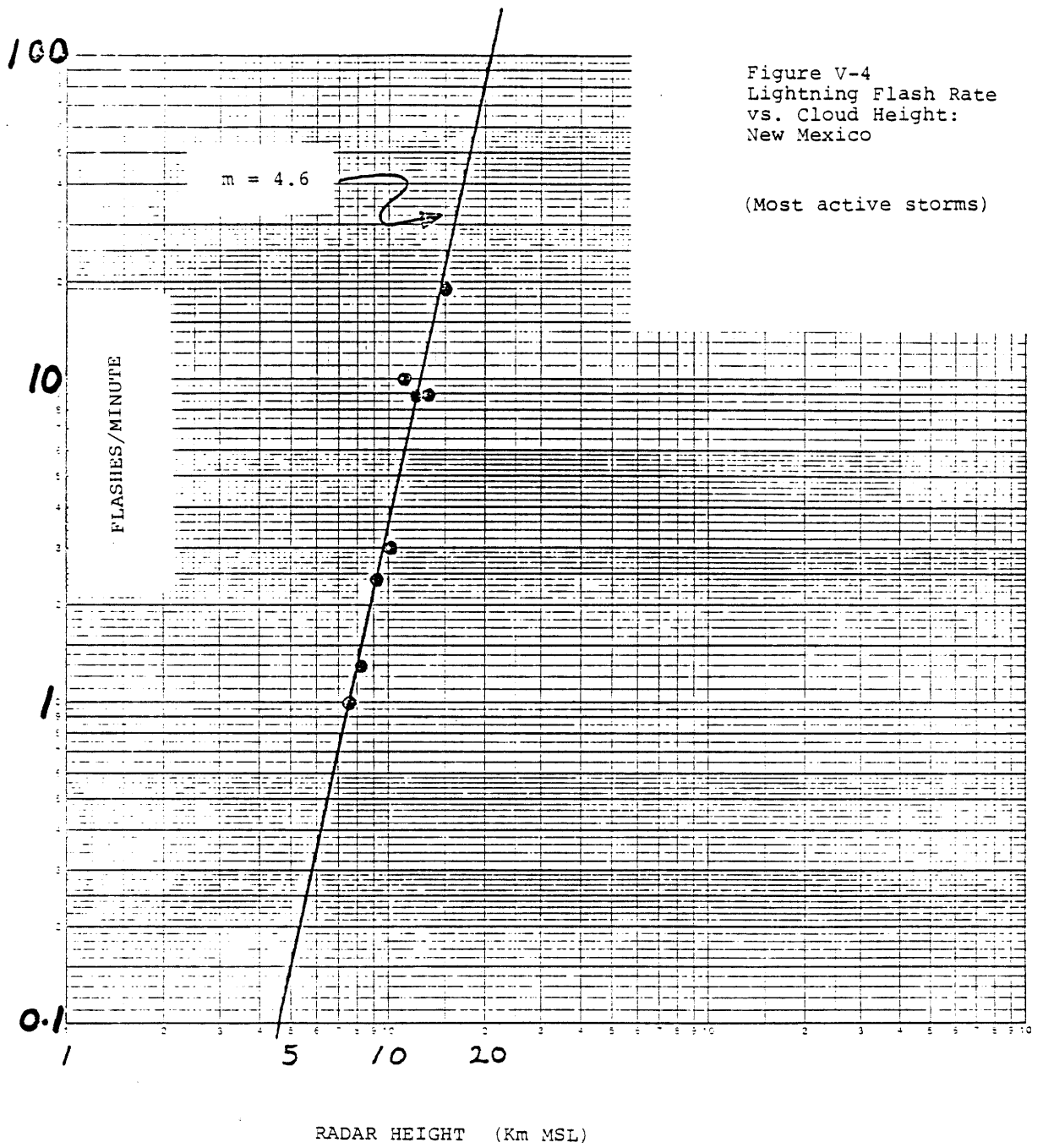
A final test of the scaling law predictions is a flash rate versus cloud height comparison over the lifetime of a storm. Dr. Marx Brook has kindly supplied fast vertical scanning radar data and field change data for an unusually tall (>17 km MSL) Florida thunderstorm (August 10, 1976), with which we can make this comparison. The radar cloud top and flash rate data (at 1 minute intervals) are plotted in Figure V-5. Also calculated and plotted are the cloud heights raised to the 5th power. Note that this parameter and the flash rate track very closely for more than an hour. Phase shifts which we have noted in short duration thunderstorms, for which the steady state assumption is not upheld, are small for this case. Only in the decaying phase of the storm do the plotted parameters diverge, but it is at this time that the storm is shallow and widespread and the assumption of equidimensionality is least likely to be upheld.

V-6 Flash Energy Scaling

In the simple thunderstorm scaling model presented in Figure V-1, the electrical power is generated continuously. To get a measure of this rate in real thunderclouds in the last section, we time averaged the lightning flash dissipation rate (Section V-5), and in so doing, implicitly assumed that the energy per flash was independent of cloud size and flash rate. In this section we examine possible constraints on the validity of this assumption.

We first examine two cases of an alternative assumption, referred to here as the total neutralization assumption and

101

Figure V-5
Temporal Variation of
Lightning Flash Rate
and Cloud Height:
Florida Day 223, 1976
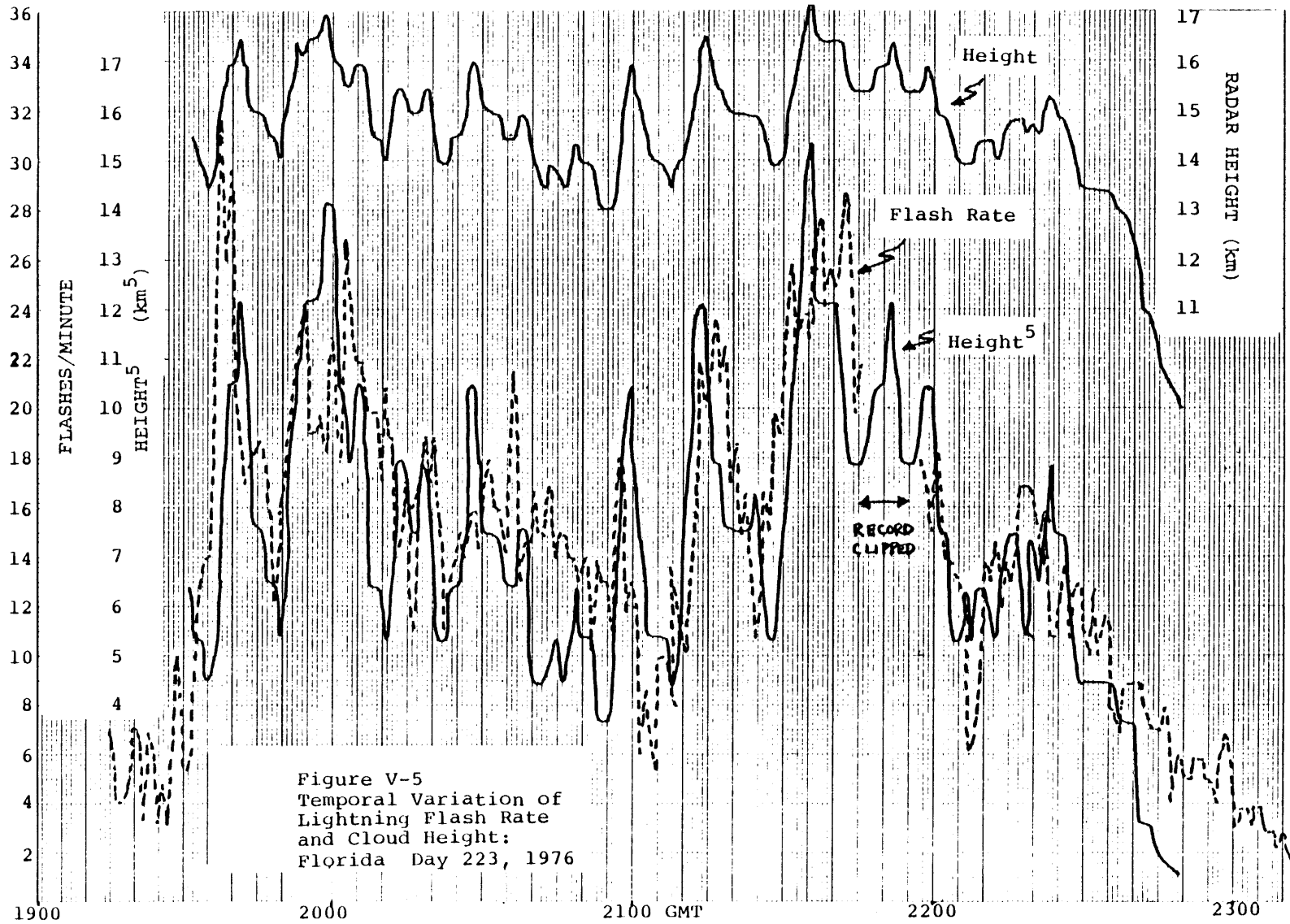
summarized in Figure V-6. In Case I we assert that the charge

neutralized by lightning closely coincides with the charge

which produced the lightning. Retaining the assumption of

space charge density scale invariance, one would predict that

the neutralized charge would depend on the cloud volume, as L^3.

In this case the flash energy would scale as the fifth power of

the storm size, and combined with the empirical results on

flash rate, would result in a 10th power dependence for

electrical power, which is grossly inconsistent with both the

simple scaling model predictions.

In Case II, we assume that the accumulation of

electrostatic energy is terminated by a critical field

conditions. Electric charge $\pm Q$ accumulates in the upper and

lower spheres of a thunderstorm dipole until

$$E_{crit} = \frac{Q}{4\pi\varepsilon\left(\frac{L}{4}\right)}$$

and so $Q \sim E_{crit}L^2$. If E_{crit} is independent of cloud size and

again all the energy is destroyed by the discharge, then the

energy $\sim Q\Delta V \sim \frac{Q^2}{L} \sim L$. In this case, therefore, the electrical

power scaling will be $L^5 \cdot L^3 \sim L^8$, and is again inconsistent with

the predictions.

The breakdown of the total neutralization assumption is

consistent with Vonnegut's (1979) criticism of the inferences

drawn from the charge location technique (Krehbiel et al.,

1979), in which the identity between Q and ΔQ is implicitly

assumed.

103

Figure V-6

Flash Energy Scale Dependence

Total Neutralization Assumption

Case I ΔQ coincides with initial Q

$$\Delta Q \sim \rho L^3 \sim L^3$$

$$\text{Energy} \sim (\Delta Q)(\Delta V) \sim \rho L^3 \cdot L^2 \sim L^5$$

$$\text{Power} \sim \left(\begin{array}{c}\text{Flash}\\\text{Energy}\end{array}\right)\left(\begin{array}{c}\text{Flash}\\\text{Rate}\end{array}\right) \sim L^5 \cdot L^5 \sim L^{10}$$

Case II   Critical Field Condition

$$E_{crit} \sim \frac{Q}{L^2}$$

$$Q \sim E_{crit} L^2 \sim L^2$$

$$\text{Energy} \sim \frac{Q^2}{L} \sim \frac{L^4}{L} \sim L^3$$

$$\text{Power} \sim (L^3) \cdot (L^5) \sim L^8$$

Flash Energy Scale Invariance

$$\text{Energy} \sim L^0$$

$$\text{Power} \sim (L^0)(L^5) \sim L^5$$

$$\Delta Q \sim \frac{\text{Energy}}{\Delta V} \sim \frac{L^0}{L^2} \sim L^{-2}$$

If however we adhere to our original (implicit) assumption of lightning energy scale invariance, we predict that the net charge redistributed by lightning will be inversely related to the flash rate and cloud size. We now present further evidence for this unexpected result.

A common feature of electric field records beneath (see for example Figure V-7 from Livingston and Krider (1978)) thunderstorms is for the magnitude of the field changes to decrease as the flash rate increases. A similar trend is observed within the cloud. Winn and Byerley (1975) found fractional field changes of about 40% for New Mexico clouds producing 1-2 flashes per minute, whereas Christian (1976) found smaller fractional changes in a larger, more active storm at the same location (see Figure V-7).

The currently available data on lightning neutralized charge magnitudes support the view that the smaller field changes are associated with higher flash rates and (presumably) larger clouds. Figure V-8 includes cloud-to-ground data from Winn and Byerley (1975), Jacobson and Krider (1976), Uman et al., (1978), and Krehbiel et al., (1979), as well as intra-cloud estimates (Nakano, 1979, and personal communication). Cloud heights were not reported for most of these measurements and we have therefore used the flash rate F as the scaling parameter. The resulting scaling relationship is easily shown to be $\Delta Q \sim F^{-2/5}$ if the flash rate is proportional to L^5 and if the flash energy is scale invariant. Although the ΔQ data exhibit considerable scatter,

Figure V-7
Variation of Field Change
Magnitude with Lightning
Flash Rate

Livingston &
Krider (1978)
Ground Records

(1)

6-14-74
SITE 7

7-1-74
SITE 25A

6-17-75
SITE 8

6-17-75
SITE II

7-8-76
SITE 12

ELECTRIC FIELD (kV/m)
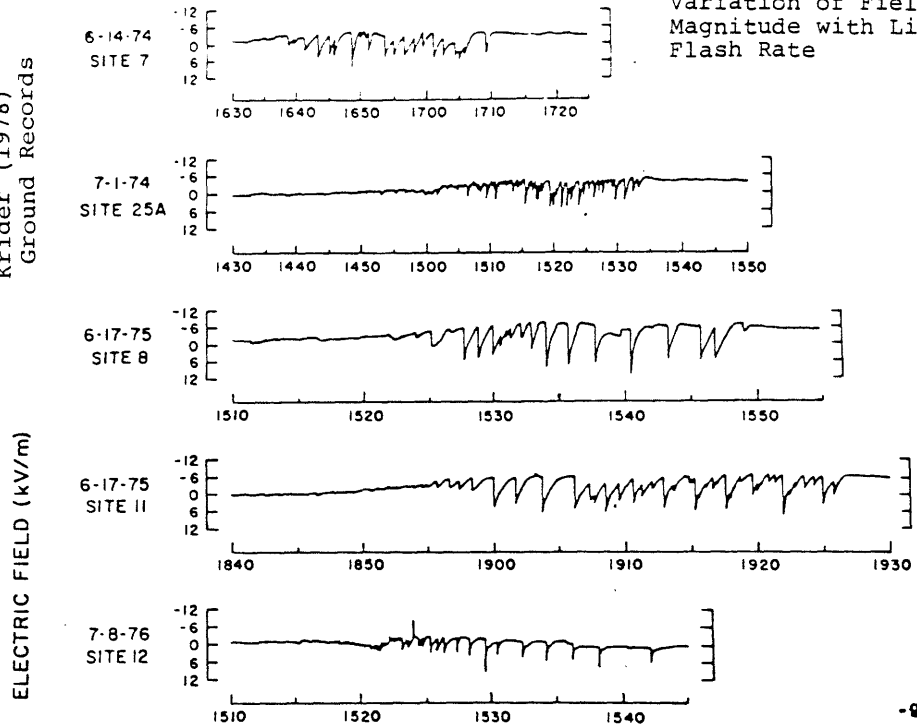
(2) Winn &
Byerley
(1975)
In Cloud

(3) Christian (1976)

In Cloud

E (kv/m)

TIME (msl)

ALTITUDE (km)

106
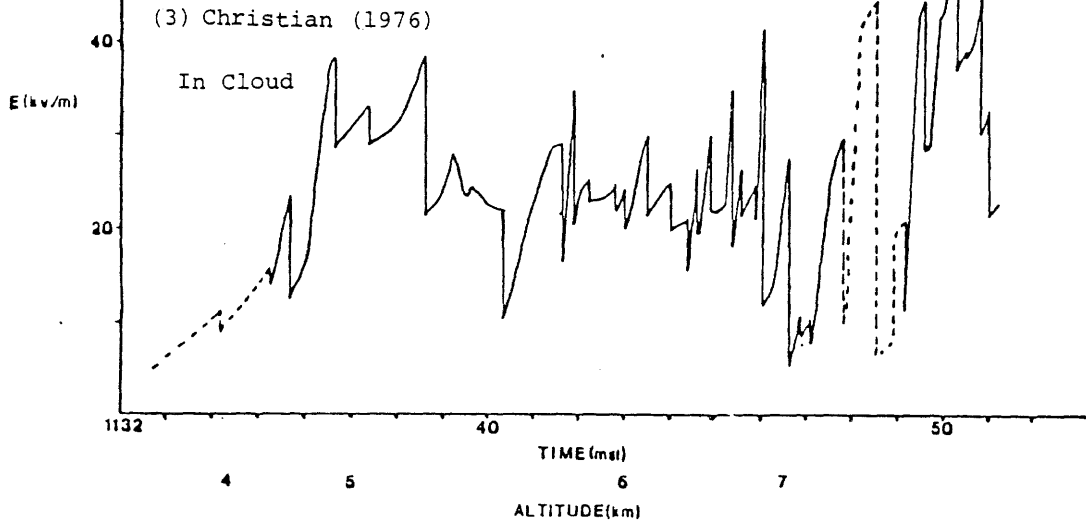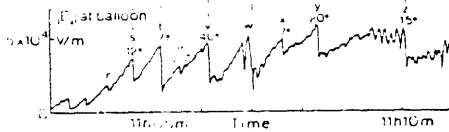
Figure V-8
Net Charge Change
vs. Lightning Flash
Rate
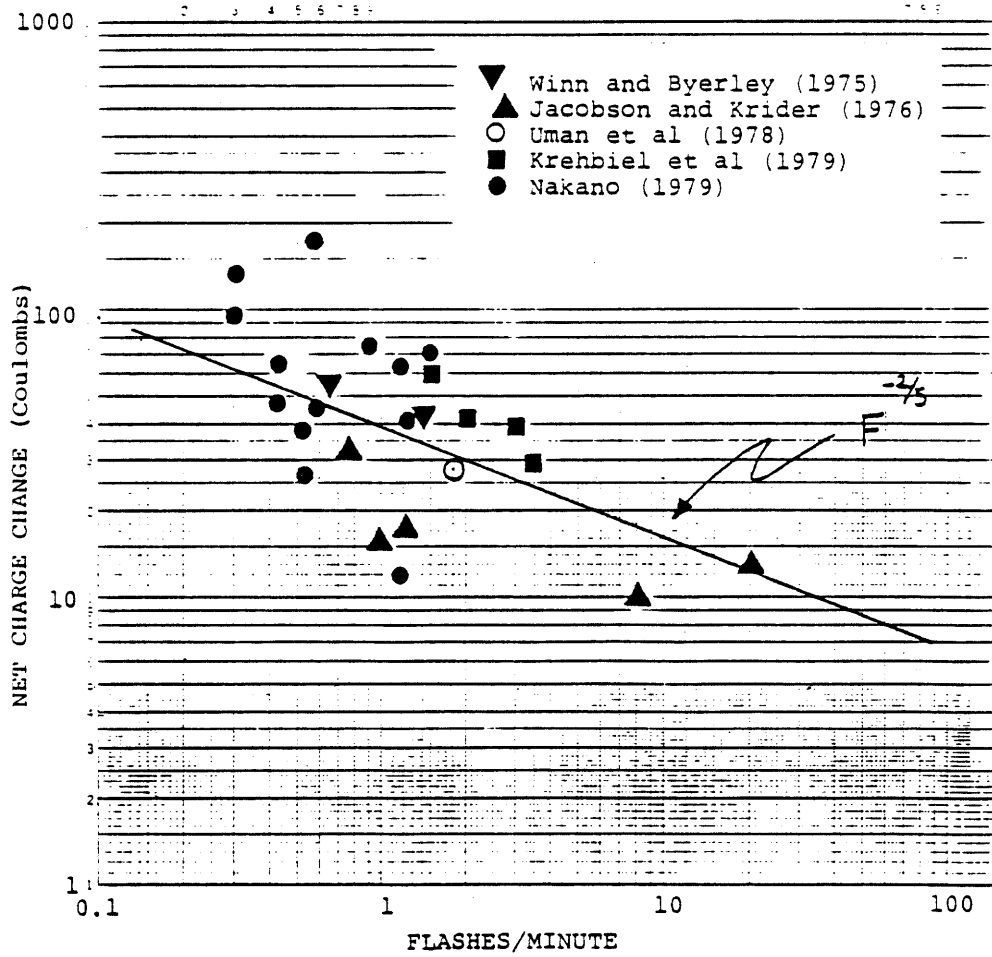
they are not inconsistent with the $F^{-2/5}$ prediction.
Consistency with the total neutralization assumption (Figure
V-6) would require $\Delta Q \sim F^{+2/5}$ in Case I and $\Delta Q \sim F^{+2/5}$ in Case II,
neither of which is supported by these data.

V-7 Behavior of Externally Derived Charge Flow

An important item in the electrical budget of a
thunderstorm and a vital element in Vonnegut's (1953)
convection theory is the surface corona current. This section
considers the scaling behavior of this parameter, and a
comparison with other currents relevant to electrification.

Although the corona current from land surfaces is known to
depend strongly on surface field (see Figure VIII-4, Chapter
VIII), the field strengths beneath active thunderclouds are
corona space charge limited and do not vary in any systematic
way with storm size or flash rate.* We are in agreement with
Livingston and Krider (1978) in concluding that the total
corona current will be proportional to the affected surface
area beneath the cloud ($\sim L^2$).

This L^2 scaling for corona current may fall short of the
mark in providing the main charging current for thunderstorms.
Consistency with the simple scaling relationships in Figure
V-1 and our flash rate versus cloud height data requires a

_____

*The exception to this result, emphasized by Livingston and
Krider (1978), is the tendency for larger surface fields and
corona current densities during the final end of storm
oscillation (EOSO) when the flash rate is very small.

charging current scaling of $L^{3/2}$ to L^3, which may outrun the available charge supply from the earth's surface.

The corona current is one of two distinct charging currents in the convective theory (Vonnegut, 1953) and the crucial test is whether the overall charging current can provide for the negative charge flow to ground in cloud-to-ground lightning activity. This average current will scale as the product of charge per flash and the flash rate. Recalling the results that the energy per flash is scale invariant (Section V-6) and that the flash rate scales as $L^{9/2}$ to L^5, we conclude that this current scales as $L^{5/2}$ to L^3 if it is also assumed that the ratio of intra-cloud to cloud-to-ground lightning is independent of cloud size. The modelling of convective transport of negative space charge from the upper part of the cloud (Chapter VIII) shows a current scaling of $L^{3.2}$ (see specifically Figure VII-5, Chapter VII), which is therefore adequate to supply the cloud-to-ground lightning current for all cloud sizes if it can be effectively transported downward in screening layers.

Livingston and Krider (1978) have suggested that the average current associated with cloud-to-ground lightning may predominate over the total corona current during active lightning periods. Although noting that the average surface field and the resulting corona current density may be less during these periods, they have ignored the tendency for smaller lightning charge neutralizations at such times (see Figure V-8). In any case the magnitudes of the corona and

lightning currents will be of the same order, contrary to the results of earlier analyses (e.g., Wormell, 1930) in which the corona current always predominates.

V-8   The Scaling of Precipitation Gravitational Power

In Chapter II, the energetics of the precipitation hypothesis were examined, and the gravitational power associated with falling precipitation was calculated. Since we have a prediction for the scaling behavior (L^4) for precipitation-driven electrification (see Section V-4), it is of interest to determine how the available gravitational power scales with cloud size.

The available gravitational power is MgV, where M is the total mass of precipitation, g is the acceleration due to gravity, and V is the center of mass terminal velocity. We can also express this quality as

$$MgV = \int \overline{p} \cdot \overline{g} \; d(vol)$$

where $\overline{p}$ is the mean momentum density of falling precipitation and the integration is performed over the cloud volume.

The momentum density is really the precipitation rate when expressed in appropriate units (of mass flux). Considerations of accretional growth in geometrical sweepout readily show that peak precipitation rates vary linearly with cloud depth L and radar observations support this prediction
(Austin and Houze, 1972). The available gravitational power should then scale as $L \times L^3 = L^4$.

110

Since the observed electrical output of a thunderstorm scales more like the convection prediction ($L^{9/2}$ to L^5), it follows that the <u>apparent</u> gravitational-to-electrical efficiency should increase with storm size, and this is confirmed in our storm data (replotted in Figure V-9 from Figure II-6 in Chapter II). For very electrically active clouds (Vonnegut and Moore, 1958), the electrical outputs would appear to outrun the capacity of the precipitation gravitational power, but we lack data of this kind for large clouds to confirm this suspicion.

V-9 <u>Scaling</u> <u>Law</u> <u>Extrapolation</u> <u>to</u> <u>Small</u> <u>Clouds</u>: <u>A</u> <u>Possible</u> <u>Explanation</u> <u>for</u> <u>the</u> <u>Infrequent</u> <u>Occurrence</u> <u>of</u> <u>Lightning</u> <u>in</u> <u>Warm</u> <u>Clouds</u>

Although the range of lightning producing cloud sizes is not great, the flash rate versus cloud size data we have presented in section V-5 (Figures V-3 and V-4) show that thunderstorms tend to follow a consistent power law scaling relationship over this range and thereby suggest self-similar behavior. Such a power law behavior could not extend to small cloud sizes if the presence of ice were essential for electrification, since some clouds are everywhere lower than the 0°C isotherm and yet produce lightning (Foster, 1950; Pietrowski, 1960; Moore et al., 1960). In view of these observations, we will assume self-similarity and see what conclusions may be drawn by extrapolating to warm cloud sizes.

Figure V-9
Apparent Gravitational-
to-Electrical Power
Efficiency vs. Radar
Storm Height

RADAR HEIGHT   (km)
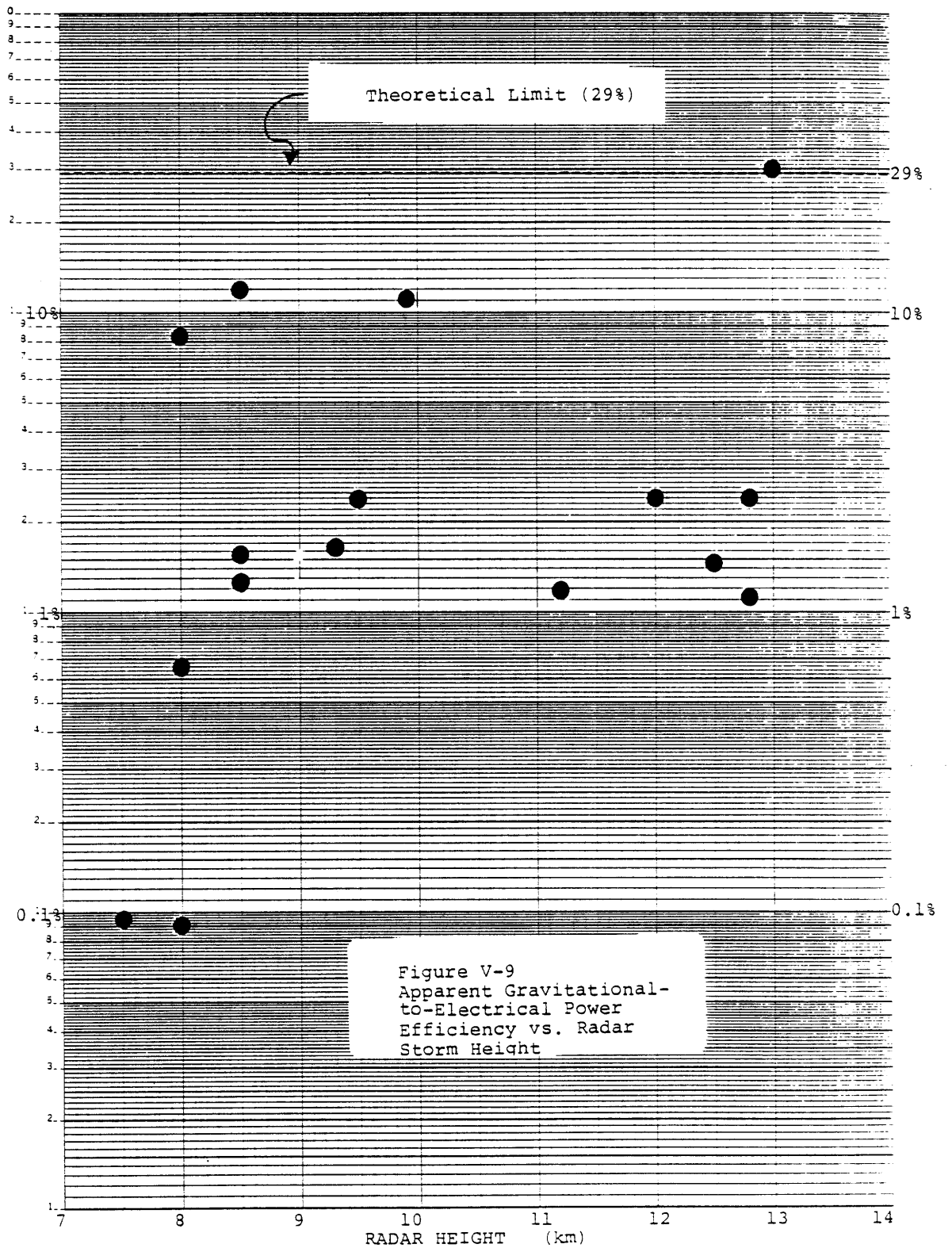
To measure the probability of observing lightning in shallow clouds, we have plotted the reciprocal flash rate (the mean time interval between flashes) versus cloud size, using the same data presented in Figures V-3 and V-4, and compare these times with the expected lifetimes of these clouds (Austin and Houze, 1972; Battan, 1953) in Figure V-10. For clouds of size 10 km, the cloud lifetime exceeds the reciprocal flash rate by two orders of magnitude. However, the smaller the cloud, the shorter is its lifetime, and for clouds less than 4-5 km deep, the wait time for lightning exceeds the lifetime of the cloud. Since the atmospheric temperature structure constrains warm clouds to be of this size and smaller, it seems likely that many warm clouds are potential thunderstorms but seldom have time to make lightning.

V-10 The Electric Reynolds Number as a Thunderstorm Figure of Merit

A commonly used scaling parameter for electrohydrodynamic generators is the electric Reynolds number (Stuetzer, 1962). This dimensionless parameter is the ratio of the electrical relaxation time of the medium to the convective time scale required to transport electric charge through a characteristic length scale L

$$R_E = \frac{\varepsilon V}{\sigma L}$$

One normally associates the electrical conductivity σ with charge leakage and electrical dissipation, and the velocity V

Figure V-10
Cloud Lifetime and Mean
Time Interval between
Lightning Flashes vs.
Cloud Size

114
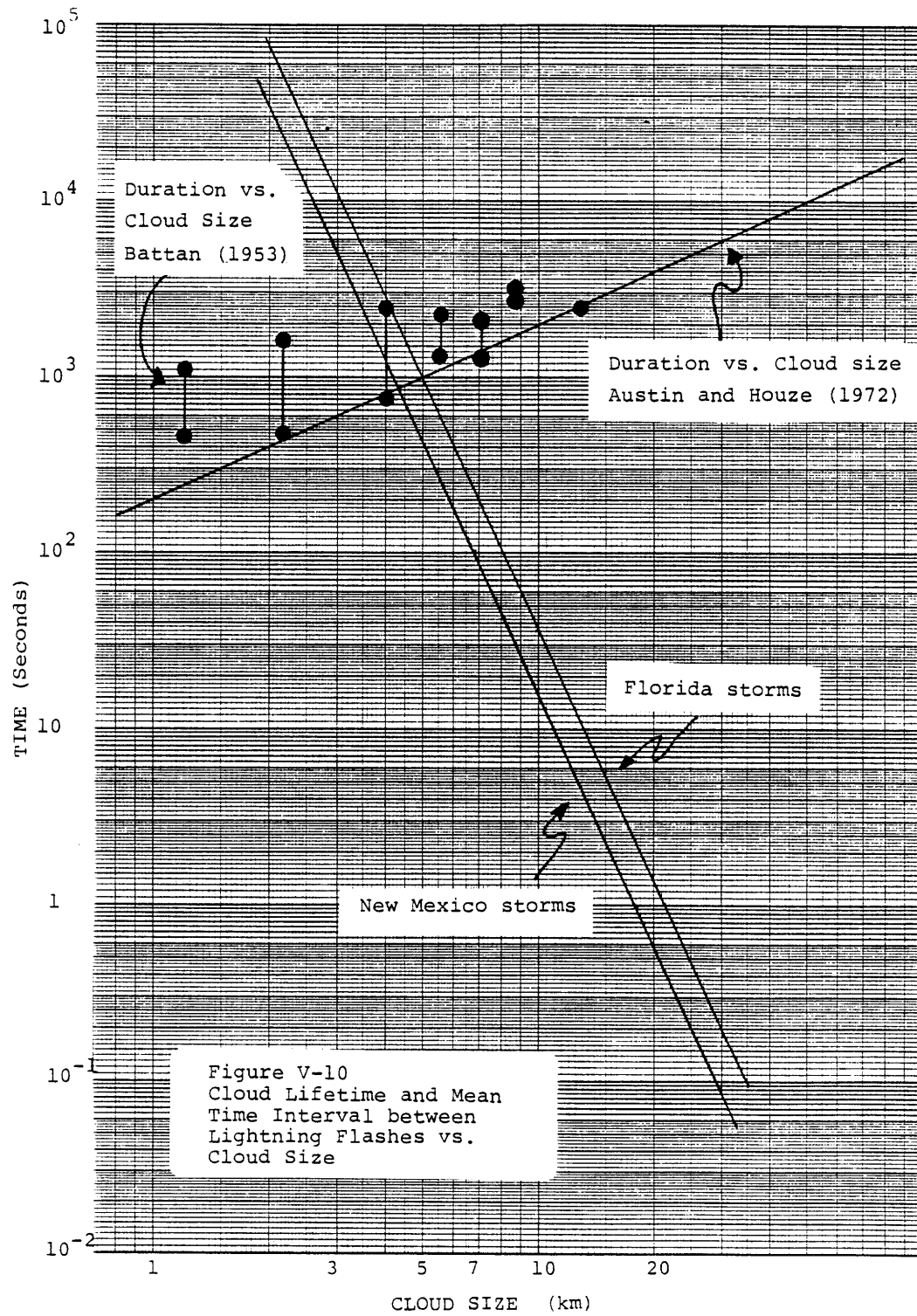
with generative charge transport which works against this leakage. In this view, the larger the electric Reynolds number, the more potent is the EHD generator. Though this number may provide a meaningful figure of merit for streaming potential generators, Kelvin water droppers, or Van de Graaff machines, its predictions are inconsistent with the scaling behavior of thundercloud electrification, since its value is smaller for taller storms (larger L) which penetrate into the more conductive regions (higher σ) of the atmosphere, and such storms are electrically more efficient and more energetic.

Similar arguments have been presented by Vonnegut and Moore (1958), who contested the applicability of Gunn's electrical index (Gunn, 1954) $\rho V/\sigma E$, to thunderstorms. Since the electric field E at the surface of a uniformly charged cloud of radius L and space charge density ρ is $\rho L/3\varepsilon$, it is clear that Gunn's index is the electric Reynolds number in another form. Gunn's argument was based on the precipitation hypothesis, in which case electric charge is produced solely by precipitation particle-cloud particle interactions and the finite conductivity of the atmosphere plays only a passive dissipative role.

The convection hypothesis (Vonnegut, 1953), on the other hand, relies on the finite conductivity of the atmosphere for the accumulation of space charge. A model for screening layer charge transport to test this hypothesis in Chapter VII indicates the existence of optimal, finite electric Reynolds numbers rather than infinite ones.

A closely parallel situation in magnetohydrodynamics concerns the magnetic Reynolds number and the generation of magnetic fields by convecting dynamos. In this case the electrical conductivity must be sufficiently large that magnetic diffusion does not destroy the field, but not so large that the field lines are truly frozen to the fluid. Viable MHD dynamos are therefore characterized by optimal magnetic Reynolds numbers, rather than infinite ones.

The implications of this EHD/MHD analogy for electrification are examined further in Chapter IX, in which the electrical conductivities of planetary atmospheres are explored.

Chapter VI

Pressure Variations Beneath
Thunderstorms

VI.-1 Introduction

This chapter explores the relationship between the
electrical evolution of thunderstorms and the pressure
variations beneath them, which are manifestations of convective
motions within and around the cloud.

Section VI-2 is concerned with specific causes for these
pressure variations. Section VI-3 includes a brief discussion
of instrumentation and measurement procedures beneath
thunderstorms in both New England and New Mexico. The next
three sections are concerned with selected observations and
emphasize the close association between pressure and electric
field in various phases of storm development. The correlated
behavior with other parameters like cloud height and lightning
flash rate is also treated. Pressure variations accompanying
excursions in electric field are examined in Section VI-7, and
possible hypotheses for this phenomenon are discussed in light
of the observations in the final Section.

VI-2 Atmospheric Pressure Perturbations and Their Causes

The convective phenomena and associated pressure
fluctuations with which we are concerned result from departures
in hydrostatic equilibrium. To examine these departures, we
need to consider the balance of forces for vertical atmospheric

117

motions, i.e. Newton's Law. Conservation of vertical momentum density, ρw, requires

$$\frac{D(\rho w)}{Dt} + \frac{\partial P}{\partial Z} - \rho g = 0 \qquad (1)$$

where ρ is the atmospheric density, w is the vertical velocity, and P is the pressure. The motions of interest involve large Reynolds numbers ($10^7 - 10^9$) and a friction force has been ignored.

If we expand the total derivative in (1), invoke mass conservation ($\nabla \cdot V = 0$), and integrate the equation in Z, the vertical coordinate from the Earth's surface Z_0 to some height Z_1, we obtain a general expression for the surface pressure P with respect to Z_1,

$$\rho = \int_{Z_0}^{Z_1} \rho q dz - \int_{Z_0}^{Z_1} \frac{\partial(\rho w^2)}{\partial z} dz - \int_{Z_0}^{Z_1} \frac{\partial(\rho w)}{\partial t} dz - \int_{Z_0}^{Z_1} \frac{\partial(\rho w)}{\partial x} dz \qquad (2)$$

$$\#1 \qquad\qquad \#2 \qquad\qquad \#3 \qquad\qquad \#4$$

To further simplify the above result we have assumed zero horizontal velocity in the y direction.

Equation (2) shows the pressure contributions which may arise in addition to the hydrostatic load, term #1. The descriptor "static" for this term is however misleading, since this implies constancy over all time scales. During thunderstorm conditions, the effective density of air, ρ, in a vertical column may change with time and perturb the "hydrostatic" contribution over time scales of interest (5-10 minutes).

These perturbations are small but so are the pressure
fluctuations we measure. Evidence for this possibility will be
presented shortly.

The second term is the vertical advective acceleration
contribution and represents the impact or stagnation pressure
for downward motions. Note however that steady upward motion
can make a negative contribution to surface pressure via this
term. Term #3 is the vertical acceleration component and
represents a negative pressure contribution for upward
acceleration. Finally the advection of velocity structures
affects the pressure; this contribution is represented in term
#4.

An important common factor in all terms in (2) is the
atmospheric density $\rho(z)$. Since this parameter is an
exponentially decreasing function of height in the atmosphere,
the pressure measurements made near the surface will be more
influenced by fluctuations near the ground than to fluctuations
aloft. The surface electric field beneath a storm is also more
influenced by space charge in closer proximity, and this
circumstance may contribute to the remarkable correlation
between pressure and electric field records.

The convective time scales which we believe are important
for electrification lie in the range of 5-30 minutes, and the
bandpass of our pressure recorders has been correspondingly
configured (see Appendix E). A simple order of magnitude
analysis of the pressure fluctuations expected from each of the
four terms in equation (2) shows values of a few hundred

microbars per minute; all terms have contributions of the same order. This situation confuses the interpretation a bit, but since different contributions have different signs, we can still make meaningful interpretations. Peripheral information from radar and the sorting out of advecting features through the use of an array of pressure recorders has helped guide this interpretation.

VI-3 **Pressure Measurements**

Pressure measurements beneath thunderstorms were carried out with sensitive microbarographs formerly used in gravity wave studies at MIT (Claerbout, 1967). The original bandpass was modified only slightly to (1) dampen contributions from high frequency turbulence and (2) to extend the low frequency response. These instruments were particularly well suited to our study, since the recorder outputs are closely in phase with the actual pressure for convective time scales of interest (5-30 minute periods). The details of microbarograph operation and an equivalent circuit for determining their frequency response are presented in Appendix E.

For our New England observations (1978), only a single station was available. In New Mexico (1979, 1980), an array of identical recorders was installed in a manner similar to that of the gravity wave studies (Claerbout, 1967), though our purposes were somewhat different. We wished to distinguish propagating or advecting perturbations which were potential sources of noise in this study, from possible stationary

120

disturbances associated with local convection. Also of interest
was the spatial variation of the convective disturbance away
from the source region. Unfortunately, the stations in New
Mexico were constrained to lie on the mountain ridge and
inter-station distances (~ 1 km) were smaller than the
characteristic cloud dimensions. Figure VI-1 shows the pressure
recorder array geometry for New Mexico. As a check on the
response of the microbarographs to common pressure fluctuations,
all instruments were operated at the same location before
locating them at their respective sites in Figure VI-1. Figure
VI-2 shows a segment of this simultaneous record. Except for
the Solar Tower instrument which passes long period (diurnal)
variations, all instrument responses are reasonably well
matched.

VI-4   Pressure Behavior Associated with Cloud Development and Initial Electrification

A noticeable feature of the pressure behavior in the early
stages of cloud development is the tendency for falling pressure
at the time of initial foul weather field (negative charge
overhead). Figure VI-3 shows three examples of this effect for
developing isolated thunderstorms in New Mexico. (Small arrows
mark the approximate onset of foul weather field in this
Figure.) Although this effect is more pronounced at some
stations than others, the pressure variations are closely in
phase, suggesting a common stationary source overhead.

121

Doppler Radar Site (1980)   ○   Barograph Locations
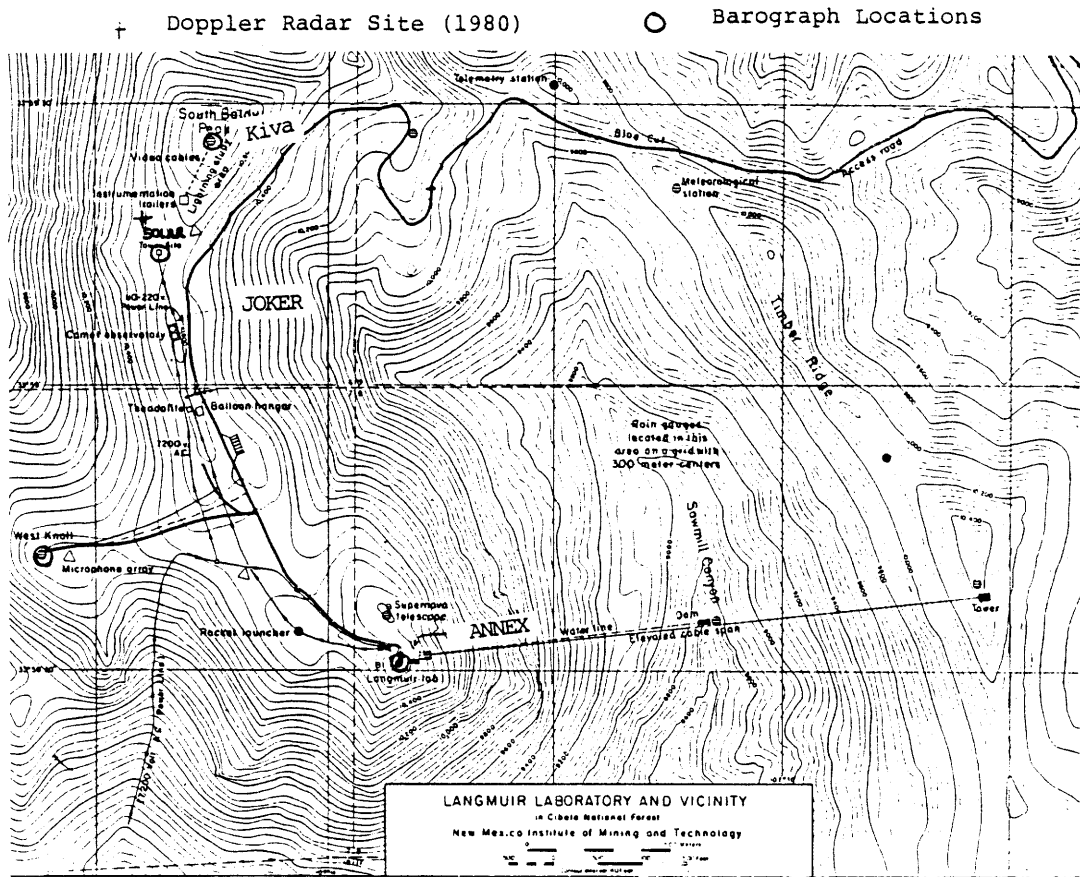
Figure VI-1
Microbarograph Array, Radar
Locations, Field Mill
Locations : New Mexico

Figure VI-2
Microbarograph Cross
Calibration

123

Figure VI-3
Declining Pressure during
the initial growth of
Foul Weather Field

124
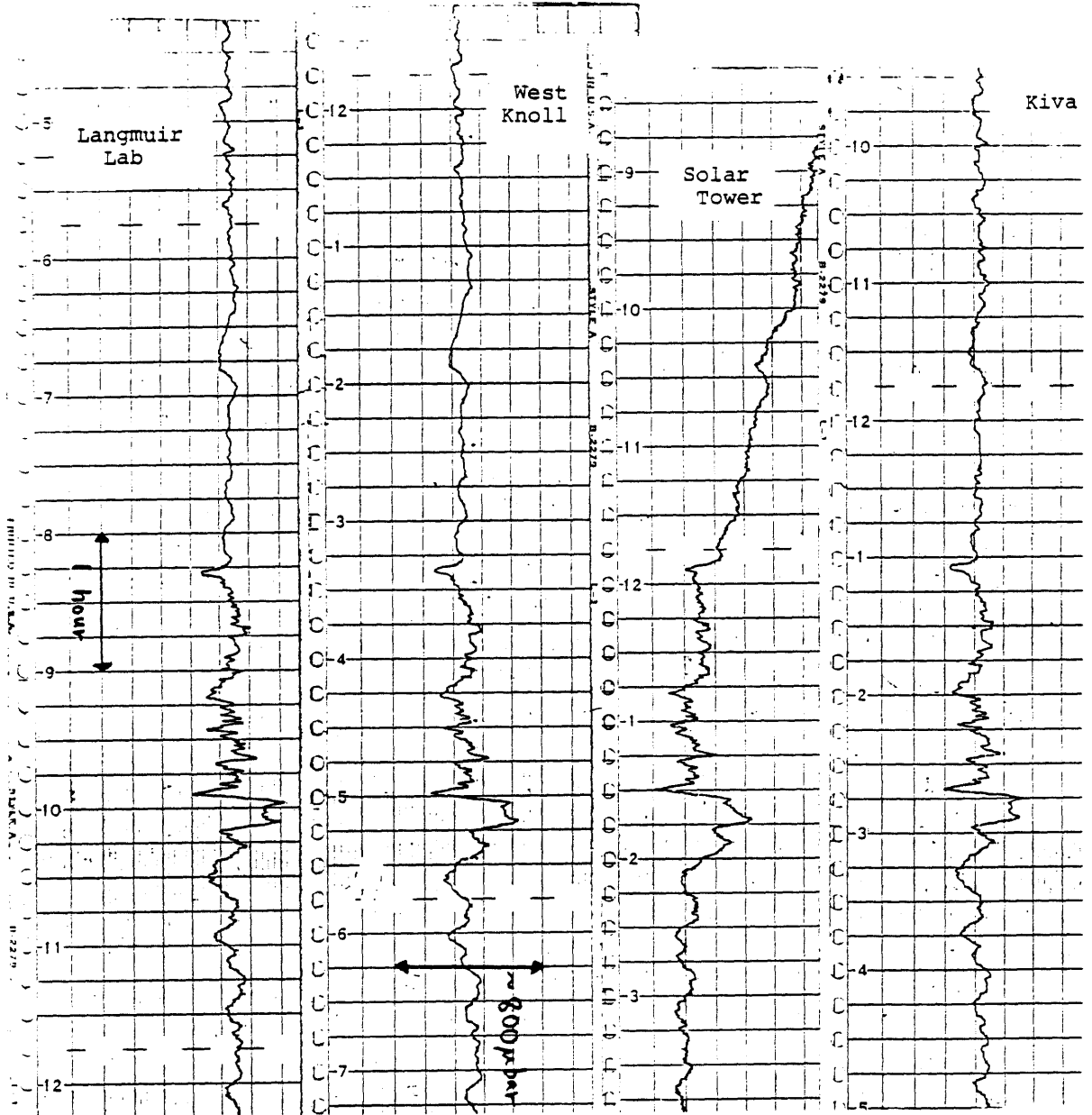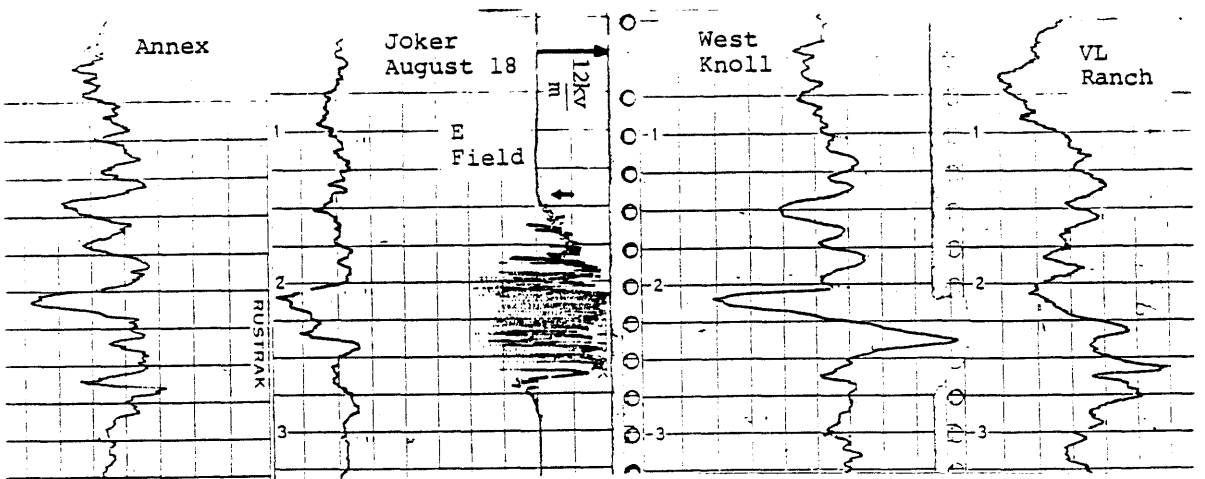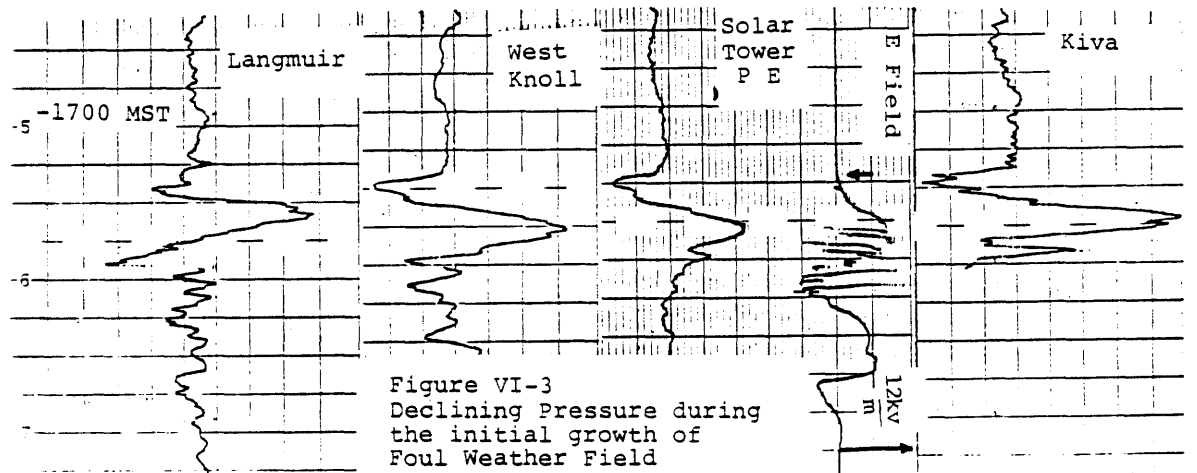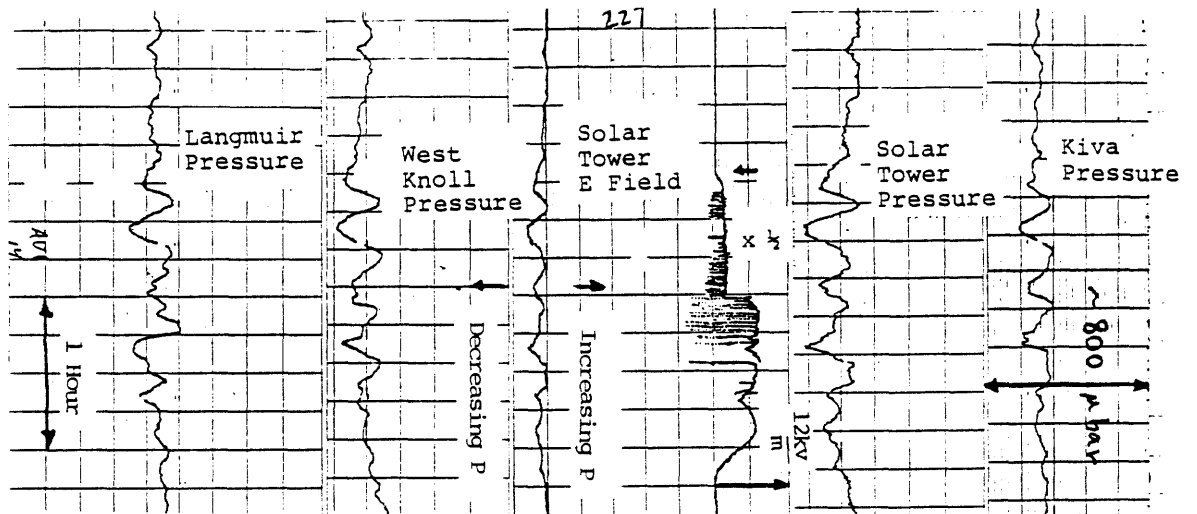
We attribute the pressure decreases to upward acceleration of air associated with latent heat-induced buoyancy forces. The close association with the initial electric field behavior suggests that the inferred convective motion is a causal agent in enhancing the foul weather field.

Falling precipitation, which can only act to accelerate the air downward, does not appear to play a prominent role in the pressure behavior at this stage, but could possibly contribute to the observed electrification. We do not have radar data for the cases in question, but a relevant finding of the surface pressure-radar comparisons in the Thunderstorm Project (Byers and Braham, 1949) was the tendency for "pressure to begin to fall a few minutes prior to the first appearance of the PPI echo." Unfortunately, the electric field was not recorded in these latter experiments.

These pressure and electric field observations at the ground are consistent with the findings of Moore et al. (1958), who found convective surges in the cloud to precede the reversal of potential gradient there.

VI-5 Coupled Electric Field-Pressure Variations

For times beyond the relatively simple early development, the pressure-electric field relationship is often muddled. The simultaneous existence of multiple sources (cells) of convection and multiple pressure contributions (recall Section VI-2) are responsible for this confusion. Another potential source of

pressure noise is the gravity waves which may be generated by the convective motions we wish to monitor. Yet another drawback in these comparisons is the effect of surface point discharge which "clips" the electric field (see for example the 1st and 3rd examples in Figure VI-3) and obscures the true electrical variation in the clouds overhead (Standler and Winn, 1979).

In spite of these complicating factors, a remarkably close coupling between the electric field and pressure records is often observed. We first noticed this effect during an electrically inactive nocturnal thunderstorm in New England when only single station pressure data was available. Figure VI-4 shows the simultaneous electric field and pressure records. Note the marked tendency for low pressure to accompany foul or foul-tending electric field.

We attribute this quasi-periodic behavior to convective overturn of the cloud overhead and a systematic redistribution of charge controlled by that overturn. The falling pressure/low pressure we again associate with the expansion of air due to latent heat release (term #1, equation 2) and to upward acceleration of air (term #2 and #3, equation 2). These segments of the record are associated with the growth and maintenance of foul weather field, suggesting that the inferred upward motion is responsible for the generation of the characteristic positive thunderstorm dipole.

Foul

7.5 kv/m

Fair

A   B

Decreasing Pressure

650 μbar.

Increasing Pressure

10 min.

Time
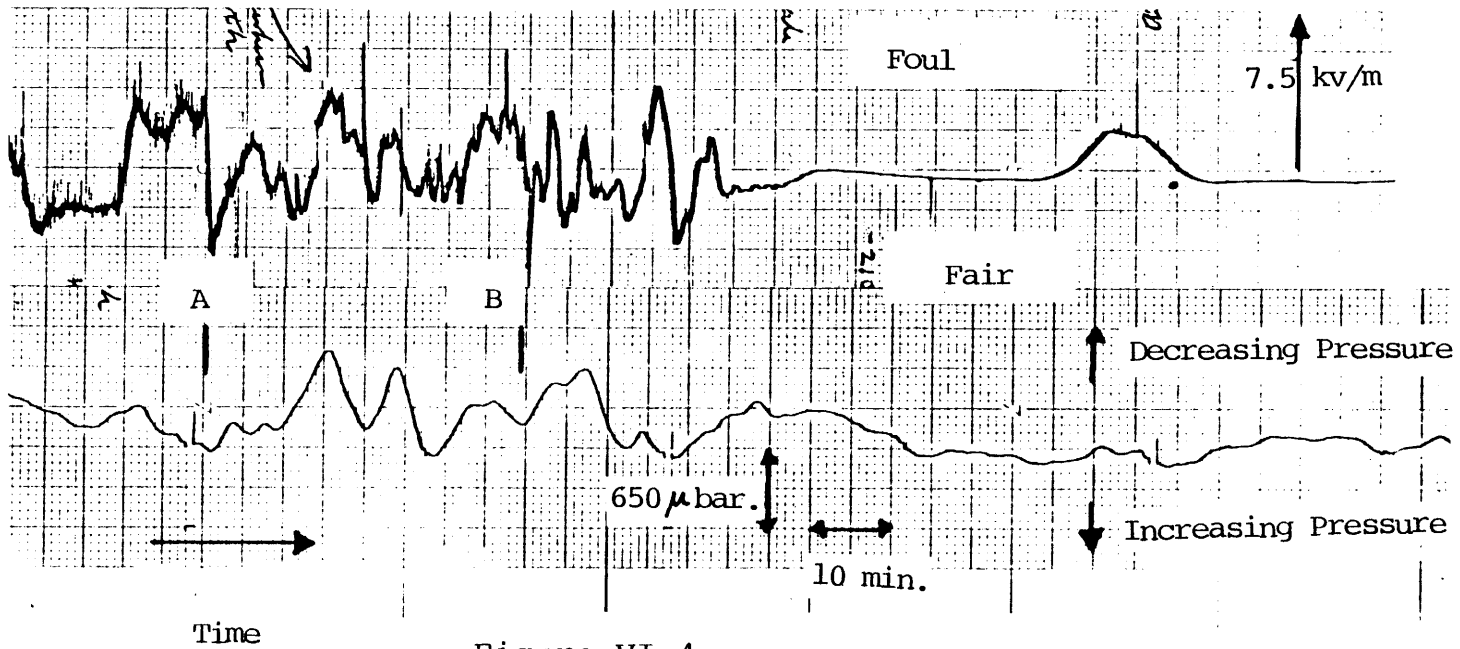
Figure VI-4
Pressure and Electric
Field Records, Millstone
Hill, August 4, 1978

127

The pressure increases which follow the convective upsurges may have multiple causes. The convergence of water vapor-laden air at lower levels in response to the initially low pressure will reverse the pressure trend by contributing to the static load in the overhead column. An additional contribution to increasing pressure will arise through the establishment of precipitation-driven downdrafts. Such features may be self-intensifying due to a shear flow instability (Mollo-Christensen, 1961) which will induce precipitation particles to move toward the region of maximum downward motion.

Although we are of the opinion that precipitation-associated downdrafts are responsible for pressure maxima and the accompanying fair weather fields in Figure VI-4, we are uncertain about the nature of source charge for the field reversals. Holden et al. (1980) have attributed fair weather field excursions to the descent of positively charged precipitation. Standler and Winn (1979) have recorded positively charged hail coincident with a field excursion. We have, however, detected a preponderance of negatively charged precipitation arriving at the Earth's surface at the time of field reversals A and B in Figure VI-4. This result suggests that in these cases, the charged precipitation is not the cause of the field reversal. A more complete discussion of possible hypotheses for such features can be found at the end of Section VI-7 of this chapter.

An additional example of correlated electric field and pressure signals for a New Mexico cloud which was electrified but which did not produce lightning is shown in Figure VI-5. Slight phase shifts in the pressure records suggests an advecting disturbance, but the high pressure-fair field/low pressure-foul field behavior is still upheld.

VI-6   Cloud Height Variation and Associated Pressure Fluctuations

Further insight into the pressure fluctuations of the convective cycle and the relationship with electrification can be gained through comparisons with radar data.

In Figure VI-6 we compare the pressure records at the West Knoll, Annex, and Joker sites with the radar-determined cloud height over the Joker site for the thunderstorm of August 13, 1979. The three pressure signals are closely in phase and are well correlated with the cloud top variation from 1330 MST to 1500 MST. Such behavior confirms our earlier assertion that the pressure recorded at the ground can be an accurate indication of convective activity.

The electric field at the ground during this electrically active storm is not a reliable index of the electrical behavior of the cloud for reasons stated earlier, and we have used the lightning flash rate as an index of this behavior in Figure VI-6.

To explain the pressure-cloud top correlation, we resort to a somewhat simpler physical situation. Imagine a pressure

129 .
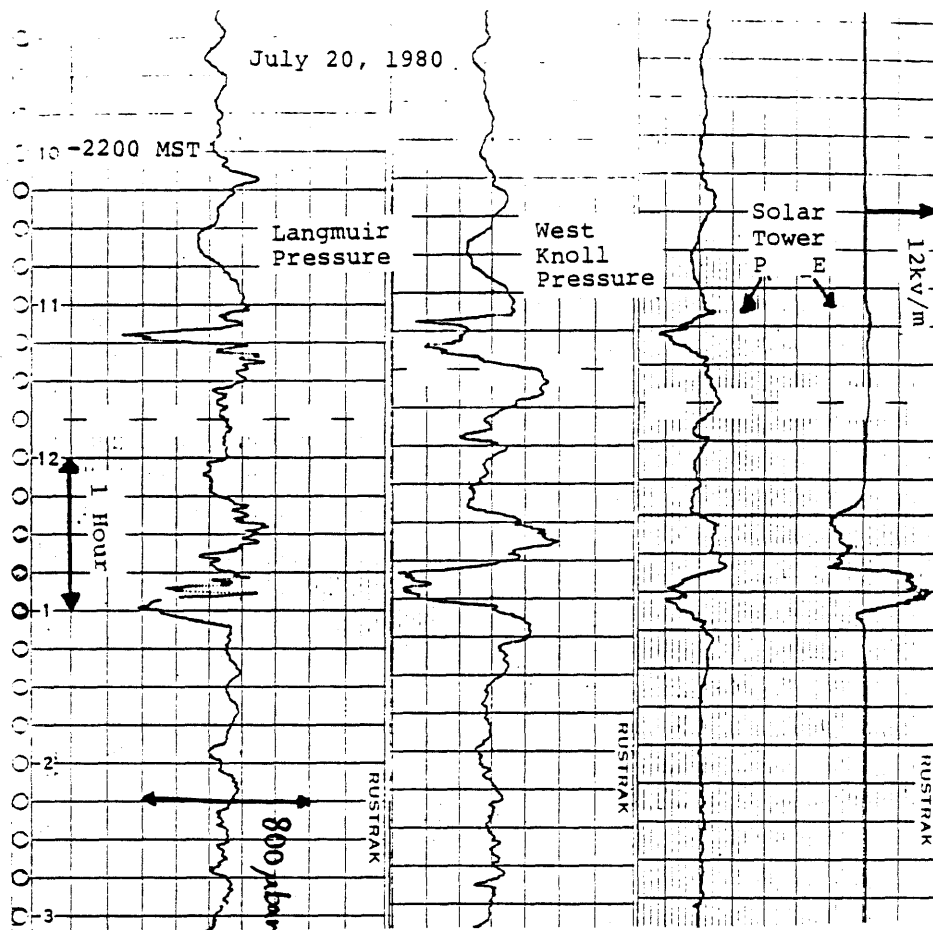
Figure VI-5
Pressure and Electric
Field Records, New Mexico,
July 20, 1980

130

Figure VI-6
Pressure, Radar Cloud Top,
Flash Rate;
New Mexico, August 13, 1979

131
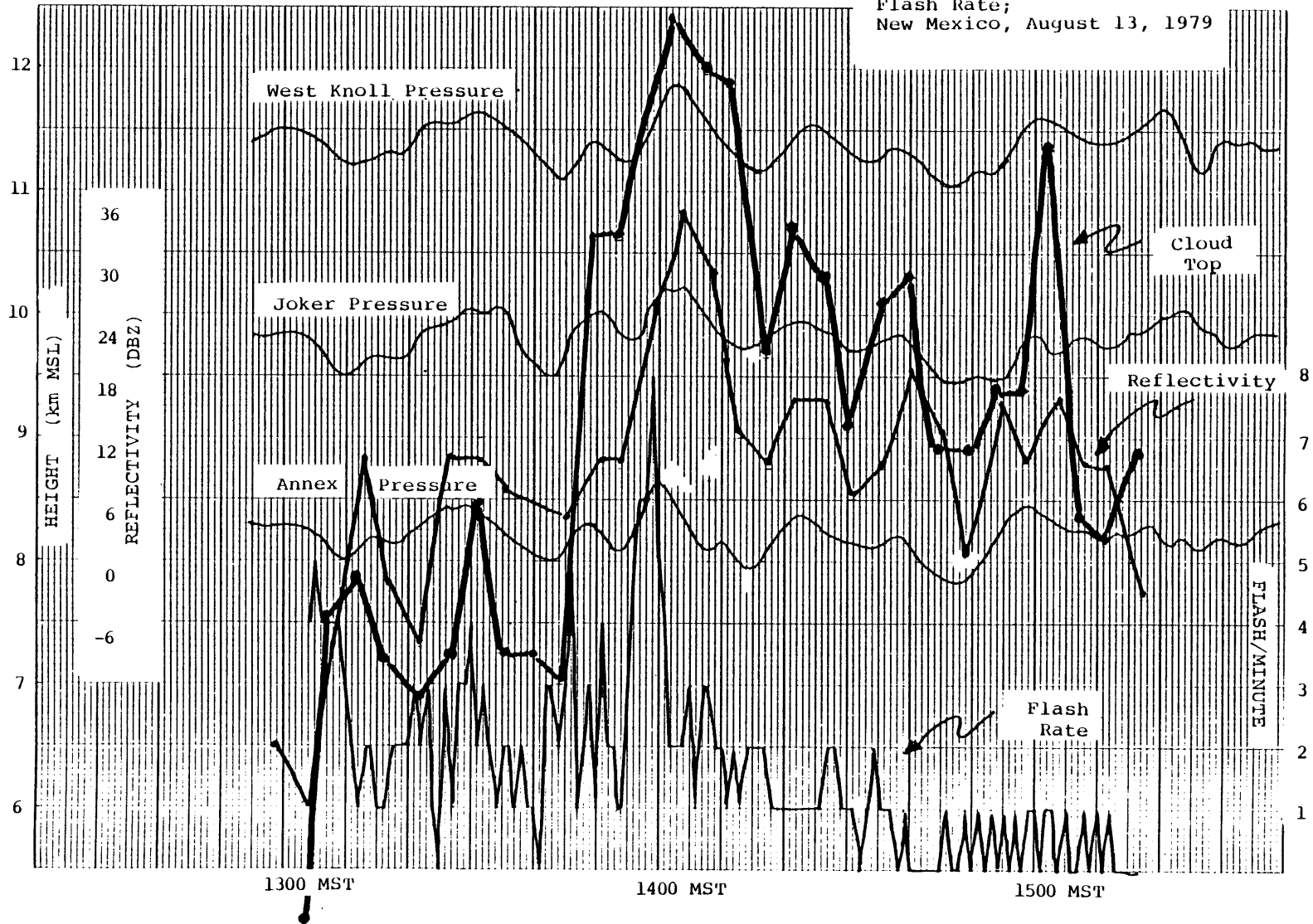
recorder resting on the bottom of a swimming pool. If the fluid surface above is disturbed (displaced upward, say), mass is drawn into the column of water beneath. The increased depth results in increased pressure and a radical pressure gradient which opposes further upward displacement and ultimately reverses the vertical velocity. The then descending fluid surface overshoots its equilibrium position, resulting in mass flux out of the water column and a pressure deficit. The pressure gradient force is now radially inward, restoring mass to the fluid column, causing it to rise and overshoot its equilibrium position, and so on.

In the absence of dissipation, the fluid column undergoes simple harmonic motion. With gravity as the restoring force, this phenomenon is very similar to the atmospheric Brunt oscillation, though the latter is, strictly speaking, an infinitesimal amplitude oscillation. Nonetheless, the characteristic oscillation period in Figure VI-6 is about 15 minutes, which is a reasonable Brunt period.

Thunderstorm convection is obviously a more complicated phenomenon, but this simple picture goes a long way in explaining the behavior shown in Figure VI-6. Pressure beneath the growing cell increases with the depth and density of the cell, together with the effect of growing, downward accelerating precipitation. The reflectivity data shows that the precipitation intensity in mid cloud is nearly in phase with the cloud top. The increased pressure retards the

convergence which supplies the cell with water vapor energy, and after the cell overshoots its equilibrium position, it rebounds downward as the pressure beneath falls. Decreased pressure allows for renewed convergence, latent heat release, and enhanced vertical motion.

We do not have vertical velocity data for this storm but following the harmonic oscillation picture we may predict that maximum vertical motion will precede the time of maximum cloud height by as much as a quarter cycle. The fact that flash rate maxima also precede the maximum cloud heights by about a quarter cycle is evidence that the inferred vertical motion is responsible for generative charge transport. Maximum flash rates preceding maximum cloud heights occur at 1305, 1330, 1346, 1359, and 1434 MST.

The argument that precipitation is playing the major role in electrification in this case is less convincing, since mid-cloud precipitation maxima lag flash rate maxima by as much as 2-3 minutes.

VI-7 Pressure Behavior Accompanying Electric Field Excursions: Case Studies

Reversals of electric field polarity at the Earth's surface which are not directly connected with lightning discharges are a common feature of thunderstorms, but are not well understood (Moore and Vonegut, 1977). The field excursion may take place in less than a minute and may be sustained for a period which varies from a few minutes to many tens of minutes. The

133

pressure signals often show pronounced correlations with these field excursions. In this section we examine the electric field and pressure relationship for a relatively short field excursions on August 16, 1979, for several long duration field excursions on August 17, 1979, and for a field excursion associated with the end of storm oscillation (EOSO) on July 19, 1980. Finally we shall discuss possible hypotheses for the consistent features of the behavior.

Simultaneous pressure records and the electric field signal from the Solar Tower site are shown in Figure VI-7 for the thunderstorm of August 16, 1979 over Langmuir Laboratory. Although these records exhibit a number of interesting features, the feature with which we are immediately concerned is the field excursions from foul to fair weather polarity which is denoted by the heavy vertical line (1442 MST). The sequence of events prior to, including, and following this excursion is as follows:

Growth of the cloud top (as observed with the zenith-pointing Doppler radar at the Joker site) continued from 1433 MST as the storm produced flashes at a rate of 1-2 per minute. The pressure at the Joker site increased simultaneously. At 1440 MST, the cloud reached its apogee at about 9 km MSL, coinciding closely with maximum pressure, and suddenly the cloud top began to collapse, continuing to descend for at least 15 minutes. The rate of decline of the cloud top was 5-7 m/sec from 1440 to 1445 MST. Coincident with this decline are large pressure falls at all sites. At 1441 MST,
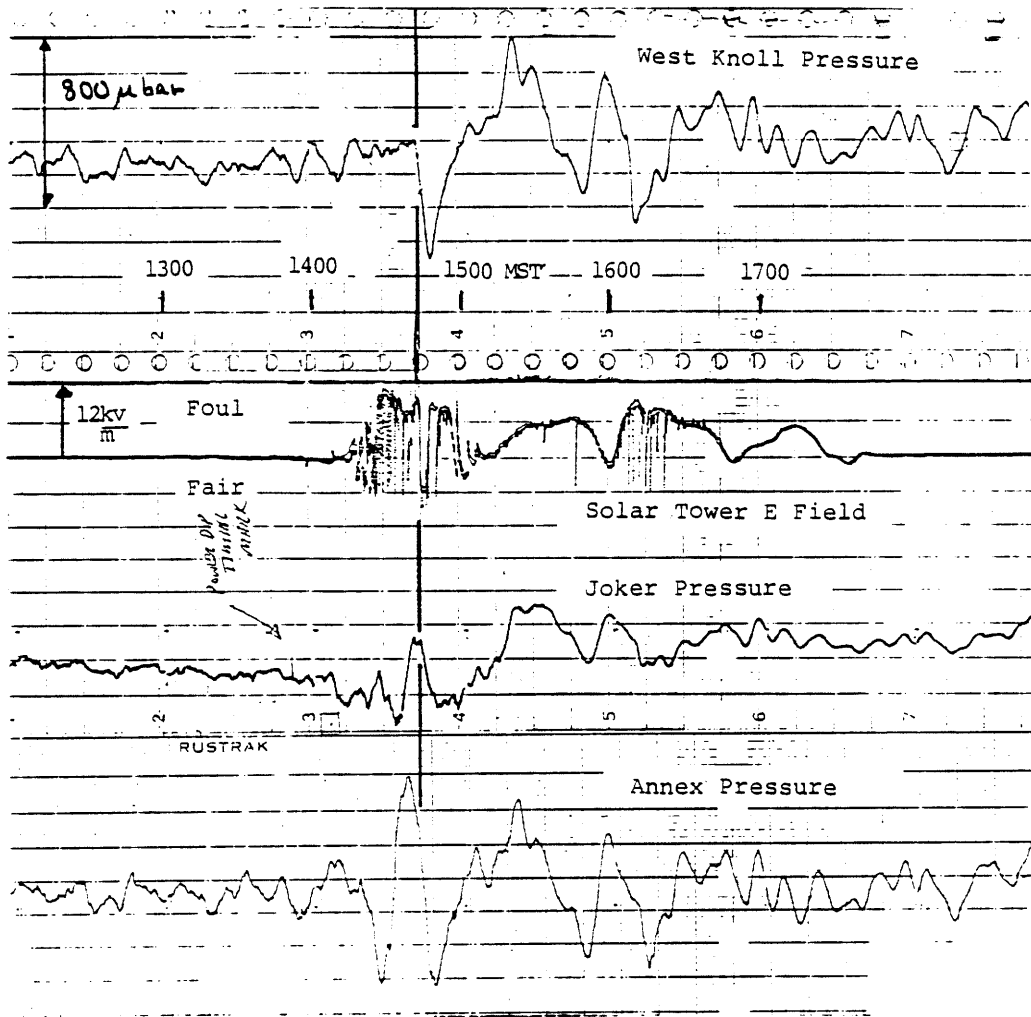
Figure VI-7
Pressure and Electric
Field Records, New Mexico,
August 16, 1979

135

the single gate at 6.8 km MSL indicates a weak downdraft, consistent with the declining cloud top behavior. At 1442 MST, the field excursion commences at the Solar Tower site, carrying the electric field from about 10 kV/m foul weather polarity to 7 kV/m fair weather polarity. The average flashing rate declines by at least a factor of two at this time. The field recovers to strong foul weather polarity by 1447 MST as the pressure reaches its minimum level.

The squall line thunderstorms of August 17, 1979 contained several field excursions with sustained reversals 5-10 times longer than the August 16 case, yet the systematic phase relationships between the electric field and pressure signals are often still upheld. Figure VI-8 shows the August 17 records with four major field excursions marked successively A, B, C, and D.

As with the August 16 case, the foul to fair transition A coincides with maximum pressure and the fair to foul polarity recovery B coincides with a pressure minimum. The pressure then increases again and the second foul-to-fair excursion (C) coincides with maximum pressure, also as before.

Also consistent with the August 16 behavior is the coincidence of foul-to-fair excursions A and C with extrema in cloud height. Unlike the August 16 case, these extrema are cloud top minima rather than maxima. Figure VI-9 shows the cloud height variation and the times of the four electric field excursions.

136
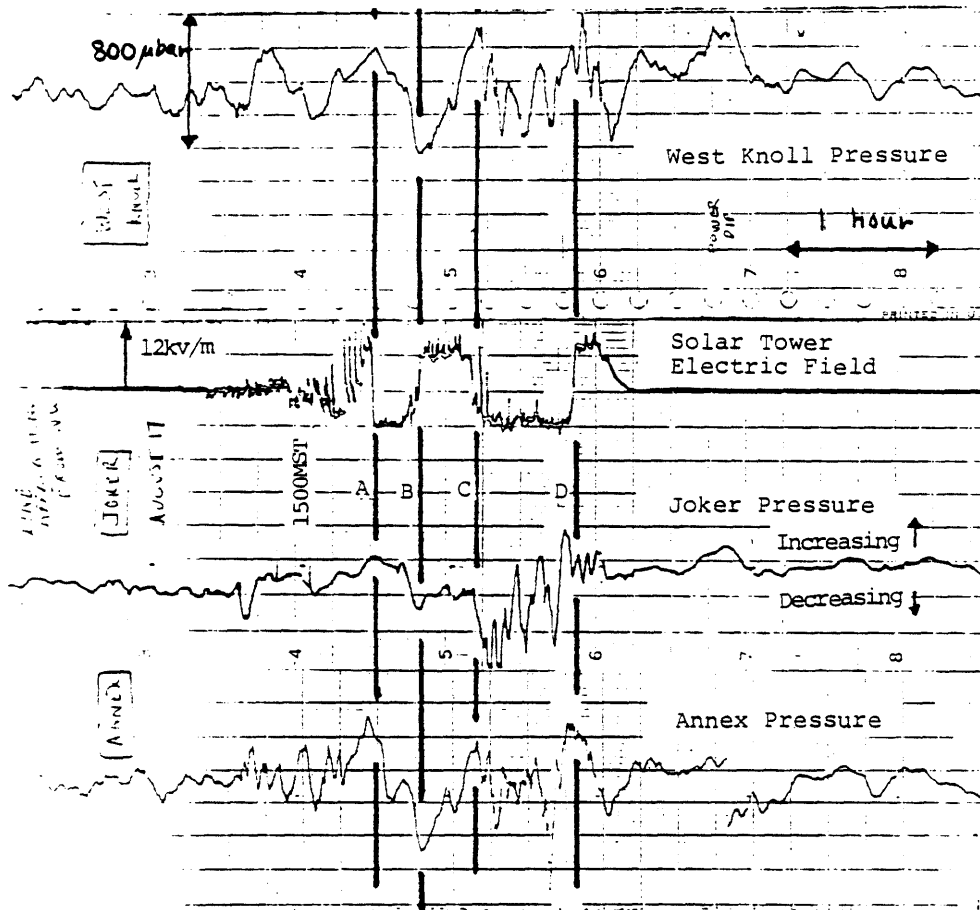
Figure VI-8
Pressure and Electric
Field Records, New Mexico,
August 17, 1979

137

Figure VI-9
Joker Radar Cloud Top and
Electric Field Excursion
Times, New Mexico,
August 17, 1979
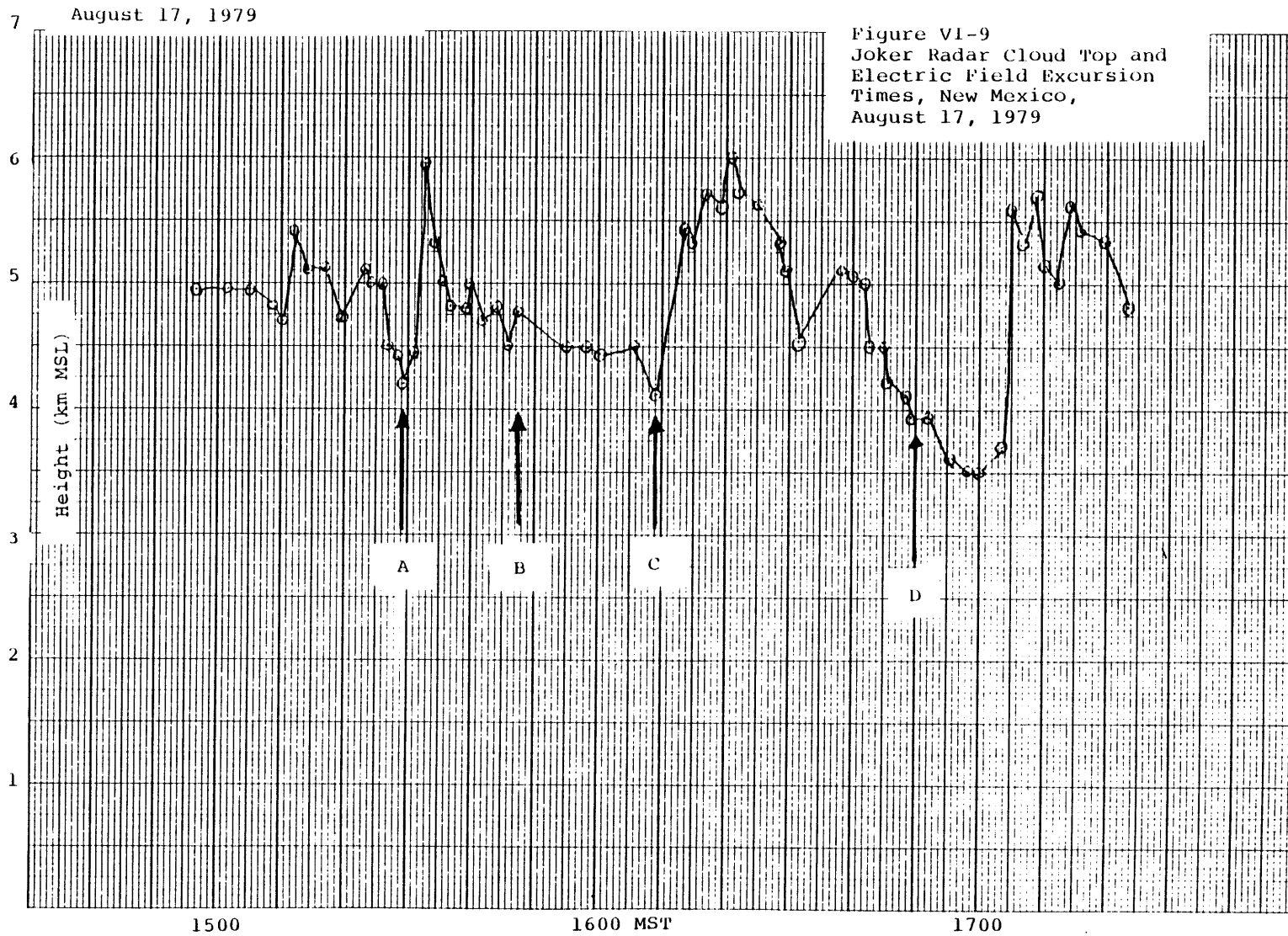
Excursion C, which marks the beginning of a rather extended end of storm oscillation (Moore and Vonnegut, 1977), also coincides with an abrupt transition in the dynamics of the storm. Violent wind gusts were noted during this period which we associate with downdrafts impinging and diverging on the mountaintop. Precipitation at the ground was very light.

The transition in dynamical behavior is readily apparent in the pressure signals. The relatively large energy in the high frequency portion of the pressure spectrum suggests that this period of the storm may be a likely time for gravity wave generation. Moo (1976) has proposed a mechanism associated with thunderstorm convection for the generation of 2-5 minute period oscillations. The sinusoidol oscillations prior to 1700 MST have 4-minute periods, and are therefore in the right range.

In a third and final case, we wish to describe the behavior of electric field and pressure during an end of storm oscillation which occurred during 1980, when more detailed vertically-pointing Doppler information was available. Figure VI-10 shows the pressure signal at the Solar Tower site which is nearest the radar, the electric field at the Solar Tower site, the radar reflectivity observed 500 meters above the ground, and vertical profiles of mean Doppler velocity at 2 minute intervals. No radar reflectivity information was available below 500 meters altitude (3.8 km MSL), and no velocity information below 750 meters altitude (4.0 km MSL).

139
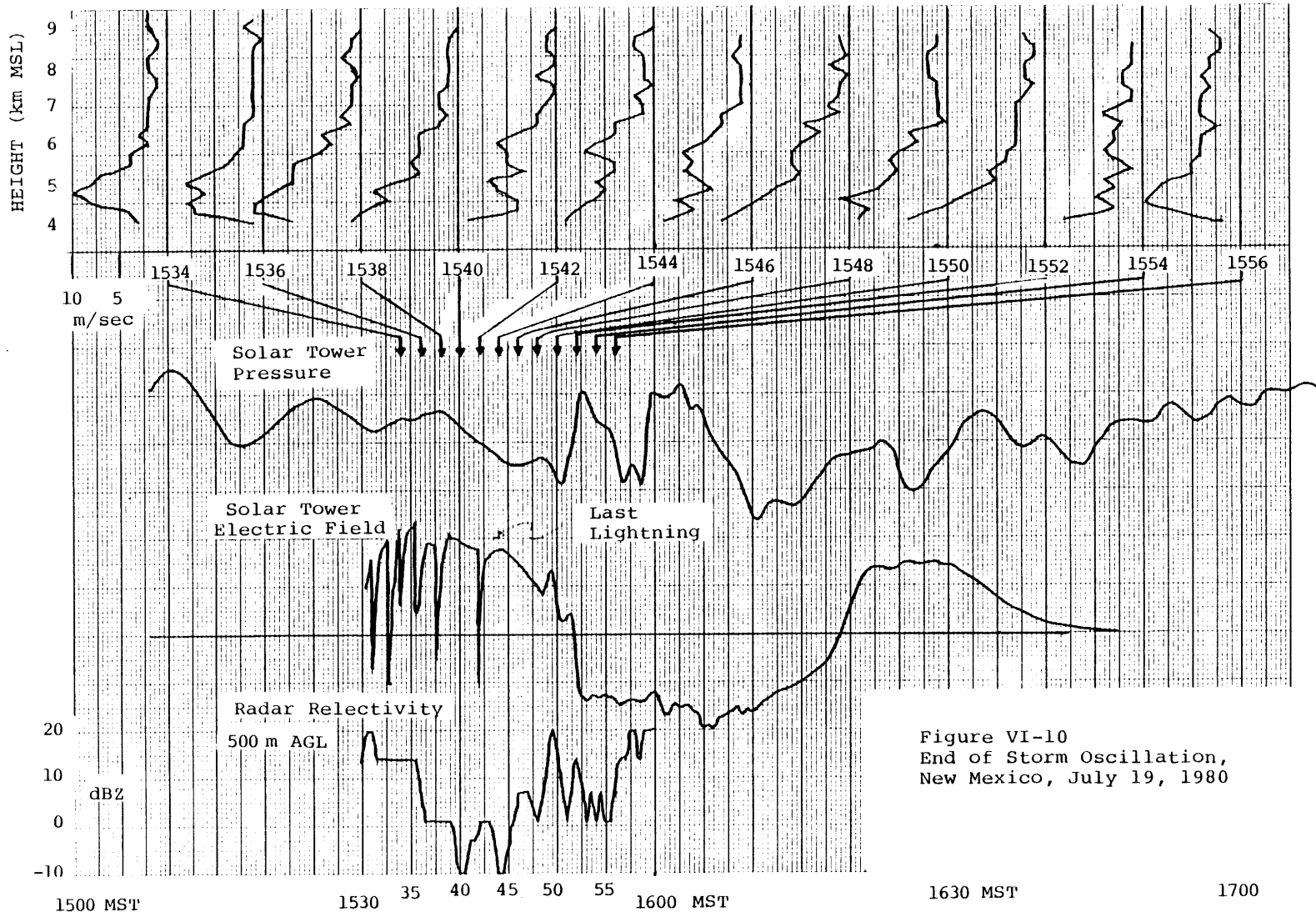
Figure VI-10
End of Storm Oscillation,
New Mexico, July 19, 1980

From 1534-1538 MST, the foul weather field began its
delcine as the last few lightning flashes occurred. The three
Doppler profiles for this period show pronounced downward
maxima at 1-2 km altitude, with a downward trend in this
altitude with time. The pressure is increasing slightly but is
on a longer term downward trend. Between 1538 and 1540 MST,
the vertical velocity gradient at the bottom of the profile
changes sign, and the associated divergence of flow at the
ground may account for the pressure maximum around 1538 MST.
The pressure then continues to fall as air at higher levels
continues to accelerate earthward. The profiles of 1542-1546
show successive increases in downward velocity in mid-cloud.
By 1548 MST, the rate of decline of foul weather field has
increased, and the velocity near the ground is again maximum.
A wind gust was noted at 154830, and was probably associated
with divergence of flow. A small pressure rise accompanies the
velocity maximum. The 1550 profile shows a reduced velocity
maximum, and coincides with a brief pressure fall. At
1552 MST, an abrupt pressure increase coincides with the
largest downward velocity (14 m/sec) and the largest rate of
change of electric field. This strongest convective surge
drives the field into fair weather polarity corona saturation.
By 1554 MST the downdraft is substantially less and the
pressure is falling again. Two minutes later (at 1556 MST),
the vertical velocity gradient near the ground has reverted to
its pre-oscillation direction. Doppler radar data is
unavailable after this time, but the high frequency content in

the pressure signals and our own observations of wind gusts during this fair weather polarity period suggest that this EOSO is very similar to the August 17, 1979 case already discussed (Figure VI-8).

The well documented vertical motions for this case and their close association with an electric field excursion to fair weather polarity leave little doubt that net positive charge is conveyed toward the ground by air motions. The two transient reversions toward foul weather polarity between 1548 and 1552 MST (and which we did not discuss in the play-by-play for this sequence) suggest that the downward moving air contained "pockets" of negative charge. Unfortunately we have no way of knowing on what particles the charges reside. Although the maximum reflectivities associated with the observed downdrafts are quite small (20 dBZ), the fact remains that both cloud and precipitation particles are potential charge carriers.

VI-8 Pressure Behavior Accompanying Field Excursions: Hypotheses

Several mechanisms have been proposed to explain field excursions from foul to fair weather polarity. In this section, we examine the hypotheses in light of the measurements discussed here. The pertinent charge configurations and their relative motions are illustrated schematically in Figure VI-11. The classical positive dipole structure of a thundercloud is shown in Figure VI-11(a). The lower positive charge center has

142

(A) Classical Electrical Structure

Simpson & Robinson (1940)
Malan (1963)

(B) Charge Deposition by Lightning

Holden et al (1980)

(C) Electrical Convection Structure

Moore & Vonnegut (1977)
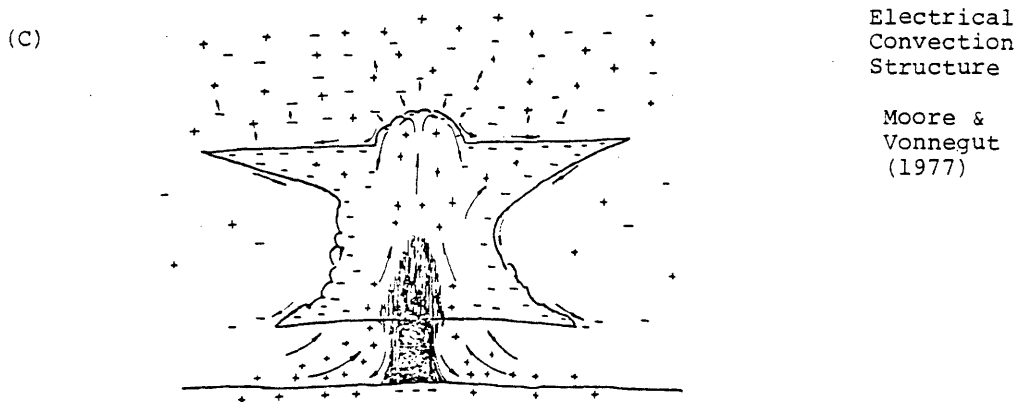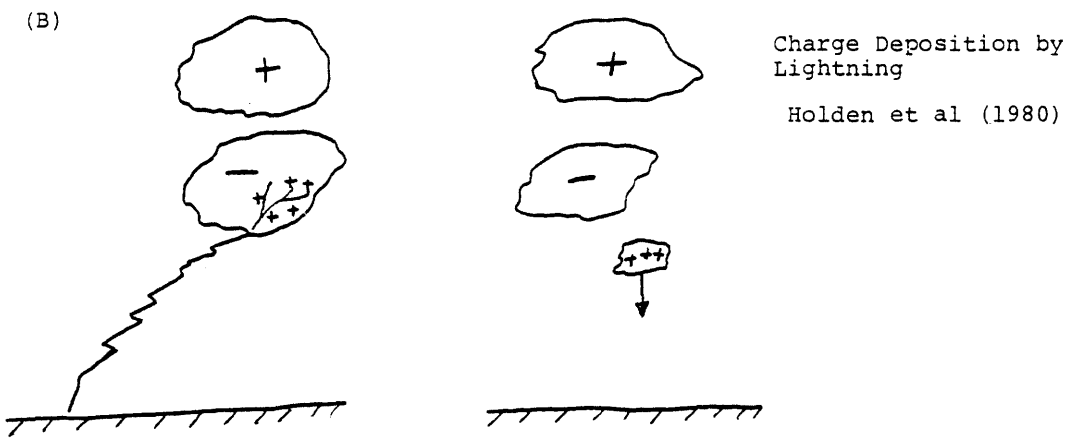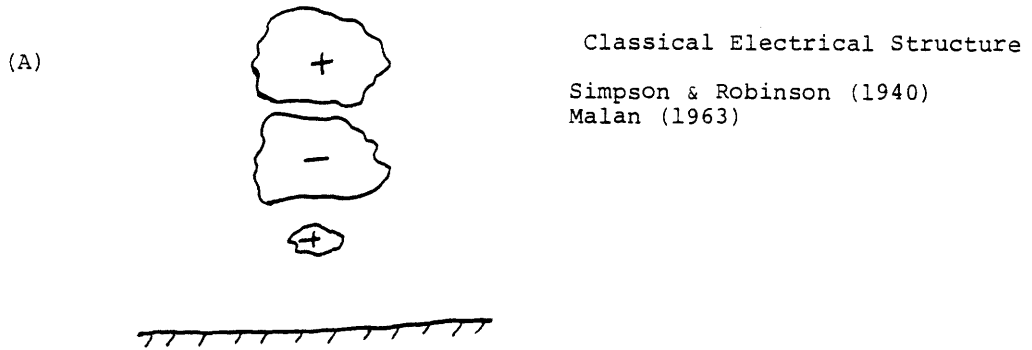
Figure VI-11
Electrical Structures
Associated with Hypotheses
for Electric Field
Excursions

143

been attributed to positive precipitation charging (Simpson and Robinson, 1940) and to the accumulation of positive point discharge ions from the Earth's surface (Malan, 1952). All hypotheses for field excursions involve the perturbation of this basic electrical structure.

Holden et al. (1980) have suggested that lightning may deposit positive charge on precipitation particles, which subsequently fall from the cloud to produce the so-called field excursion associated with precipitation (FEAWP) (See Figure VI-11(b)). Though this hypothesis will adequately explain the highly localized (~ 1 km) and short duration (a few minutes or less) nature of some excursions, it appears inadequate to account for sustained field reversals which are large scale in nature (in the examples we have described). This hypothesis also does not account for the associated dynamical variation in cloud top height and surface pressure, which suggest a global modification of the thundercloud generator.

An additional problem with the FEAWP hypothesis (Moore and Vonnegut, 1977) is the observation of negatively charged precipitation arriving at the Earth during an excursion, which would tend to drive the electric field in the opposite direction. We have already commented on observations of such an occurrence (see Figure VI-4).

Another hypothesis for field excursions was proposed by Moore and Vonnegut (1977) and is closely tied to Vonnegut's picture of convective electrification. This hypothesis is illustrated in Figure VI-4(c). Downdrafts displace the

negative charge in the lower part of the cloud to the sides, thereby exposing to ground observers the positively charged core in the central part of the cloud and causing a reversal in electric field.

Although we do not discount the possible importance of negatively charged downdrafts at the cloud periphery (see Chapter VII), we believe that centrally located downdrafts carrying net positive charge are responsible for field excursions. These motions are best documented for the July 19, 1980 end of storm oscillation (EOSO), a situation which Moore and Vonnegut (1977) do attribute to descending positive charge. Since the pressure signals and cloud motions associated with the foul to fair weather polarity excursion in the EOSO bear so many simlarities with other field excursions, we are of the opinion that they all have common origins. The EOSO is simply the last (and perhaps most vigorous) field excursion to occur in the storm.

Analysis of the evolution of vertical Doppler velocity profiles during field excursions have shown a systematic behavior which is consistent with this interpretation and with the pressure records beneath the storms. The development of the downdraft and commencement of the field excursion followed by a few minutes a rising updraft in the upper half of the cloud and the attainment of maximum cloud height. The fair weather field may grow and persist for several minutes following the decline of maximum downdraft near the ground, and only recovers to its original foul weather polarity after

the initiation of a new surge of convection and the appearance of upward air motion in the top half of the cloud.

We are uncertain about the origin of the positive charge in these downdrafts, but it is likely the result of positive point discharge ions released in the strong foul weather field which invariable precedes a field excursion. Near the ground, the motions of these ions will be largely governed by the electric field, and the ions will move upward toward the cloud until intercepted and immobilized by larger cloud particles. Since the Doppler derived vertical air motions in the lower central portions of thunderclouds are small and more often downward than upward, the positive charge may not make rapid upward progress. The accumulation of this positive charge, as suggested by Malan (1963), therefore seems reasonable under these conditions.

If the convective transport of this positive charge is of importance to electrification (Vonnegut, 1953), then the hypothesized downward motion of positive charge will oppose that process. Although the Doppler observations raise skepticism about efficient vertical transport of corona space charge in precipitation regions, this latter prediction is consistent with the decline in flash rate which often follows a field excursion (as for example on August 16, 1979).

Since precipitation particles contained within the hypothesized positively charged downdraft will grow by accretion of positively charged cloud particles, positively

146

charged precipitation should be observed at the ground during a field excursion. This prediction is consistent with <u>some</u> of the observations (Standler and Winn, 1979; Winn <u>et</u> <u>al</u>., 1980).

VI-9 <u>Conclusions</u>

A close association has been found between the electrical configuration of the cloud and the surface pressure manifestations of vertical air motions. Possible interfering effects (simultaneous updrafts and downdrafts, for example) and variable distance to the pressure source make phase relationships between the variables of interest difficult to pin down, but a correlated behavior frequently persists for the duration of individual thunderstorms. Such closely coupled behavior strongly suggests that the convective motion of electrically charged air plays a controlling role in cloud electrification.

Chapter VII

A Convective Kinematic Dynamo

VII-1   Introduction

Conceptual qualitative discussions of electrical screening layer formation in thunderclouds were put forth by Grenet (1947) and Vonnegut (1953, 1963). Subsequent numerical (Brown et al., 1971) and analytical (Klett, 1972) treatments of screening layer evolution at stationary cloud boundaries have concluded that such structures have a potential for playing significant roles in cloud electrification. Different sorts of evidence for the existence of screening layers in real clouds have been provided by Vonnegut et al. (1966) and Winn et al. (1978, 1980).

In this chapter, we examine a simple steady state kinematic screening layer dynamo with two goals in mind: (1) to establish reasonable upper bounds on the contribution of convective screening layer motion to thunderstorm electrical power and (2) to examine the scaling behavior of this electrification mechanism. The major obstacle to goal (1), in general, has been the complicated nature of the wind field in a thunderstorm, which we bypass by prescribing the motion (a kinematic model). The obstacle to goal (2) has been the nonlinear nature of screening layer formation in an atmosphere whose electrical conductivity increases exponentially with altitude. This problem, however, can be handled analytically, as we will presently demonstrate.

1 (a)

Model geometry

$$c(z) = c_t \exp(-Kz)$$

Z=0

Screening layer

Z=4R
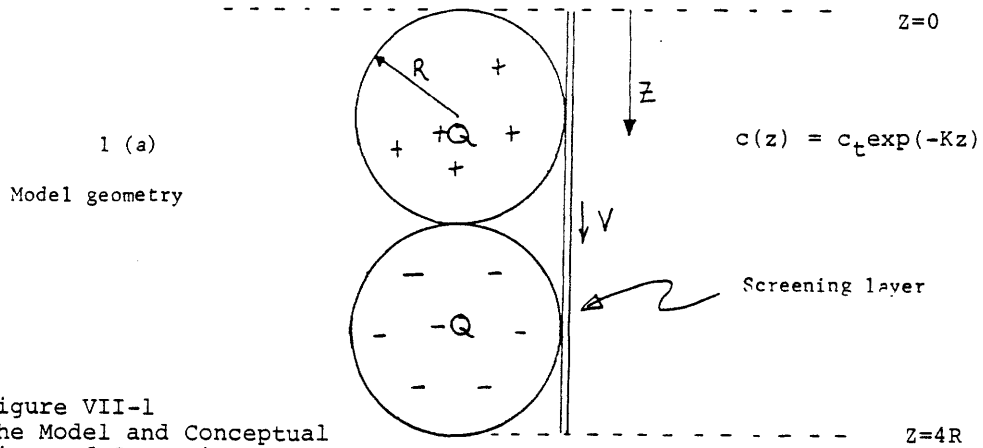
Figure VII-1
The Model and Conceptual
Views of Screening Layer
Convection

1(b)
from Vonnegut (1955)

A   B   C   D

Convective electrification process

1(c)
from
Vonnegut (1963)

CONDUCTION CURRENT

CLOUD BASE

POINT DISCHARGE FROM EARTH
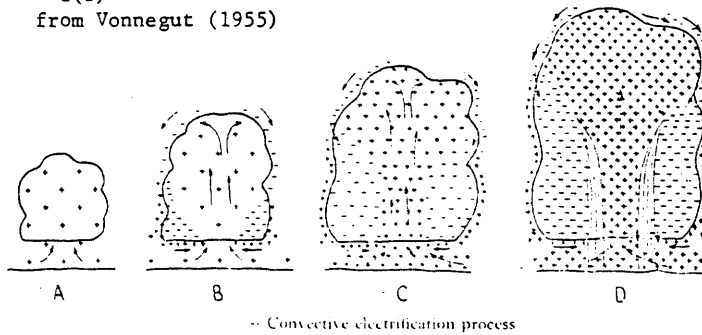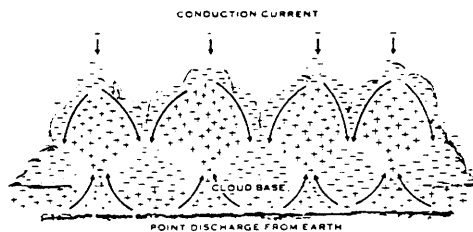
Schematic representation of a group of thunderstorm cells illustrating how the electrification process might be maintained by convection. According to this representation the negative charge attracted to the top of the cloud is carried to the lower part of the cloud by downdrafts while positive charge created by point discharge at the ground is carried to the upper part of the cloud by updrafts.

149

An additional goal, pursued further in Chapter IX, is to investigate the possible importance of a finitely conducting medium for electrification in other planetary atmospheres.

VII-2 Formulation of the Model and Its Predictions

The model, illustrated in Figure VII-1(a), consists of an evolving screening layer (downdraft) which descends vertically at velocity V along a fixed (time independent) distributed positive vertical dipole structure. The downdraft, whose source may be a rebounding turret, "peels off" at the cloud top as fresh uncharged cloudy air, but immediately begins to acquire negative ions from the relatively conductive clear air in its vicinity, in response to the horizontal component of the dipole field, E_{xdip}, at the edge of the cloud. (Conceptual illustrations of this process taken from Vonnegut (1953, 1963) are also shown in Figure VII-1(b,c).) The clear air conductivity is a prescribed exponential function of altitude, with an e-folding scale height of K^{-1}. The ions which flow to the screening layer are captured by ice crystals and cloud droplets and are effectively immobilized. This immobilized negative charge is then conveyed downward in the vertical dipole field, E_{zdip}, to make a $-J \cdot E$ contribution to electrical power.

The horizontal electric field $E_x(z)$ at the screening layer surface has contributions from both the dipole field and the screening layer charge density. Since screening layer thicknesses are usually much less than the cloud size (Brown et al., 1971), we ignore the finite thickness of this charged

zone. For two-dimensional geometry:

$$E_x(z) = E_{xdip}(z) - \frac{\sigma(z)}{2\varepsilon} \qquad (1)$$

where σ is the net charge per unit area in the descending screening layer. This charge density in turn is the result of the unipolar current flow to the cloud surface, integrated from the "peel off" time $t=0$.

$$\sigma(t) = \int_o^t c(z) \, E_x(t) \, dt \qquad (2)$$

where $c(z) = c_{top} \exp(-Kz)$ is the unipolar clear air conductivity. For constant velocity descent

$$t = z/V$$

where z is the distance down from the cloud top and $\sigma(t)$ becomes

$$\sigma(z) = \frac{1}{v} \int_o^z c(z) E_x(z) \, dz \qquad (3)$$

Substituting (3) onto (1) yields

$$E_x(z) = E_{xdip}(z) - \frac{1}{2\varepsilon V} \int_o^z c_t \exp(-Kz) E_x(z) \, dz \qquad (4)$$

Differentiating with respect to z we obtain the following

151

differential equation for $E_X(z)$

$$E_X(z) + (\frac{c_t}{2\varepsilon V} \exp(-Kz))E_X(z) = \frac{dE_{xdip}(z)}{dz} \qquad (5)$$

whose solution can be shown to be

$$E_X(z) = (\frac{1}{\exp(\frac{-c_t}{2\varepsilon vK}[\exp(-Kz)-1])})(E_{xdip}(z=o) +$$

$$\int_o^z (\frac{dE_{xdip}(z')}{dz'})(\exp(\frac{-c_t}{2\varepsilon VK}[\exp(-Kz)-1]))dz' \qquad (6)$$

For the model illustrated in Figure VII-1(a), the expression for E_{xdip} is analytic, and so the integral in the solution (6) could perhaps be eliminated by clever integration tricks. We have preferred to solve equation (6) numerically.

Given $E_X(z)$, we can determine the screening layer charge density from (3), and then calculate the electrical power density contribution

$$-J \cdot E(z) = \sigma(z) \cdot W \cdot V \cdot E_{zdip}(z) \text{ watts/m} \qquad (7)$$

where W is the width of the screening layer (in a direction perpendicular to x and z). Integrating this quantity along the extent of the dipole (along z) yields the net power production:

152

$$\text{Power} = W \cdot V \int_{O}^{z=4R} \sigma(z) \, E_{zdip} \, dz$$

Before discussing the model results, it is useful to point out two dimensionless parameters which have emerged in the foregoing analysis. The first of these is the quantity $\frac{\varepsilon v K}{c_t}$ (see equation (6)), which is the ratio of cloud top clear air relaxation time $\frac{\varepsilon}{c_t}$ to the convective transport time $(VK)^{-1}$ for screening layer air to transit one conductivity scale height. This quantity might be referred to as the electric Reynolds number for this EHD dynamo.

The other dimensionless quantity (see equation (3)) is KR, the ratio of electric dipole size (or cloud size) to the conductivity scale height. The deep tropospheric convection which characterizes thunderstorms occurs on scales which are at least as large, but of the same order of magnitude, as an atmospheric (pressure) scale height. Electrical conductivity is the product of ion density and mobility, each of which has its own scale height, with the result that the conductivity scale height will always be somewhat less than the atmospheric (pressure) scale height. For the earth's troposphere, KR will always be of order 1.

The significance of these two parameters is readily shown by calculating the net dynamo power (8) as a function of each parameter.

Figure VII-2 shows the electric Reynolds number dependence, where we have chosen $K = 1/(3\text{km})$ (following Israel, Vol. II, p. 341), $V = 10\text{m/sec}$, $Q=400$ C, $R = 3\text{km}$, $\varepsilon = 8.85 \times 10^{-12}$ MKS,

153
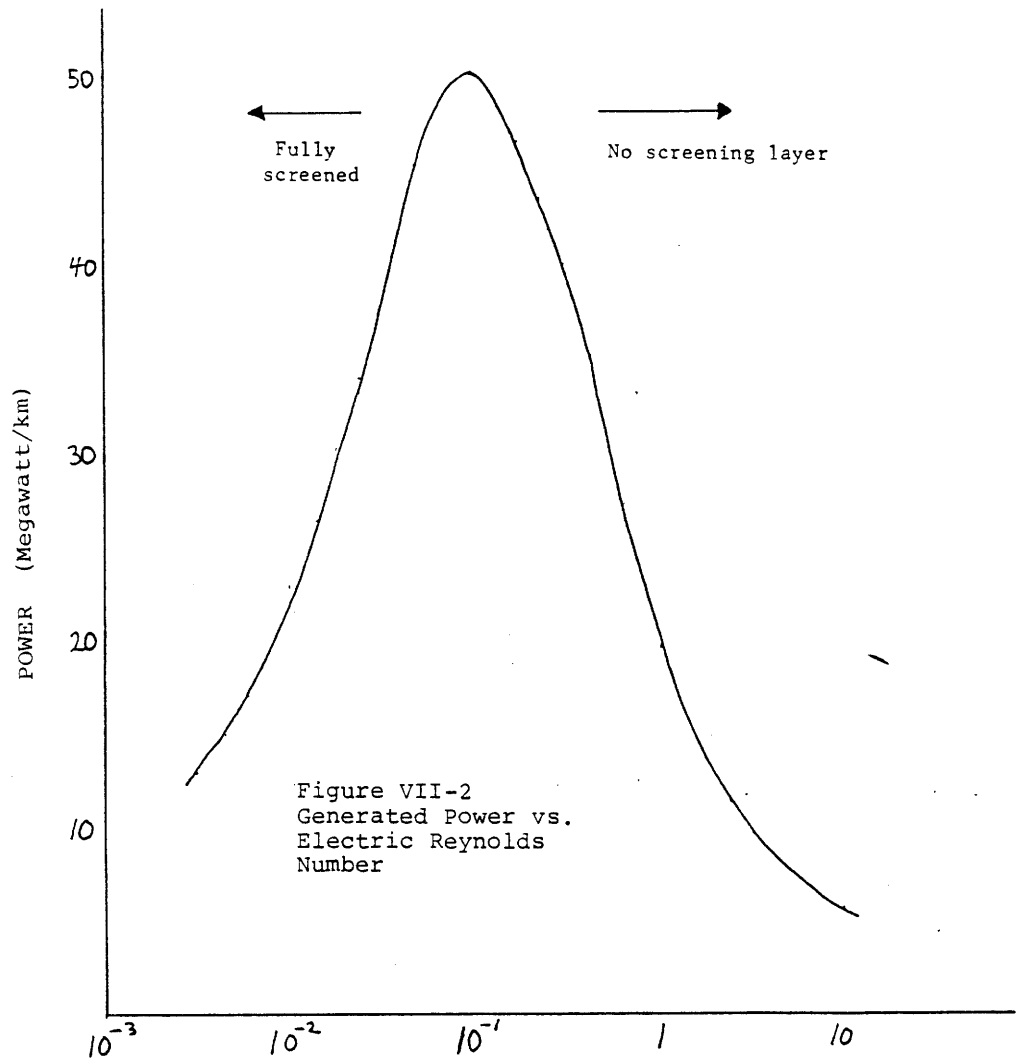
Figure VII-2
Generated Power vs.
Electric Reynolds
Number

$$Re_E = \frac{\epsilon K V}{c_T}$$

154

and varied the conductivity c_t at the dipole top to vary Re_E.
The resulting "bandpass" behavior indicates that the dynamo will
be "tuned" when $Re_E \approx 0.1$. For larger electric Reynolds
numbers, the screening layer descends too fast for appreciable
charge to collect, and less power is produced. At smaller Re_E,
the descending screening layer approaches a fully screened
situation $(E_x(z)=0)$ and the screening layer charge saturates.
Interestingly, the optimum Re_E may often exist for real
thunderstorms (e.g., with reasonable values $K=1/(3$ km$)$,
$V=10$m/sec, $c_{top}=3\times10^{-13}$mho/m, we have $Re_E = 0.1$).

In Figure VII-3 we have calculated the KR dependence for
electrical power, using the same values for the other parameters
as before. Once again, an optimal value exists (KR$\approx$1) which is
of the order of its value in the real atmosphere, as was
mentioned earlier. It can also be seen in Figure VII-3 that the
descending screening layer will generate power even in a medium
with constant conductivity (1/K>>R, KR<<1), but only about half
as much as for the optimum situation. A sort of resonance
situation appears to be at work when the vertical charge scale
and the vertical conductivity scale are comparable. In the
other extreme, when 1/K<<R, KR>>1, the conductivity decreases
very rapidly from the dipole top and again little charge will be
available for transport against the vertical dipole field.

In Figure VII-4 we show vertical profiles of the quantities
of interest for the case of optimum $Re_E = 0.1$. E_{xdip} and

Figure VII-3
Generated Power
vs. KR

Z=0

$E_x(z)$

$\sigma(z)$

E_{xdip}

E_{zdip}

+Q

Z=2R

$-J \cdot E_{zdip}$

Figure VII-4

Numerical results of
model calculations
Q = 400 C
R = 3 KM
c_t = 3 x 10^{-13} mho/m
K^{-1} = 3 KM

-Q

σ	10	5		-5	-10	$\mu C/m^2$
E	-400	-200		200	400	kV/m
POWER				5	10	15	kW/m

Z=4R=12 km
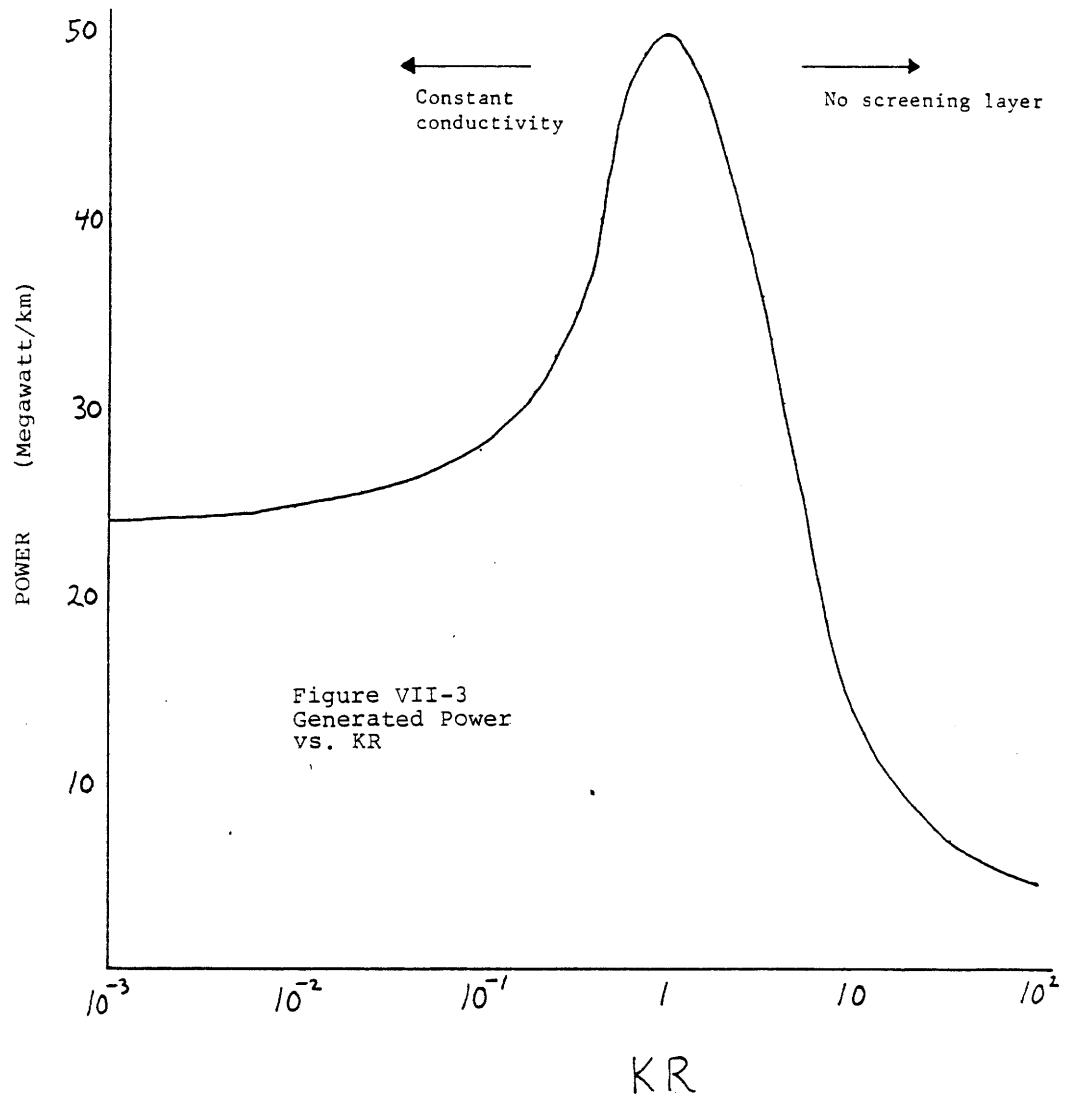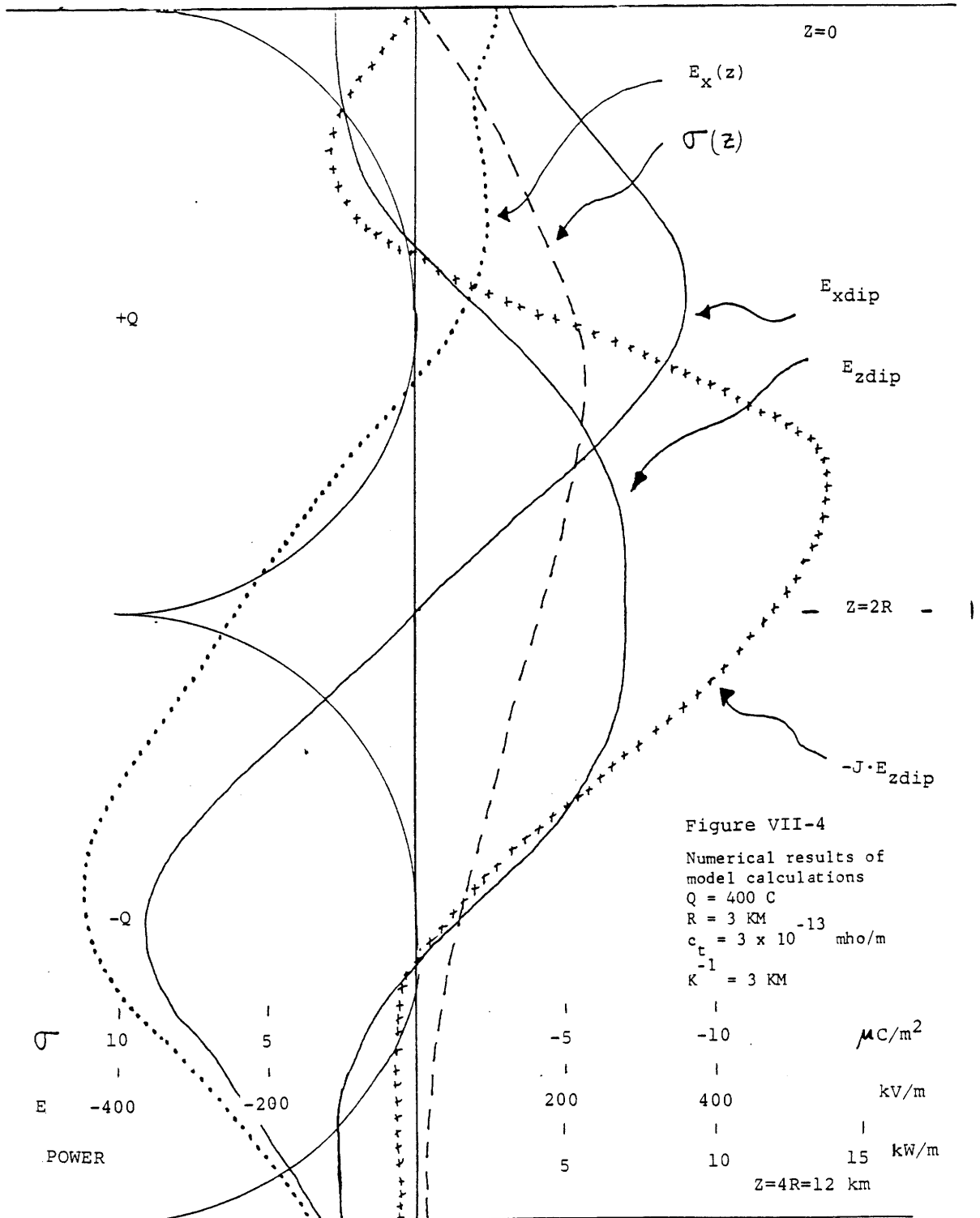
E_{zdip} are calculated along the screening layer from well known analytic expressions. The horizontal field at the screening layer is then calculated from (6), the screening layer charge density σ from (3), and the power per unit length of screening layer from equation (7).

The magnitude of the electric field near the electrically screened cloud top (a few tens of kilovolts per meter to 10^5 volt/m) are consistent with aircraft measurements near the tops of thunderclouds (Bly and Nanevicz, 1977).

Noteworthy is the fact that the net charge in the screening layer is negative over the entire extent (z=0 to 4R) of the layer. Except near the dipole top where negative charge is approaching the positive end of the dipole, and near the bottom where negative charge is conveyed away from the negative end of the dipole, electrical power is generated as a result of screening layer charge transport. The bulk of this power is generated in the upper half of the dipole, where the product of screening layer charge and vertical dipole field strength is maximum. (This latter situation may have some relevance to our real world observations in Chapter IV of VHF emission predominating in the upper draft regions of thunderstorms.) Additionally, we note that the negative screening layer charge makes a significant contribution to the horizontal electric field in the lower portion of the dipole.

These profiles demonstrate that the effectiveness of this sort of dynamo is due to the quasi-orthogonality property of

158

the horizontal and vertical component of a dipole field. The maximum screening tendency occurs when E_{xdip} is maximum (near the dipole top). The trapped charge is then conveyed through the maximum in E_{zdip} a quarter wavelength further down to generate power.

VII-3 The Scaling Behavior of the Dynamo

The purpose of this section is to examine the scaling behavior of certain parameters for this dynamo model. A cursory scaling comparison between electrification mechanisms which derive charge from within the cloud and mechanisms which derive it externally indicates that the internal mechanism should produce charge at a rate proportional to the cloud volume and the external supply should be controlled by the surface area of the cloud. From this viewpoint, the availability of internally derived charge would be highly favored for large clouds. This argument, however, ignores, among other things, the exponential scaling of clear air conductivity with cloud size, a point first emphasized by Vonnegut and Moore (1958). With the model we have formulated, we are able to incorporate this dependence, and can investigate how the negative charge flow to the cloud surface and the electrical power generation scale with storm (dipole) size.

Following our assumptions in Chapter V on scaling laws, we take the dipole space charge density to be scale invariant, and so the steady-state dipole charges $\pm Q$ vary as R^3. The vertical velocity is assumed to depend linearly on dipole size,

159

consistent with the results presented in Figure V-2 of
Chapter V. The screening layer is wrapped around the dipole in
cylindrical fashion and therefore has an effective width of
$2\pi R$. The clear air electrical conductivity, C_T, increases
exponentially with cloud size. Calculations for the unipolar
negative ion flow to the cloud and the electrical power due to
screening layer charge transport for a range of dipole sizes
are shown in Figures VII-5 and VII-6, respectively.

The most significant feature of Figure VII-5 is that the
rate at which externally derived charge is supplied to the
cloud tends to scale more like the cloud volume ($\sim L^3$) than like
its surface area ($\sim L^2$). This stronger scaling is primarily the
result of the exponential increase of atmospheric conductivity,
but is also a consequence of the greater negative-seeking
positive charge in the larger clouds and the larger velocity
with which negative is transported away (downward).

As far as electrical power scaling is concerned (see
Figure 6), over the range of sizes 4R = 6 km to 22 km the
behavior follows closely an L^5 dependence, in closer agreement
with the flash rate-cloud height data than the L^4 dependence
(also drawn in Figure VII-6) predicted for precipitation charge
transport.

VII-4 The Model's Applicability to Real Thunderclouds
The applicability of these results will depend in large
part on the shortcomings of the model. Some of these
shortcomings are addressed below:

160

Figure VII-5
Charge Flow to Cloud Top
vs. Cloud Size

CURRENT (Amperes)

EQUIVALENT HEIGHT (km)

161

Figure VII-6
Electrical Power Scaling
for the Kinematic Dynamo

⊕ Model Calculations

$K^{-1} = 3$ km

m=5

m=4

GENERATED POWER (Watts)

DIPOLE SIZE (=4R)
(km)
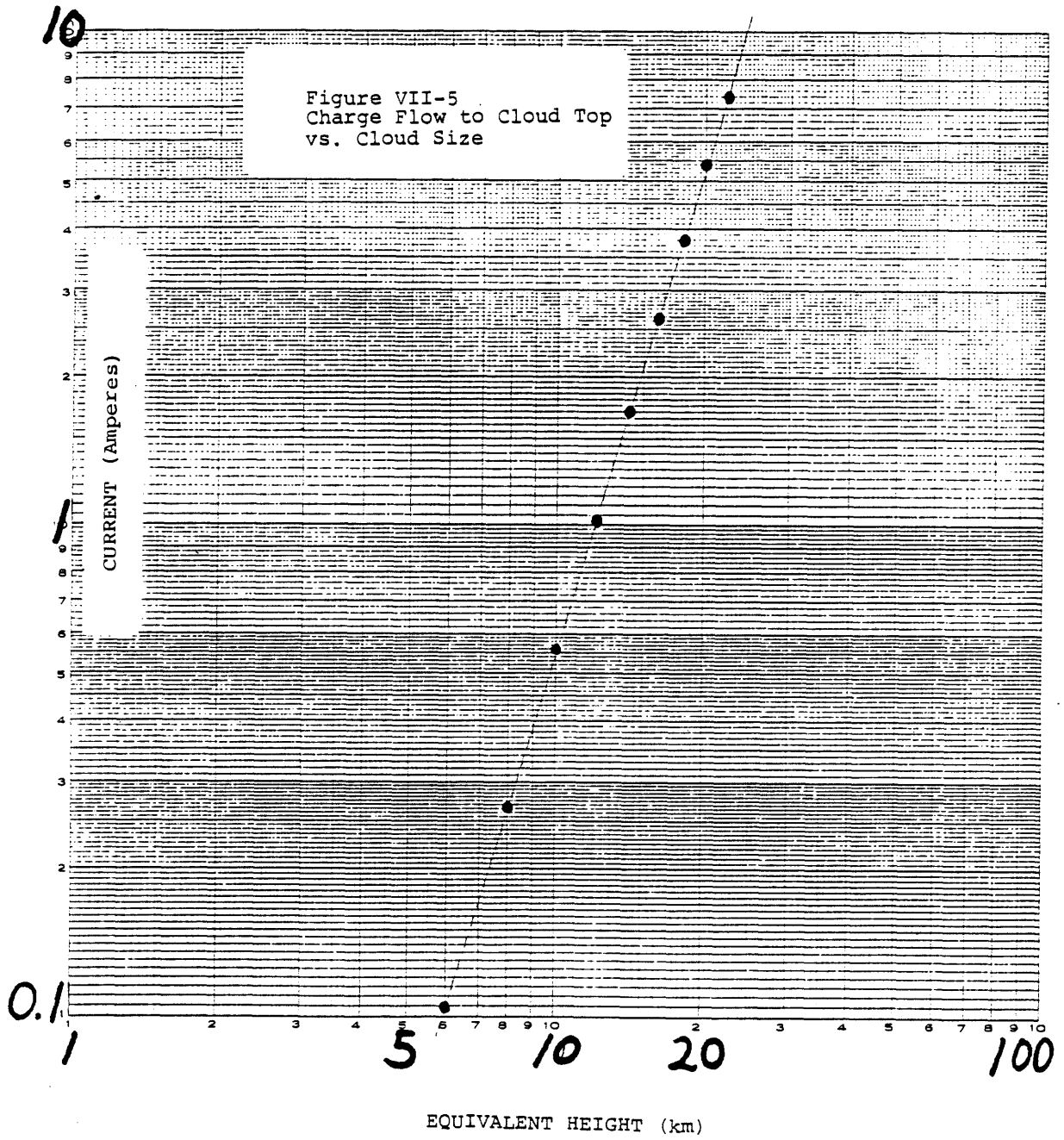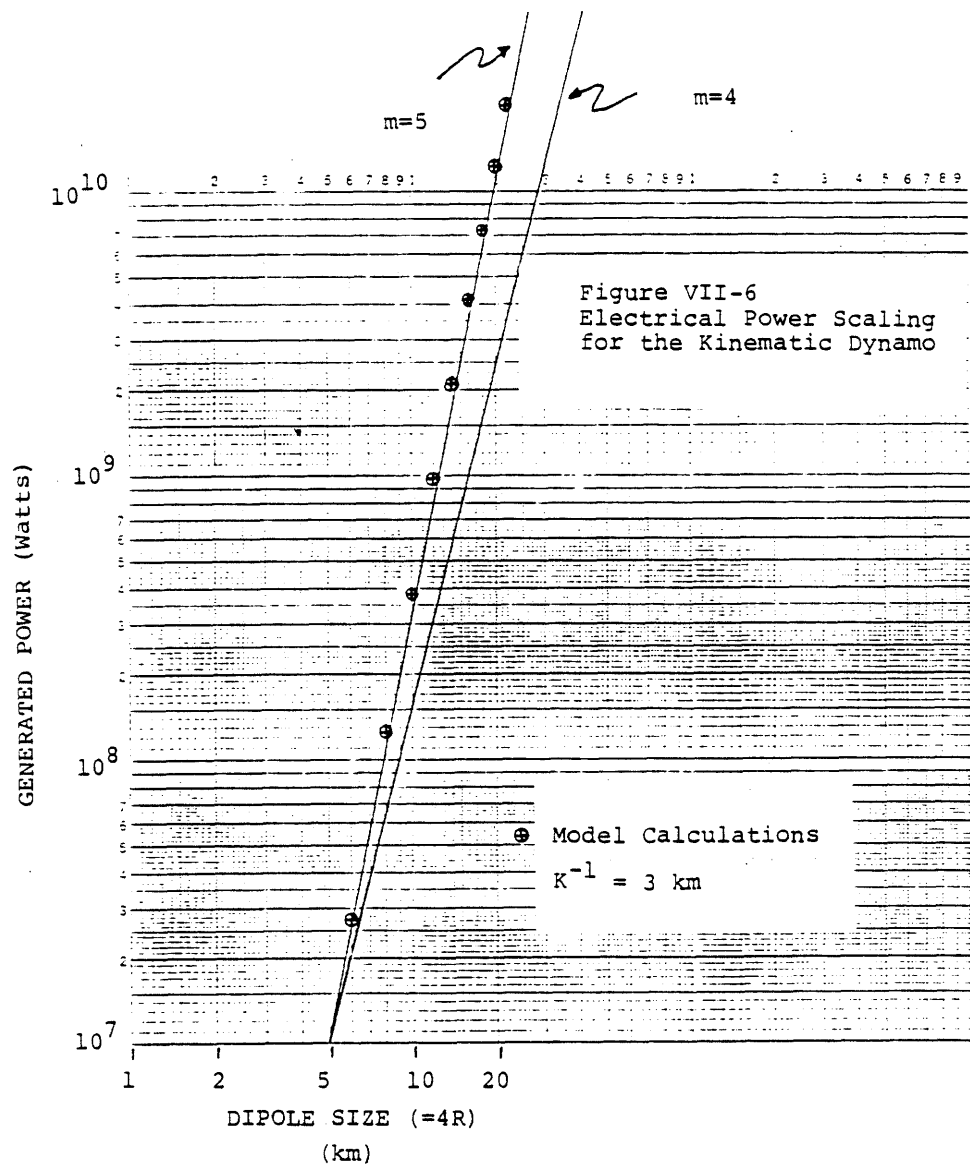
(1) Neglect of turbulent mixing. This question has been raised by Klett (1972) (to name one) and is probably the major obstacle in evaluating the importance of screening layer charge transport to thunderstorm electrification. Eddies whose sizes are comparable with the screening layer thickness will tend to destroy the structure of such a feature in times which may be short in comparison with the larger scale convective transport time. This problem will be mitigated somewhat when screening layers are hundreds of meters thick as they may be in the ice crystal region of a mature thunderstorm, but according to Klett (1972) the 'stir-up' time is not a strong function of screening layer thickness.

The existence of strong large scale downdrafts responsible for the hypothesized charge transport is now well established through doppler radar observations (see for example, Lhermitte and Krehbiel, 1979). These features are driven in part by evaporative cooling at the cloud boundary, which in turn should be enhanced by strong mixing in this region. It is possible that such mixing works against the preservation of a screening layer. Downward motion may also be driven by the negative buoyancy of overshooting cloud turrets.

(2) Fixed conductivity at the cloud boundary. Our assumption is equivalent to that of Brown et al. (1971) which fixes the ion concentration at the cloud boundary. Klett (1972) has questioned this assumption but his analysis for a stationary cloud is not applicable here. In reality, the screening layer evolution at the cloud top depletes the

surrounding clear air of negative ions and an electrode layer

forms. This is a nonlinear problem (see for example, Hoppel

and Phillips, 1971), but an order of magnitude estimate of the

electrode layer thickness is the ion flux at the cloud boundary

divided by the ion production rate in the clear air at the same

altitude. This calculation results in electrode layer

thicknesses of a few kilometers, which suggests that this

omission is significant, though I am unaware of any

observational evidence for this electrode layer. The

calculations in the model of course ignore the details of ion

population on both sides of the cloud boundary. These details

could be incorporated numerically but such an effort hardly

seems justified in view of our ignorance about the field of

motion in the vicinity of the cloud boundary.

It is important to note here that the radar reflectivity

within a screening layer at a cloud boundary may be small, and

therefore conventional Doppler radar techniques will be

ineffective in probing the motion field in this region.

(3) Neglect of the effect of screening layer charge on the

vertical component of electric field through which the charge

is transported. Though this effect has not been included in

the equations presented ((1) through (8)), we have included it

in subsequent numerical calculations. In many cases this

inclusion increases the upward component of vertical dipole

field near the dipole top. Power profiles with and without

this inclusion are shown in Figure VI-7. In extreme cases, the

discrepancies in total power were factors of two.

Z=0

Effect of Screening layer
charge on E_z included

+Q

— Z=2R

Effect of screening
layer charge on E_z
neglected

-Q

Figure VII-7
Power Generation
Profiles

-10   -5   5   10   15 kW/m

Z=4R=12 km

165
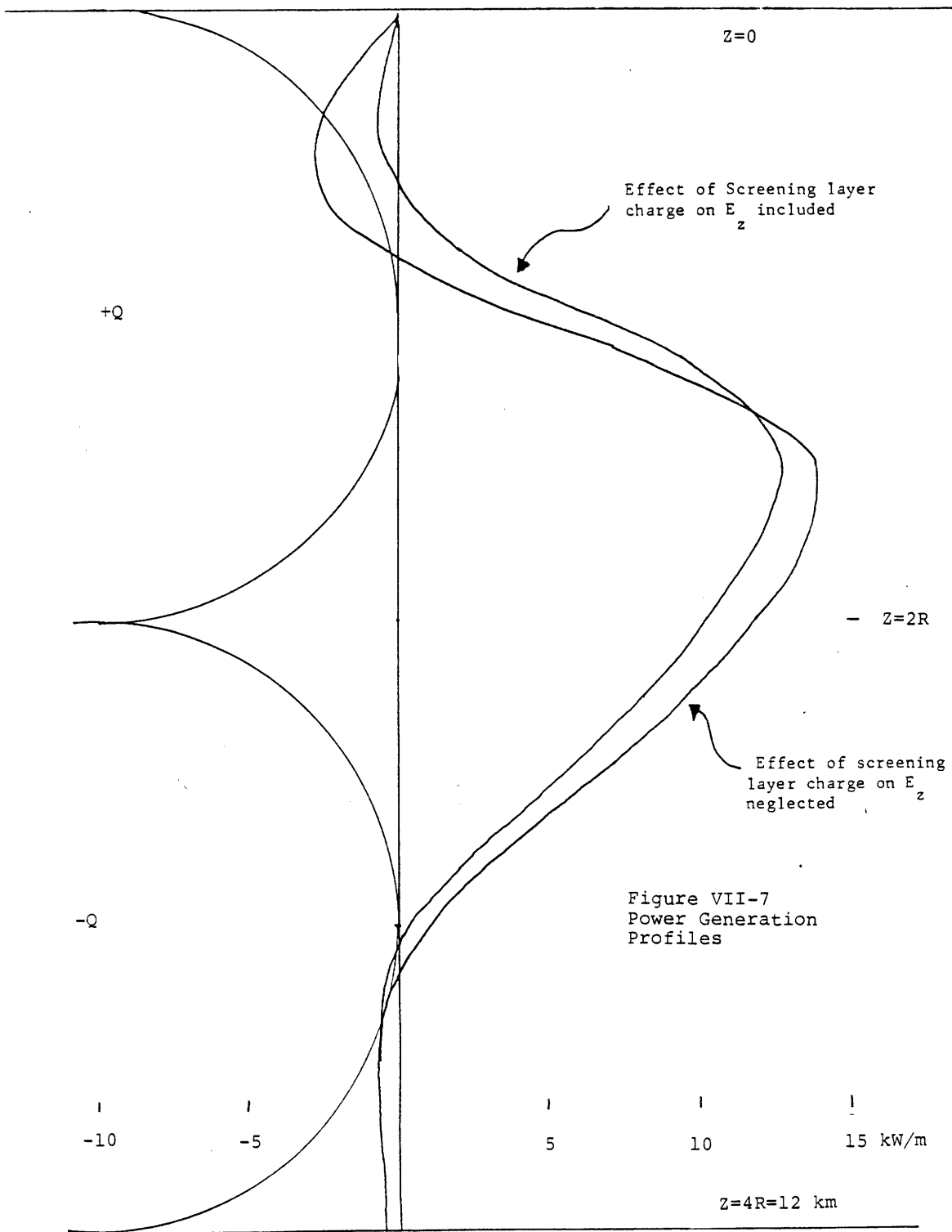
(4) The assumption concerning the immobilization of ions on cloud particles in the screening layer. This assumption is never strictly upheld and it is generally recognized that cloud particles may carry sufficient charge to achieve velocities of several meters per second in fields of thunderstorms magnitude. We have ignored the dissipative contribution of such motions. The magnitude of this contribution has been a controversial issue (Vonnegut et al., 1966; Kamra, 1979). Because we have ignored the finite mobilities of the screening layer particles, as well as the effect of screening layer mixing (item (1) above), both of which will degrade the performance of the generator, our results can be considered only upper limits on available power from screening layer convective charge transport.

(5) Bootstrapping and the absence of feedback. We have made no attempt to explain the pre-existing dipole field, nor does the dynamo pump any charge back to the dipole to maintain or enhance it. Recently, Moore et al. (1980) have used pairs of delay differential equations to describe the feedback effects of space charge transport by convection. Their model evolves from a primed zero electrification state, and grows exponentially. Since the thrust of our study has been to investigate electrical power generation in quasi-steady state systems which are active lightning producers, our model is steady state. To include the effects of feedback (which are unquestionably important) and still maintain a steady state requires the inclusion of the dissipative and discontinuous

166

contribution of lightning. Such an inclusion will add

considerably to the complexity of the problem, and has not yet

been pursued.

Chapter VIII

Continental versus Oceanic Thunderstorm Electrification

VIII-1   Introduction

Although both continental and oceanic cumulonimbus clouds have long been recognized as lightning producers, only in recent years (with the advent of satellite data) has the disparity between continental and oceanic lightning been realized (Vorpahl (1967), Edgar (1978), Orville and Spencer (1979), Orville (1981)). This chapter is concerned with the land-ocean disparity in flash rate per storm, and the possible implications for the origin of thunderstorm electrification.

VIII-2   The Available Data

The disparity between continental and oceanic electrical activity has appeared in both global lightning flash counts and in global sferics counts.

Orville and Spencer (1979) have completed the most thorough optical flash count to date. Their results show an area-normalized land/ocean flash ratio of 18/9 for dusk/midnight observations if all flashes occurring within 50 km of the coast are counted as land lightning. With strict separation at the coastline in another data set, Orville (1981) finds area normalized ratios ranging from 3.6 to 4.5 for midnight lightning.

A point worth emphasizing is that ratios obtained from the necessarily nighttime satellite data will all be biased in favor of oceanic events, since the local diurnal variation of open ocean thunderstorm activity has a broad maximum between 2100 and 0600 Local Time (Sanders and Freeman, (to be published)). According to the analysis of the diurnal variation of potential gradient (Whipple, 1929), the most intense thunderstorm activity occurs over the continental regions of tropical Africa and South America during local afternoon. The flashes in these daytime storms cannot be "seen" in the satellite data.

For comparison with the optical results are the hard-to-come-by global sferics data. Figure VIII-1 from Freeman (unpublished, 1974) shows the distribution of observed sferics in the Eastern Hemisphere for all of 1972. A comparison between land and ocean counts yields a ratio of 4.9. Though these data lack the resolution necessary for strict coastline separation, this latter estimate agrees closely with Orville's (1981) results.

Part of the explanation for these large land/ocean ratios is the greater probability of occurrence of thunderstorms over land than over water. Brooks (1925) assumed that thunderstorm occurrence probabilities were proportional to thunderstorm day counts, and using the then available data, he estimated a land/ocean thunderstorm ratio (per unit area) of 2.5. A similar

Figure VIII-1
Distribution of Sferics in the
Eastern Hemisphere for 1972
from Freeman (1974)
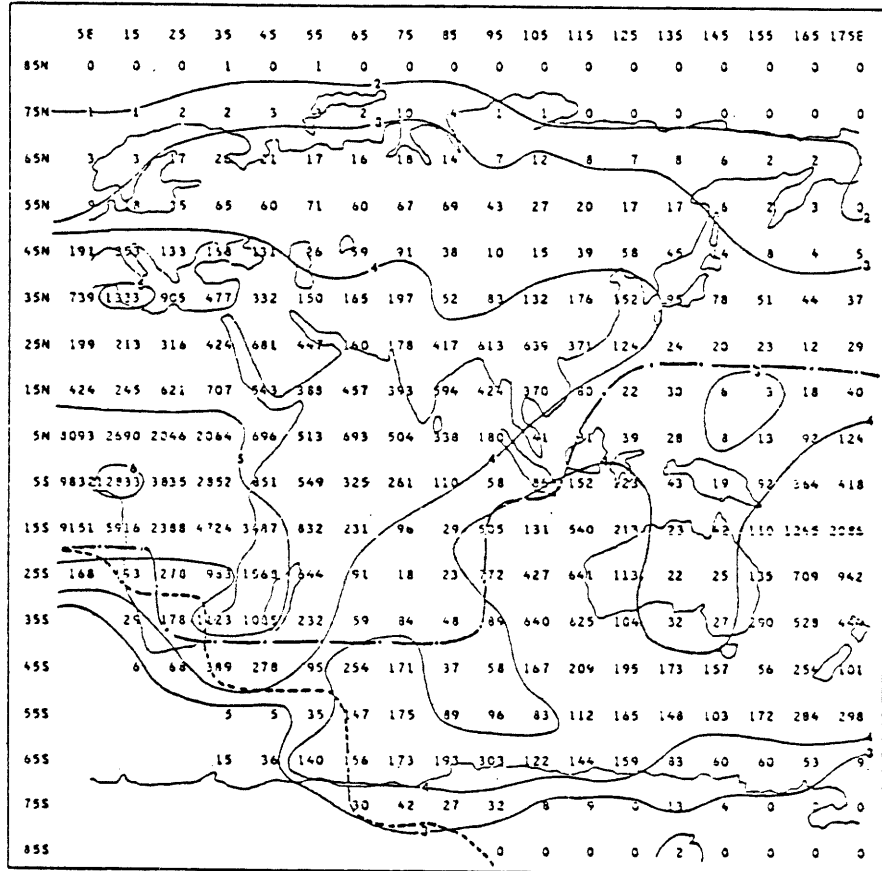
Distribution of the estimated number of lightning discharges for 1972. The broken line is the average threshold-sector line for the period January to July 1972 and the dash-dot line is that for the period August to December 1972. Values are in hundreds of discharges for 10-deg data blocks centered at the points shown. Isolines are number of discharges in powers of 10.
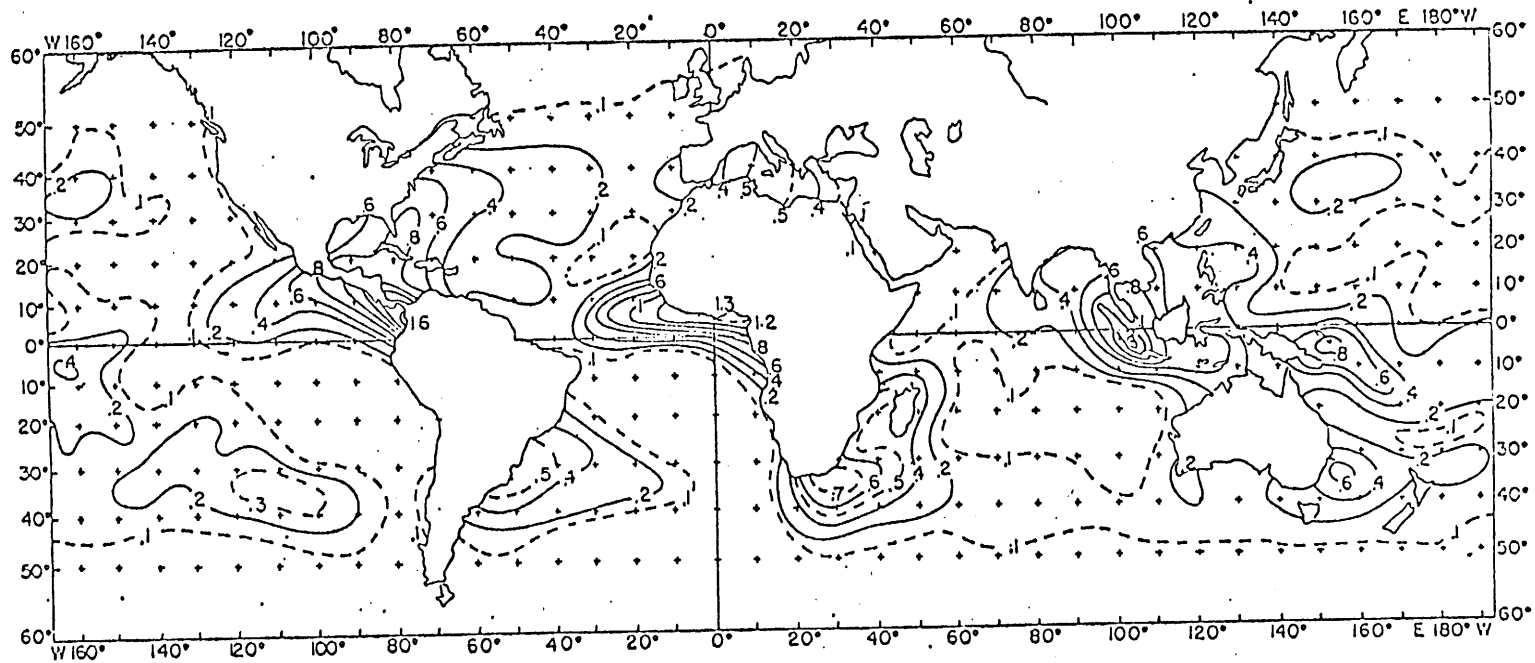
Figure VIII-2
Oceanic Thunderstorm
Probability:
WMO Data
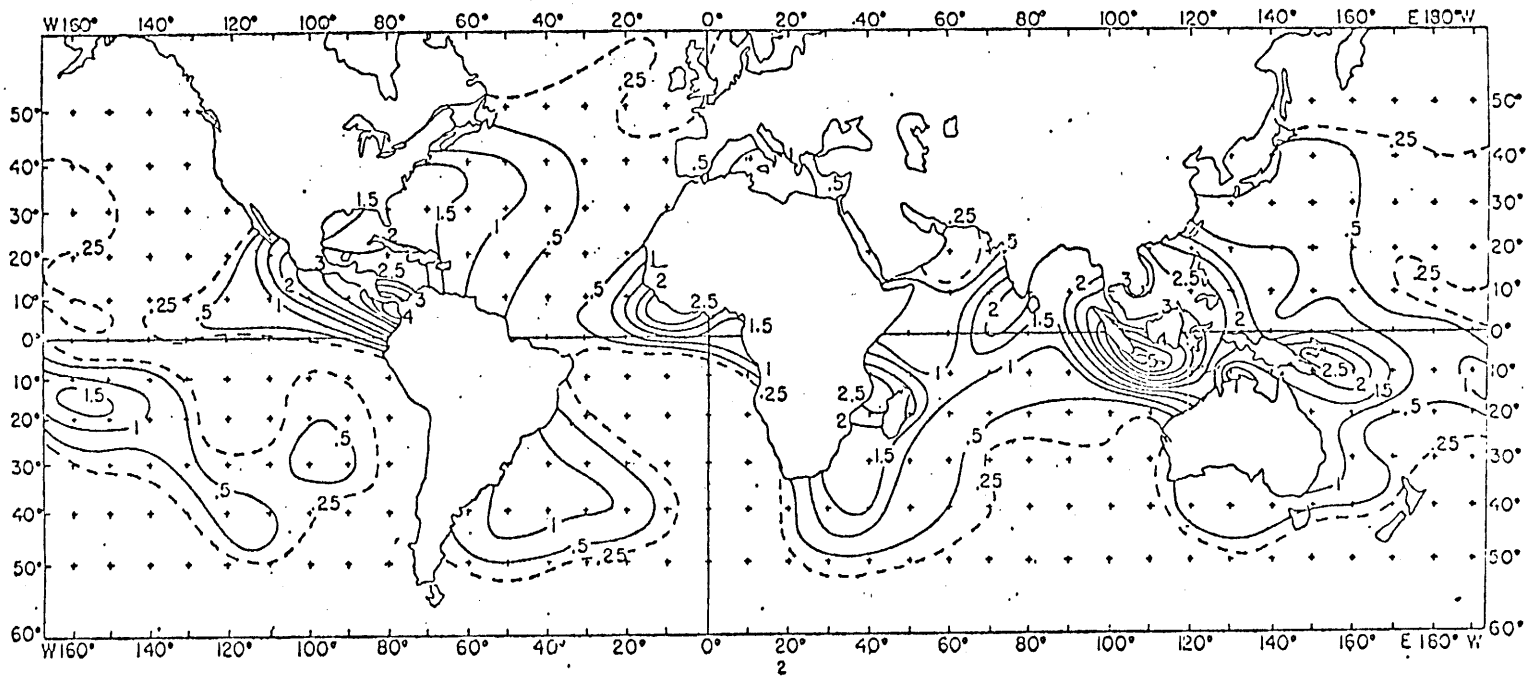
Figure VIII-3
Oceanic Thunderstorm
Probability:
Trent and Gathman(1972)

calculation with global thunderstorm statistics published by
the World Meteorological Organization (1956), which shows
greater frequencies of both continental and oceanic
thunderstorms, yields a ratio of 2.4.

Still more recent (and presumably more complete) oceanic
thunderstorm data, compiled by Trent and Gathman (1972) and
summarized by Sanders and Freeman (to be published),
indicates that the probability of occurrence of oceanic
thunderstorms is still larger (often by a factor of two) than
the WMO estimates. Figures VIII-2 and VIII-3 from Sanders and
Freeman illustrate the discrepancies in these two data sets.[*]
If the WMO data is reliable for land thunderstorms and if the
Trent and Gathman data is more representative for oceanic
thunderstorms, the inferred land/ocean storm ratio could be as
small as 1.5.

One final estimate of this latter ratio may be made. Both
total flashes and total storms were counted in one early
satellite lightning study (Vorpahl, 1967; Vorpahl et al.,
1970). The total area land/ocean flash ratio of 50 (Vorpahl,
1967) is larger than other estimates (Orville and Spencer,
1979), as is the land ocean storm ratio of 10

---

[*] Sanders and Freeman attribute this discrepancy to the
"inclusion of observations of lightning alone, which were
evidently excluded from the WMO data." However, the
Introduction to the WMO publication states explicitly that
"percentage frequencies of lightning seen for ocean regions
poleward of latitude 30 in both hemispheres" were included in
the compilation.

(Vorpahl et al., 1970). Combining these two results, we have a land/ocean flash rate per storm ratio of 5, which is only slightly larger than our other estimates.

From a purely statistical standpoint, we conclude that the flash rates of continental thunderstorms exceed the flash rates of oceanic storms by a factor of 2 to 5. Recalling the tentative result in Chapter V that the energy per flash tends to be independent of cloud size, we can further conclude that the electrical power generation for land storms is greater than for those over the sea.

Possible explanations for this discrepancy are discussed in the following two sections.

VIII-3 A Possible Difference in Cloud Size

The most obvious explanation for the greater electrical activity in continental storms is that these clouds are on the average larger than those over the ocean. We demonstrated in Chapter V on scaling laws that the flash rate of a thunderstorm depends roughly on the fifth power of its size. A factor of two in flash rate therefore corresponds with a factor $2^{1/5}$ (on the average) in cloud size. If oceanic thunderstorms are (on the average) 12 km high, then continental thunderstorms would need be 13.8 km high to explain a factor of two in the land/ocean flash rate ratio. A factor of 4 in this ratio would require a 32% edge for continental cloud heights (15.8 km vs. 12 km). The predicted height difference could be checked with

174

currently available infrared satellite data (Minzer et al.,
1978), but we are unaware of any study on the global statistics
of thunderstorm cloud heights.

Other parameters which increase with thunderstorm size may
be compared for particular cases, but the results of these
comparisons are contradictory.

The vigor of convection is known to increase with storm
size, a key point in Chapter V. A recent comparison (LeMone
and Zipser, 1980) of updraft velocities for oceanic
cumulonimbus clouds off the west coast of Africa and
thunderstorms in Ohio (Byers and Braham, 1949) show a factor of
two discrepancy in updraft velocity in favor of the continental
storms. Unfortunately, we do not know how representative these
two storm types are of oceanic and continental thunderstorms.
Cloud height comparisons are not available, nor are flash rate
data.

Larger storms are expected to consume greater quantities of
water vapor and estimates of the global water vapor
distribution are available (Bannon and Steele, 1957). These
data show that the greater part of the water vapor mass resides
over the oceans (land/ocean ratio per unit area $\simeq$ 0.4), and
although maxima in the water vapor distribution exist in the
tropical regions of South America, Africa, and Southeast Asia,
they are never a factor of 2 larger than the corresponding
oceanic values at the same latitude.

Larger storms are also likely to produce greater quantities
of precipitation (see Chapter V, Section 8), and here too

175

oceanic and continental comparisons may be made. Consistent with the water vapor data, the global oceanic precipitation exceeds that over land (land/ocean ratio = 0.64) (Haurwitz and Austin, 1944; Budyko, 1962). (We do not know what fraction of the global precipitation is produced by thunderstorms.) However, over tropical islands where both water vapor and convection-triggering local heating are available, the island rainfall may exceed that over the adjacent ocean. Reed (1980) finds an average island/ ocean rainfall ratio of 1.9.

We repeat that comparisons of this kind are not definitive and stress the need for satellite storm size comparisons to fully test the hypothesis presented in this section. We now turn attention to what we believe is a clear-cut distinction between continental and oceanic thunderstorms, and which may offer another explanation for the discrepancy in electrical output.

VIII-4 Differences in Subcloud Current

The corona current which flows from asperities on the Earth's surface beneath continental thunderstorms is acknowledged to be a significant item in the cloud electrical budget (Wormell, 1930; Standler and Winn, 1979). Whereas this flow of charge is contributing to Vonnegut's (1953) convection mechanism, it can only dissipate the electrostatic energy which may accumulate due to falling precipitation (Illingworth and Latham, 1977).

The smoothness of a water surface can suppress corona, and surface electric fields beneath thunderclouds over water may be

far larger than those observed over land (Toland and Vonnegut, 1977). In the case of oceanic thunderstorms, the sea surface is likely to be very agitated through the effects of wind and splashing precipitation particles. Under such circumstances, charge transfer from the ocean surface is possible by at least two processes which have been studied in the laboratory: (1) the production of corona resulting from raindrop impingement on a water surface in strong electric fields (Phelps et al., 1973; Griffiths et al., 1973), and (2) the induction charging of jet drops in sea surface spray in response to the surface electric field (Blanchard, 1961).

The impact corona mechanism is inoperative in fields less than 180kV/m, but depends markedly on both electric field and the distribution of drop sizes above this threshold field (Griffiths et al., 1973). We have assumed Marshall-Palmer type raindrop distributions to calculate current densities for electric fields in excess of threshold. The behavior of the current density for three different precipitation rates is shown in Figure VIII-4.

The other possible charge transfer mechanism, the induction charging of jet drops, has been shown by Blanchard (1961) to be linear with field to 450 kV/m. Using jet drop size distributions for various wind speeds presented in his thesis, we have estimated the surface current density expected from this mechanism. These results for various surface wind speeds are also included in Figure VIII-4.

177

Figure VIII-4
Charge Transfer from
Continental and Oceanic
Surfaces Beneath
Thunderstorms

50mm/hr

10mm/hr

P = 2mm/hr

Corona
Associated with
Precipitation
Impingement

Standler & Winn
(1979)
Cubic Relation

30
20
10 knots

Wind Speed

Jet Drop
Induction Current
Blanchard (1961)

SURFACE CURRENT DENSITY (Ampere/m^2)

SURFACE ELECTRIC FIELD (VOLT/M)

10^{-1}

10^{-3}

10^{-5}

10^{-7}

10^{-9}

10^{-11}

10^{-13}

10^{-15}

10^3

10^4

10^5

10^6
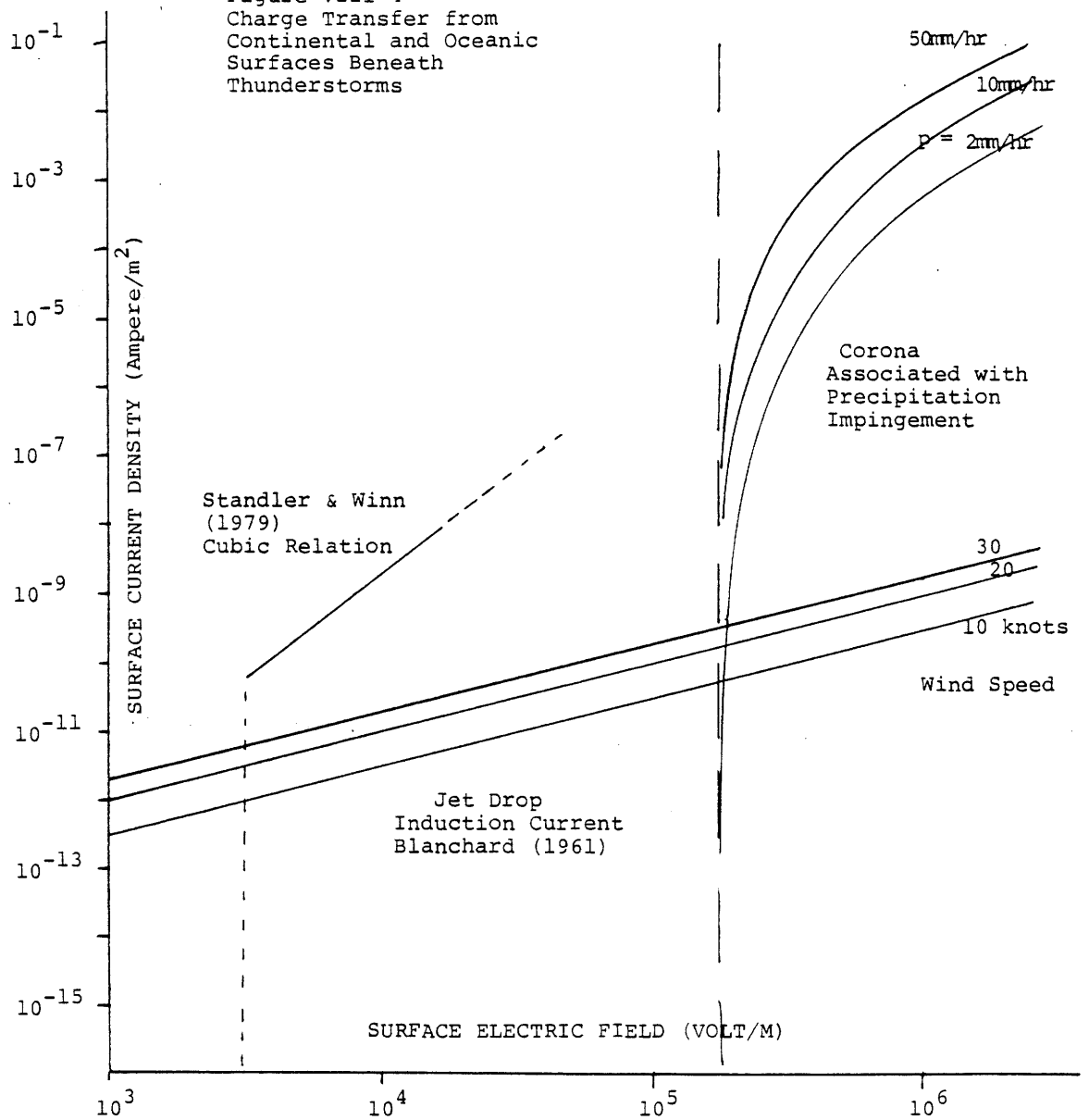
The most recent results on corona beneath continental thunderstorms (Standler and Winn, 1979) indicate threshold fields of a few kilovolts per meter and a cubic dependence of corona current density on surface electric field. For comparison with the charge transfer predictions for oceanic storms, this relationship is also included in Figure VIII-4.

For fields less than the 180 kV/m threshold (in a range expected for surface fields beneath thunderclouds) the continental current density is at least an order of magnitude greater than one might expect in the oceanic case (from induction charging). Much larger oceanic current densities are possible in the presence of precipitation and surface fields greater than 180 kV/m, but as Griffiths et al. (1973) have pointed out, this contribution will quickly self-limit and never provide sustained charge transfer. We therefore believe that the steady component of charge transfer beneath oceanic thunderstorms is negligible in comparison with that from the land.

With the absence of the dissipative effects of subcloud corona current, the oceanic clouds are expected to produce more frequent lightning than a continental storm of comparable size. This prediction is contrary to the observations. It is therefore quite possible that the subcloud corona current may contribute to the electrification of continental clouds, as Vonnegut (1953) first suggested.

VIII-5 Conclusion

The presently available information on global lightning frequency shows that the flash rate of continental thunderstorms is greater than for oceanic storms. This discrepancy may be due to a difference in respective cloud size, or to a difference in the subcloud corona current. More data are needed to distinguish between these two hypotheses.

Chapter IX

Comparative Planetary Electrification

IX-1   Introduction

The relative importance of precipitation and convection to electrification is not a question applicable only to terrestrial thunderstorms. Within the last five years lightning has been identified in the atmospheres of both Venus and Jupiter. This chapter is concerned with comparisons of planetary atmosphere electrification parameters which may shed additional light on this central question. These parameters are discussed in Section IX-2.

A parameter of particular interest is the atmospheric electrical conductivity. Field independent precipitation mechanisms should operate most effectively in an atmosphere with vanishing conductivity, whereas the convective mechanism proposed by Vonnegut (1953) and treated in Chapter VII relies on a finite atmospheric conductivity as a source or electric charge. The general validity of the latter mechanism would provide a symmetry between electrohydrodynamic and magnetohydrodynamic field generation: magnetic dynamos require a finitely conducting (not infinite) fluid for field regeneration and thunderstorms require finitely conducting (not zero) atmospheres to produce lightning.

Procedures for determining the verical structure of electrical conductivity in a planetary troposphere are developed in IX-3, and applied to both terrestrial and Jovian planets. The influence of the planetary magnetic field, which

181

is important for the atmospheres of the Jovian planets, is also treated.

In the final Section IX-4 each planetary atmosphere is discussed in light of the electrification parameter comparisons and the conductivity structure predictions.

IX-2 Atmospheric Parameters Relevant to Electrification

Because of the relatively conductive nature of space plasmas, stellar interiors, and the deep interiors of planets, large scale electrification and dielectric breakdown phenomena in the universe are confined to the gaseous media of planetary atmospheres. In this section we briefly examine those parameters of significance to electrification in the atmospheres of the terrestrial and Jovian planets. A summary of these parameters may be found in Table IX-1.

IX-2.1 Energy Supply for Electrification

The common energy source for all solar system atmospheric processes is of course the Sun. The solar flux at each planet relative to the terrestrial value (=1) are given in Table IX-1. Present areal flash rate results for the Earth, Venus (Borucki et al., 1981) and Jupiter (Lewis, 1980) follow the trend in solar flux (Table IX-1).

An additional energy source for the Jovian planets is the internal heat generated by gravitational collapse, and for Jupiter and Saturn is estimated (Stone, 1976; Erickson et al., 1978) to be of the same order as the respective solar fluxes.

Table IX-1

Parameters Relevant to Electrification in Planetary Atmospheres

	gravity (m^2/sec)	Scale Height (km)	Solar Flux Relative to Earth	Atmospheric Density (kg/m^3)	Precipitation Particle Terminal Velocity (m/sec)	Wind Velocity Horiz. (m/sec)	Vert. (m/sec)	Cloud Forming Condensates	Dielectric Strength v/m	Lightning Flash/km^2/ year
Mars	3.7	11	0.43	1.6×10^{-2}	Precip. Unlikely	120		CO_2 H_2O	7×10^4	Doubtful
Venus	8.7	7	1.94	0.9	8	200	40	H_2SO_4	2×10^6	30 Yes
Earth	9.8	8	1.0	1.0	7	50	80	H_2O	2×10^6	6 Yes
Jupiter	26	19 (NH_3)	3.7×10^{-2}	0.2	21	100	64	NH_3 NH_4SH	4×10^5	3×10^{-3}
		40		0.7	14		110	H_2O	1×10^6	Yes
Saturn	11	53 (NH_3)	1.1×10^{-2}	0.5	9	450		NH_3 NH_4SH	1×10^6	?
		93 (H_2O)		1.6	6		110	H_2O	4×10^6	
Uranus	10	36 (H_2O)	2.7×10^{-3}	0.5	8	?	110	Ch_4 NH_3	1×10^6	?
		67 (NH_3)		1.6	6			H_2O NH_4SH	4×10^6	
Neptune	15	22 (H_2O)	1.1×10^{-3}	1	7	?	110	Ar Ch_4 H_2O NH_3	2×10^6	?
		47 (NH_3)		5	4			NH_4SH	8×10^6	

183

IX-2.2 Cloud Size

The discussion on scaling laws for electrification in Chapter V emphasized the importance of cloud size for convection and electrical activity. Cloud sizes in any atmosphere will be highly variable but will generally be of the order of the atmospheric scale height ($H_s = kT/mg$). This statement is readily confirmed by the terrestrial case ($H_s \sim 8$ km), but is further emphasized by the Venusian case ($H_s = 7$ km). The depth of the latter atmosphere from planetary surface to tropopause is about 10 scale heights, yet the three principal cloud layers have thicknesses of the order of one scale height (Knollenberg et al., 1981).

Owing to the relatively low molecular mass of the Jovian planetary atmospheres, their respective scale heights are significantly larger (by as much as an order of magnitude) than for the terrestrial planets. The expectation of larger clouds is consistent with space probe observations of "puffy" convective elements 100-200 km in size (Smith et al., 1979).

IX-2.3 Cloud and Atmospheric Chemistry

The planetary atmospheres in question are marked by very distinct differences in chemical composition. The predominant gaseous constituent for Mars and Venus is carbon dioxide, whereas the Jovian planets consist of solar composition hydrogen (86%) and helium (11%).

184

Principal cloud condensates are sulphuric acid (H_2SO_4) for Venus (Knollenberg, et al., 1981), and solid ammonia (NH_3), ammonium hydrosulfide (NH_4SH), and H_2O for Jupiter and Saturn (Weidenschilling, 1973). In the colder atmospheres of Uranus and Neptune, argon and methane may condense to form clouds (Weidenschilling and Lewis, 1973).

IX-2.4 Precipitation Particle Terminal Velocities

Though there exists no direct evidence for precipitation in atmospheres other than our own, we have little reason to doubt that precipitation is a common feature of all the planetary atmospheres dealt with in Table IX-1 (with the possible exception of the extremely thin Martian atmosphere). The cloud depths of several kilometers on Venus and the anticipated deep clouds in the Jovian planets will contribute to the colloidal instability which results in the formation of precipitation.

Since it is the differential fall speed of precipitation particles which determines the charge separation rate for precipitation mechanisms, we have made estimates of terminal velocities in other planetary atmospheres. Values for atmospheric density at specific altitudes of interest were obtained from space probe data in the case of Mars and Venus (Seiff and Kirk, 1977; Seiff et al., 1981) and from atmospheric models of the Jovian planets (Weidenschilling and Lewis, 1973). Table IX-1 shows that only in the case of Jupiter, whose surface gravity is anomalously large, are the terminal velocities for 1 mm precipitation particles significantly different from terrestrial values (~ 7 m/sec).

185

IX-2.5 <u>Wind</u> <u>Velocities</u>

Since we are of the opinion that motions of the atmospheric
gas play a major role in the generation of electrical energy,
it is of interest to examine the wind velocities in other
planetary atmospheres.

The maximum observed horizontal wind velocities for Venus
(Counselman <u>et</u> <u>al</u>., 1981), Jupiter (Ingersoll <u>et</u> <u>al</u>., 1979),
and Saturn (Ingersoll, 1981) are all in excess of 100 m/sec and
are all, like the terrestrial case, significantly larger than
the predicted terminal velocities of precipitation particles
(Table IX-1).

If intense vertical convection is a phenomenon common to
other atmospheres, a more relevant parameter for comparison is
the vertical velocity. Unfortunately, only in the case of
Venus do any such measurements exist. These space probe entry
measurements (Counselman, private communication) show vertical
velocities of a few meters per second --comparable to what one
might expect to see in the terrestrial atmosphere for
atmospheric entry at arbitrary locations. Unfortunately, we
have little information concerning "disturbed weather"
conditions on either Venus or the Jovian planets.

Since the cloud forming processes of condensation and
latent heat release are likely common to these other
atmospheres, we may use currently available information on
cloud vapor quantity and composition to estimate upper bounds
on vertical motion. We make the limiting assumption that all
the latent heat energy in the condensable vapor near cloud base

186

is used to expand the parcel and increase its vertical kinetic energy through buoyant acceleration. With this assumption it can be shown that, after accelerating through one atmospheric scale height, the parcel's vertical velocity will be:

$$V_{MAX} = \left(\frac{2(MR)L}{\gamma+1}\right)^{1/2}$$

where MR is the vapor mixing ratio at cloud base, L is the latent heat energy per unit mass, and γ is the ratio of specific heats for the atmospheric gas in question.

NH_3 and H_2O vapor mixing ratios for the Jovian planets were calculated from the abundance estimates of Sato and Hansen (1979) for Jupiter. Mixing ratio estimates for Venus were derived from Pollack et al. (1978).

The calculated bounds on vertical velocity are shown again in Table IX-1. For purposes of comparison, the same technique was used for vertical convection in the Earth's atmosphere; the 80 m/sec result is only slightly higher than the largest documented vertical velocity in a terrestrial thunderstorm (Steiner and Rhyne, 1964). Estimated maximum vertical velocities are, like the wind observations, significantly greater than the estimated fall speeds of precipitation particles.

IX-2.6 Dielectric Strength of Atmospheres

The breakdown strength of a planetary atmosphere will place bounds on the accumulation of electrostatic energy, and also on

187

the local ohmic conduction current density if the electrical conductivity is known. Vonnegut (1980) has discussed the potential importance of the former condition to the dynamics of the deep atmospheres of Jupiter and Venus.

Here we confine our attention to the dielectric strength in the observed or predicted cloud forming levels of planetary atmospheres. Since the breakdown strength of many gases and liquids depends to first order only on their densities (Cooke, 1978), we may immediately estimate breakdown fields using the already tabulated atmospheric densities in Table IX-1. The breakdown fields calculated on this basis (and presented in the same Table) do not differ by more than a factor of 2 or 3 from the terrestrial value (2×10^6 v/m). Again the sole exception is in the relatively thin atmosphere of Mars, which may not even sustain electrification, as we will argue later.

IX-2.7 Electrical Conductivity

The finite atmospheric conductivity plays only a passive role for precipitation mechanisms for thunderstorm electrification, but is a vital ingredient to screening layer convection (Vonnegut, 1963). It is therefore of interest and of value to this study to examine the conductivity structure in electrified atmospheres other than our own. Section IX-3 is concerned with the details and results of such calculations. These results and the comparisons in this section are then applied to the interpretation of existing evidence for extraterrestrial planetary electrification in the final section of this chapter.

188

IX-3 Electrical Conductivity Structures

IX-3.1 The Determination of Electrical Conductivity

Any planetary atmosphere will be electrically conducting by virtue of the mobile charge (ions) it contains. Energetic radiation from the Sun (uv radiation) and deep space (cosmic radiation) is responsible for the ionization of atmospheric species. The ultraviolet component from the Sun is readily absorbed high in the atmosphere to maintain the highly conductive planetary ionosphere, and this mechanism is apparently at work on both Mars and Venus (McConnel, 1976), and on the Jovian planets (Huntress, 1974). Only the very energetic (10^9 to 10^{19} eV) cosmic rays remain as ionizing agents in the lower tropospheres of these atmospheres.

A quantification of the attenuation (and resultant ionization) of cosmic rays in an atmosphere is greatly simplified by an empirical result known as the mass absorption law. At relativistic energies the loss of particle energy to ionization depends only on the integrated mass of traversed matter, and is roughly independent of the atomic constitution of the material. This integrated mass per unit area, the so called equivalent depth, has been computed from recently available space probe data for the atmospheres of Mars (Seiff and Kirk, 1977) and Venus (Seiff et al., 1980), and is shown in comparison with the terrestrial profile in Figure IX-1. In spite of the larger molecular mass in the CO_2-rich atmosphere

Figure IX-1
Equivalent Depth versus
Altitude: Terrestial
Planets
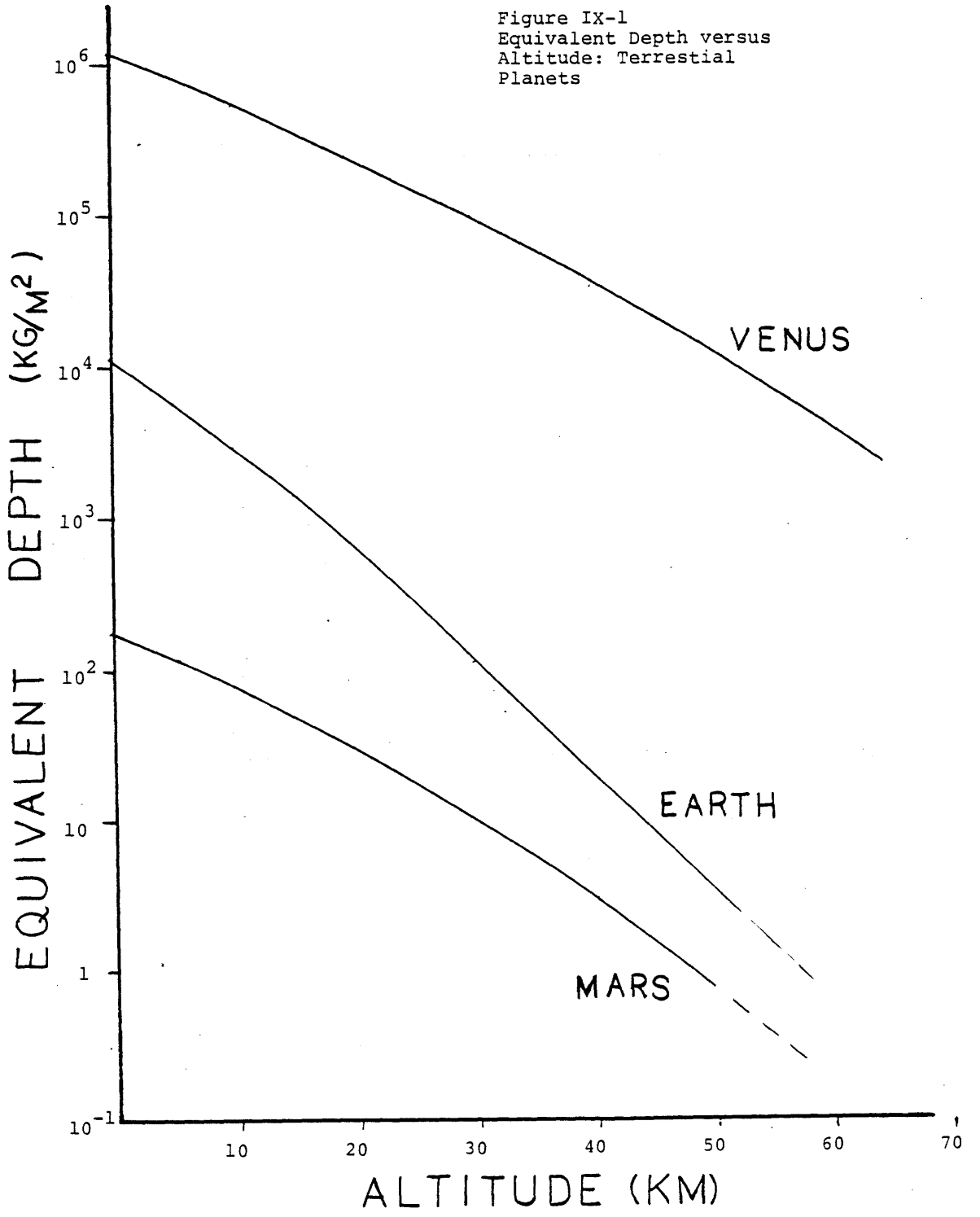
(44 amu) than that of Earth's (29 amu), the scale heights for both Mars and Venus are larger than that for Earth, owing to reduced gravity (Mars) and substantially higher temperature (Venus).

In Figure IX-2 are shown the equivalent depth curves for the Jovian planets Jupiter, Saturn, Uranus, and Neptune. These values are based on the solar composition, adiabatic atmosphere models of Weidenschilling and Lewis (1973), which agree closely with recently available space probe information from Jupiter (Lindal et al., 1981). Because the Jovian planets lack solid surfaces which are the usual benchmarks for atmospheric altitude, we have plotted the equivalent depth versus temperature in Figure IX-2. Note that the equivalent depth at any given temperature increases with the planet's distance from the Sun.

The isotropy in space and time and spatial uniformity of the primary cosmic radiation is well established (Sandstrom, 1965). We may therefore assume that the cosmic ray intensity outside the atmospheres of other planets in the solar system will be similar to that in the Earth's environment. This result, together with the mass absorption law, allows us to use terrestrial cosmic ray intensity data to construct a universal curve which is applicable to any penetrated medium.

Fortunately, the earliest quantifications of cosmic ray intensity were in terms of the local ionization rate (Bowen et al., 1933). (It was in fact this ionization which was

191

Figure IX-2
Equivalent Depth versus
Temperature: Jovian
Planets

192
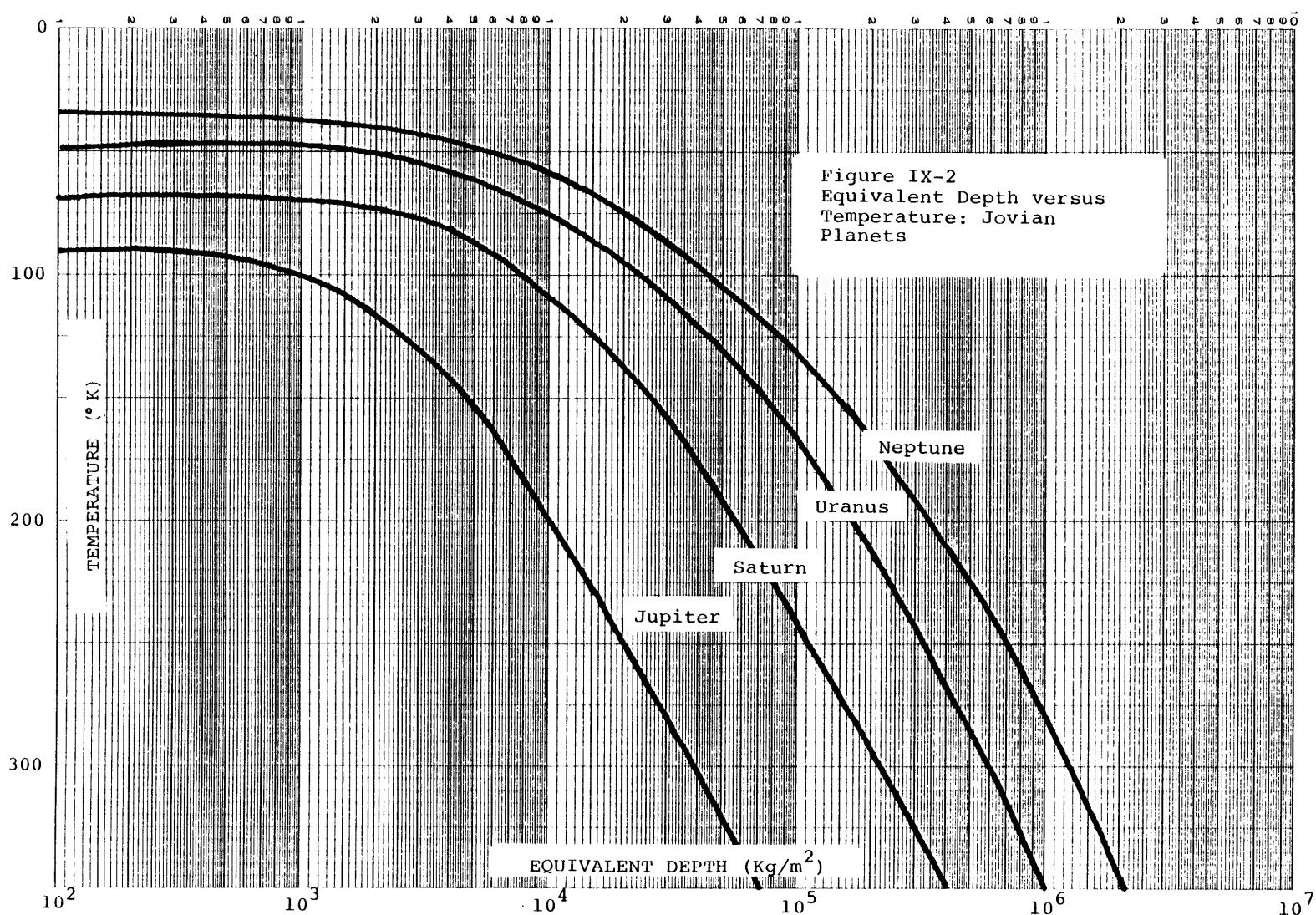
responsible for the slow decay of voltage in electroscopes, a situation which spurred the initial discovery of cosmic radiation (Wilson, 1901).) A compilation of measurements of this kind in the Earth's atmosphere (Bowen et al., 1938), in deep water lakes (Regener, 1933; Bowen et al., 1933), in the deep ocean (Higashi et al., 1966), and in deep mines (Wilson, 1938) results in a universal curve if the equivalent depth parameter is used and is shown in Figure IX-3. For shallow penetrations, the ionization rate shows a slight increase with equivalent depth (owing to the cascade process), and then decreases dramatically as the radiation is attenuated. The deep mine and deep ocean measurements were actually carried out with Geiger counters, but it is seen that the data track closely with the ionization measurements when normalized at the upper ends of their respective ranges. This data is particularly valuable since it allows us to extend our calculations into planetary atmospheres "deeper" than our own, such as that of Venus. In this context it is interesting to note that Regener's (1933) cosmic ray ionization chamber was filled with CO_2!

The curve in Figure IX-3 is not strictly universal since the terrestrial magnetic field influences charged particle trajectories and slightly modifies the upper atmosphere ionization rates. We have selected high latitude data (60°N) (Bowen et al., 1938) in this region to minimize this effect. Fortunately, the magnetic fields of both Mars and Venus are

Figure IX-3
Universal Cosmic Ray
Ionization Curve

Data from:

Bowen et al. (1933,1938)

Wilson (1936)

Higashi et al. (1966)
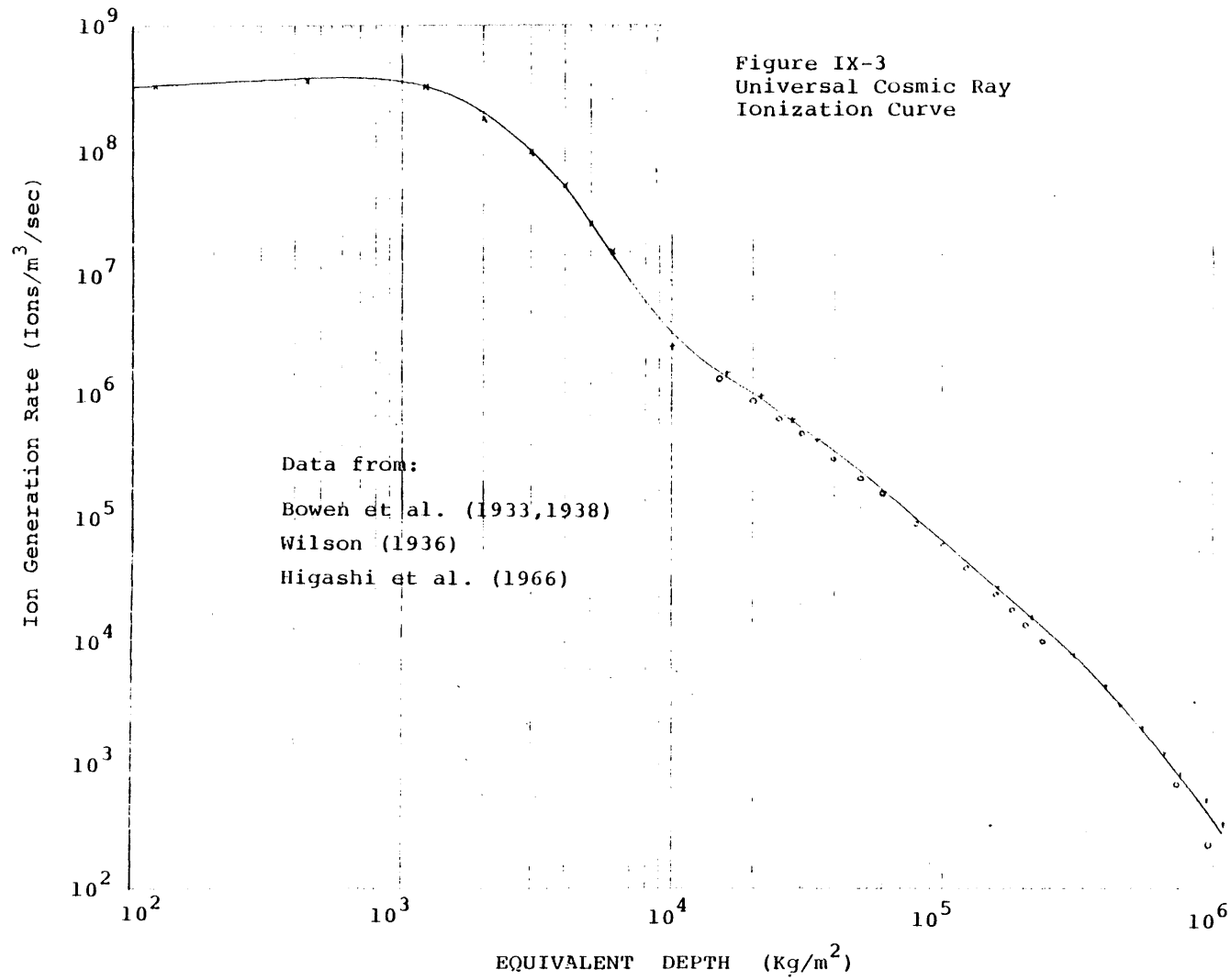
anomalously weak and may be safely ignored in the calculations of ionization rate. Such is not the case for the Jovian planets, and the cosmic ray shielding by these magnetic fields and its effect on electrical conductivity must be taken into account (see IX-3.3).

It is to be noted that the ion production rates on the ordinate in Figure IX-3 are those rates which would be recorded in ionization chambers filled with atmospheric air at standard conditions. Actual ion production rates will be directly proportional to the ratio of the in situ density to the standard density (1.2 kg/m^3), again following the mass absorption law. The energy expenditure per ion pair in air and in CO_2 differ by only a few percent (Valentine and Curran, 1959) and so Figure IX-3 is directly applicable to the determination of ion production rates in the atmospheres of both Mars and Venus.

The atmospheres of the Jovian planets consists chiefly of molecular hydrogen, whose ionization behavior departs from the mass absorption law. Corrections based on the laboratory measurements of Merrymon (1926) were implemented in our ionization predictions in these atmospheres.

In summary, to determine the ion generation rate at a prescribed altitude in a planetary atmosphere, we first check the equivalent depth for that altitude in Figures IX-1 or IX-2. We then find the corresponding ion generation rate, using available atmospheric density data (Seiff and Kirk, 1977; Seiff et al., 1980). Our computed profiles for ion generation rate

on Mars (Weidenschilling and Lewis, 1973) and Venus are included in Figures IX-4 and IX-5, respectively.

The determination of equilibrium small ion density now proceeds as in calculations for the terrestrial case (Sayers, 1938; Callahan et al., 1951; Shreve, 1970). A steady state balance is assumed to exist between small ion generation and ion recombination, in which case the equilibrium ion concentration n is given by

$$n = \left(\frac{g}{\alpha}\right)^{1/2}$$

where g is the ion generation rate and α is the ion recombination coefficient, and all three quantites are ultimately functions of altitude Z. Calculated profiles for these quantities are also shown in Figures IX-4 and IX-5.

Carbon dioxide, which is the dominant atmospheric constituent for Mars and Venus, is an electron-attaching gas (like oxygen in the terrestrial atmosphere) and therefore the Thomson theory for ion-ion recomination is applicable. This theory (as presented by Loeb, 1955) was used for calculations of ion recombination coefficient α for the low pressures encountered on Mars and in the upper levels (z > 65 km) on Venus. For deeper levels in that atmosphere, the high pressure Langevin theory (Langevin, 1903) was used, in which α is inversely proportional to ion mobility. This behavior was upheld in laboratory recombination experiments on CO_2 by Machler (1936).

196
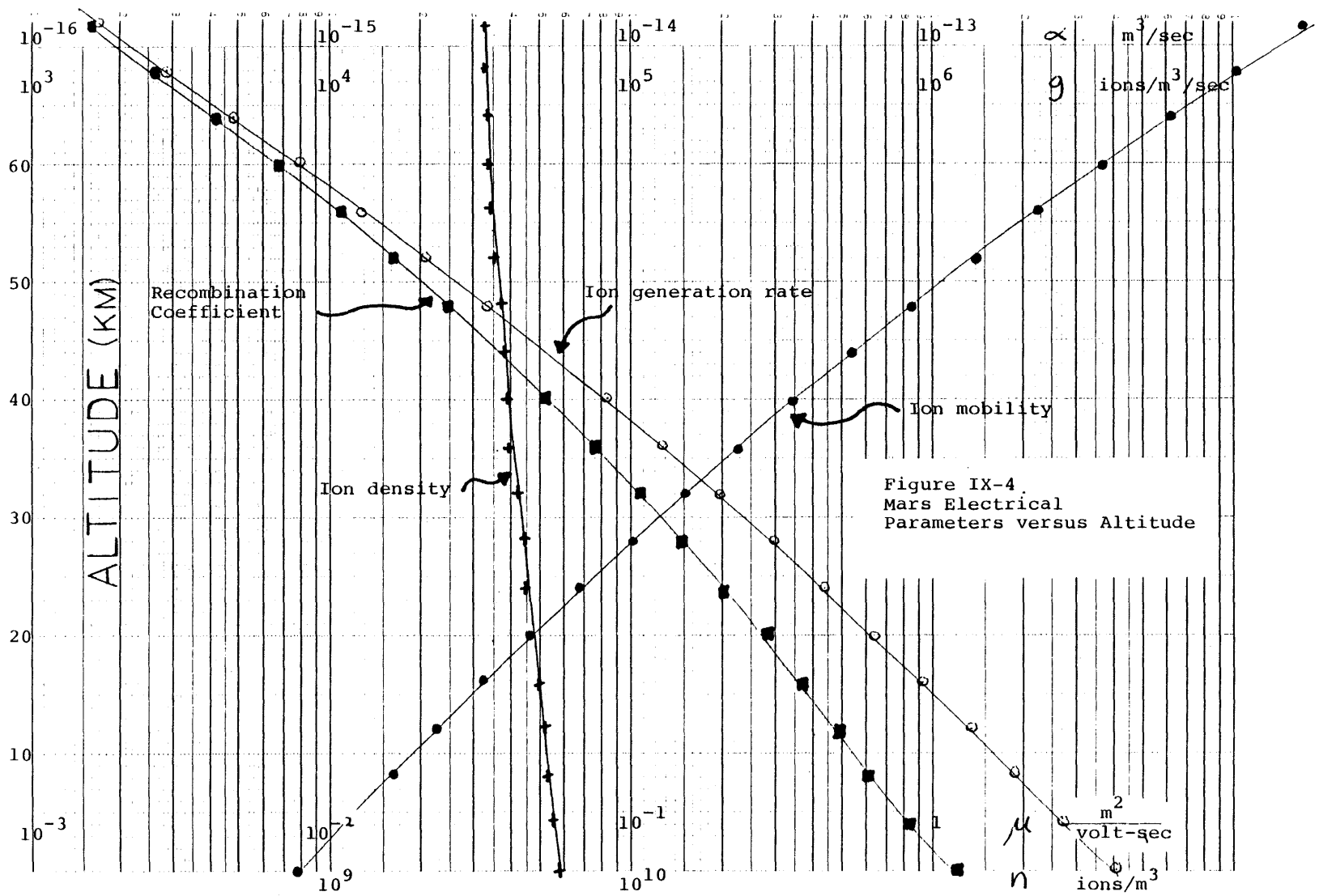
Figure IX-4
Mars Electrical
Parameters versus Altitude

197

Figure IX-5
Venus Electrical Parameters
versus Altitude
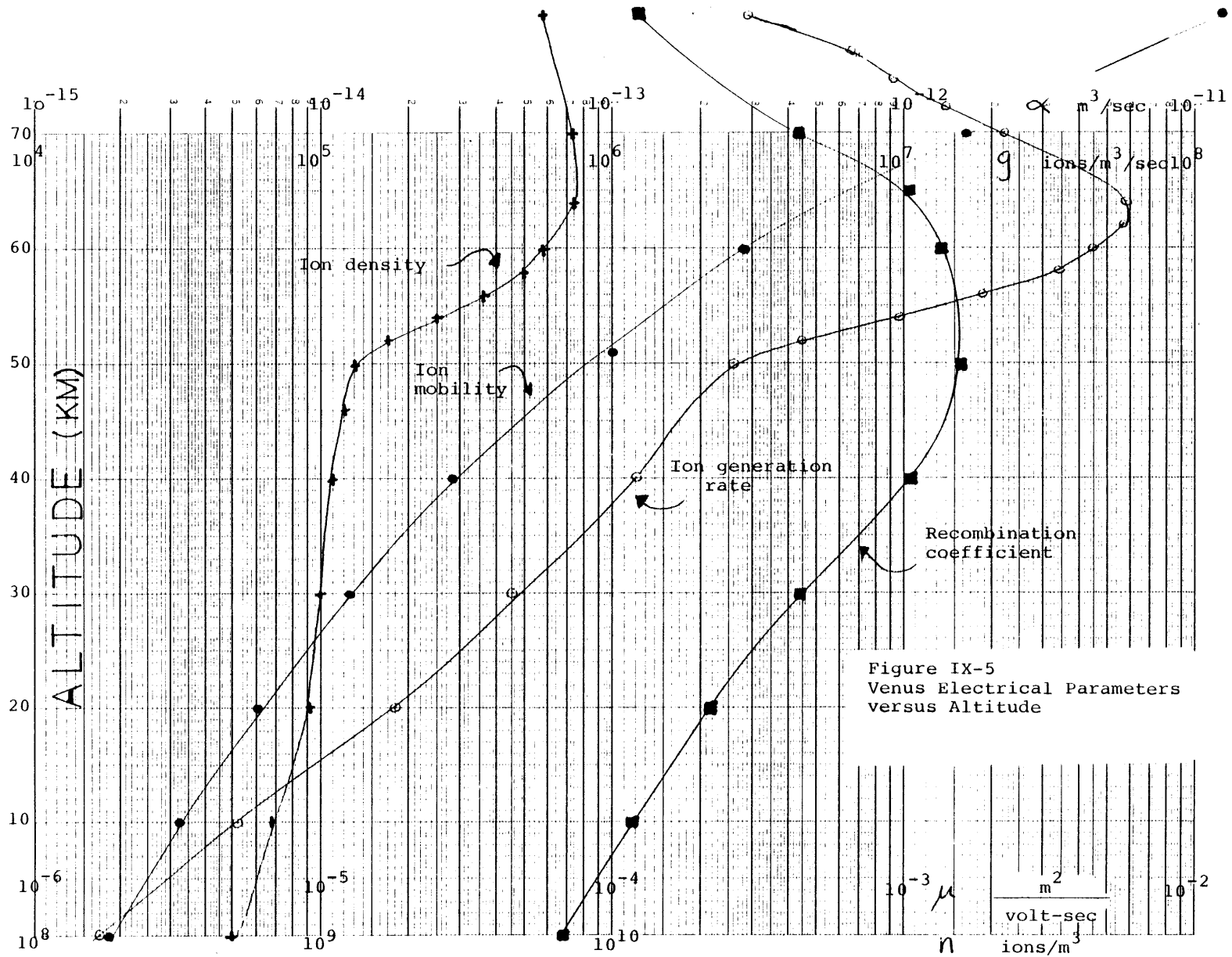
The ion chemistry in the Jovian tropospheres is somewhat obscure. Huntress (1974) emphasizes the rarity of negative ions in the Jovian ionospheres and the consequent greater number of free electrons than at commensurate altitudes in the Earth's ionosphere. In the Jovian planet troposphere, however, where a far greater number of electron-hydrogen molecule encounters takes place, the dissociative electron attachment reaction

$$e + H_2 \rightarrow H^- + H$$
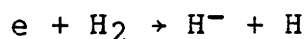
may be prominent in producing negative ions. These hydride ions, H^-, then recombine with H_2^+ and H_3^+, the dominant positive ion species (Johnson and Biondi, 1974), via the Thomson or Langevin process. Except for the case of Jupiter, the large pressures encountered in the atmospheres of the Jovian planets make the simple Langevin relation applicable over most of the depth range.

Finally, the ionic conductivity is calculated according to

$$\sigma = 2en\mu$$

where we have assumed equal positive and negative ion mobilities, μ.

In our ignorance concerning the ion chemistry in CO_2 atmospheres, we assume terrestrial atmospheric values for small ion mobilities ($10^{-4} \frac{m^2}{volt-sec}$) at standard density (consistent with the early laboratory determinations in CO_2 (Thomson,1928)) and compute mobilities at other levels consistent with an

199

inverse dependence on atmospheric density, following the
Langevin (1905) theory. The mobility profiles are included in
Figures IX-4 and IX-5.

The ion species predicted for the Jovian atmospheres are
smaller than those encountered in the atmospheres of the
terrestrial planets, and consequently have larger mobilities.
We have chosen a value of $10^{-3} \frac{m^2}{volt-sec}$ at standard conditions,
consistent with laboratory ion mobility determinations in
molecular hydrogen (Saporoschenko, 1965; Albritton et al.,
1968). Final conductivity determinations are shown in Figures
IX-6 and IX-7 for the tropospheres of Mars and Venus,
respectively. The vertical conductivity structures for the
Jovian planets, again plotted against atmospheric temperature,
are shown in Figure IX-8.

IX-3.2 Neglected Contributions to Electrical Conductivity

There can be little doubt that natural radioactivity present
in the crusts of Mars and Venus will act to enhance the near
surface atmospheric conductivity. However, we currently have
no quantitative information on this point for either planet,
and have ignored it in our calculations. The influence of
radioactivity in the Earth's troposphere extends only 2-3 km
above the surface (Israel, 1973), a distance associated with
the boundary layer thickness. It is possible that the lowest
portion of the Venusian atmosphere is stably stratified,

Figure IX-6
Mars Tropospheric
Electrical Conductivity

RELAXATION TIME (SEC)

ALTITUDE (KM)

PRESSURE (μ BARS)

CONDUCTIVITY (MHO/M)

201

Figure IX-7
Venus Tropospheric Structure
and Electrical Conductivity

Figure IX-8
Electrical Conductivity versus
Atmospheric Cosmic Ray
Ionization and Electrical
Conductivity: Jupiter

203
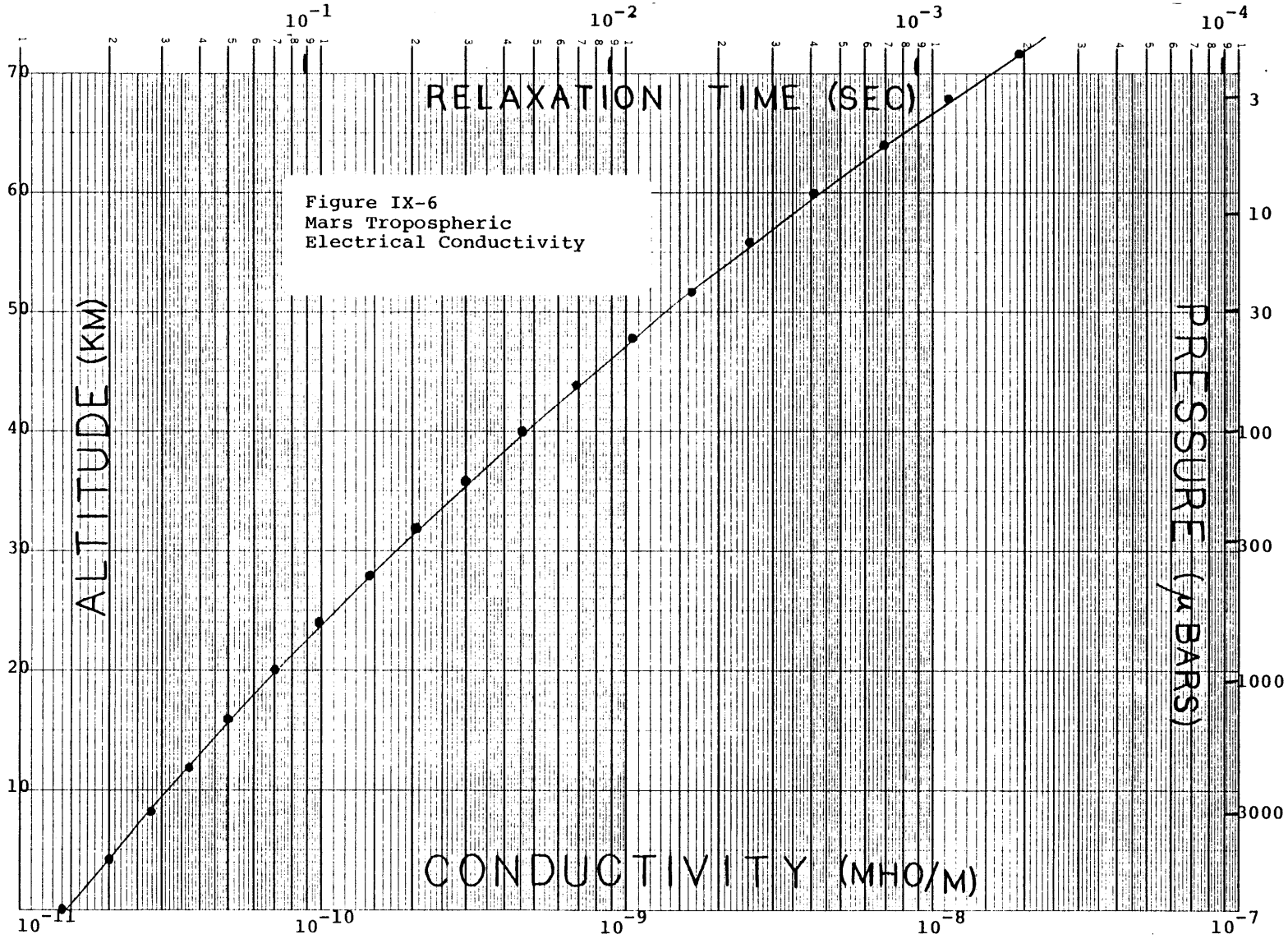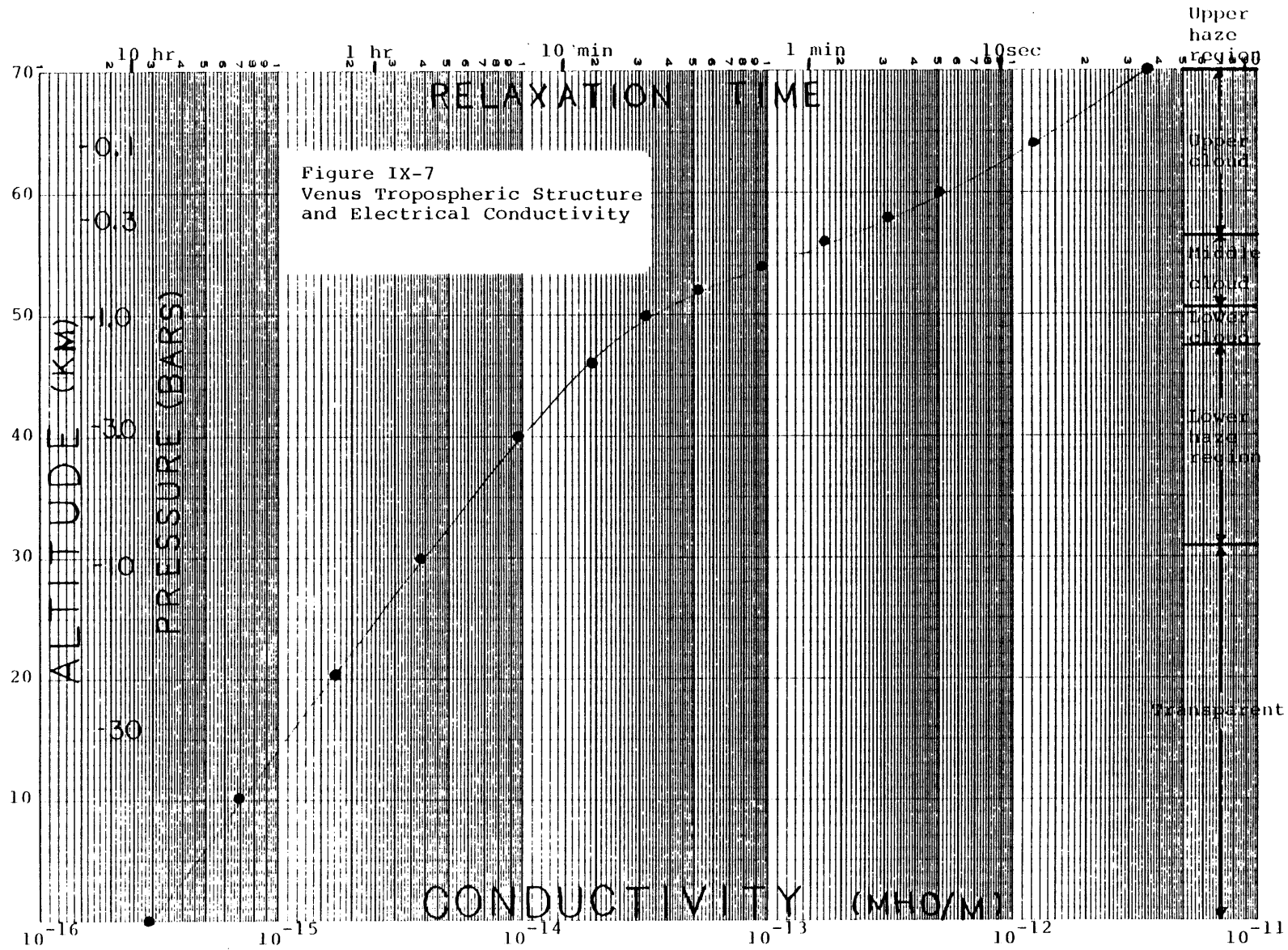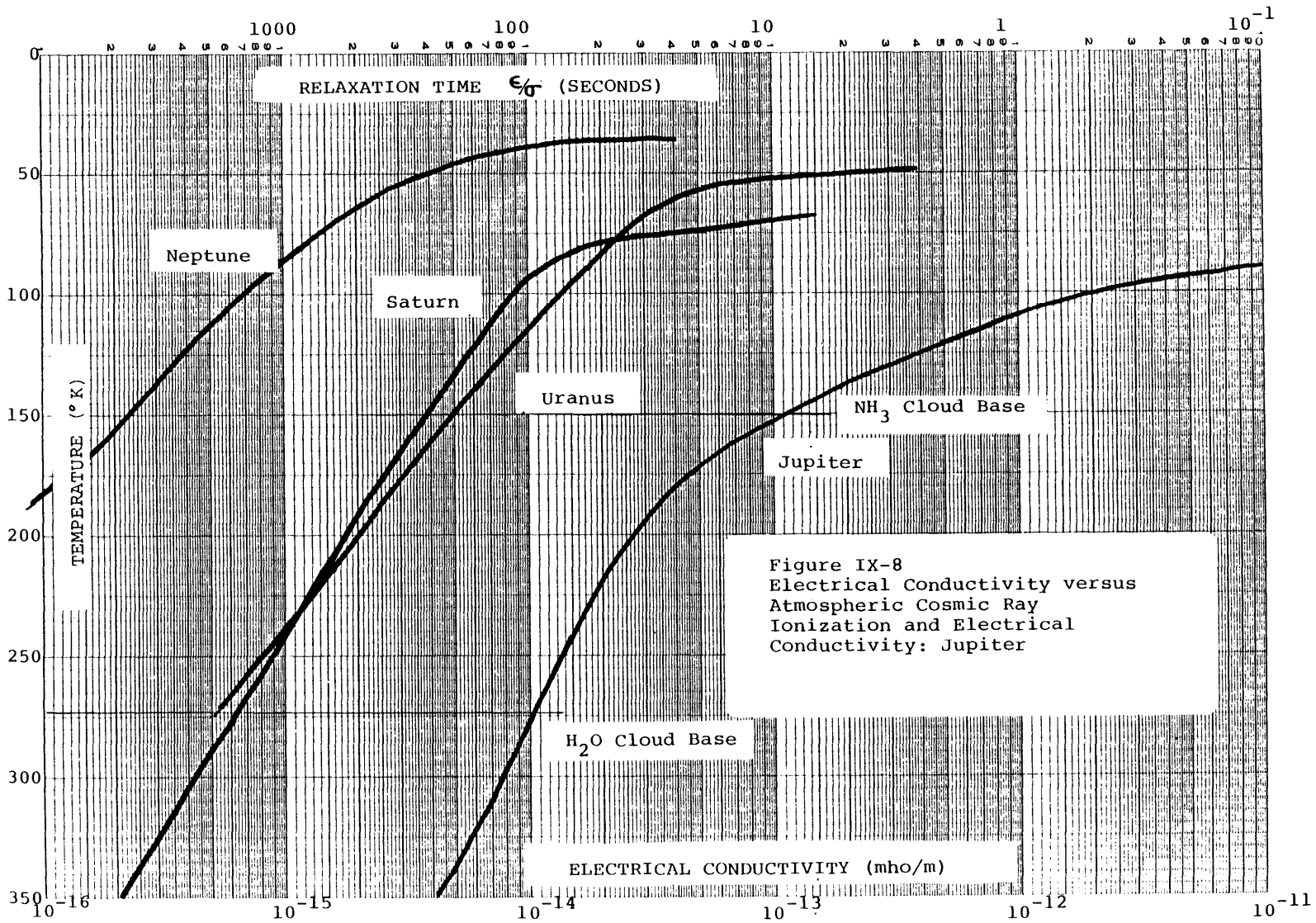
thereby minimizing the role of surface radioactivity as an ionizing agent. On Mars, the boundary layer may be 1 to 1.5 km thick (Seiff and Kirk, 1977), and radioactivity may make a significant contribution to conductivity in this region.

The depletion of ions which may occur in the electrode layer near a planetary surface is also neglected in these calculations. This omission will tend to offset the effect of neglecting the radioactivity contribution.

The Jovian planets lack solid surfaces and have solar composition atmospheres in which light elements are abundant and in which heavy radioactive elements may be relatively scarce. It therefore appears improbable that radioactivity is making a major contribution to ionization and electrical conductivity in these atmospheres.

We have also ignored the possible effects of atmospheric condensates on electrical properties. The calculations presented here are strictly applicable only to regions of "fair weather" atmosphere (no clouds, weak electric fields). The non-ohmic effects on conductivity, treated in papers by Phillips (1967) and Griffiths et al. (1974), are likely to prevail in any atmosphere in which both clouds and strong electrification are known to occur.

We have until now ignored the influence of the planetary magnetic field on the cosmic ray ionization and electrical conductivity. This effect is important, particularly for Jupiter and Saturn, and must be examined before the final conductivity results are discussed.

IX-3.3 Magnetic Field Effects on Cosmic Ray Ionization and Electrical Conductivity

The magnetic field of a planet will alter the trajectory of a charged cosmic ray particle, and in certain circumstances may prevent it from reaching the planetary atmosphere. The result may be diminished ionization and a reduced conductivity. The atmospheric ionization variation with latitude within the Earth's dipole field (the "latitude effect") has been exploited to deduce features of the cosmic ray energy spectrum (Bowen et al., 1938). In this section, we will work backward from known features of the cosmic ray spectrum in order to quantify the effects of planetary magnetic field on atmospheric ionization and electrical conductivity.

The magnetic field effects are negligible for Mars and Venus and modest for the Earth, but are appreciable in the large fields of the Jovian planets. The relevant parameters are listed in Table IX-2, which includes planetary radii, magnetic dipole moments, surface magnetic fields, and calculated values for the cutoff rigidities, R_c, at the magnetic equator.

These latter values represent the threshold particle energies (momenta) below which a particle at vertical incidence cannot reach the planetary troposphere. This value applies at the dipole equator, where the magnetic field component perpendicular to particle motion is maximum. Particles approaching along the dipole axis (toward the magnetic poles) will experience no deflection and the critical rigidity

Table IX-2

	Planetary Radius (m)	Magnetic Dipole Moment (G-cm^3)	Surface Magnetic Field (T)	Critical Rigidity* (BeV/c)
Earth	6.28×10^6	8.06×10^{25}	5×10^{-5}	15
Jupiter	7.14×10^7	1.55×10^{30}	4.3×10^{-4}	2300
Saturn	5.98×10^7	4.7×10^{28}	2.2×10^{-5}	100
Uranus	2.36×10^7	2×10^{27} **	1.5×10^{-5} **	26
Neptune	2.23×10^7	2×10^{27} **	1.8×10^{-5} **	40

*   Vertical incidence at dipole equator

**   Scaling law extrapolations (Williams, 1980)

vanishes there. The critical rigidity latitude dependence in a dipole field has been shown to be $\cos^4 \lambda$ (LeMaitre and Vallarta, 1936).

To determine the cosmic ray energy available for atmospheric ionization at any latitude, we need to know how much cosmic ray energy is available for energies greater than the cutoff rigidity at that latitude. Such information is contained in the integral cosmic ray spectrum, which exhibits a power law behavior with slope -1.6 for energies greater than 10-20 BeV (Sandstrom, 1965), but flattens out at lower energies (Johnson, 1938). We may therefore predict that the cosmic ray energy available for atmospheric ionization will vary as $(\cos^4 \lambda)^{-1.6}$ for cutoff rigidities in the power law region. For lower cutoffs (toward the magnetic poles) the total ionization rate latitude dependence will weaken considerably. The predicted latitude dependence for the Jovian planets Jupiter and Saturn is shown in Figures IX-9 and IX-10, respectively.

More important to this study is the effect of planetary magnetic field on atmospheric electrical conductivity, which we know will depend locally on the square root of the ionization rate. In the above calculations, we have determined the ionization rate integrated throughout the atmospheric depth and have ignored its variation with depth. Such a calculation would require keeping track of the entire cosmic ray particle spectrum as it passed through the planet's magnetic field "filter" and then through every layer of the atmosphere. This

Figure IX-9
Magnetic Field Effects on
Atmospheric Cosmic Ray
Ionization and Electrical
Conductivity: Jupiter

Relative
Conductivity

Relative
Ionization

Equator

Pole

Magnetic Latitude (Degrees)
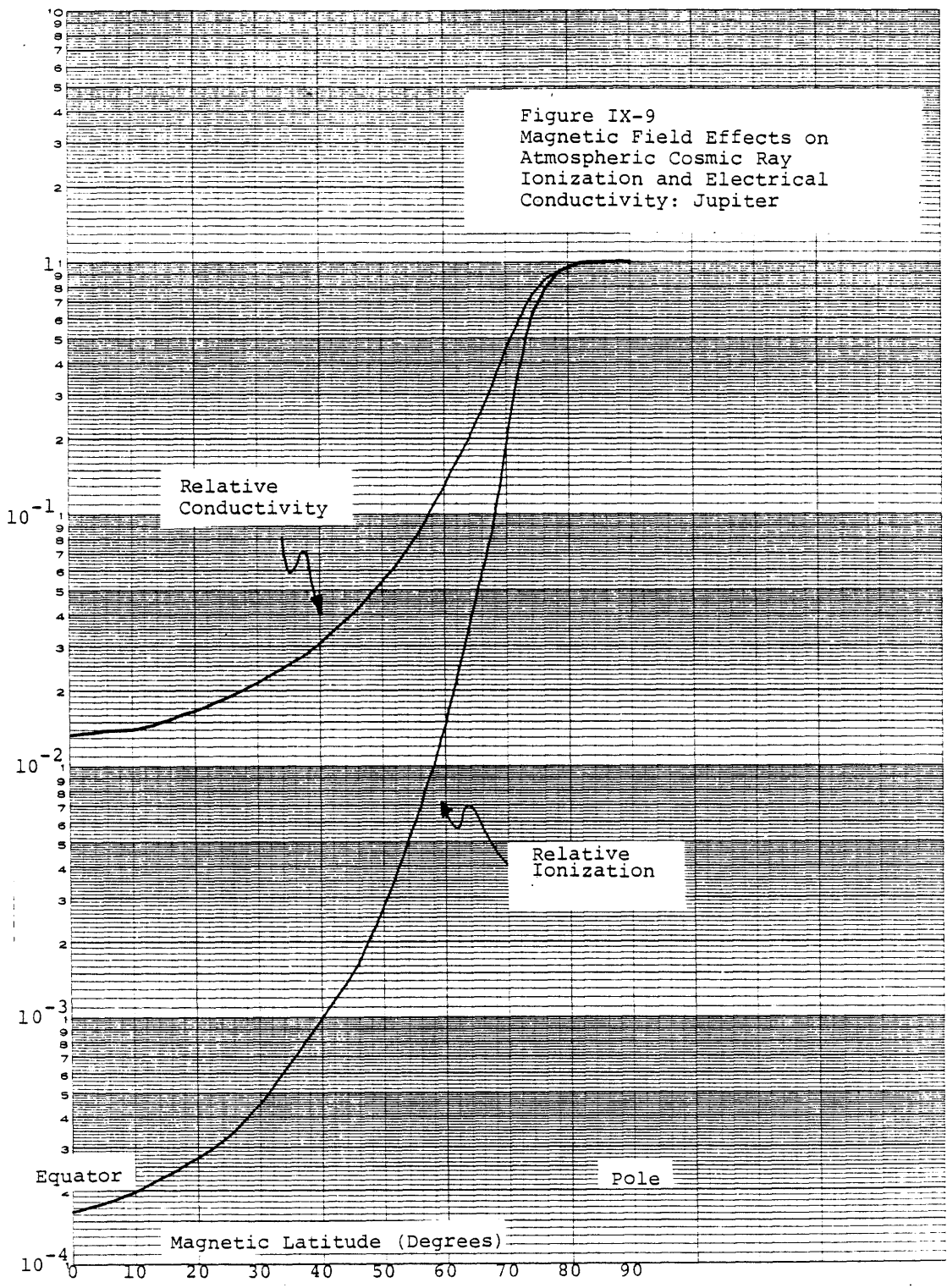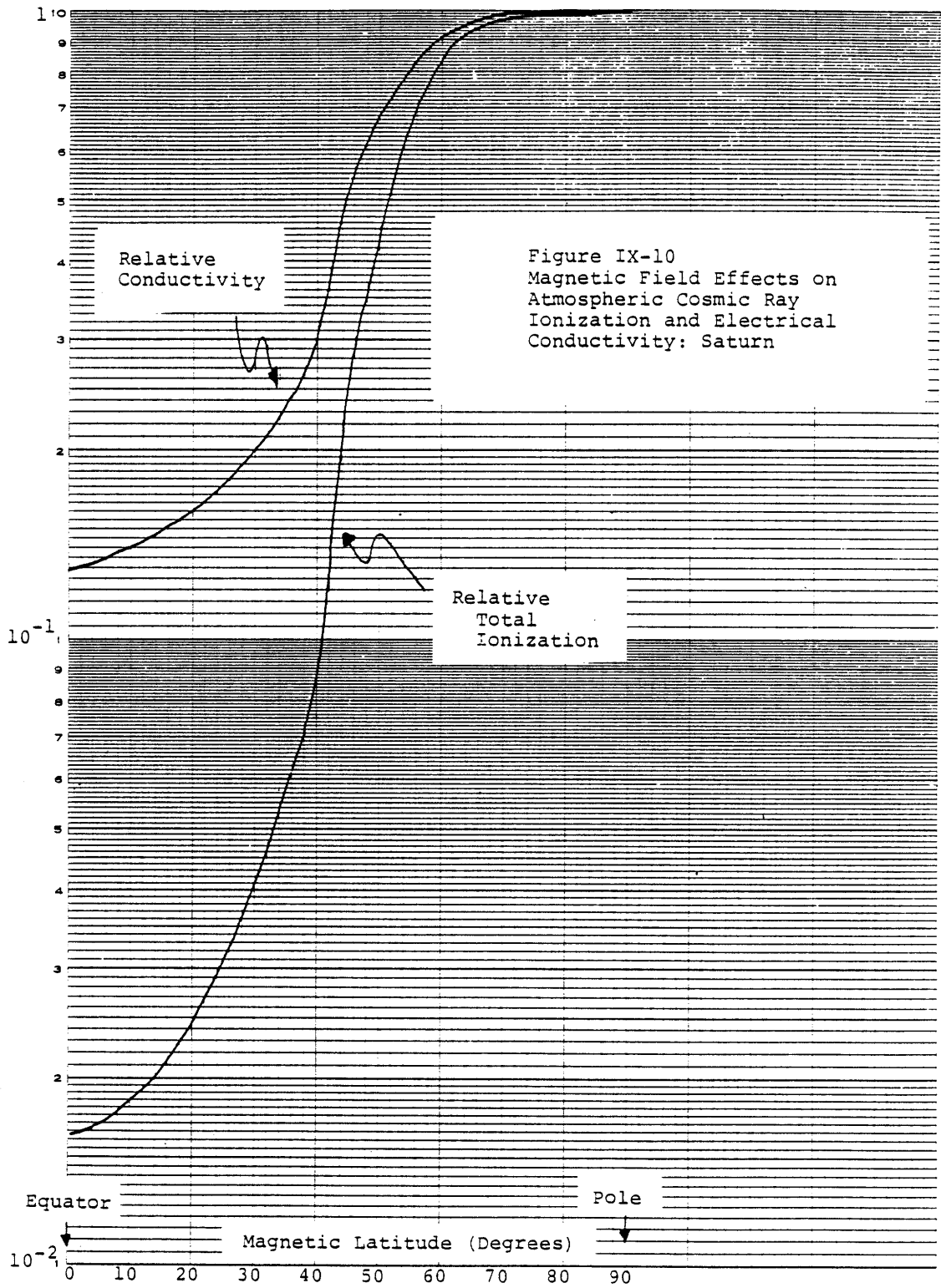
Figure IX-10
Magnetic Field Effects on
Atmospheric Cosmic Ray
Ionization and Electrical
Conductivity: Saturn

Relative
Conductivity

Relative
Total
Ionization

Equator

Pole

Magnetic Latitude (Degrees)

would appear to be a formidable problem, but fortunately is not justified for the following reason. Terrestrial ionization versus depth curves at different magnetic latitudes (Bowen et al., 1938) show only slightly different shapes, and their areas (representing the integrated ionization rate) are roughly commensurate with their peak values. Therefore, for the purposes of rough (factors of two) comparisons, we can take the square root of the integrated ionization rate as a measure of the relative atmospheric conductivity at any given latitude. These conductivities (relative to the maximum value expected in polar regions) for Jupiter and Saturn are also included in Figures IX-9 and IX-10, respectively.

By far the largest magnetic field effects occur in the case of Jupiter, in which the cosmic ray ionization at the magnetic equator is reduced by a factor of 6000 and the electrical conductivity by a factor of 75, relative to their respective values at the poles. These factors for Saturn are less, but still significant (60 and 8, respectively). Predicted effects for Uranus and Neptune are more modest (Uranus: 4,2; Neptune: 16,4). Possible implications of these results will be discussed in the following Section.

IX-4 Discussion of Results

IX-4.1 Discussion of Results: Mars

The Martian atmosphere is sufficiently thin that the cosmic ray flux incident on its exterior arrives at the planetary surface virtually unattenuated. This condition, together with

the existence of highly mobile ions (see Figure IX-4), tend to make a conductive atmosphere throughout. The minimum conductivity at the surface of 1.4 x 10^{-11} mho/m (neglecting any contribution from natural radioactivity) corresponds with a relaxation time $\frac{\varepsilon}{\sigma}$ of only 0.6 seconds. The conductivity increases exponentially with altitude with a scale height of about 13 km. The validity of the calculations above 30 km is questionable, however, since the Thomson recombination theory loses its applicability at these low pressures.

Although both dust particles and cloud particle condensates exist in this atmosphere (Pollack et al., 1979), which may serve as electric charge carriers, the short relaxation time will likely prevent any large scale charge accumulation. Even with a wind velocity of 120 m/sec, which may typify a large Martian dust storm, the charge transport time over any reasonable distance is signficantly larger that the sub-second (maximum) relaxation times. The ion scavenging effects of the existing particles may reduce the predicted conductivity, but their general sparsity suggests that this will not be an order of magnitude effect as it may be in terrestrial clouds (Griffiths et al., 1974).

Since the existence of precipitation in this atmosphere appears unlikely, we can be reasonably sure that if local electrification does occur, it will be the result of convective/ advective charge transport.

It has been suggested that glow discharges may be important in the low pressure Martian environment (Eden and Vonnegut,1973;

211

Mills, 1977). In light of the present results, however, it appears that conclusions drawn from earth-based laboratory simulations of Mars need to be reevaluated.

This author is unaware of any report of electrification phenomena in the Martian atmosphere, and this is consistent with the present findings on electrical conductivity.

IX-4.2 Discussion of Results: Venus

The atmosphere of Venus, whose near surface density is 50-60 times that of Earth's, is a strikingly more resistive environment. The calculated conductivity near the surface is 4×10^{-16} mho/m, with an associated electrostatic relaxation time of about 8 hours. The conductivity (Figured IX-7) increases exponentially with altitude with a scale height of 12 km, and then more rapidly (scale height 3-4 km) beginning at about 50 km. This transition is associated with both a change in the ion generation rate with height and with change in pressure regimes for the behavior of the ion recombination coefficient (see Figure IX-4). The profile in Figure IX-7 may be integrated to obtain the planet-ionosphere DC resistance, which is 8.6×10^4 ohms. If the Venus global electrical circuit were configured as it is on Earth, with a comparable global current of 2000 amperes (consistent with the preliminary charge (Ksanfomaliti, 1980) and flash rate (Borucki, 1980) estimates for Venus), the planet-ionosphere voltage difference would be 170 million volts.

The suggestion that electric charge is transported throughout the depth of the Venusian troposphere is however at odds with current information on atmospheric structre. Relevant features from Schubert et al. (1981) and Knollenberg et al. (1981) are included in Figure IX-7. The atmosphere appears to be stably stratified over large vertical scales and the large scale features of the wind field are dominated by horizontal motions.

For purposes of this discussion, three major altitude intervals may be distinguished: (1) the stratiform cloud deck region from 48 km to 70 km, consisting of three distinct cloud layers; (2) a region containing haze below the clouds extending from 31 to 48 km; and (3) an apparently transparent region from 31 km to the surface of the planet.

Consider first the cloud region. The one bar pressure level is at 50 km and it is no surprise that the conductivity structure above that level is very similar to that in the Earth's atmosphere. The predicted relaxation time above the thick upper cloud layer is however somewhat less than that above terrestrial thunderstorms. Although the measured cloud liquid contents are modest (Knollenberg, et al., 1981) and no precipitation particles have been directly detected, the cloud layers are of sufficient thickness that local regions of precipitation cannot be ruled out. The strong horizontal shear in the wind profile (Figure IX-11) (Counselman et al., 1981) will result in a large relative velocity (30-40 m/sec) between

Figure IX-11
Zonal Wind Profiles for
Various Venus Probes
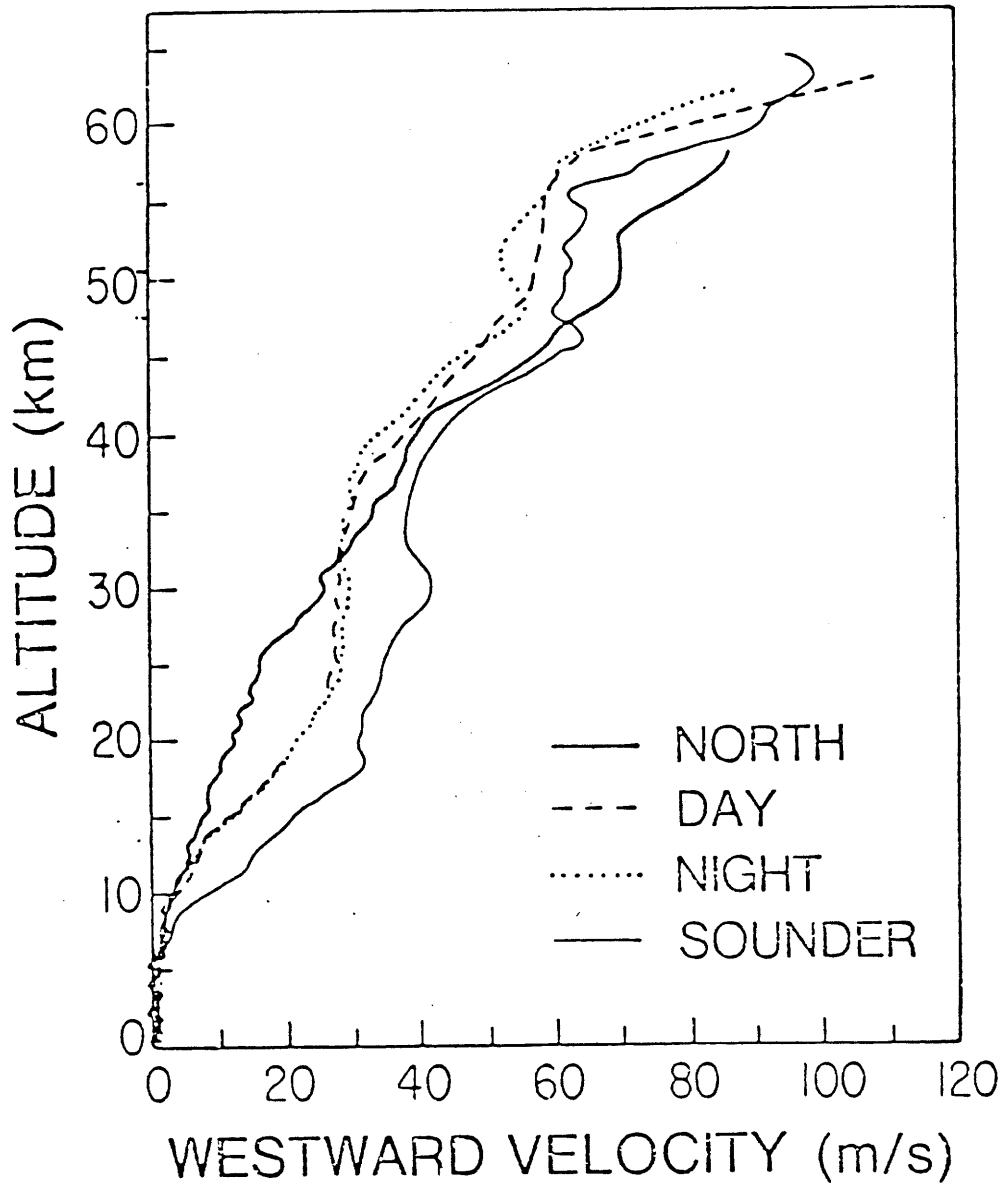
portions of the upper and middle cloud layers, and could act to amplify any charge separation mechanism at work there.

Ksanfomaliti (1980) has already speculated that the cloud layer is the site of electrification. Esposito (private communication), on the other hand, concludes from a preliminary analysis of uv spectrometer data that lightning occurs below 50 km.

The ion generation rate falls off dramatically in the haze region below the clouds, and the electrical conductivity is less than that in the Earth's atmosphere. If Venusian thunderstorms exist here and are separating charge at terrestrial rates, we would be forced to conclude that the finite conductivity of the atmosphere was not playing a dominant role. Cimino and Elachi (1979) have proposed the existence of H_2SO_4 solution precipitation in this region, extending as deep as 28 km altitude. If this prediction is correct and if the particles are suitably charged (Section II-4), it is expected that they will make a signficant contribution to electrification.

In spite of the extremely low conductivity in the lowest region of the Venusian atmosphere (31 km to the surface), the observed absence of aerosol and cloud particles (Knollenberg et al., 1981), the predicted absence of precipitation (Cimino and Elachi, 1979), and the scarcity of ions (Figure IX-5) all suggest that electrification local to this region is unlikely. There remains the possibility that electrified dust particles are occasionally blown up from the surface to create well

215

insulated charged clouds, which may in turn produce lightning. Of course, Venusian cloud to ground lightning would necessarily transit this region, but the requisite energy may be enormously larger than that for terrestrial events (Vonnegut, 1980).

The need to identify the altitude region or regions responsible for the observed Venusian lightning is obvious. Efforts in this direction using lightning spectroscopy (Vonnegut and Orville, 1980) and radio wave path reconstructions (Taylor and Scarf, 1980) are currently in progress.

IX-4.3 Discussion of Results: Jupiter

The equivalent depths of the cloud levels on Jupiter are less than for the other Jovian atmospheres (see Figure IX-2), and consequently its electrical conductivity is the largest of the group (see Figure IX-8). In the absence of magnetic field shielding effects (i.e., at the magnetic poles) the predicted electrical conductivity near the NH_3 cloud tops is $\sim 5 \times 10^{-12}$ mho/m, corresponding to a relaxation time of a few seconds. Cosmic ray shielding effects are maximum at the equator (see Figure IX-9), where we estimate the cloud top relaxation time to be ~ 1000 seconds. The polar and equatorial cloud top relaxation times therefore bound the range of values at the tops of terrestrial thunderclouds (10-100 seconds).

The possible importance of cloud top conductivity to electrification is strengthened by the currently available latitudinal distribution of lightning on Jupiter. Unlike

216

terrestrial lightning which predominates near the equator where more solar energy and moisture are available, the Jupiter lightning has been observed at higher altitudes (Cook et al., 1979). Lewis (1980) has pointed out that 19 of the 20 optical flashes originated in the complex polar region (> 45°N). Whistler data (Gurnett et al., 1979; Menietti and Gurnett, 1980) support the existence of high latitude (~ 66°N) lightning. Though it is possible that many other factors are influencing this distribution, we suggest that the predicted latitudinal conductivity dependence (Figure (IX-9) is playing a role.

The cloud top acquisition of electric charge in the nonlinear feedback process originally proposed by Vonnegut (1953) and examined in Chapter VII of this thesis requires the existence of large electric fields near the cloud tops. Estimates of the dielectric breakdown strength for this region on Jupiter (Table IX-1) show that fields in excess of 10^5 v/m are possible. Recalling the cloud top conductivity predictions, we estimate that cloud top current densities may be in excess of 10^{-7} amp/m^2, which is a large number when measured against values in terrestrial thunderclouds.

Unfortunately, the existence of large electric fields at the Jovian cloud tops is not well constrained by the presently available lightning observations. The optical data with long time exposure images (Cook et al., 1979) shows evidence for luminous spots whose projected diameters on the planetary disc are several hundred kilometers.

It is possible that the observed lightning is confined to the NH_3 cloud layer and has a large horizontal extent characteristic of terrestrial squall line lightning (Ligda, 1956). In this case one might expect electric field strengths approaching breakdown levels at the cloud tops.

Alternatively, the luminous spots may have originated from lightning deeper in the atmosphere --in the NH_4SH or H_2O cloud layers, or deeper still. Since the optical depth of the uppermost NH_3 cloud is of order 10 (Sato and Hansen, 1979), the extinction of light which may originate below it will be substantial, in which case the Jovian lightning energy may have been grossly underestimated (Smith et al., 1979).

A third possibility is that multiple smaller scale lightning sources are illuminating a large scale convective system. The limited spatial and temporal resolution in the optical data prevent us from examining the details of what appear to be local thunderstorms.

IX-4.4 Discussion of Results: Saturn

The atmospheric structure of Jupiter and Saturn are similar in so many ways (see Table IX-1) that the verification of lightning on Jupiter points to its existence on Saturn. If the observable flash rate per unit area varies with the solar flux incident on the planet (as it appears to do for Venus and Jupiter), we may expect a readily observable lightning rate on Saturn.

On the other hand, if cloud top conductivity is important to electrification as we argued for Earth and have suggested

218

for Jupiter, the prospects for lightning on Saturn are diminished. The predicted cloud forming levels for this planet are at greater equivalent depths (see Figure IX-2). The cosmic ray shielding effect is less severe fr Saturn than for Jupiter (Figures IX-10 and IX-9), but the Saturnian cloud top conductivity may still be two orders of magnitude smaller than for Jupiter.

The finding that electrification is confined to deep levels within the atmospheres of either Jupiter or Saturn would be strong evidence against the view that a finite atmospheric conductivity is essential for strong electrification. The electrical conductivity decreases monotonically with depth in both cases. We expect no significant conductivity contribution from radioactivity, and since there is no conductive planetary surface, we can expect no surface corona contribution.

A search for lightning in the Voyager dark side images of Saturn is currently in progress (B. Smith, private communication). Detection may be impaired by the presence of sunlight reflected by Saturn's ring system, which will compete with potential lightning sources.

IX-4.5 Discussion of Results: Uranus and Neptune

All currently available observations of the atmospheres of Uranus and Neptune are Earth-based and are limited because of the great distances involved. The possibility of a space probe flyby in 1986 has encouraged the conductivity calculations in spite of the present lack of observational information.

If we extrapolate the flash rate per unit area versus solar flux trend set by Venus, Earth and Jupiter, we may predict infrequent lightning on both Uranus and Neptune.

The electrical conductivity decreases with the increasing equivalent depths of cloud features in these colder, more remote atmospheres. Figure IX-8 shows that the predicted electrical conductivity for Neptune is at least an order of magnitude smaller than for Uranus at every temperature level. If cloud top conductivity is essential for electrification, this trend does not favor the existence of lightning on Neptune.

Massive NH_3-H_2O solution clouds have been predicted (Weidenschilling and Lewis, 1973) at deep levels in these atmospheres. Our estimates of electrostatic relaxation times at such depths (see Figure IX-8) range from hours to days. This would seem to be an ideal environment for precipitation driven electrification. The atmospheric opacity would almost certainly prevent the optical detection of lightning, and RF sensing may be necessary.

IX-5 Conclusions

What do these comparisons have to say about the relative importance of precipitation and convection for planetary electrification?

The most striking differences in the lightning producing planetary atmospheres are their chemical compositions. Such differences may mean that a unique microphysical charge

generation process is at work in every atmosphere, or alternatively, that a more general process is operative, governed by the common features of planetary atmospheres.

Such a general process does not exclude the possible contribution of precipitation, which we have noted as a probable common feature, but other common features support the role of convective charge transport. As one example, both the observed and predicted atmospheric motions are signficantly larger than the predicted fall speeds of precipitation particles.

The most striking example of a common feature is the adjacency of a conductive upper troposphere (relaxation time < convective time scale) to the planetary cloud tops, where the dielectric strength of the atmosphere is still substantial (10^5 -10^6 v/m). Such a configuration is vital to the convective theory proposed by Vonnegut (1953) (which we examined in Chapter VII), and may help to explain the latitudinal distribution of lightning on Jupiter.

Chapter X

Conclusions

X-1 The Prospects for Precipitation

The energy analysis (Chapter II) of the precipitation hypothesis for thunderstorm electrification has led to the conclusion that the electrical power of active thunderstorms is a substantial fraction of the gravitational power associated with falling precipitation. A corollary to this conclusion is the necessary modification in precipitation particle fall velocities by electric forces if precipitation is responsible for the electrical energy.

A Doppler radar search (Chapter III) has revealed the existence of a few velocity changes at the times of nearby lightning discharges, but contrary to expectation, these changes do not support the view that falling precipitation is responsible for the pre-discharge accumulation of electrostatic energy. Instead, net dissipative precipitation motion was observed.

In the vast majority of cases, no velocity changes were noted, and such a null result might be expected in cases in which the gravitational power associated with falling precipitation far exceeded the electrical power (Section II-8). In such cases the Doppler experiment is not a critical test for the energy contribution of precipitation. However, both the induction mechanism and the ice mechanism predict an electric force modification of the precipitation particle fall

222

velocities (Section II) which should have been frequently observable in the Doppler experiments regardless of the constraint which energy conservation imposes for electrically active storms.

Although the Doppler radar results do not support an energy contribution from precipitation, they do provide strong evidence for the systematic charging of a substantial volume of precipitation particles in the upper regions of thunderclouds ($>$ 6.8 km MSL). This evidence is consistent with the observations of clouds during initial electrification and during the mature stage of electrical development.

The appearance of precipitation at an altitude of 6-8 km MSL during the initial growth of foul weather field at the ground, and the absence of vertical air motion at lower levels which might promote initial electrification by convection (Vonnegut, 1953), together suggest that precipitation at upper levels is playing a role in segregating electric charge which may be fundamental to initiating the electrification process.

The rapid growth of precipitation above 6 km which is closely correlated with discharge rate (Section II-8) points further to a contribution from precipitation to this region. The gravitational energy associated with the precipitation appears inadequate to account for the electrification, but the flow configuration may promote a cooperative interaction between convection and precipitation. Horizontal air motion near the top of the precipitation core may transport segregated

charge forward and into the updraft at the leading edge of the storm to account for the systematic displacment of VHF sources away from regions of radar reflectivity.

It is possible that the accumulations of negative charge inferred from electric field studies (Krehbiel et al. 1979; Winn et al., 1981) are the result of a precipitation mechanism in mid-cloud which is responsible for initiating the electrification process. However, regardless of the nature of the particles which carry the negative charge, we believe that the air motions in and around the cloud will be the major factor in determining the location of negative charge accumulations.

Krehbiel et al. (1980) have argued in favor of the ice precipitation mechanism (Reynolds et al., 1957) on the basis that negative charge centers inferred from multiple field change studies are all at the same temperature in clouds of different size and in different geographical locations. This point has been raised against the scaling arguments presented in Chapter V (M. Brook, private communication), which imply a self-similarity of cloud electrical structure and therefore higher charge centers in larger clouds. In response to this criticism, we point out that negative charge centers in Florida thunderstorms (Jacobson and Krider, 1978), storms which are generally larger than those in New Mexico, do in fact show higher charge locations at lower cloud temperatures (mean: -23°C) than the data for New Mexico storms (mean: -13°C) (Krehbiel et al., 1979). The corresponding discrepancy in

224

altitude between New Mexico and Florida is significantly larger than the respective charge location error estimates. The charge locations in Japanese winter thunderstorms (Brook et al., 1980) are at lower altitudes, but the clouds are also significantly smaller than those in either New Mexico or Florida. The smallest known thunderstorms are lightning-producing warm clouds (Moore et al., 1960) and though the location of negative charge in such clouds is not known, it is unlikely that the charge is at -10°C.

These findings suggest that it may be more fruitful to correlate the locations of negative charge centers with heights of near zero vertical air motion than with the local air temperature.

If the charge transfers observed in laboratory experiments (Reynolds et al., 1957; Gaskell and Illingworth, 1980) are taking place systematically in thunderclouds, there is no question that the ice precipitation mechanism will make a substantial contribution to the accumulation of electric charge therein. If falling precipitation particles are principal contributors to thundercloud electrical energy, however, we should have seen evidence for this in our zenith pointing Doppler radar observations. The results of this experiment are puzzling but would be all the more puzzling if no energy source larger than the gravitational potential energy of precipitation were available for electrification. This alternative is of course convection and is discussed in the next section.

X-2 The Prospects for Convection

This study has shown convection to be a vital ingredient in the electrification of thunderstorms. This contribution must be assessed in light of both the existing convective theory (Vonnegut, 1953) and the evidence provided in this study.

The prospects for convective feedback effects relying upon externally derived electric charge (Vonnegut, 1953) were examined in Chapter VII, in which we demonstrated that under appropriate conditions the transport of screening layer charge from the cloud top can make a substantial contribution to electrical power. Documentation of the screening layer structures and penetrative downdrafts in the upper cloud, which are both necessary for this generative feedback, have proliferated in recent years. Furthermore, a negative charge accumulation near the top of a thunderstorm (13.7 km MSL) has been inferred to have participated in a lightning discharge (Rustan et al., 1980). The proximity to the cloud top and the fact that existing precipitation mechanisms do not predict negative charge accumulations at such high altitudes, both suggest a negative screening layer source.

Screening layer thicknesses are small in comparison with the size of the cloud and must necessarily form at the clear air-cloud boundary. The radar reflectivity of such structures may be insufficient to probe with long wavelength Doppler radar. Evidence for downturn in the Doppler derived wind field is often seen at the edge of the detectable cloud volume.

Only a fraction of the negative ions which flow to the cloud top can be expected to contribute to electrification (Grumm and Vonnegut, 1980). The paucity of information concerning the electrical and dynamical conditions in and around the cloud tops makes this fraction difficult to evaluate. However the requisite current flow has been documented (Gish and Wait, 1950), and forms the basis for the global circuit theory (Wilson, 1920). Cloud top currents as large as 6.5 amperes have been estimated with average values of 0.8 amperes. These estimates are consistent with the charge flow predictions (Figure VII-1) to our model screening layer.

If the negative screening layer charge is the major contributor to the negative charge center in mid-cloud (inferred from acoustic (Teer and Few, 1974) and electric field measurements (Krehbiel et al., 1979; Winn et al., 1981)), then an initially downward moving screening layer space charge must accumulate at this level. Curiously, a dual-Doppler radar analysis of a thunderstorm (Kropfli and Miller, 1976) has shown predominantly horizontal motion and a line of near zero vertical air motion at about 6 km MSL, and the vertically pointing Doppler profiles in New Mexico show systematic evidence for a zero in vertical air motion at a height which varies from 5 to 8 km. We also note that the Winn et al. (1981) balloon sounding experienced a distinct horizontal motion in passing upward through a negative charge region centered at -3°C (5.3 km).

Additional indirect support for the importance of screening layer charge accumulation to electrification is provided by the comparisons in Chapter IX. A common feature of all planetary atmospheres known to produce lightning is the proximity of a conductive atmosphere adjacent to the visible cloud tops. Furthermore, in the case of Jupiter, both the predicted and the observed lightning activity tend to increase with planetary latitude. These observations support the view that externally derived electric charge and a finite atmospheric conductivity are essential for electrification, as Vonnegut (1953) has argued for the terrestrial case.

The conductivity predictions also support the analogy between EHD and MHD dynamo theory in which dynamo action is characterized by optimal electric/magnetic Reynolds numbers.

The other feedback in the convection theory (Vonnegut, 1953) results from the point discharge current from the Earth's surface, and we are less optimistic about this contribution. Estimates both by Standler and Winn (1979) and Livingston and Krider (1978) indicate that the steady state corona current from the ground is of the same order as the current associated with lightning. Since only some fraction of the charge released at the ground can be expected to contribute to electrification, it is unlikely that point discharge is a primary charge source for thunderstorms.

If the positive space charge from the Earth's surface has inadequate time to reach the upper portion of the cloud in the early stages of storm development (as the Doppler observations

have suggested and which convective transport models

(Winn et al., 1980) have shown), then it is unlikely that

screening layer charge, hypothetically induced by this positive

charge in the upper cloud, can make a major contribution to

initial electrification. It is possible, however, that

positive charge segregated by a precipitation mechanism could

induce a screening layer.

The most damaging evidence for the convective theory

(Vonnegut, 1953) is the presence of lightning in oceanic

thunderstorms, where the existence of a quasi-steady state

corona current is unlikely (Fig. VIII-4). We further note

that the most electrically active thunderstorm ever documented

(Vonnegut and Moore, 1958) was observed over the ocean. Warm

cloud lightning (Foster, 1950; Moore et al., 1960) has been

characteristically oceanic, and so convected corona space

charge cannot be of much help in explaining this phenomenon.

Nevertheless, the continental and oceanic lightning comparisons

in Chapter VIII provide possible indirect evidence that the

corona space charge plays a contributory role in cloud

electrification.

Tests for convection versus precipitation based not on how

the electric charge is generated, but on the velocity with

which it is transported were pursued in Chapter V. (This test

therefore does not distinguish between internally derived

charge by precipitation mechanisms and externally derived

charge (Vonnegut, 1953).) Scaling law comparisons with three

independent data sets from three geographical locations all

support electrification by convection. In this context, we re-emphasize the point that, because of their large numbers, the total surface area of the cloud particles may be two orders of magnitude larger than the total surface area of the precipitation particles.

The frequently correlated behavior between pressure and electric field is strong evidence for a controlling role of the dynamics in cloud electrification, but does not rule out a contribution from precipitation. The coincidence of maximum flash rate with maximum rate of pressure change, prior to the maximum radar cloud top overhead (Figure VI-6), could be caused by a surge of convected space charge, or by the rapid proliferation of charge associated with the growth of precipitation at higher levels. In other data, dielectric breakdown evidenced by VHF emission occurs in a region of intense vertical air motion and ahead of and above the region of intense precipitation. These observations suggest that the convective air motion is responsible for the electrical energy, but the close proximity of the upper level precipitation hints that it may be important as a charge source for the updraft. Again we question the sustained contribution of charged precipitation to electrical energy since the flash rate has declined by the time of maximum cloud top. The gravitational power associated with ice phase precipitation can scarcely be expected to be _less_ at the time of maximum cloud height.

The Doppler profile and pressure comparisons with surface electric field during the end of storm oscillation confirm the

view (Moore and Vonnegut, 1977) that this phenomenon is caused by large scale convection of space charge.

Our original goal in this thesis as stated in the Introduction was to evaluate the relative contributions of precipitation and convection to thunderstorm electrification. We have demonstrated that convective energy is essential to the electrification process, but that convection alone appears inadequate to account for the initial electrification of developing clouds. Since a precipitation mechanism appears to be necessary in early stages of electrical development, there is little doubt that it will play an important role in segregating electric charge in later stages, when our calculations show that externally derived charge is also likely to make a substantial contriubution. The impression gained, however, is that the largest and most convectively active clouds rely most heavily on the kinetic energy of air motion for electrical energy. The small fractional field changes during high flash rate periods indicate that a large fraction of the existing space charge in the cloud remains unaffected by lightning and continues to move with the air to generate electrical energy. Since both the space charge and convection volumes are likely to be far greater than the precipitation volume, and since the air velocities will be far greater than the precipitation particle terminal velocities, the electrical contribution of convection may far outweigh the contribution of precipitation.

231

X-3   Suggestions for Future Work

(1) The vertically pointing Doppler work has opened up a new approach to evaluating the contribution of precipitation particle motion to thunderstorm electrification. The few cases of abrupt velocity changes at the times of nearby lightning make it worthwhile to "look" again. Improvements in sensitivity to velocity changes may be implemented by looking at sequential differences in complete Doppler spectra during lightning discharges.

(2) The infrequent occurrence of velocity changes in the Doppler results is inconsistent with the predictions of the ice precipitation mechanism (Section II-6). These predictions are based on the assumption that the graupel particle charge increases monitonically in constant increments, each of which represents the charge transfer in single ice crystal collisions as measured in laboratory experiments (Gaskell and Illingworth, 1980). Experiments need to be conducted to see whether graupel particles can accumulate (through repeated collisons) sufficient charge to influence their motion in fields of tens of kilovolts per meter within a realistic cloud particle environment.

(3) The motion field at the cloud boundary is often inaccessible to conventional Doppler radar investigation, but needs to be examined if the contribution of convective screening layer charge transport is to be evaluated. Millimeter wavelength Doppler techniques, currently being

developed by Dr. Roger Lhermitte, may provide a solution to this problem.

(4) A complete assessment of the contribution of external currents to thundercloud electrification (Vonnegut, 1953) will require a thorough charge budget study of an individual thunderstorm. Techniques for the measurement of the cloud top current, the corona current, and the current associated with lightning must be implemented simultaneously in a single thundercloud.

(5) Great progress has been made in recent years in measuring the electric charge carried by precipitation particles within thunderclouds. The more difficult task of measuring the charge on cloud particles, whose total charge carrying capacity is many times greater than the precipitation, needs further attention.

(6) The scaling law approach has produced the approximate result that the lightning flash energy is scale invariant, but we have not come up with a good physical basis for this somewhat surprising finding. The small field changes which characterize rapid flash rate periods must be a reflection of breakdown physics in space charge regions, but the details have continued to elude us.

(7) The Brook-Krehbiel hypothesis concerning the location of negative charge centers needs further testing to determine whether the heights of negative charge are controlled by cloud temperature, pressure or by cloud dynamics. Existing data could be used to determine the locations of lightning net

charge changes in very tall clouds (for example, the data used in Figure V-5) for which we would predict negative charge centers at higher altitudes.

(8) The cloud size hypothesis for the discrepancy in the lightning flash rates of oceanic and continental thunderstorms should be checked by examining existing satellite data and looking for systematic differences in the heights of these two storm types.

(9) Experiments designed to locate the depths of lightning sources in planetary atmospheres should accompany future space probes. The location of lightning deep within an atmosphere where the electrical relaxation time is predicted to be hours or days would contradict the assertion concerning the importance of conductivity for electrification, and would point to the existence of a precipitation mechanism. This finding would also have important implications for Vonnegut's (1980) predictions concerning the effect of electric fields on dynamics in dense atmospheres.

References

Albritton, D.L., T.M. Miller, D.W. Martin, E.W. McDaniel, Mobilities of mass-identified H_3^+ and H^+ ions in hydrogen. Phys. Rev., <u>171</u>, 1968, pp. 94-102.

Bohannon, J.L., Infrasonic Thunder: Explained, PhD. Thesis, Rice University, 1980, 61 pp.

Bannon, J.K. and L.P. Steele, Average water-vapour content of the air, Meteorological Research Paper #1075, (Air Ministry, Meteorological Office, London, England), 1957, 6 pp.

Battan, L.J., Duration of convective radar cloud units, Bull. Amer. Met. Soc. <u>34</u>, 1953, pp. 227-228.

Battan, L.J., <u>Radar Observations of the Atmosphere</u>, Univ. of Chicago Press, 1973.

Battan, L.J. and J.B. Theiss, Observations of vertical motions and particle sizes in a thunderstorm, J. Atmos. Sci., <u>23</u>, 1965, pp. 78-87.

Blanchard, D.C., The electrification of the atmosphere by particles from bubbles in the sea, PhD. Thesis, MIT, 1961.

Bly, R.T. and J.E. Nanevicz, Aerial measurements of the electric field in the vicinity of Florida thunderstorms: analysis and results, Final report, Stanford Research Institute, 1977.

Borucki, W.J., J.W. Dyer, G.S. Thomas, J.C. Jordan, and D.A. Comstock, Optical search for lightning on Venus, Geophy. Res. Lett., <u>8</u>, 1981, pp. 233-236.

Bowen, I.S., R.A. Millikan, and H.V. Neher, New high-altitude study of cosmic-ray bands and a new determination of their total energy content, Phys. Rev., <u>44</u>, 1933, pp. 246-252.

Bowen, I.S., R.A. Millikan, and H.V. Neher, New light on the nature and origin of the incoming cosmic rays, Phys. Rev., <u>53</u>, 1938, pp. 855-861.

Braham, R.R., Jr., The water and energy budgets of the thunderstorm and their relation to thunderstorm development, J. Met., <u>4</u>, 1952, pp. 227-242.

Brook, M., N. Kitagawa, and E.J. Workman, Quantitative study of strokes and continuing currents in lightning discharges to ground, J.G.R., <u>67</u>, 1962, pp. 649-659.

Brook, M., P. Krehbiel, P. MacLaughlan, T. Takeuti, and M. Nakano, Positive ground stroke observations in Japanese and Florida storms. Paper presented at 6th Int'l Conf. on Atmospheric Electricity, Manchester, England, July 1980.

Brooks, C.E.P., The distribution of thunderstorms over the globe, Geophys. Memo. 3, No. 24, (Air Ministry, Meteorological Office, London, England), 1925, pp. 147-164.

Brown, K.A., P.R. Krehbiel, C.B. Moore, G.N. Sargent, Electrical screening layers around charged clouds, J.G.R., 76, 1971, pp. 2825-2835.

Budyko, M.I., Climate and Life, Academic Press, 1974, 508 pp.

Busse, F.H., Theory of planetary dynamos, in Solar System Plasma Physics, vol. II, ed., C.F. Kennel, L.J. Lanzonotti, and E.N. Parker, North Holland Publ. Co., 1979.

Byers, H.R. and R.Braham, Jr., The Thunderstorm, U.S. Government Printing Office, Washington, D.C., 1949, 53 pp.

Callahan, R.C., S.C. Coroniti, A.J. Parziale, and K. Patten, Electrical conductivity of air in the troposphere, J.G.R., 56, 1951, p. 545.

Chiu, C. -S., Numerical study of cloud electrification in an axisymmetric, time-dependent cloud model, J.G.R., 83, 1978, pp. 5025-5049.

Christian, H., C.R. Holmes, J.W. Bullock, W. Gaskell, A.J. Illingworth, and J. Latham, Airborne and ground based studies of thunderstorms in the vicinity of Langmuir Laboratory, Quart. J. Roy. Met. Soc., 106, 1980, pp. 159-175.

Christian, H.J., Jr., Vector electric field structure inside a New Mexico thundercloud, PhD. Thesis, Rice University, 1976, 70 pp.

Cimino, J.B. and C. Elachi, Precipitation on Venus: properties and possibilities of detection, J. Atmos. Sci., 36, 1979, p. 1168.

Claerbout, J., Electromagnetic effects of atmospheric gravity waves, PhD. Thesis, MIT, 1967.

Colgate, S.A., Enhanced drop coalescence by electric fields in equilibrium with turbulence, J.G.R., 72, 1967, pp. 479-787.

Colgate, S.A., Differential charge transport in thunderstorm clouds, J.G.R., 77, 1972, pp. 4511-4517.

236

Cook, A.F., T.C. Duxbury, and G.E. Hunt, First results on Jovian lightning, Nature, 180, 1979, pp. 794.

Cooke, C.M. IEEE Trans. on Elec. Insulation, vol. EI 13, 1978, p. 239.

Counselman, C.C., S.A. Gourevitch, R.W. King, G.B. Loriot, and E.S Ginsberg, Zonal and meridional circulation in the lower atmosphere of Venus determined by radio interferometry, J.G.R., 85, 1981, pp. 8026-8030.

Dawson, G.A., C.N. Richards, E.P. Krider, and M.A. Uman, Acoustic output of a long spark, J.G.R., 73, 1968, pp. 815-811.

Eden, H.F. and B. Vonnegut, Electrical breakdown caused by dust motion in low-pressure atmospheres; considerations for Mars, Science, 180, 1973, pp. 962-963.,

Edgar, B.C., Global Lightning distribution at dawn and dusk for August-September 1977 as observed by the DMSP Lightning Detector, Space Sciences Lab. Rept. SSL-78, (3839-02)-1, Aerospace Corp., 1978.

Elster, J. and H. Geitel, Uber die Elektrizitatsentwicklung bei der Regenbildung, Annls. Phys. Chemy., 25, 1885, pp. 121-131.

Erickson, E.F., D. Goorvitch, J.P. Simpson, and D.W. Strecker, Far-infrared spectrophotometry of Jupiter and Saturn, Icarus, 35, 1978, pp. 61-73.

Few, A.A., H.B. Garrett, M.A. Uman, and L.E. Salanave, Comments on letter by W.W. Troutman 'Numerical calculation of the pressure pulse from a lightning stroke', J.G.R., 75, 1970, pp. 4192-4195. Foster, H., An unusual observation of lightning, Bull. Amer. Met. Soc. 31, 1950, pp. 140-141.

Freeman, W.B., Jr., The distribution of thunderstorm and lightning parameters over the eastern hemisphere for 1972, M.S. Thesis, Texas A. & M. Univ., 1974, 102 pp.

Gaskell, W. and A.J. Illingworth, Charge transfer accompanying individual collisions between ice particles and its role in thunderstorm electrification, Quart. J. Roy. Met. Soc., 106, 1980, pp. 841-854.

Gaskell, W., A.J. Illingworth, J. Latham, and C.B. Moore, Airborne studies of electric field and the charge and size of precipitation elements in thunderstorms, Quart. J. Roy. Met. Soc., 104, 1978, pp. 447-460.

Gay, M.J., R.F. Griffiths, and C.P.R. Saunders, The terminal velocities of charged raindrops and cloud droplets falling in strong fields, Quart. J. Roy. Met. Soc., 100, 1974, pp. 682-687.

Geotis, S.G., Thunderstorm water contents and rain fluxes deduced from radar, J. Appl. Met., 10, 1971, pp. 1233-1237.

Gish, O.H. and G.R. Wait, Thunderstorms and the Earth's General Electrification, J.G.R., 55, 1950, pp. 473-484.

Grenet, G., Essai d'expliquation de la charge electrique des nuages d'orages, Extrait Annls. Geophys., 3, 1947, pp. 306-307.

Griffiths, R.F., J. Latham, and V. Myers, The ionic conductivity of electrified clouds, Quart. J. Roy. Met. Soc., 100, 1974, p. 181.

Griffiths, R.F., C.T. Phelps, and B. Vonnegut, Charge transfer from a highly electrically stressed water surface during drop impact, J. Atmos. Terr. Phys., 35, 1973, pp. 1967-1978.

Griffiths, R.F. and Latham, J., Field Generation and Dissipation currents in thunderstorm clouds as a result of the movement of charged hydrometers, J. Atmos. Sci. 32, 1975, pp. 958-964.

Griffiths, R.F. and V. Myers, The ionic conductivity of electrified clouds, Quart. J. Roy. Met. Soc., 100, 1974, pp. 181-190.

Grumm, R.H. and B. Vonnnegut, Mechanisms of charge transfer in the upper part of the thundercloud, Trans. American Geophys. Union, 61, 1980, p. 974.

Gunn, R., Electric field regeneration in thunderstorms, J. Met., 11, 1954, pp. 130-138.

Gunn, R., The electrification of precipitation and thunderstorms, Proc. IRE, October, 1957, pp. 1331-1358.

Gurnett, D.A., R.R. Shaw, R.R. Anderson, and W.S. Kurth. Whistlers observed by Voyager 1: detection of lightning on Jupiter, Geophys. Res. Lett., 6, 1979, pp. 511-514.

Hallett, J. and C.P.R. Saunders, Charge separation associated with secondary ice crystal production, J. Atmos. Sci., 36, 1979, pp. 2234-2235.

Haurwitz, B. and J.M. Austin, Climatology, McGraw-Hill, 1944, 410 pp.

Higashi, S., T. Kitamura, S., Mivamoto, Y. Mishuma, et al., Cosmic ray intensities under seawater at depths down to 1400 meters, Nuovo Cimento, 43, 1966, p. 334.

Hill, R.D., Energy dissipation in lightning, J.G.R., 82, 1977, pp. 4967-4968.

238

Hill, R.D., A survey of lightning energy estimates, Rev. Geophys. Space Phys., 17, 1979, pp. 155-164.

Hilst, G.R., Analysis of the audio-frequency fluctuations in radar storm echoes: a key to the relative velocities of the precipitation particles, Tech. Rep't. #9, MIT Weather Radar Research, 1949.

Holden, D.N.; C.R. Holmes, C.B. Moore, W.P. Winn, J.W. Cobb, J.E. Griswold, and D.M. Lytle, Local charge concentrations in thunderclouds, paper presented at 6th Int'l. Conf. on Atmospheric Electricity, Manchester, England, July, 1980.

Hoppel, W.A. and B.B. Phillips, The electrical shielding layer around charged clouds and its role in thunderstorm electricity, J. Atmos. Sci., 28, 1971, pp. 1258-1271.

Huntress, W.T., A review of Jovian ionosphere chemistry, Advan. Atmos. Molec. Phys., 10, 1974, pp. 295-340.

Illingworth, A.J. and J. Latham, Calculations of electric field growth, field structure and charge distributions in thunderstorms, Quart. J. Roy. Met. Soc., 103, 1977, pp. 281-295.

Ingersoll, A.P., Saturn's atmosphere and interior, EOS, 62, 1981, p. 254.

Ingersoll, A.P., R.F. Beebe, S.A. Collins, et al., Zonal velocity and texture in the Jovian atmosphere inferred from Voyager images, Nature, 280, 1979, pp. 773-775.

Israel, H., Atmospheric Electricity, vol. I, Israel Program for Scientific Translations, Jerusalem, 1970, 316 pp.

Israel, H., Atmospheric Electricity, vol. II, Israel Program for Scientific Trans., Jerusalem, 1973, 341 pp.

Jacobson, E.A. and E.P. Krider, Electrostatic field changes produced by Florida lightning, J. Atmos. Sci., 33, 1976, pp. 103-117.

Johnson, R. and M.A. Biondi, Measurements of positive ion conversion and removal relating to the Jovian ionosphere, Icarus, 23, 1974, pp. 139-143.

Johnson, T.H., Cosmic ray intensity and geomagnetic effects, Reviews of Mod. Phys., 10, 1938, pp. 193-244.

Kamra, A.K., Contributions of cloud and precipitation particles to the electrical conductivity and the relaxation time of the air in thunderstorms, J.G.R., 84, 1979, pp. 5034-5038.

Klett, J.D., Charge screening layers around electrified clouds, J.G.R., 77, 1972, pp. 3187-3195.

Knollenberg, R., L. Travis, M. Tomasko, et al., The clouds of
    Venus: a synthesis report, J.G.R., 85, 1981, pp. 8059-8081.

Krehbiel, P.R., M. Brook, and R.A. McCrory, An analysis of the
    charge structure of lightning discharges to ground, J.G.R.,
    84, 1979, pp. 2432-2456.

Krehbiel, P.R., M. Brook, R. Lhermitte, and C.L. Lennon,
    Lightning charge structure in thunderstorms, paper presented
    at 6th Int'l. Conf. on Atmospheric Electricity, Manchester,
    England, July, 1980.

Krider, E.P., G.A. Dawson, and M.A. Uman, Peak power and energy
    dissipation in a single stroke lightning flash, J.G.R., 73,
    1968, pp. 3335-3339.

Kropfli, R.A. and L.J. Miller, Kinematic structure and flux
    quantities in a convective storm from dual-Doppler radar
    observations, J. Atmos. Sci., 33, 1976, pp. 520-529.

Ksanfomaliti, L.V., Discovery of frequent lightning discharges
    in clouds on Venus, Nature, 284, 1980, pp. 244-246.

Langevin, P., Recombinaison et mobilities des ions dans les
    gaz, Annls. Chim. Phys., 1, 1903, p. 433.

Langevin, P., Une formule fondamentale de theorie cinetique,
    Annls. Chim. Phys., 8, 1905, p. 245.

Latham, J., A quantitative assessment of precipitation
    mechanisms for thunderstorm electrification, J. Met. Soc.
    Japan, 49, 1971, pp. 359-365.

Latham, J. The electrification of thunderstorms, Quart. J. Roy.
    Met. Soc., 107, 1981, pp. 277-298.

Le Maitre, G. and M.S. Vallarta, Geomagnetic analysis of cosmic
    radiation, Phys. Rev., 49, 1936, pp. 719-726.

LeMone, M.A. and E.J. Zipser, Cumulonimbus vertical velocity
    events in gate. Part I; diameter, intensity, and mass flux,
    J. Atmos. Sci., 37, 1980, pp. 2444-2457.

Lewis, J.S., Lightning on Jupiter: rate, energetics, and
    effects, Science, 210, 1980, pp. 1351-2.

Lhermitte, R., Real time processing of meteorological Doppler
    radar signals, preprints, 15th Conf. on Radar Meteorology,
    A.M.S., Boston, Massachusetts, 1972, pp. 364-367.

Lhermitte, R., Real time velocity observations by multi-doppler
    radar, 10th Conf. on Radar Meteorology, A.M.S., April 22-24,
    1975.

Lhermitte, R.M. and P.R. Krehbiel, Doppler radar and radio observations of thunderstorms, IEEE Trans. on Geoscience Electronics, GE-17, 1979, pp. 162-171.

Ligda, M.G.H., The radar observation of lightning, J. Atmos. Terr. Phys., 9, 1956, pp. 329-346.

Lindal, G.F., G.E. Wood, G.S. Levy, J.D. Anderson, D.N. Sweetham, H.B. Hotz, B.J. Buckles, D.P. Holmes, and P.E. Doms, The atmosphere of Jupiter: an analysis of the Voyager radio occultation measurements, to be published, J.G.R., 1981.

Livingston, J.M. and E.P. Krider, Electric fields produced by Florida thunderstorms, J.G.R., 83, 1978, pp. 385-401.

Loeb, L.B., Basic Processes of Gaseous Electronics, Berkeley, Univ. of Calif. Press, 1955.

McConnel, J.C., The ionospheres of Mars and Venus, Ann. Rev. Earth Planet. Sci., 4, 1976, p. 319.

McKenzie, D.P., Speculations on the consequences and causes of plate motions, Geophys. J. R. Astr. Soc., 18, 1969, pp. 1-32.

Machler, W., 2ur Druck-und Temperaturabhangkeit des Wieder vereinigungskoeffizienten und der ionization durch gammastrahlen in luft und Kohlensaure, Zeit. f. Physik., 104, 1936, p. 1.

Malan, D.J., Les decharges dans l'air et la charge inferieure positive d'un orage orageux, Annales due Geophysique, 8, 1952, pp. 385-401.

Malan, D.J., Physics of Lightning, English Univ. Press, London, 1963, 1976 pp.

Marshall, B.J.P., J. Latham, and C.P.R. Saunders, A laboratory study of charge transfer accompanying the collision of ice crystals with a simulated hailstone, Quart. J. Roy. Met. Soc., 104, 1978, pp. 163-178.

Marshall, J.S. and W.M.K. Palmer, The distribution of raindrops with size, J. Met., 5, 1948, pp. 165-166.

Marshall, T.C. and W.P. Winn, Preliminary measurements of charge on individual precipitation particles inside thunderstorms, paper presented at 6th Int'l. Conf. on Atmospheric Electricity, Manchester, England, 1980.

Mason, B.J., The physics of the thunderstorm, Proc. Roy. Soc. London, 327, 1972, pp. 433-466.

241

Menietti, J.D. and D.A. Gurnett, Whister propagation in the Jovian magnetosphere, Geophys. Res. Lett., 7, 1980, pp. 49-52.

Merrymon, W.W., Variation with pressure of the residual ionization in gases, Phys. Rev., 27, 1926, pp. 659-671.

Mills, A.A., Report in Science News, Science News, 112, 1977, p. 183.

Minzer, R.A., W.E. Shenk, R.D. Teagle, and J. Steranka, Stereographic cloud heights from imagery of SMS/GOES satellites, G.R.L., 5, 1978, pp. 21-24.

Mollo-Christenson, E., The distribution of raindrops and gusts in showers and squalls, J. Atmos. Sci., 10, 1962, pp. 191-192.
Moo, C.A., Non-linear interactions of atmospheric gravity waves, PhD. Thesis, MIT, 1976.

Moore, C.B., B. Vonnegut, B.A. Stein, and H.J. Survilas, Observations of electrification and lightning in warm clouds, J.G.R., 65, 1960, pp. 1907-1910.

Moore, C.B. and B. Vonnegut, The Thundercloud, a chapter in The Physics of Lightning, ed., R.H. Golde, Academic Press, London, 1977, pp. 51-98.

Moore, C.B., W.P. Winn, and A.S. Cooper, The effect of transport time delays on convective cloud electrification, paper presented at 6th Int'l. Conf. on Atmospheric Electricity, Manchester, England, July, 1980.

Muller-Hillebrand, D., Charge generation in thunderstorms by collision of ice crystals with gravel, falling through vertical electric field, Tellus, 6, 1954, pp. 367-381.

Nakano, M., Initial streamers of the cloud discharge in winter thunderstorms of the Hokuriku coast, J. Met. Soc. Japan, 57, 1979, pp. 452-457.

Ogawa, T. and M. Brook, Charge distribution in thunderstorm clouds, Quart. J. Roy. Met. Soc., 95, 1965, pp. 513-525.

Orville, R.E., Global distribution of midnight lightning-September-November 1977, Monthly Weather Review, 109, 1981, pp. 177-181.

Orville, R.E. and D.W. Spencer, Global lightning flash frequency, Monthly Weather Review, 107, 1979, pp. 934-943.

242

Phelps, C.T., R.F. Griffiths, and B. Vonnegut, Corona produced by splashing of water drops on a water surface in a strong electric field, J. Appl. Phys., 44, 1973, pp. 3082-3086.

Phillips, B.B., Ionic equilibrium and the electrical conductivity in thunderclouds, Mon. Weather, Rev., 95, 1967, p. 854.

Pietrowski, E.L., An observation of lightning in warm clouds, J. Met., 17, 1960, pp. 562-563.

Poehler, H.A., LDAR observations of a developing thunderstorm correlated with field mill, ground strike location, and weather radar data including the first report of the design and capabilities of a new time-of-arrival ground-strike location system (GSLS), NASA Contractor Report CR-154626, 1978, 134 pp.

Pollack, J.B., F.M. Flasar, R. Kahn,, C.E. Carlson, and D. Pidek, Properties and effects of dust particles suspended in the Martian atmosphere, J.G.R., 84, 1979, p. 2929.

Pollack, J.B., D.W. Strecker, F.C. Witteborn, E.F. Erickson and B. Baldwin, Properties of the clouds of Venus, as inferred from airborne observations of its near-infrared reflectivity spectrum, Icarus, 34, 1978, pp. 28-45.

Ray, P.S., et al., Triple-Doppler observations of a convective storm, J. Appl. Met., 17, 1978, pp. 1201-1212.

Reed, R.K., Comparison of ocean and island rainfall in the tropical N. Pacific, J. Appl. Met., 19, 1980, pp. 877-880.

Regener, E., Die absorptionskurve der ultrastrahlung und ihre deutung, Physik, Zeitschr., 34, 1933, p. 306.

Reynolds, S.E., M. Brook, and M.F. Gourley, Thunderstorm charge separation, J. Met., 14, 1957, pp. 426-436.

Reynolds, S.E. and H.W. Neill, The distribution and discharge of thunderstorm charge centers, J. Met., 12, 1955, pp. 1-12.

Rust, W.D. and C.B. Moore, Electrical conditions near the bases of thunderclouds over New Mexico, Quart, J. Roy. Met. Soc., 100, 1974, pp. 450-468.

Rustan, P.L., M.A. Uman, D.G. Childers, W.H. Beasley, Lightning source locations from VHF radiation data for a flash at Kennedy Space Center, J.G.R., 85, 1980, pp. 4893-4903.

Sanders, F. and J. Freeman, Thunderstorms at Sea, to be published.

Sandstrom, A.E., Cosmic Ray Physics, Amsterdam, North Holland Publ. Co., 1965.

Saporoschenko, M., Mobility of mass-analyzed H^+, H_3^+, and H_5^+ ions in hydrogen gas. Phys. Rev., 139, 1965, pp. 349-351.

Sartor, J.D., The role of particle interactions in the distribu-tion of electricity in thunderstorms, J. Atmos. Sci., 24, 1967, pp. 601-615.

Sato, M. and J.E. Hanson, Jupiter's atmospheric composition and cloud structure deduced from absorption bands in reflected sunlight, J. Atmos. Sci., 36, 1979, pp. 1133-1167.

Sayers, J., Ionic recombination in air, Proc. Roy. Soc. A., 169, 1938, p. 83.

Schonland, B.F.J., The Flight of Thunderbolts, Oxford Univ. Press, 1950, pp. 150-151.

Schubert, G., C. Covey, A. Delbenio, et al., Structure and circulation in the Venus atmosphere, J.G.R., 85, 1981, pp. 8007-8025.

Scorer, R.S., Natural Aerodynamics, Pergammon Press, New York, 1958.

Seiff, A. and D.B. Kirk, Structure of the atmosphere of Mars in summer at midlatitudes, J.G.R., 82, 1977, p. 4364.

Seiff, A. D.B. Kirk, R.E. Young, et al., Measurements of thermal structure and thermal contrasts in the atmosphere of Venus, and related dynamical observations-results from the four Pioneer Venus probes, J.G.R., 85, 1981, pp. 7903-7933.

Shackford, C.R., Radar indications of a precipitation-lightning relationship in New England thunderstorms, J. Met., 17, 1960, pp. 15-19.

Simpson, G.C. and G.D. Robinson, The distribution of electricity in thunderclouds II, Proc. Roy. Soc. A., 161, 1940, pp. 281-329.

Shreve, E.L., Theoretical derivation of atmospheric ion concentrations, conductivity, space charge density, electric field and generation rates from 0 to 60 km, J. Atmos. Sci., 27, 1970, p. 1186.

Smith, B.A., L.A. Soderblum, A.P. Ingersoll et al., The Jupiter system through the eyes of Voyager, Science, 204, 1979, pp. 951-972.

Standler, R.B. and W.P. Winn, Effects of coronae on electric fields beneath thunderclouds, Quart. J. Roy. Met. Soc., 105, 1979, pp. 285-302.

Steiner, R. and R.H. Rhyne, Atmospheric turbulence and airplane response in convective-type clouds, J. Aircraft, 1, 1964, pp. 13-17.

Stone, P., in Jupiter, T. Gehrels, ed., Univ. of Arizona Press, Tucson, 1976.

Stuetzer, O.M. Magnetohydrodynamics and electrohydrodynamics, Phys. Fluids, 5, no. 3, 1962.

Takahashi, T., Riming electrification as a charge generation mechanism in thunderstorms, J. Atmos. Sci., 35, 1978, pp. 1536-1548.

Taylor, W.W.L. and F.L. Scarf, Atmospheric refraction and lightning on Venus, Trans. A.G.U., 61, p. 1017.

Taylor, W.W.L., F.L. Scarf, C.T. Russell, and L.H. Brace, Evidence for lightning on Venus, Nature, 279, 1979, p. 614.

Thomson, J.J. and G.P. Thomson, The Conduction of Electricity Through Gases, Cambridge, University Press, 1928.

Toland, R.B. and B. Vonnegut, Measurement of maximum electric field intensities over water during thunderstorms, J.G.R., 82, 1977, pp. 438-440.

Trent, E.M. and S.G. Gathman, Oceanic thunderstorms, Pageophys., 100, 1972, pp. 60-69.

Uman, M.A. et al., An unusual lightning flash at Kennedy Space Center, Science, 201, 1978, pp. 9-16.

Valentine, J.M. and S.C. Curran, Average energy expenditure per ion pair in gases and gas mixtures, Reports of Prog. in Phys., 21, 1958, pp. 1-29.

Vonnegut, B., Possible mechanism for the formation of thunderstorm electricity, Bull. Am. Met. Soc., 34, 1953, p. 378.

Vonnegut, B., Some facts and speculations concerning the origin and role of thunderstorm electricity, Met. Monogr., 5, 1963, pp. 224-241.

Vonnegut, B., Discussion of paper by J.B. Mathews 'Mass Loss and Distortion of Freely Falling Water Drops in an Electric Field', J.G.R., 73, 1968, p. 1501.

245

Vonnegut, B., Locations of charged regions in thunderclouds inferred from electric field changes associated with lightning, 1979, unpublished note.

Vonnegut, B., Possible role of atmospheric electricity in the dynamics of atmospheres more dense than that of Earth, paper presented at 6th Int'l. Conf. on Atmos. Electricity, Manchester, England, July, 1980.

Vonnegut, B. and C.B. Moore, Giant electrical storms, in: Recent Advances in Atmospheric Electricity, Pergammon Press, London, 1958, pp. 399-411.

Vonnegut, B. and C.B. Moore, A possible effect of lightning discharge on precipitation formation process, in: Physics of Precipitation, Monogr. No. 5, A.G.U., 1960, pp. 287-290.

Vonnegut, B., C.B. Moore, R.P. Espinola, and H.H. Blau, Jr., Electric potential gradients above thunderstorms, J. Atmos. Sci., 23, 1966, pp. 764-770.

Vonnegut, B. and R.E. Orville, Venusian lightning -a spectroscopic study of spark discharges in CO_2 at pressures from one to eighty atmospheres, Trans. from Geophys. Union, 61, 1980, p. 978.

Vorpahl, J.A., The frequency and intensity of lightning within 30° of the equator, M.S. Thesis, Univ. of Minnesota, 1967, 66 pp.
Vorpahl, J.A., J.G. Sparrow, and E.P. Ney, Satellite observations of lightning, Science, 169, 1970, pp. 860-862.

Wang, P.K. and H.R. Pruppacher, Acceleration to terminal velocity of cloud and raindrops, J. Appl. Met., 16, 1977, pp. 275-280.

Weidenschilling, S.J. and J.S. Lewis, Atmospheric and cloud structures of the Jovian planets, Icarus, 20, 1973, pp. 465-476.

Whipple, F.J.W., On the association of the diurnal variation of electric potential gradient in fine weather with the distribution of thunderstorms over the globe, Quart. J. Roy. Met. Soc., 55, 1929, pp. 1-17.

Williams, E., Scaling of planetary magnetic moment with core size, revisited, Trans. A.G.U., 61, 1980.

Wilson, C.T.R., On the ionization of atmospheric air, Proc. Roy. Soc. A., 68, 1901, p. 151.

Wilson, C.T.R., Investigations on lightning discharges and on the electric field of thunderstorms, Phil. Trans. Roy. Soc. London A., 221, 1920, pp. 73-115.

Wilson, C.T.R., Investigations on lightning discharges and on the electric field of thunderstorms, Trans. Roy. Soc., 221A, 1920, pp. 73-115.

Wilson, D.A., The kinematic behavior of spherical particles in an accelerating environment, ESSA. Rept., 1970.

Wilson, V.C., Cosmic ray intensities at great depths, Phys. Rev., 53, 1938, pp. 337-343.

Winn, W.P. and L.G. Byerley, Electric field growth in thunderclouds, Quart. J. Roy. Met. Soc., 101, 1975, pp. 979-993.

Winn, W.P., C.B. Moore, and C.R. Holmes, Electric field structure in an active part of a small, isolated thundercloud, J.G.R., 86, 1981, pp. 1187-1193.

Winn, W.P., C.B. Moore, C.R. Holmes, and L.G. Byerley III, A thunderstorm on July 16, 1975 over Langmuir Laboratory: a case study, J.G.R., 83, 1978, pp. 3080-3092.

Winn, W.P., G.W. Schwede, and C.B. Moore, Measurements of electric fields in thunderclouds, J.G.R., 79, 1974, pp. 1761-1767.

Winn, W.P., R.B. Standler, C.B. Moore, C.R. Holmes, L.G. Byerley, III, Electric structure of New Mexico thunderstorms from balloon-borne instruments, paper presented at 6th Int'l. Conf. on Atmos. Elec., Manchester, England, July, 1980.

World Meteorological Organization, World distribution of thunderstorm days, Part I: Tables WMO/OMN-No. 21, TP.21, 1953.

World Meteorological Organization, World distribution of thunderstorm days, Part II: Tables of marine data and world maps, WMO/OMN-No. 21, TP.21, 1956.

Wormell, T.W., Vertical electric currents below thunderstorms and showers, Proc. Roy. Soc. A., 127, 1930, pp. 567-590.

Appendix A

Maximum Gravitational to Electrical Power Conversion Efficiency in the Stokes Regime

The treatment of energy extraction for precipitation mechanisms in Chapter II dealt with particles in a high Reynolds number regime. The solution for particles in the Stokes regime is not applicable to thunderstorm precipitation particles but is analytic and is therefore included here.

The balance of forces for a particle of radius a and electric charge q immersed in a vertical gravity field g and a vertical electric field E is

$$mg - qE = 6\pi\eta aV \qquad (1)$$

and in absence of an electric field the particle's terminal velocity is

$$V_o \equiv \frac{mg}{6\pi\eta a} \qquad (2)$$

By multiplying equation (1) though by V, we obtain the energy conservation equation

$$mgV - qEV = 6\pi\eta aV^2 \qquad (3)$$

which says that the difference between the gravitational energy given up and the electrical energy generated is the energy dissipated by viscosity.

By rearranging (3) and invoking equation (2) we can write the power equation in terms of the electrical power qEV

$$qEV = 6\pi\eta aV(V_o - V) \qquad (4)$$

To determine the condition for maximum electrical power generation, we differentiate with respect to V.

$$\frac{d(qeV)}{dV} = 6\pi\eta a (V_o - 2V) = 0$$

$$V = V_o/2 \qquad (5)$$

An exact halving of the zero-field terminal velocity is required for maximum power conversion. Recalling the linearity between force and velocity which is characteristic of Stokes flow (equation (1)), we may immediately conclude that condition (5) is satisfied when the magnitude of the electric force is half that of the oppositely directed gravitational force.

To determine what fraction of the available gravitational potential energy of Stokes particle may be converted to electrical energy, we examine the power conversion efficiency

$$\text{Eff} = \frac{mgV - 6\pi\eta aV^2}{mgV} = \left(\frac{qE}{mg}\right)\left(\frac{V}{V_o}\right)$$

$$= \left(\frac{1}{2}\right)\left(\frac{1}{2}\right) = 0.25 \tag{6}$$

We conclude that for every joule of electrical energy produced, three joules will be lost to viscous dissipation and heat.

These analytic results (5) and (6) are quite close to the precipitation particle results derived in Chapter II, in spite of the differences in flow regime.

Appendix B

Radar Measurements of Precipitation Gravitational Power

The gravitational power associated with falling
precipitation may be expressed as the product of the momentum
density and the acceleration due to gravity. Since the
rainfall rate is really a momentum density when expressed in
appropriate units, and since the rainfall rate is a quantity
commonly determined with incoherent meteorological radars,
estimates of the gravitational power of a thunderstorm may be
readily obtained.

Table B-1 shows reflectivity dBZ values, rainfall rates
(R), gravitational power per unit volume, and precipitation
water contents (M), for Z-R and Z-M relationships which we have
used and which were used in a prior study of New England
thunderstorm total water contents (Geotis, 1971). Reflectivity
corrections for the existence of ice above 4 km were
implemented as in the latter study.

Nearly all estimates of thunderstorm gravitational power
were obtained from New England squall line observations with
MIT radar data. Radar reflectivity values were digitally
recorded with 1 kilometer spatial resolution and with estimated
uncertainties in the 1-2 dB range. This data was used to
evaluate the gravitational power within an arbitrary 10
kilometer radius cylinder centered on the electric field
measurement location at Millstone Hill, Westford, Massachusetts
as shown in Figure B-1.

.

250

Table B-1

dBZ	R (mm/hr)	P (Mwatt/km^3)	M (gm/m^3)
20	0.34	0.92	0.02
25	0.83	2.3	0.05
30	2.0	5.5	0.12
35	4.9	13.3	0.27
40	11.9	32.3	0.59
45	28.8	78.4	1.33
50	70.0	190	2.98
55	169	461	6.70

Z-R Relation

$$z = 400R^{1.3}$$

Z-M Relation

$$z = (2.1 \times 10^4)M^{1.43}$$
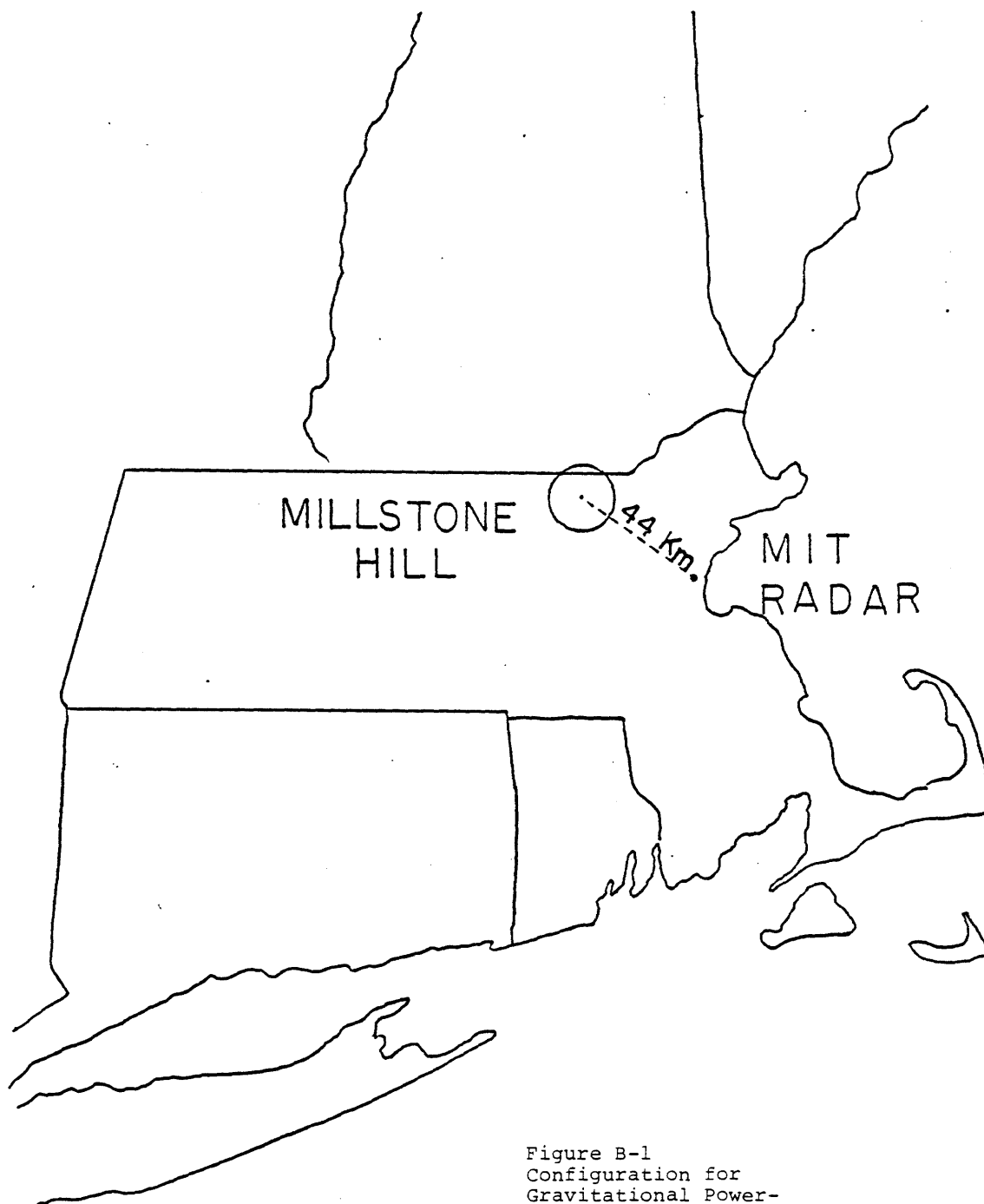
MILLSTONE
HILL

44 Km.

MIT
RADAR

Figure B-1
Configuration for
Gravitational Power-
Lightning Comparisons:
New England

Total gravitational power calculations with data made available to us later from thunderstorms in Florida and New Mexico, in which the origin of the electrical activity was better specified, indicated that the earlier New England calculations for gravitational power were exaggerated.

Appendix C

Doppler Radar Instrumentation

The Doppler radars used in the experiments described in Chapter III were designed and built by Dr. Roger Lhermitte. The characteristics of these radars are summarized in Table C-1 and a block diagram of their operation is shown in Figure C-1. The meteorological Doppler methodology is now well established (Lhermitte, 1973; Battan, 1973) and will not be reviewed here.

For the 1979 observations we used a sample-and-hold circuit to monitor the Doppler audio signals at a single range gate in altitude (6.8 km MSL). The real and imaginary Doppler signals (See Figure C-1) were recorded on two of the four channels of a Sony Quadraphonic tape recorder. We recorded either the electric field or the output of a HF radio receiver, and a timing signal, on the third and fourth channels, respectively. The Doppler signals could be played back in post-storm analysis through an audio amplifier to check for the presence of frequency changes at the times of lightning discharges. For quantitative analysis, the mean Doppler frequency was determined by counting zero crossings of these audio signals with a digital processing technique.

For the 1980 observations, a mean Doppler frequency processor was available to provide the mean velocity in real time at 150 msec intervals at each of 128 range gates spaced by 255 meters each. The pulse-pair technique for evaluation of the mean velocity in real time was first implemented by Lhermitte (1972) and is discussed in detail by Lhermitte

Table C-1

Radar Characterisitcs

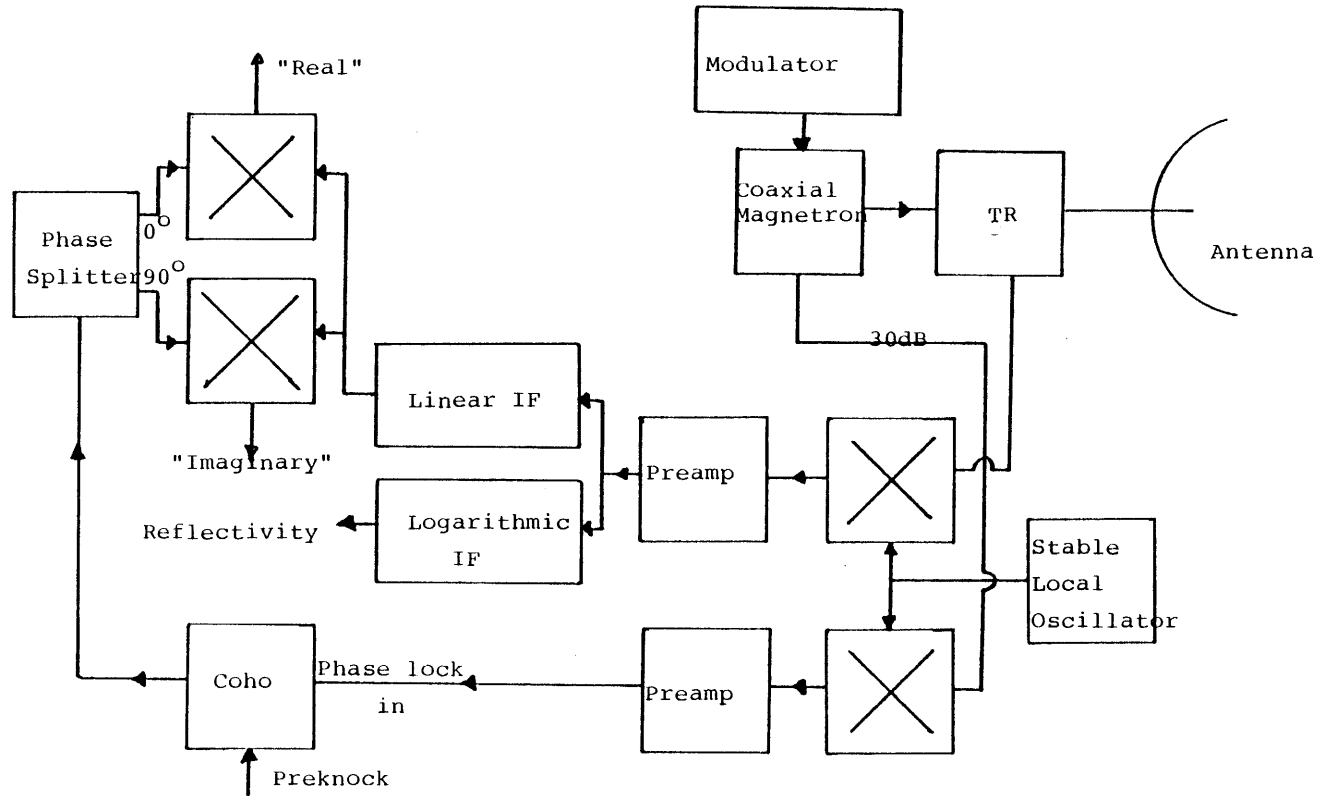|		
Wavelength	3.2 cm	3.2 cm
Peak power	30 kW	50 kW
Beamwidth	1.0°	0.8°
Pulse width	0.25 μsec	0.25 μsec
Pulse repetition frequency	2000 sec^{-1}	1900 sec^{-1}
Data acquisition	Single gate mean velocity	Multiple gate mean velocity; reflectivity

255

Figure C-1
Doppler Radar Transmitter-Receiver

(1975). These digitally computed mean Doppler velocities were color coded and displayed on the screen of a color CRT during the storm so that the occurrence of sudden velocity changes associated with nearby lightning discharges could be instantly recognized.
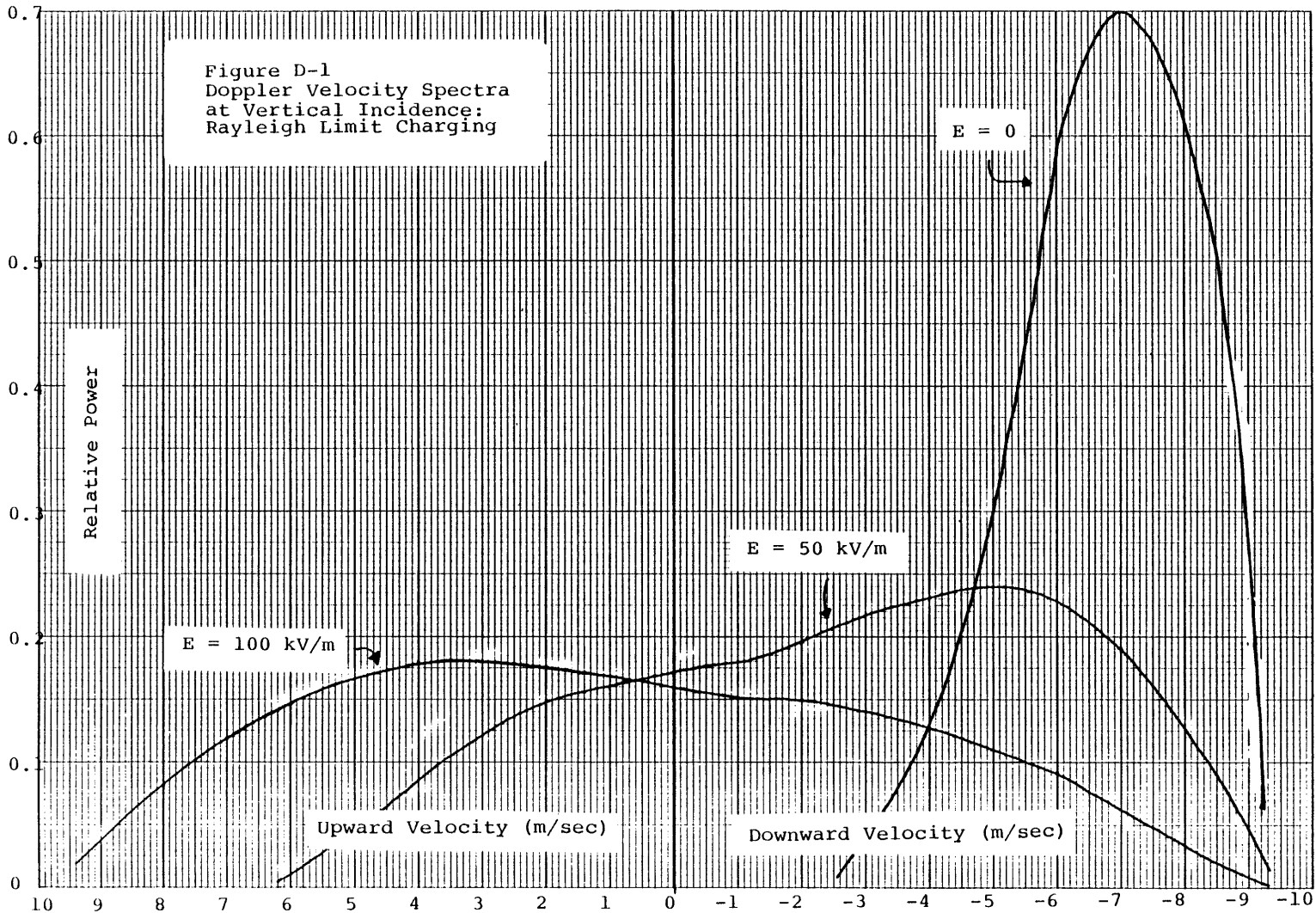
Appendix D

A Possible Effect of Electric Field on the Spectrum of Doppler Velocity at Vertical Incidence
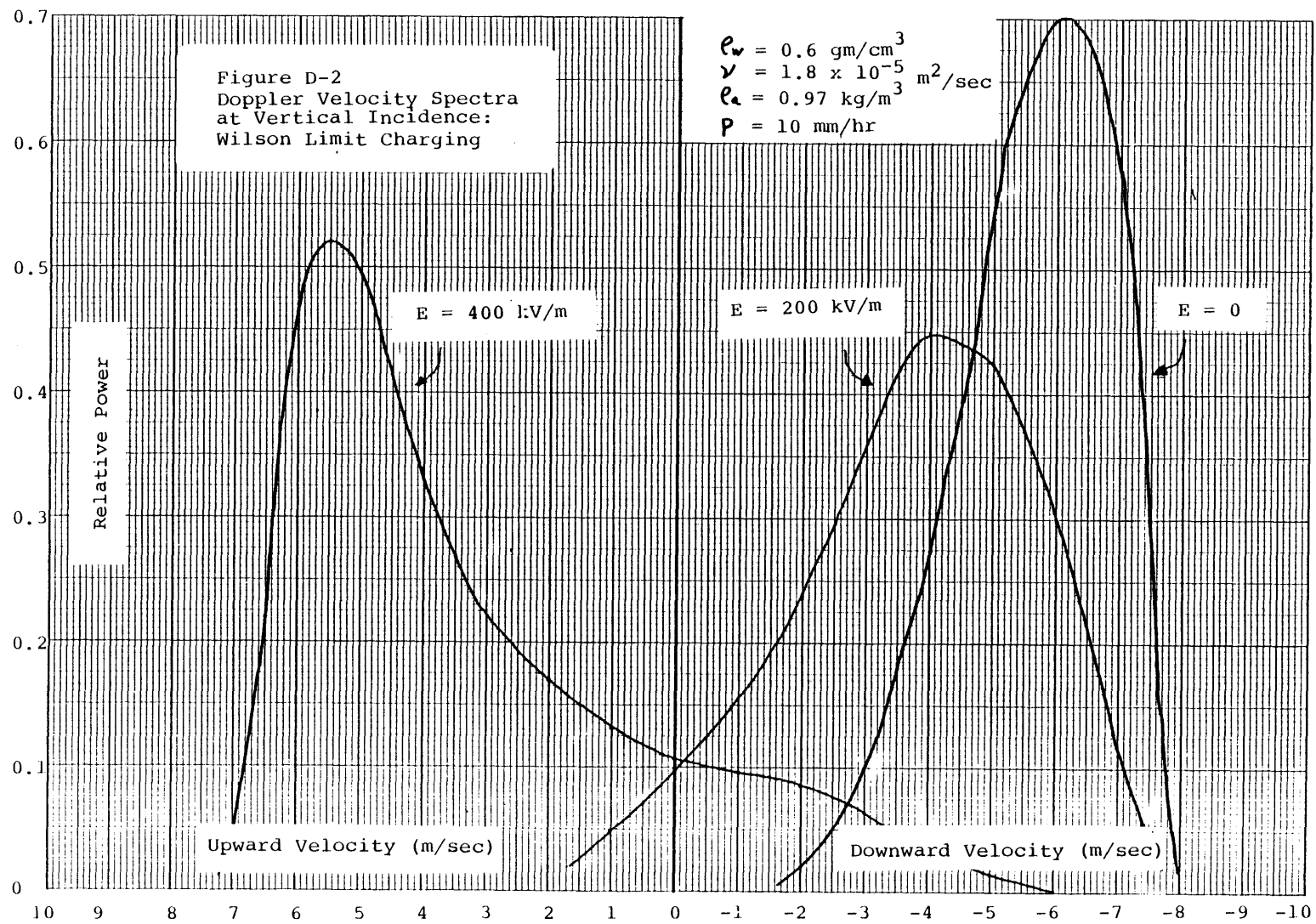
In Chapter III we discussed the tendency for greater scatter in the mean Doppler velocity estimate before the lightning discharge then after it. As possible explanations, we proposed a rapidly varying electric field prior to the discharge, or an effect of the electric field on the width of the Doppler spectrum. In this Appendix, we examine this latter explanation more closely by calculating Doppler spectra at vertical incidence for specified particle size distributions, specified particle charge distributions, and specified vertical electric fields.

Figure D-1 shows Doppler power spectra calculated for a Marshall-Palmer (1948) distribution of raindrops which are all charged with single polarity to the Rayleigh limit:

$$q_R = (8\pi \ \varepsilon_0 \gamma)^{1/2} \ R^{3/2}$$

which represents the largest possible charge for liquid precipitation particles. When the imposed vertical electric field is zero, all particles move downward under the influence of gravity, (The mutual coulombic repulsion of the particles is ignored.) When a vertical electric field of 50 kv/m is applied so that the electric force acting on the particles opposes that of gravity, the smaller size particles in the distribution are levitated and the downward velocities of the larger particles are reduced. Velocity modifications have been calculated following Gay et al. (1974). The result is a considerable

258

Figure D-1
Doppler Velocity Spectra
at Vertical Incidence:
Rayleigh Limit Charging

E = 0

E = 50 kV/m

E = 100 kV/m

Relative Power

Upward Velocity (m/sec)

Downward Velocity (m/sec)

259

Figure D-2
Doppler Velocity Spectra
at Vertical Incidence:
Wilson Limit Charging

$\rho_w = 0.6$ gm/cm^3
$\nu = 1.8 \times 10^{-5}$ m^2/sec
$\rho_a = 0.97$ kg/m^3
$P = 10$ mm/hr

E = 400 kV/m

E = 200 kV/m

E = 0

Relative Power

Upward Velocity (m/sec)

Downward Velocity (m/sec)

260

broadening in the distribution of spectral energy, and an anticipated larger standard deviation in the mean Doppler velocity estimate. The application of a field of 100 kv/m results in still greater energy in upward motion.

Another set of calculations were performed for a hypothetical Marshall-Palmer distribution of graupel particles, each charged to the induction limit: the Wilson charge

$$q_W = 12\pi\epsilon_O \ E \ R^2$$

In this case the maximum charge is a function of the electric field E. Figure D-2 shows the results of the calculations. In a field of 200 kv/m, the spectrum has broadened slightly and the mean velocity has decreased from the zero field case. In a field of 400 kv/m, which is considered close to dielectric breakdown, a larger fraction of the particles are levitating and the Doppler spectrum has narrowed again. Because the spread of electric forces ($\sim R^2$) in this case is less than the spread of gravitational forces ($\sim R^3$) in the zero field case, this spectral narrowing is expected.

Although the cases considered here are highly artificial, they do serve to illustrate the possible importance of electric fields on the shape of the Doppler spectrum.

261

Appendix E

Microbarograph Instrumentation

A functional diagram of the instrument used to measure pressure variations is shown in Figure E-1. A Sanborn model 270-300 gas pressure transducer (see Figure E-2) connects two 16 oz. glass bottles, each of which is open to the atmosphere via capillary tubes of different diameters. The large capillary provides a fast leak and controls the high frequency side of the instrument bandpass response, whereas the small capillary has a slow leak time and controls the low frequency end of the bandpass.

The instrument response is better appreciated by considered its equivalent electrical circuit. If voltage differences correspond with pressure differences and electric currents correspond with air flows, we can represent the 16 oz. air reservoirs with capacitors, C, and the capillary flow permeabilities with resistors R_1 and R_2. The equivalent electrical circuit is shown in Figure E-1.

The final instrument bandpass and phase angle between actual pressure and recorded signal are shown in Figure E-3. Note that the phase angle is small over the range of periods of interest in thunderstorm convection.

The pressure signals were recorded with Rustraks running at 1 inch per hour with nominal post-amplifier outputs of ±700 bar for ±5 volts (±3cm) full scale. Time synchrony at the multiple recorder sites was guaranteed with common timing marks at hourly intervals.

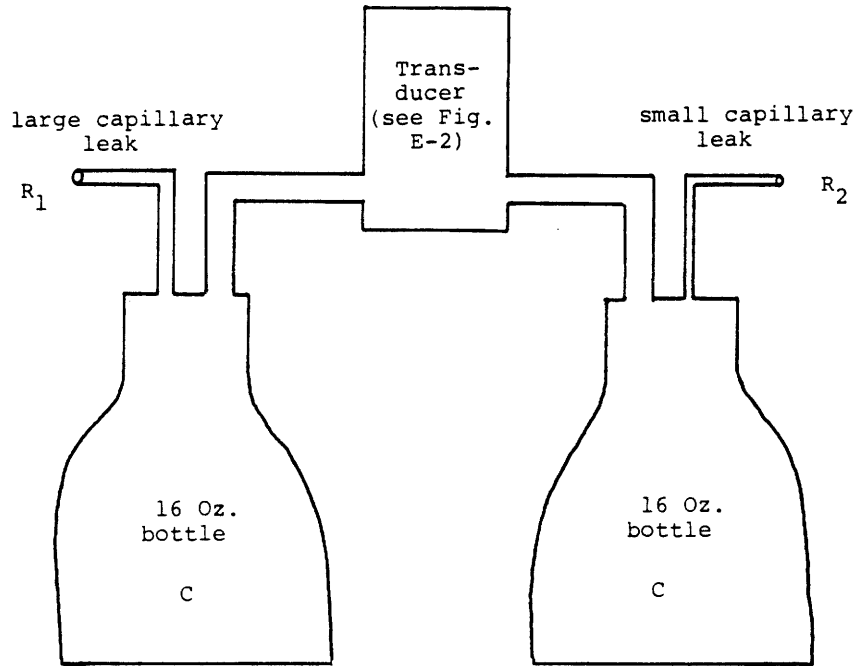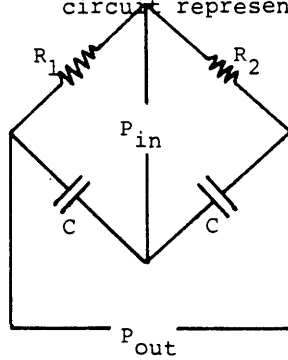large capillary
leak

Trans-
ducer
(see Fig.
E-2)

small capillary
leak

R_1

R_2

16 Oz.
bottle

C

16 Oz.
bottle

C

Figure E-1
Functional diagram
of microbarograph
and its electrical
circuit representation

R_1 R_2

P_{in}

C   C

P_{out}

263
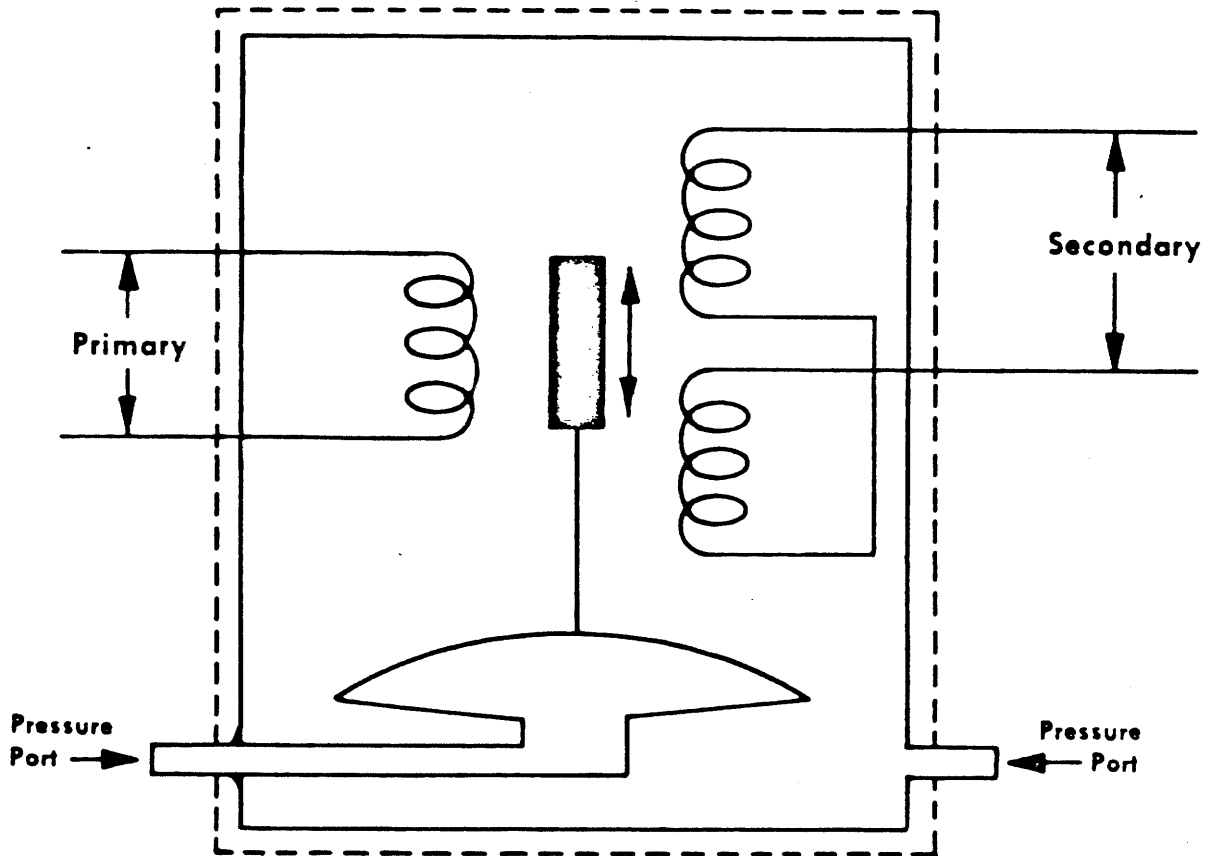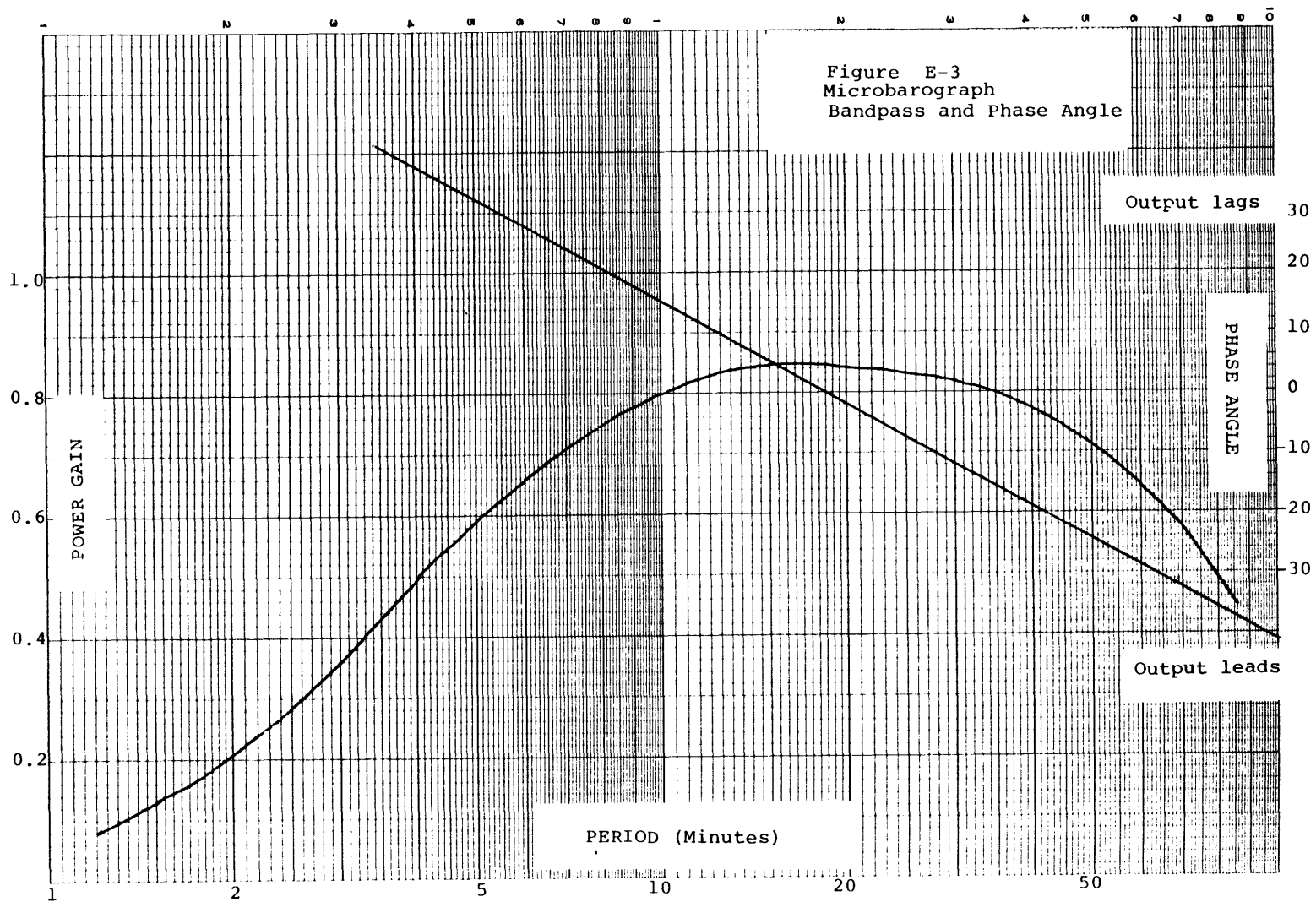
Figure E-2

Functional Diagram
Of Differential Gas
Pressure Transducer

Figure E-3
Microbarograph
Bandpass and Phase Angle

265

BIOGRAPHICAL NOTE

Earle R. Williams was born December 20, 1951 in
South Bend, Indiana. He attended preparatory school at Culver
Military Academy in his home town. He graduated from
Swarthmore College in Pennsylvania with a BA degree in physics
in June of 1974, and entered graduate school at MIT in the Fall
of that year. These graduate studies were supported by a
research grant from the National Science Foundation and by a
Hertz Foundation Fellowship.